

**A novel membrane-binding probe for the morphological and  
molecular characterization of synaptic vesicle recycling pathways**

PhD Thesis

In partial fulfilment of the requirements  
for the degree “*Doctor rerum naturalium (Dr. rer. nat.)*”  
in the Neuroscience Program  
at the Georg August University Göttingen,  
Faculty of Biology

Submitted by  
Natalia Hasel Revelo Nuncira

Born in  
Bogota, Colombia

Göttingen, May 2014



Members of the Thesis Committee:

Supervisor, reviewer: **Prof. Dr. Silvio O. Rizzoli**  
Department of Neuro- and Sensory Physiology  
University Medical Center Göttingen, Germany

Reviewer: **Prof. Dr. Mikael Simons**  
Max Planck Institute of Experimental Medicine  
Department of Neurology, University of Göttingen, Germany

Committee member: **Prof. Dr. Tobias Moser**  
InnerEarLab  
Department of Otolaryngology  
University Medical Center Göttingen, Germany

Date of oral examination: June 11, 2014



# Affidavit

I hereby declare that I prepared the PhD thesis “**A novel membrane-binding probe for the morphological and molecular characterization of synaptic vesicle recycling pathways**” on my own and with no other sources and aids than quoted.

**Natalia Hasel Revelo Nuncira**



*To my family and Christian,  
for embracing me with love and support*

*“Invention, it must be humbly admitted,  
does not consist in creating out of void but out of chaos.”*

From *Frankenstein*,  
by Mary Shelley





# LIST OF PUBLICATIONS

---

Parts of this thesis have been or will be published in the following research articles:

**Revelo N.H.\***, Kamin D.\*, Truckenbrodt S., Wong A.B., Reuter K., Reisinger E., Moser T., Rizzoli S.O. (2014) A new probe for super-resolution imaging of membranes elucidates trafficking pathways. *J Cell Biol.* 205(4), 591–606.

Kamin, D.\*, **Revelo N.H.\***, Rizzoli S.O. (2014) FM Dye Photo-oxidation as a Tool for Monitoring Membrane Recycling in Inner Hair Cells. *PLoS One.* 9:e88353. doi:10.1371/journal.pone.0088353.

\* Equal contribution

Techniques used in this thesis were summarized in the following book chapter:

**Revelo N.H.°**, Rizzoli S.O. Application of STED microscopy to cell biology questions. In: Verveer P. Advanced Fluorescence Microscopy: Methods and Protocols. *Methods Mol Biol. In press.*

° Corresponding Author



# TABLE OF CONTENTS

---

List of Publications .....	ix
Table of Contents.....	xi
List of Figures .....	xvii
List of Tables .....	xix
List of Abbreviations.....	xx
Acknowledgements .....	xxii
Abstract .....	xxiv
1 Introduction .....	1
1.1 Constitutive endocytosis and the endocytic pathway .....	1
1.1.1 Modes of endocytosis.....	1
1.1.1.1 Clathrin-mediated endocytosis (CME).....	1
1.1.1.2 Endocytosis of caveolae.....	3
1.1.1.3 Other mechanisms of membrane retrieval .....	3
1.1.2 Endosomal sorting .....	3
1.2 Membrane trafficking at a specialized cell junction: the neuronal synapse .....	6
1.2.1 Synaptic transmission in chemical synapses .....	7
1.2.2 Diversity among synaptic vesicles .....	8
1.2.2.1 The three main synaptic vesicle pools: readily releasable, recycling and reserve.....	8
1.2.2.2 The spontaneously released pool of vesicles.....	9
1.2.2.3 The readily retrievable or surface pool of vesicles .....	10
1.2.3 Synaptic vesicle recycling.....	12
1.2.3.1 Kiss-and-run .....	12
1.2.3.2 Clathrin mediated endocytosis (CME) of synaptic vesicles.....	13
1.2.3.3 Bulk endocytosis.....	14

## Table of Contents

---

1.2.3.4 Endosomal sorting of recycled vesicles.....	15
1.3 Membrane trafficking at specialized sensory synapses.....	16
1.3.1 The highly efficient ribbon-type sensory synapses.....	16
1.3.2 Ribbon synapses in the auditory system .....	18
1.3.2.1 The hearing process .....	18
1.3.2.2 The transduction process at IHCs .....	20
1.3.2.3 Mechanisms of synaptic vesicle recycling in hair cells.....	21
1.4 High-resolution STED microscopy for the study of membrane trafficking pathways ..	27
1.5 Aims of this work.....	30
2 Materials and Methods.....	33
2.1 Materials.....	33
2.1.1 Reagents.....	33
2.1.2 Buffers and solutions .....	34
2.1.3 List of Antibodies.....	35
2.1.4 Microscopes and equipment.....	37
2.1.5 Software.....	38
2.2 Methods .....	39
2.2.1 Generation of tools for the study of membrane traffic .....	39
2.2.1.1 Generation and dialysis of membrane-binding molecules .....	39
2.2.1.2 mCLING generation and concentration estimation .....	39
2.2.2 Experiments performed with cultured mammalian cells .....	40
2.2.2.1 Preparation of coverslips for cell culture seeding.....	40
2.2.2.2 Endocytosis assays in COS7 cells.....	40
2.2.2.3 mCLING toxicity assay in COS7 cells.....	41
2.2.2.4 Culture methods for rat hippocampal neurons .....	42
2.2.2.5 Neuronal transfection with SynaptopHluorin construct.....	42
2.2.2.6 SynaptopHluorin experiments in neuronal hippocampal cultures .....	43
2.2.2.7 mCLING applications to cultured rat hippocampal neurons .....	43

2.2.2.8	Preparation of Mowiol embedding medium .....	44
2.2.3	Dissection and uses of the mouse organ of Corti.....	44
2.2.3.1	Animals .....	44
2.2.3.2	Dissection of the organ of Corti (OC).....	45
2.2.3.3	Testing commercial fluorescent dyes in living IHCs.....	45
2.2.3.4	mCLING labeling and immunostaining of OCs .....	46
2.2.3.5	Vesicle release estimation by cell surface quenching of mCLING in IHCs .....	48
2.2.3.6	Application of endocytosis inhibitors to IHCs .....	49
2.2.3.7	Experiments with otoferlin knockout ( <i>Otof<sup>-/-</sup></i> ) mice.....	49
2.2.4	mCLING application on the larval neuromuscular junction (NMJ) of <i>Drosophila</i> ..	50
2.2.4.1	Dissection of <i>Drosophila</i> larvae and mCLING labeling.....	50
2.2.5	Sample embedding, sectioning and imaging .....	50
2.2.5.1	Melamine preparation, embedding and sectioning .....	50
2.2.5.2	STED and confocal microscopy .....	51
2.2.5.3	Thin-section imaging .....	52
2.2.6	Experiments with microorganisms .....	52
2.2.6.1	mCLING validation on yeast cells.....	52
2.2.6.2	mCLING validation in bacteria .....	52
2.2.7	Data analysis .....	53
2.2.7.1	Image analysis and processing.....	53
2.2.7.2	Statistical analysis.....	54
2.2.7.3	Data presentation.....	54
3	Results.....	55
3.1	Testing commercial membrane markers in IHCs .....	55
3.1.1	FM dyes, their analogs and fluid phase markers fail to label endocytosis in IHCs.	55
3.2	Design, synthesis and evaluation of novel membrane-binding probes .....	59
3.2.1	Requirements for the generation of suitable membrane probes to study IHCs.....	59
3.2.2	Strategies for probe design .....	60

## Table of Contents

---

3.2.2.1 Lessons from protein-based probes .....	61
3.2.2.2 PLLs conjugated to Atto 647N fail to fix on membranes .....	64
3.2.3 mCLING, a novel membrane-binding fluorescent probe .....	66
3.2.3.1 Design and validation of mCLING .....	66
3.2.3.2 mCLING is superior in fixability to commercially available probes .....	70
3.2.3.3 mCLING is taken up into organelles involved in ligand trafficking .....	72
3.3 mCLING elucidates membrane trafficking pathways in IHCs.....	75
3.3.1 Challenges in the study of endocytic events in IHCs.....	75
3.3.2 mCLING does not permeate the MET channels of IHCs.....	76
3.3.3 mCLING labeling and sample processing for the study of recycling organelles in IHCs at nano-resolution.....	76
3.3.4 mCLING uptake is endocytosis-dependent and therefore inhibited by low temperature .....	79
3.3.5 mCLING reveals that stimulation-induced synaptic vesicle recycling occurs at the IHC base.....	81
3.3.6 mCLING unloading reports SV exocytosis at the IHC base .....	84
3.3.7 Endocytic processes reported by mCLING are dynamin- and clathrin-dependent.....	87
3.3.8 Impairment of synaptic vesicle exocytosis reduces mCLING-reported endocytosis .....	89
3.3.9 Membrane recycling at the active zones of IHCs.....	90
3.3.10 Organelles recycling at the basal levels of IHCs colocalize with vesicular markers .....	93
3.3.11 Tubular structures at the top and nuclear levels of IHCs have an endosomal nature.....	95
3.3.12 mCLING-labeled organelles surrounding the cuticular plate participate in constitutive traffic to lysosomes .....	98
3.3.13 Functional separation of constitutive and synaptic recycling in IHCs is confirmed by multi-color epifluorescence imaging.....	99
3.4 Studies on synaptic vesicle recycling and protein distribution in hippocampal neurons using mCLING .....	102

3.4.1	Actively and spontaneously released synaptic vesicles differ in protein composition.....	103
3.4.2	mCLING surface labeling for the study of membrane-associated proteins.....	106
3.4.3	Organization of t-SNARE proteins on the plasma membrane and organelles .....	108
3.5	Application of mCLING to other biological preparations .....	111
3.5.1	mCLING uptake in stimulated neuromuscular junctions of the <i>Drosophila</i> larva.....	111
3.5.2	Membrane labeling in microorganisms with mCLING.....	112
3.5.2.1	mCLING can be used to study membrane uptake in yeast cells .....	112
3.5.2.2	High-resolution imaging of <i>Escherichia coli</i> membranes with mCLING .....	114
4	Discussion .....	117
4.1	The correct recipe for a fixable membrane probe.....	119
4.2	mCLING labels endocytosis and stays on membranes upon fixation and permeabilization .....	120
4.3	Membrane trafficking in IHCs.....	121
4.3.1	Technical improvements for the application of mCLING to the organ of Corti ...	121
4.3.2	Endocytosis in IHCs .....	123
4.3.3	Synaptic vesicle recycling in IHCs .....	124
4.3.3.1	Synaptic-related membrane trafficking occurs at the IHC base.....	124
4.3.3.2	Dynamin and clathrin as molecular players of synaptic vesicle recycling .....	125
4.3.3.3	A local model for synaptic vesicle recycling.....	127
4.3.4	The constitutive recycling pathway in IHCs .....	133
4.3.4.1	The identity of constitutively recycling organelles.....	134
4.3.4.2	Membrane traffic at the cuticular plate.....	135
4.3.4.3	Molecules driving constitutive membrane uptake.....	136
4.3.5	A membrane recycling model for IHCs .....	136
4.4	New insights into neuronal function .....	138
4.4.1	Molecular differences between spontaneously and actively released synaptic vesicles.....	138

## Table of Contents

---

4.4.2 Synaptic vesicle proteins stranded on the plasma membrane .....	139
4.4.3 Differences in protein clustering between SNAP-25 and Syntaxin 1 .....	141
4.5 mCLING uses in other biological preparations .....	142
4.5.1 Perspectives in <i>Drosophila</i> larva neuromuscular junction .....	142
4.5.2 Microorganisms.....	142
4.5.3 Following endocytosis with mCLING in cells with permeable channels .....	143
5 Outlook.....	144
References .....	146
Appendix.....	175
<i>Curriculum vitae</i> .....	195



# LIST OF FIGURES

---

Figure 1.1 Synaptic vesicle pools and mechanisms of synaptic vesicle recycling.....	11
Figure 1.2 SynaptopHluorin: a fluorescent tool for the of study synaptic vesicle recycling..	12
Figure 1.3 Structure of the organ of Corti. ....	19
Figure 1.4 Models of synaptic vesicle recycling in hair cells. ....	22
Figure 1.5 FM 1-43 photo-oxidation supports the local model of synaptic vesicle recycling taking place at the IHC basal level. ....	27
Figure 1.6 Working principle of high-resolution STED microscopy. ....	29
Figure 2.1 Customized chamber for IHC imaging at low temperature. ....	46
Figure 2.2 Experimental workflow for the membrane labeling, immunostaining and plastic embedding of OCs ....	48
Figure 3.1 Commercial membrane markers label IHCs in an endocytosis-independent process. ....	57
Figure 3.2 Differences in fixability and labeling distribution among protein-based membrane-binding probes. ....	62
Figure 3.3 PLL molecules conjugated to Atto 647N do not fix to membranes. ....	65
Figure 3.4 mCLING, a novel probe that successfully labels endocytosis.....	67
Figure 3.5 mCLING is not toxic for cells at working concentrations for membrane labeling.	68
Figure 3.6 mCLING does not affect endosomal traffic in COS7 cells. ....	69
Figure 3.7 In contrast to fixable FM dyes, mCLING labeling is preserved after permeabilization. ....	71
Figure 3.8 mCLING labels endocytic organelles involved in ligand trafficking.....	74
Figure 3.9 mCLING does not permeate the MET channels of living IHCs. ....	76
Figure 3.10 A 1-minute incubation period is not long enough for mCLING to penetrate into OCs and label IHCs homogeneously.....	79
Figure 3.11 mCLING uptake into IHCs is endocytosis-dependent and therefore inhibited by low temperature.....	80
Figure 3.12 mCLING reveals recycling organelles in IHCs. ....	84
Figure 3.13 mCLING unloading, evidenced by BPB fluorescence quenching, locates SV exocytosis exclusively at the IHC basal level. ....	86
Figure 3.14 Effects of clathrin and dynamin inhibition visualized by mCLING labeling in	

IHCs .....	88
Figure 3.15 Impaired SV exocytosis by deletion of the protein otoferlin is accompanied by reduced levels of endocytosis in IHCs.....	90
Figure 3.16 mCLING reveals the morphology of the organelles that locally recycle SVs at the IHCs active zone.....	92
Figure 3.17 mCLING-labeled organelles at the cell base show better colocalization with SV markers than those at the top and nuclear levels .....	94
Figure 3.18 Tubular structures at top and nuclear level are not related to ER or cis-Golgi....	96
Figure 3.19 The tubular organelles endocytosed at the IHC top and nuclear levels have endosomal identity.....	97
Figure 3.20 mCLING-labeled organelles surrounding the cuticular plate contain the late endosome/lysosome marker LAMP1 .....	99
Figure 3.21 Separation of constitutive and synaptic recycling pathways is confirmed by multi-color imaging.....	101
Figure 3.22 mCLING does not affect synaptic vesicle recycling in hippocampal neurons....	103
Figure 3.23 mCLING reveals differences in molecular composition between actively and spontaneously released SVs .....	105
Figure 3.24 mCLING labeling allows the distinction between the organelle- and the membrane-associated fractions of synaptic vesicle proteins. ....	108
Figure 3.25 Analysis of membrane-associated protein clusters at high resolution using mCLING.....	109
Figure 3.26 mCLING uptake in the <i>Drosophila</i> larva neuromuscular junction. ....	112
Figure 3.27 mCLING is taken up in endocytic compartments in yeast cells.....	113
Figure 3.28 High-resolution imaging of mCLING-labeled membranes of <i>E. coli</i> cells.....	115
Figure 4.1 Local model of synaptic vesicle recycling in hair cells.....	130
Figure 4.2 Membrane trafficking pathways in IHCs.....	137

# LIST OF TABLES

---

Table 2.1 List of reagents used in this study..... 33

Table 2.2 List of buffers and solutions used in this study..... 34

Table 2.3 List of antibodies used in this study..... 35

Table 2.4 List of microscopes and equipment used in this study..... 37

Table 2.5 List of software used in this study ..... 38

Table 3.1 List of commercial dyes tested on IHCs..... 56

# LIST OF ABBREVIATIONS

---

AP	Action potential
BPB	Bromophenol blue
BSA	Bovine serum albumin
CCD	Charge-coupled device
CME	Clathrin-mediate endocytosis
CTBA	Cholera toxin B subunit conjugated to Alexa 594
Da	Dalton
DAB	3,3'-Diaminobenzidine
DiI	1,1'-dioctadecyl-3,3,3'-tetramethylindocarbocyanine
DIV	<i>Days in vitro</i>
DMSO	Dimethyl sulfoxide
<i>E. coli</i>	<i>Escherichia coli</i>
EGF	Epidermal growth factor
EGTA	Ethylene glycol tetraacetic acid
EM	Electron microscopy
ER	Endoplasmic reticulum
FM	Fei Mao, name of the chemist who developed FM dyes
FWHM	Full width at half maximum
GFP	Green Fluorescent Protein
GM130	130 kDa cis-Golgi matrix protein
HBSS	Hank's Balanced Salt Solution
HEPES	4-(2-hydroxyethyl)-1-piperazineethanesulfonic acid
HRP	Horseradish peroxidase
IHCs	Inner Hair Cells
IPA	Insulin-palmitoyl-Atto 647N
kDa	kiloDalton
LAMP1	Lysosome membrane associated protein 1
LDL	Low-density Lipoprotein
MET	Mechanoelectric transducer or mechanotransduction (channels)
mV	Millivolt
NA	Numerical aperture
NHS	N-Hydroxysuccinimide

---

NMJ	Neuromuscular junction
OC	Organ of Corti
<i>Otof</i> <sup>-/-</sup>	Otoferlin knockout
PBS	Phosphate buffer saline
PFA	Paraformaldehyde
PI	Propidium iodide
PLL	Poly-L-lysine
PMT	Photomultiplier tube
PSF	Point spread function
Rab	Ras-like protein in brain
ROI	Region of interest
RRP	Readily releasable pool of synaptic vesicles
RT	Room temperature
<i>S. cerevisiae</i>	<i>Saccharomyces cerevisiae</i>
SEM	Standard error of the mean
SNAP-25	25 kDa synaptosomal-associated protein
SNARE	Soluble N-ethylmaleimide-sensitive factor attachment protein receptor
STED	Stimulated Emission Depletion Microscopy
SV	Synaptic vesicle
Sx 1	Syntaxin 1
Sx 6	Syntaxin 6
Sx 13	Syntaxin 13
Sx 16	Syntaxin 16
Syt	Synaptotagmin
TfPA	Transferrin-palmitoyl-Alexa 594
TGN	Trans-Golgi network
TTX	Tetrodotoxin
VAMP	Vesicle-associated membrane protein, also known as synaptobrevin
VGLUT1	Vesicular glutamate transporter 1
VGLUT3	Vesicular glutamate transporter 3
Vti1a	Vps10p-tail-interactor-1a
YNB	Yeast nitrogen base medium

# ACKNOWLEDGEMENTS

---

First and foremost, I would like to thank my supervisor Prof. Dr. Silvio Rizzoli for his support, trust and encouragement during the last three years (especially after every journal rejection!). Thank you for teaching me that science is not only constructed by following preestablished protocols and dogmas, but also by our curiosity and innovation, pushing unconventional ideas forward. And finally, thanks for giving me the opportunity to become a better scientist and helping me see what I am capable of.

I am also grateful to the members of my thesis committee Prof. Dr. Tobias Moser and Prof. Dr. Mikael Simons for the fruitful discussions during the committee meetings. I would also like to thank Prof. Moser for the collaborative work and his great effort in organizing the Ribbon Synapse Symposium, which was a wonderful setting to meet researches leading the sensory physiology field.

Many thanks to Prof. Dr. Michael Hörner and Sandra Drube from the Neuroscience Program for their superb support since I arrived to Göttingen. They did not only take care of academic issues but also made the start of a new life so far from home easier.

I would like to thank Dirk Kamin for guiding me in the first experiments I performed in the lab and for being a great co-author, backing me up when I needed it. I would also like to thank my colleague Sven Truckenbrodt for his excellent work contributed to our manuscript.

I am grateful to Christina Schäfer and Katharina Kröhnert for their excellent technical assistance, always making sure that the laboratory is running well so that we can focus on our research.

I would also like to thank all the people from the Rizzoli lab. Dr. Eugenio Fornasiero for his dedication in helping me to establish new experimental routines, the exciting scientific discussions and for the great company in the Friday singing afternoons while doing experiments in the lab. Sinem Saka Kırılı (or Kırılı Saka) for her friendship and constant support, always having friendly and encouraging comments. Many thanks to Ingrid Vreja, William Zhang, Katharina Seitz, Manuel Maidorn, Dr. Benjamin Wilhelm, Dr. Anette Denker, Dr. Angela Gomes, Dr. Nikhil Sasidharan, Dr. Nora Wender and Dr. Felipe Opazo for making

the time in the lab so enjoyable and rich in scientific discussions.

Thanks to my friends in Göttingen: Chepe, Melanie, Carlos Eduardo (Cadu), Koray, Sinem, Aaron and Wendy, for making of our life here an unforgettable experience.

To my co-mentees Dominika Lytzw, Tamara Vázquez and Andreea Scacioc, and my mentor Sharmishtha Dattagupta, I would like to express my deepest thanks for sharing with me fruitful sessions that helped me to find a balance in my life and respond to challenges with my best face.

The completion of my studies would not have been possible without the constant support and encouragement of my family. A mis padres agradezco su amor y esfuerzo incondicional por darnos a mi y a mi hermano la oportunidad de ir a la Universidad y ofrecernos un ambiente de bienestar. A toda mi familia, por enseñarme a luchar y mirar con optimismo las situaciones difíciles.

Finally, I would like to thank Christian for his unconditional love and support, and for constructing with me a place I can call home. Thank you for constantly believing in me and helping me reach all my dreams, small and big. Thank you for being the sunshine of my life.

# ABSTRACT

---

An important anatomical feature of neuronal synapses is the presynaptic bouton, a structure that isolates synaptic vesicle recycling from constitutive membrane trafficking pathways. However, in some neurotransmitter-releasing cells this structure is not present and instead they develop active zones directly located at the cell soma (somatic active zones). This is the case for the auditory inner hair cells (IHCs), polarized cells responsible for sound encoding in mammals, with somatic active zones located at their basal pole. As most sensory synapses, IHCs present particularly high rates of synaptic vesicle release, which need to be compensated by equally efficient membrane retrieval mechanisms. Up to now, two models of synaptic vesicle recycling have been proposed in IHCs: 1) apical membrane retrieval that involves organelles of constitutive pathways in vesicle reformation (e.g. endoplasmic reticulum and Golgi apparatus), and 2) local basal recycling, in proximity to the vesicle release sites. Establishing which of these models is correct has been difficult, since conventional endocytosis markers have failed to accurately report membrane uptake events in these cells.

In this study a new membrane-binding probe, called mCLING (membrane-binding fluorophore-Cysteine-Lysine-Palmitoyl Group), was developed to study membrane uptake and trafficking in IHCs, under high-resolution Stimulated Emission Depletion (STED) microscopy. mCLING is not toxic and does not affect membrane trafficking physiology. Moreover, mCLING can be fixed and combined with immunostaining, in order to establish the molecular composition of recycling organelles. mCLING uptake combined with immunostaining against vesicular markers confirmed that synaptic vesicle recycling in IHCs exclusively localizes at the cell base. Synaptic vesicles seem to reform from endocytic intermediates, such as membrane infoldings and cisterns that arise in the vicinity of synaptic active zones. mCLING labeling also revealed that constitutive recycling pathways take place at the top and nuclear IHC levels, in the form of large tubulo-cisternal structures related to recycling endosomes. These results indicate that IHCs functionally and spatially separate synaptic vesicle recycling from constitutive membrane traffic. Moreover, they evidence the importance of keeping synaptic vesicle recycling as a separate trafficking pathway, especially in the absence of a synaptic bouton.



The applicability of mCLING to other biological preparations was further explored. In hippocampal cultured neurons, mCLING allowed to answer still open questions on synaptic function and protein organization: 1) are the same synaptic vesicles undergoing active and spontaneous release? mCLING labeling combined with immunostaining revealed that actively and spontaneously released vesicles differ in molecular composition, being the latter more related to constitutive endosomal traffic. 2) What is the fraction of synaptic vesicle proteins that remains stranded on the plasma membrane as a potential readily retrievable pool of vesicles? This quantification has been difficult, since it has been estimated mainly by overexpression of different proteins fused with the pH sensor pHluorin. Surface labeling with mCLING combined with immunolabeling of endogenous synaptic proteins allowed to establish that ~12 to 22% of them remain stranded on the plasma membrane. 3) What is the organization of SNAP-25 and syntaxin 1 on intracellular organelles? So far clusters of these proteins have only been studied on the plasma membrane. Using mCLING as a surface marker, it was possible to establish that SNAP-25 forms clusters of similar size on the plasma membrane and in intracellular organelles. In contrast, Syntaxin 1 forms larger clusters on the plasma membrane.

Additionally, mCLING labeling and endocytosis were compatible with immunolabeling in COS7 cells, the *Drosophila* larva neuromuscular junction and yeast cells.

I conclude that mCLING is the first fixable endocytosis marker that can be successfully combined with immunolabeling techniques, and is also compatible with a high-resolution microscopy technique. mCLING helped to answer long-standing questions in a conventional and a sensory synapse, and has a strong potential in the study of membrane traffic in any biological preparation, from cultured cells to complex tissues.



# 1 INTRODUCTION

---

## 1.1 Constitutive endocytosis and the endocytic pathway

In his theory on the origin of life (1957), Oparin suggested that for the early precursors of life (coacervates) to persist in time “the entry of substances into the system or their expulsion into the external medium must already have ceased to depend on the simple laws of permeability and adsorption”. He further highlighted that “it is precisely this sort of interaction with the external medium, though in a considerably more highly developed form, which is the characteristic of all contemporary living things”. With these words, Oparin defined the most important function of the cell plasma membrane.

Establishing a barrier between the cell content and the environment, the plasma membrane can be considered as the main regulator of intracellular processes. While small hydrophobic molecules (e.g. CO<sub>2</sub>, N<sub>2</sub> and O<sub>2</sub>) can passively diffuse across the membrane, small and large uncharged polar molecules can only diffuse very slowly. In the case of charged molecules (i.e. ions) the membrane is completely impermeable. Transport of ions and slow diffusing molecules along their electrochemical gradients can be performed by regulated opening of transmembrane channels. Moving molecules against such gradients requires active transport at an energy cost. For the entrance of even larger molecules, bulk internalization of solutes, uptake of degradation substrates, or the regulated internalization of signaling molecules and biosynthetic precursors, a specialized mechanism involving the retrieval of membrane-bound compartments is required. This is known as **endocytosis** (Alberts et al., 2008). Throughout this study, the term **constitutive endocytosis** will be used to group the membrane retrieval events that take place regularly and preserve normal cell function. In particular, when referring to neurotransmitter-releasing cells, I will generalize as constitutive the endocytic processes not related with synaptic function.

### 1.1.1 Modes of endocytosis

#### 1.1.1.1 Clathrin-mediated endocytosis (CME)

This mode of endocytosis is responsible for the internalization of plasma membrane

molecules, including receptors and their ligands (e.g. the iron carrier transferrin, the cholesterol carrier low-density-lipoprotein (LDL), or the epidermal growth factor (EGF)). Hence, this pathway is essential for providing the cells with precursor molecules for biosynthetic pathways and for regulating signaling cascades. For many years, the conspicuous clathrin polymers seen in electron microscopy led to think of it as the major endocytic pathway taking place in cells, but recent research has unveiled more important roles for other endocytosis modes (Doherty and McMahon, 2009). CME is not only important for the retrieval of endocytic vesicles from the plasma membrane, but also for the formation of cargo vesicles from the trans-Golgi network. The term clathrin groups two different proteins, the 180 kDa clathrin heavy chain and the 30-40 kDa clathrin light chain. Six copies (3 of each) polymerize to form a three-legged structure called triskelion. While the heavy chain acts as backbone, the light chain helps in the trimerization (Pearse, 1975; Ungewickell and Branton, 1981; Winkler and Stanley, 1983; Huang et al., 1997; Edeling et al., 2006).

The main purpose of CME is the regulated formation of a coat that provides cargo selectivity and mechanical support for membrane bending and vesicle budding. First, cargo proteins are recognized by an adaptor protein complex called AP2. This is a heterotetrameric complex, formed by the  $\alpha$ ,  $\beta$ ,  $\mu$  and  $\sigma$  adaptins, which serves as coat formation coordinator: it binds to dileucine motifs in the cargo, phosphoinositides PI(4,5)P<sub>2</sub> and PI(3,4,5)P<sub>3</sub> on the plasma membrane, accessory proteins, and clathrin (Collins et al., 2002). In the next step, AP2 recruits clathrin triskelions at the site of endocytosis, which interact between them to form a lattice that progressively grows into a polygonal cage around the future cargo vesicle (Kirchhausen and Toyoda, 1993). Epsin, which also binds to cargo and phosphoinositides, induces membrane curvature by inserting an amphipathic  $\alpha$ -helix (Ford et al., 2002). Additionally, curvature can be aided by the N-BAR domain protein amphiphysin (Yoshida et al., 2004). At this point the vesicle is ready for fission. This is facilitated by dynamin, a GTPase that assembles into spirals around the neck of endocytic vesicles. Thanks to its catalytic activity, dynamin provides the energy required for membrane fission and release of the reformed vesicle (Baba et al., 1999; Hinshaw, 2000; Kessels et al., 2006). In the final step, the clathrin-binding protein auxilin recruits ATP-activated molecules of the chaperone Hsp70 for catalyzing vesicle uncoating (Lemmon, 2001). Several other accessory proteins have been described, that give specificity to the cargo or the cell type.

### **1.1.1.2 Endocytosis of caveolae**

Caveolae are flask-shaped invaginations of the plasma membrane that can undergo endocytosis (Yamada, 1955; Palade and Bruns, 1968). They are involved in nitric oxide and calcium signaling, lipid homeostasis, transcytosis and mechanosensation (Drab et al., 2001; Razani et al., 2002; Yu et al., 2006). By their composition, caveolae have been associated to plasma membrane microdomains rich in glycosphingolipids, cholesterol and glycosphosphatidylinositol (GPI)-anchored proteins, called lipid rafts (Parton and Simons, 2007). Three types of caveolin 1, 2 and 3 are the main players in caveolin formation and function. Caveolin 1 and 2 are expressed in non-muscle cells, while Caveolin 3 is enriched in muscle fibers (Parton et al., 1997). They contain a hairpin domain that inserts into the membrane and is flanked by the cytoplasmic N and C terminal domains. A model proposes that caveolin molecules induce membrane curvature thanks to oligomerization and the strong interaction with the membrane via cholesterol and palmitoylation (Dietzen et al., 1995; Monier et al., 1996; Parton et al., 2006). Fission of caveolae is performed by dynamin (Henley et al., 1998; Oh et al., 1998).

### **1.1.1.3 Other mechanisms of membrane retrieval**

Several alternative modes of endocytosis have been described. One of them is coordinated by the proteins Flotillin 1 and 2. As caveolins, these proteins are found in membrane microdomains, and seem to be responsible for internalization of GPI-anchored proteins and proteoglycans (Frick et al., 2007; Payne et al., 2007; Doherty and McMahon, 2009). Other modes include the uptake of membranes into large compartments. This is the case of macropinocytosis, or generation of membrane ruffles for gross internalization of fluid without coat formation. This process is cholesterol dependent and involves the actin cytoskeleton (Grimmer et al., 2002; Doherty and McMahon, 2009). Another mode internalizes membrane in tubular or ring like structures and has been called Clathrin-independent carrier (CLIC) endocytosis. Although its role remains elusive, it is regulated by caveolins and the small GTPase Cdc42 (Kirkham et al., 2005; Doherty and McMahon, 2009; Chaudhary et al., 2014). Finally, phagocytosis is the formation of large endocytic compartments called phagosomes, for the uptake of large particles, like microorganisms and dead cells (Alberts et al., 2008).

## **1.1.2 Endosomal sorting**

After the process of endocytosis, a set of organelles coordinate the distribution of

endocytosed cargo molecules, sorting apart proteins that need to be recycled back to their original membranes, biosynthetic precursors and molecules that need to be degraded. Elucidating the different steps of the endocytic pathway has been challenged by highly active trafficking processes that constantly exchange cargo molecules and solutes between compartments. Despite this, a complex network of proteins orchestrating fusion and fission events could be unveiled. Furthermore, it was found that some of those proteins preferentially reside in or return back to a specific type of compartment, making easier to establish a classification, sometimes also supported by morphological hallmarks. An example of such molecules is the family of Rab GTPases. These are proteins that can transiently associate with membranes via a hydrophobic tail to specifically regulate fission and fusion of organelles (Pfeffer, 2001).

The **early endosome** (also called sorting endosome) is the convergence point for endocytic vesicles taken up by clathrin-dependent and -independent mechanisms. Delivery of endocytic vesicles from the plasma membrane to early endosomes, as well as their homotypic fusion are regulated by Rab5 and the early endosome antigen 1 (EEA1) (Gorvel et al., 1991; Bucci et al., 1992; Mills et al., 1999). This organelle is responsible for the first steps of molecular sorting for proteins and lipids. Due to a low internal pH 6.3 most ligands are released from their receptors here (Sipe and Murphy, 1987). Output routes from early endosomes include recycling of molecules back to the plasma membrane, retrograde delivery to the trans-Golgi network or delivery of molecules to the recycling endosome. Additionally, the early endosome retains proteins destined for degradation and matures into a late endosome (Jovic et al., 2010). Sorting of molecules is facilitated by formation of membrane microdomains that, after cargo enrichment, turn into tubular appendages that are then detached and transported towards the plasma membrane or the recycling endosome, with the participation of Rab4 (van der Sluijs et al., 1992; Mayor et al., 1993).

Some proteins are not recycled back to the plasma membrane directly from the early endosome; instead they are first delivered to the **recycling endosome**. The reason could be to prevent their entrance into the degradative pathway (Traer et al., 2007). The recycling endosome is a tubular network with pH 6.5, located close to the centriole and supported by microtubules (Yamashiro et al., 1984). As in the early endosome, sorting processes also take place here (Presley et al., 1993). Besides directing recycled molecules to the plasma membrane, it also participates in retrograde transport to the trans-Golgi network (Bonifacino and Rojas, 2006). This compartment is characterized by association with

syntaxin 13, actin and Rab11, the latter controlling the two output routes (Trischler et al., 1999).

**Late endosomes**, also known as multivesicular bodies (MVBs), contain all the integral membrane proteins, ligands and solutes that were not extracted during sorting (e.g. LDL and EGF receptors) and that are destined to degradation. The generation of late endosomes is controversial. One model proposes that Rab7 selectively forms vesicles from the early endosome, which later aggregate into a late endosome (Vonderheit and Helenius, 2005). A second model suggests that early endosomes undergo a maturation process into late endosomes, during which Rab5 is replaced by Rab7 (Rink et al., 2005; Poteryaev et al., 2010). Late endosomes have a pH 5 and receive lysosomal hydrolases from the trans-Golgi network via Rab9 (Killisch et al., 1992; Lombardi et al., 1993; Gruenberg, 2001). The name MVBs comes from the presence of intraluminal vesicles inside the late endosome. These are formed by accumulation of proteins tagged with ubiquitin, a signal for degradation, on the surface of the late endosome. After assembly of a bilayered clathrin coat, protein accumulations are internalized by membrane inward invagination (Sachse et al., 2002; Piper and Katzmann, 2007). This is a pathway used for degradation of downregulated receptors, like the EGF receptor (Futter et al., 1996). MVBs targeting is also the preferred degradation pathway for old proteins coming from the trans-Golgi network (Piper and Katzmann, 2007).

**Lysosomes** are the final destination organelles for molecules to be degraded. They fuse with late endosomes with the coordination of Rab7 to receive their accumulated cargo (Luzio et al., 2010). They have a pH below 5 and are rich in hydrolases (Futter et al., 1996).

### 1.2 Membrane trafficking at a specialized cell junction: the neuronal synapse

The nervous system is responsible for the voluntary and involuntary actions of an animal, keeping basic physiological functions under regulation and gathering information about the individual's environment, important for its survival. Hence, the nervous system relies on highly evolved modes of information reception, generation, assessment and delivery. At the cellular level, the basic unit of the nervous system is the neuron. Although along evolution neurons have adopted a plethora of morphologies to better fulfill their function, a basic architecture is preserved: a receptive region for information input (dendritic arbor); a cell soma, hosting biosynthetic and recycling processes; and a delivery component, specialized for information transfer and output (axon). As in most cells, a polarized electric potential of around -70 to -80 millivolts (mV) is present across the plasma membrane of neurons, generated by negative charges distributing along the cytosolic surface and positive charges on the extracellular surface. Neurons are excitable cells, meaning that they can modulate this potential in order to encode information. Incoming electric stimuli induce membrane depolarization. If certain threshold is reached, voltage-gated  $\text{Na}^+$  channels open to allow the influx of  $\text{Na}^+$  ions. This electric current further depolarizes the membrane towards positive values, which increase the outward electrochemical driving force for  $\text{K}^+$  ions, leading to their efflux via  $\text{K}^+$  channels. After the membrane potential reaches a maximum of around 40 mV, the  $\text{K}^+$  current brings it back to negative values, typically below the initial resting potential. Every cycle of depolarization and repolarization is called an **action potential (AP)**. Action potentials are described as **all-or-none events**, since only by reaching the activation threshold potential of voltage-gated  $\text{Na}^+$  channels they can take place, and once started they will always have the same magnitude, independent of the stimulus strength. Instead, frequency and temporal patterning of APs are the parameters that encode information about the stimulus. Inactivation of  $\text{Na}^+$  channels and an ensuing refractory period avoid the reactivation of the same membrane regions, pushing the AP forward in only one direction (Bear et al., 2006; Kandel et al., 2013).

Once APs reach the end of the axon, information needs to be transferred to the next cell. For this, neurons tightly appose their membranes in a specialized junction called **synapse**, with the delivering region called presynapse, and the receiving region postsynapse. There are two types of synapses: electrical synapses, in which protein channels inserted across both membranes allow the direct transfer of ionic currents; and chemical synapses, where



quantal amounts of a chemical signal are released by the presynapse into the intercellular space. This signal, called **neurotransmitter**, reaches the postsynaptic surface and specifically activates receptor ion channels (ionotropic receptors) that start a new round of APs in the second neuron. Alternatively, neurotransmitters can also activate transmembrane receptors that modulate ion channel opening through intracellular signaling cascades (metabotropic receptors). Although information transfer is faster in electrical synapses, the flow of ions is bidirectional. Chemical synapses are slower, but they ensure unidirectional transmission, signal amplification and modulatory plasticity (Bear et al., 2006).

### 1.2.1 Synaptic transmission in chemical synapses

The presynaptic region of chemical synapses, commonly called **synaptic bouton** or **presynaptic terminal**, is a highly specialized anatomical compartment that isolates the molecular machinery necessary for neurotransmitter release from other ongoing cellular processes. Small neurotransmitters are directly synthesized at the presynaptic terminal by enzymes produced in the cell body, which work on precursor molecules imported from the extracellular space by transmembrane transporters. These neurotransmitters are loaded into small, round organelles called **synaptic vesicles**, by specific antiporter transporters that couple neurotransmitter influx with proton ( $H^+$ ) efflux. An electrochemical proton gradient is created across the vesicular membrane by vesicular ATPases. In the case of glutamate, the most important neurotransmitter of the mammalian central nervous system, import is done by one of the so far known Vesicular Glutamate Transporters (VGLUT1, 2 or 3). In contrast, peptide neurotransmitters are produced by the biosynthetic organelles (ER-Golgi) and transported in secretory vesicles towards the presynaptic terminal via fast axonal transport (Purves et al., 2004).

Synaptic vesicles are among the smallest organelles found in eukaryotic cells (~30 to 45 nm diameter in sensory receptors, neuronal and neuromuscular synapses) (Zhang et al., 1998; Hu et al., 2008; LoGiudice et al., 2008; Fuchs et al., 2014; Neef et al., 2014). They are the morphological substrate of what was described by Bernard Katz and José del Castillo (1954) as quantal release: fixed amounts of neurotransmitter evoke graded responses at the postsynaptic neurons in always equal steps. Upon arrival of APs to the presynaptic terminal, the presynaptic membrane is depolarized, activating voltage-gated channels that allow an inward  $Ca^{2+}$  current (Llinás and Nicholson, 1975). The increase in internal  $[Ca^{2+}]$  can be of more than 1000-fold, from 100 nM to 100  $\mu$ M. These rapid changes in  $Ca^{2+}$  concentration

trigger the exocytosis of neurotransmitter-filled synaptic vesicles preferentially at specific sites of the synaptic terminal called **active zones**, where the  $\text{Ca}^{2+}$  channels organize in clusters (Bear et al., 2006).

Before exocytosis can happen, two preparatory events are required. Synaptic vesicles need to be placed at active zones and establish an anchor or tether with the plasma membrane in a process called **docking**. Subsequently, during **priming**, the docked vesicles are prepared to become fusion competent and sensitive to  $[\text{Ca}^{2+}]$  changes (Geppert and Südhof, 1998; Klenchin and Martin, 2000). As in all membrane trafficking processes, the specificity and completion of vesicle fusion with the plasma membrane is tightly regulated by proteins located on both of the opposing surfaces (Takamori et al., 2006). The main players in synaptic vesicle exocytosis belong to the **SNARE** (SNAP (Soluble NSF Attachment Protein) Receptor) superfamily of proteins. SNAREs mediate vesicle fusion with the plasma membrane, other vesicles or organelles across the different trafficking pathways. Despite differences in their composition, some anchoring to membranes by transmembrane domains and others by lipidic post-translational modifications (e.g. palmitoyl), they all share a cytosolic domain called the *SNARE motif*. This is an unstructured stretch of 60-70 amino acids that upon approach to other three motifs, spontaneously assemble into a metastable four- $\alpha$ -helix bundle or complex. The free energy released during bundle formation fuels membrane fusion (Jahn and Scheller, 2006). Synaptic vesicle exocytosis is driven by a vesicular v-SNARE called **synaptobrevin 2** (also known as Vesicle-associated membrane protein, **VAMP2**) and two plasma membrane (or target) t-SNAREs **syntaxin 1** and **SNAP-25**, the last one providing two SNARE motifs (Südhof and Rizo, 2011). Fusion is completed with the help of another vesicular protein called **synaptotagmin**, which senses increases in  $[\text{Ca}^{2+}]$  at AP arrival, thanks to two  $\text{C}_2$  ( $\text{Ca}^{2+}$  binding) domains. Upon binding to five  $\text{Ca}^{2+}$  ions, synaptotagmin increases its affinity for the SNARE complex and phospholipids at the plasma membrane, further helping membrane fusion and the formation of a pore between the two membranes (Südhof, 2013).

### 1.2.2 Diversity among synaptic vesicles

#### 1.2.2.1 The three main synaptic vesicle pools: readily releasable, recycling and reserve

It has been noted that not all the synaptic vesicles found in a synaptic terminal undergo exocytosis or have the same release probability. By different approaches such as

electrophysiology, EM and fluorescence imaging, three different pools of vesicles have been defined (Figure 1.1): the **readily releasable pool (RRP)** includes vesicles that are close to the plasma membrane, in a docked configuration at the active zone, ready to undergo exocytosis. These vesicles are released at stimulation onset with fast kinetics. The **recycling pool** is formed by non-docked vesicles that eventually replenish the RRP after this is exhausted. They are detected in a second mode of exocytosis with slower kinetics. At physiological, moderate stimulation conditions, this pool is constantly replenished by synaptic vesicle recycling (endocytosis) for subsequent rounds of exocytosis. In contrast to the previous two pools, the **reserve pool** (also called as resting pool) is only mobilized for exocytosis at strong unphysiological stimulation. Surprisingly, this pool constitutes around 80-90% of the total pool of vesicles found in the terminal (Schikorski and Stevens, 2001; Südhof, 2004; Rizzoli and Betz, 2005).

Initially, it was thought that a difference between the three pools of vesicles would be their distance to the active zones, with vesicles from the RRP and recycling pool closer to active zones than those from the reserve pool. However, electron microscopy studies using endocytosis tracers revealed that they are highly intermixed (Akbergenova and Bykhovskaia, 2009; Denker et al., 2009, 2011a). In contrast, a molecular player called **synapsin** seems to differentiate between releasable vesicles (RRP and recycling) and reserve vesicles, by tethering only the latter to the actin cytoskeleton (Pieribone et al., 1995; Godenschwege et al., 2004; Cesca et al., 2010; Denker et al., 2011a; b). Accordingly, a novel role has been proposed for the large reserve pool of vesicles: it binds to proteins involved in vesicle recycling, acting as a buffer to keep them concentrated at the synaptic terminal. This indirect function of the reserve pool in synaptic activity would be of great importance, as transport of the recycling-involved proteins directly from the soma would delay RRP and recycling pool replenishment and increase energetic costs (Denker et al., 2011b).

### 1.2.2.2 The spontaneously released pool of vesicles

Fatt and Katz (1952) reported that resting preparations of muscle fibers would undergo spontaneous electric activity (Del Castillo and Katz, 1954). Later on, application of **tetrodotoxin (TTX)**, an inhibitor of voltage-gated Na<sup>+</sup> channels, also revealed that synaptic vesicles can be released spontaneously at a low rate, even in the absence of action potentials (Katz and Miledi, 1969). Since then, researchers have tried to establish the relation between spontaneously-released vesicles and those being released during electrical activity. Up to now, no definite conclusion has been reached (Figure 1.1).

Some studies have suggested that spontaneous activity relies on the same vesicles than stimulation-driven activity does. Therefore, the only difference between them is the release probability, which is increased at higher  $\text{Ca}^{2+}$  concentrations following AP arrival (Groemer and Klingauf, 2007; Hua et al., 2010; Wilhelm et al., 2010; Loy et al., 2014). Another line of evidence claims that spontaneously and actively-recycling vesicles actually belong to different pools that diverge not only in their release (Sara et al., 2005; Mathew et al., 2008; Fredj and Burrone, 2009; Chung et al., 2010) but also in their retrieval mechanisms (Mathew et al., 2008; Chung et al., 2010; Hua et al., 2011b). Some of these studies suggest that spontaneously released vesicles are mobilized from the reserve pool. Furthermore, spontaneously recycling vesicles have been suggested to preferentially contain molecular markers such as the endosomal SNARE proteins VAMP7 or Vti1a (Hua et al., 2011b; Ramirez et al., 2012). Spontaneous synaptic transmission keeps drawing researchers' attention, as it is believed to play an important role in the formation, maintenance and stabilization of synaptic contacts between the pre- and the post-synaptic terminals (McKinney et al., 1999; Verhage et al., 2000). Accordingly, spontaneous release seems to participate in the regulation of protein synthesis at postsynaptic dendrites (Sutton et al., 2007). Furthermore, spontaneous release can be regulated by reelin, a protein important in neocortex layering during development (Bal et al., 2013).

### 1.2.2.3 The readily retrievable or surface pool of vesicles

A mutant version of the fluorescent protein GFP was developed to sense changes in pH levels. The fluorescence of this protein, called **pHluorin**, is reversibly quenched at slightly acidic pH, with an increase in its quantum yield towards neutral pH. pHluorin can be fused to the luminal domain of synaptic vesicle proteins to study synaptic vesicle exo- and endocytosis (Figure 1.2). Its fusion with VAMP2 led to the name synaptopHluorin (Sankaranarayanan et al., 2000). It has been found that in neurons overexpressing pHluorin in tandem to different synaptic vesicle proteins, a fraction of the chimeric product remains stranded on the plasma membrane at all times. From these observations it was proposed that a readily retrievable pool of synaptic vesicle proteins sits at the membrane, probably already presorted and assembled within a clathrin coat, to be immediately endocytosed after stimulation-dependent exocytosis (Figure 1.1). This mechanism would speed up synaptic vesicle recycling while clathrin coats are still forming on the patches of recently exocytosed membrane (Gandhi and Stevens, 2003; Fernández-Alfonso et al., 2006; Wienisch and Klingauf, 2006; Hua et al., 2011a). The fraction of molecules remaining on the plasma

membrane has been calculated for different proteins using fluorescence imaging of pHluorin chimeras: ~2% for VGLUT1 (Balaji and Ryan, 2007), ~8% for synaptophysin (Granseth et al., 2006), ~10-24% for synaptobrevin (Sankaranarayanan and Ryan, 2000; Granseth et al., 2006) and ~22% for synaptotagmin (Fernández-Alfonso et al., 2006). Additionally, a study using antibodies against the intraluminal domain of synaptotagmin gave an estimation of 19% (Opazo et al., 2010). However, the variability in these percentages raises questions on how the different molecules could be retrieved in the same stoichiometry of a release-competent synaptic vesicle.

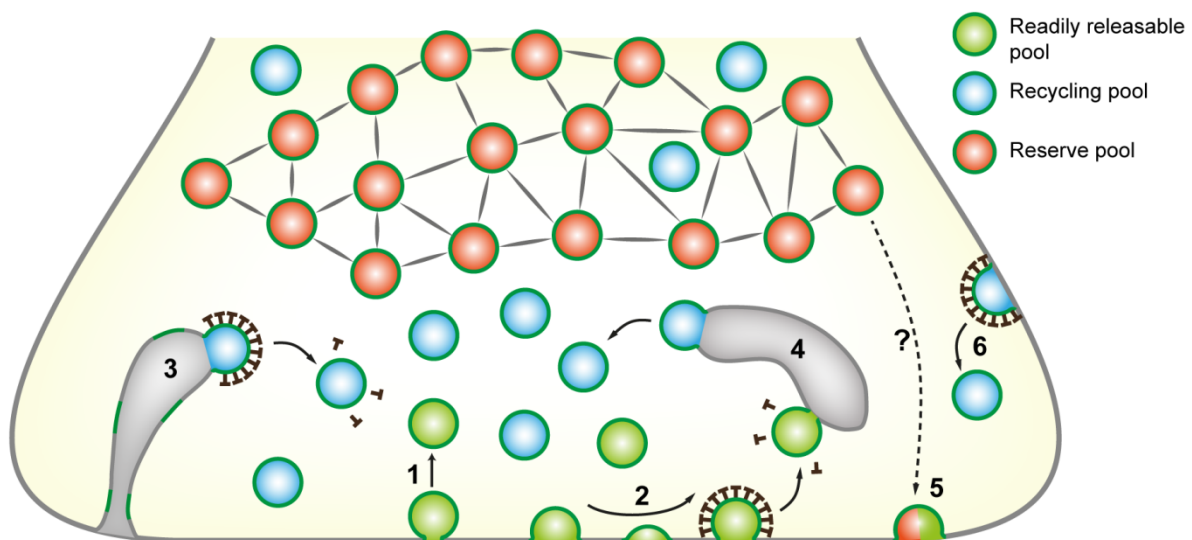


**Figure 1.1 Synaptic vesicle pools and mechanisms of synaptic vesicle recycling.**

Synaptic vesicles residing in a terminal can be classified into three main pools: the **readily releasable pool** (RRP) includes vesicles docked at the active zone, ready to undergo exocytosis at stimulus onset (green). The **recycling pool** is made of vesicles that replenish the RRP when this is exhausted and is constantly supplied by vesicle endocytosis (blue). The **reserve pool** consist of vesicles tethered to the actin cytoskeleton, reluctant to exocytose under physiological stimulation, and thought to concentrate proteins important for vesicle recycling at the terminal (orange). Upon exocytosis, synaptic vesicles can be recycled from the plasma membrane by different mechanisms: **1) Kiss-and-run**, in which vesicles avoid complete fusion with the plasma membrane by forming a transient pore that is rapidly closed after neurotransmitter release. In the case of complete vesicle-membrane fusion, **2) clathrin-mediated endocytosis (CME)** helps to selectively collect synaptic vesicle proteins from the membrane and retrieve them into a reformed synaptic vesicle by means of a proteic coat. Strong, unphysiological stimulation leads to intense exocytosis, which is compensated for by the formation of large membrane infolding, known as **3) bulk endocytosis**. Synaptic vesicles can be reformed from those infoldings with the help of clathrin. Not all recycled vesicles go directly to the recycling pool of vesicles, some (particularly from the RRP) are “cleaned” from plasma membrane proteins in a **4) sorting endosome**. Alternative pools of vesicles have been also described: a **5) spontaneously released pool**, which undergo exocytosis in the absence of APs. It is not clear if these vesicles are the same that undergo active release or are rather recruited from the reserve pool. Finally, a **6) readily retrievable pool** of vesicles has been proposed to remain stranded on the plasma membrane in a preassembled and precoated configuration, ready to undergo

endocytosis at stimulus arrival.

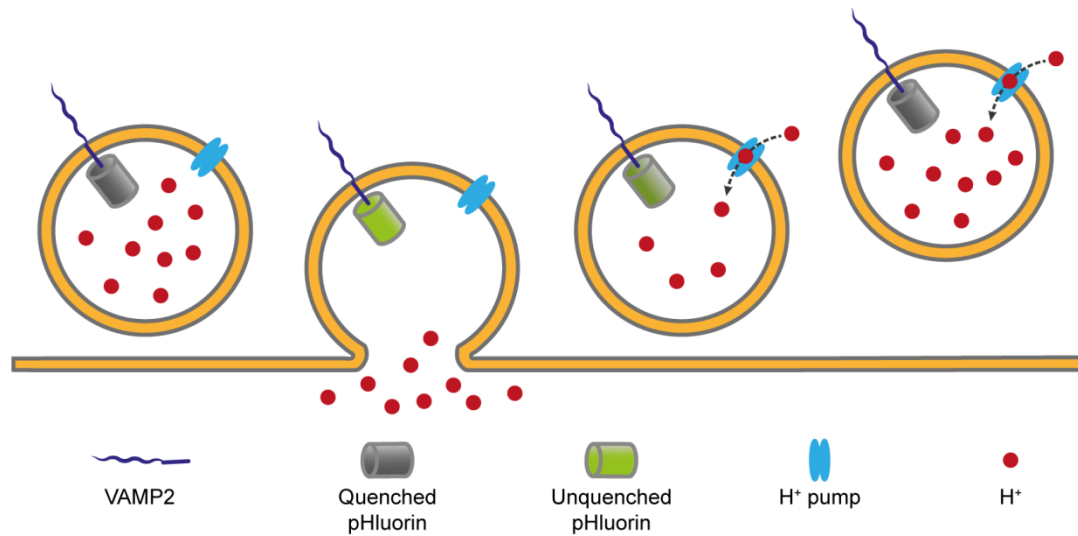


**Figure 1.2 SynaptopHluorin: a fluorescent tool for the of study synaptic vesicle recycling.**

pHluorin is a mutant version of the fluorescent protein GFP whose brightness varies according to surrounding pH levels. At the low intravesicular pH (~6.5) created by the proton pump, pHluorin is quenched and therefore undetectable in microscopy imaging. After synaptic vesicle exocytosis, pHluorin faces the neutral pH of the extracellular medium (~7.4), recovering its maximum fluorescence. The fusion of pHluorin with synaptic vesicle proteins has been called synaptopHluorin, and is used to monitor exo- and endocytosis kinetics.

### 1.2.3 Synaptic vesicle recycling

After synaptic vesicle exocytosis, compensatory endocytic mechanisms retrieve regions of membrane and their associated proteins from which synaptic vesicles are reformed. This process, called **synaptic vesicle recycling**, is important for replenishing the pool of vesicles that will undergo exocytosis upon subsequent stimulation rounds, and for keeping the surface area of the synaptic terminal constant (Südhof, 2004). Early evidence for synaptic vesicle recycling came from EM studies: stimulation strength correlates with the amount of HRP labeling taken up into synaptic terminals (Holtzman et al., 1971); the observation of  $\Omega$  (omega) shapes arising from the plasma membrane and the formation of cisterns in stimulated synapses (Heuser and Reese, 1973); and the finding that synapses exhausted by strong stimulation can resume neurotransmitter release after a recovery period (Ceccarelli et al., 1973). Since then, three main mechanism of synaptic vesicle recycling have been postulated (Figure 1.1).

#### 1.2.3.1 Kiss-and-run

This model suggests that synaptic vesicles do not undergo complete fusion with the plasma

membrane. Instead, they form a transient pore with the plasma membrane, through which neurotransmitter can exit. Thereafter, the pore closes and the synaptic vesicle can detach to be ready for a new round of neurotransmitter refilling. A variation of this model proposes that the vesicle could remain attached with the pore open for long periods, while being refilled with neurotransmitter, in what has been called “kiss-and-stay”. The pore could be walled by the fused lipid layers from both membranes, or by a protein complex similar to an ion channel (Ceccarelli et al., 1973, 1979; Fesce et al., 1994; Koenig et al., 1998; Sun et al., 2002; Aravanis et al., 2003; Gandhi and Stevens, 2003). Vesicle fission could be helped by the action of endophilin or dynamin, recruited by synaptic vesicle molecules like synaptophysin (Daly et al., 2000; Llobet et al., 2011). Although this model was postulated several decades ago, undoubtful proof of its existence has been elusive (Rizzoli and Jahn, 2007; Rizzoli, 2014). This model is attractive for the temporal and energetic benefits of not needing to reconstruct a synaptic vesicle from the membrane.

### **1.2.3.2 Clathrin mediated endocytosis (CME) of synaptic vesicles**

A wealth of studies supports the idea that synaptic vesicles completely fuse with the presynaptic membrane. After exocytosis, the vesicular membrane patch could drift away from the active zone for its retrieval by endocytosis (Miller and Heuser, 1984; Roos and Kelly, 1999). Electron micrographs showing an increase in coated pits and coated vesicles following stimulation have suggested that clathrin-mediated endocytosis (CME) is responsible for vesicle reformation (discussed in section 1.1.1.1). Further studies have confirmed that this is the main endocytosis mechanism in conventional synapses (Heuser and Reese, 1973; Zhang et al., 1998; Granseth et al., 2006), being also found in sensory synapses of retinal bipolar cells (Jockusch et al., 2005; Logiudice et al., 2009), photoreceptors (Cooper and McLaughlin, 1983; Fuchs et al., 2014) and auditory cells (Siegel and Brownell, 1986; Lenzi et al., 2002; Duncker et al., 2013; Neef et al., 2014).

The same molecules involved in CME supporting constitutive endocytic pathways have been found to play a role in synaptic vesicle recycling. Hence, synaptic vesicle reformation requires the action of the adaptor protein complex AP2 for coat formation, dynamin for vesicle fission, and amphiphysin for dynamin recruitment (Kosaka and Ikeda, 1983; Takei et al., 1995; Andrews et al., 1996; González-Gaitán and Jäckle, 1997; Shupliakov et al., 1997). But how is the clathrin machinery specifically recruited to a patch of synaptic vesicle proteins? Synaptotagmin 1 (Syt 1), the  $\text{Ca}^{2+}$  sensor triggering vesicle exocytosis, seems to be recognized as a cargo molecule by the  $\mu 2$  and  $\alpha$  subunits of the AP2 complex, leading to

coated pit nucleation. Stonin 2, a protein present in synaptic terminals, seems to facilitate the Syt1-AP2 interaction (Geppert et al., 1994b; Zhang et al., 1994; Haucke et al., 2000; Grass et al., 2004; Diril et al., 2006). In the following step of coat formation, another synapse-specific protein called AP180 has been identified. AP180 interacts with inositides and clathrin, helping in the formation of triskelia. Moreover, AP180 seems to regulate the size of the resultant synaptic vesicles, keeping in this way pool homogeneity (Zhang et al., 1998; Morgan et al., 1999).

Interestingly, it has been proposed that cycles of phosphoinositide phosphorylation/dephosphorylation may play an important role in synaptic vesicle recycling. This is supported by higher affinity of AP2 and AP180 for phosphorylated forms when anchoring to membranes, and by the presence of the inositol 5-phosphatase synaptojanin in vesicle endocytic intermediates (McPherson et al., 1994, 1996; Cremona and De Camilli, 1997).

### 1.2.3.3 Bulk endocytosis

Kiss-and-run and CME are the candidate modes of synaptic vesicle recycling happening during physiological stimulation conditions. However, in the early years of synaptic research, scientist often used unphysiological, intense stimulation protocols that revealed a third mode of membrane retrieval: after exhaustion of the RRP and recycling pool, strong stimulation mobilizes the reserve pool to also undergo exocytosis. Such rates of vesicle release outperform the endocytic machinery, creating bulging of the synaptic terminal and inducing deep membrane infoldings, known as bulk membrane retrieval (Ceccarelli et al., 1973; Heuser and Reese, 1973; Fried and Blaustein, 1978; Miller and Heuser, 1984). Dynamin I dephosphorylation by the  $\text{Ca}^{2+}$  sensor calcineurin seems to be important for bulk retrieval activation. After their formation, membrane infoldings detach from the membrane and form intracellular cisterns. During this step, syndapin and dynamin GTPase activity could be involved in membrane curvature and fission, respectively (Evans and Cousin, 2007; Andersson et al., 2008; Clayton and Cousin, 2009; Clayton et al., 2009; Nguyen et al., 2012). It is likely that infoldings and cisterns contain mixed amounts of synaptic vesicle and plasma membrane proteins, which are later on selectively segregated by clathrin coat formation and budding (Heuser and Reese, 1973; Richards et al., 2000; Teng and Wilkinson, 2000). In neuromuscular junctions, actin has been implicated in the initiation of bulk membrane retrieval, and together with dynamin in its maturation into cisternae (Nguyen et al., 2012).



Although bulk endocytosis is traditionally considered an emergency route to overcome unphysiological high rates of release, new studies have validated it in neuromuscular junctions and the large calyx of Held synapse within physiological stimulation rates (Richards et al., 2000; Wu and Wu, 2007; Clayton et al., 2008). As it will be shown in the results and discussion of this study, bulk endocytosis might have a great importance in synaptic vesicle recycling and normal function of the highly active ribbon-type sensory synapses.

#### **1.2.3.4 Endosomal sorting of recycled vesicles**

An additional step of synaptic vesicle processing has been proposed to take place intracellularly: after their retrieval and uncoating, synaptic vesicles from the RRP might rejoin the pool of vesicles waiting for next rounds of release or, alternatively, they might fuse with a sorting endosome. This compartment would fulfill the function of ridding synaptic vesicles of plasma membrane proteins that were fortuitously taken up along with the synaptic vesicle membrane patch. After sorting, regions with only synaptic vesicle proteins could bud, by a still unclear mechanism, in order to produce release-competent synaptic vesicles (Hoopmann et al., 2010).

## 1.3 Membrane trafficking at specialized sensory synapses

Sensory perception relies on the transformation of physical stimuli into electrical signals in a process called **transduction**. A sensory receptor cell encodes the strength of the stimulus into changes in its plasma membrane potential, which in turn modulate opening probability of voltage-gated  $\text{Ca}^{2+}$  channels located at active zones, triggering the release of neurotransmitter in amounts correlated with the strength of the stimulus. Hence, sensory transduction does not rely on all-or-none action potentials, but on **graded receptor potentials** that modulate constantly ongoing synaptic transmission. Sensory receptors are embedded in specialized epithelia known as the sensory organs. Within a sensory organ, the population of receptors is not homogeneous, as subgroups of them are further specialized to encode a submodality or a range of energy from the stimulus spectrum. Such receptor tuning expands the perceivable dynamic range and its levels of discrimination (Kandel et al., 2013). In the olfactory and somatosensory systems, reception is performed by neurons that directly deliver encoded sensory information to the CNS for further processing. In the auditory, vestibular, gustatory and visual systems, a cell of epithelial origin evolved the receptor and synaptic machinery required to release neurotransmitter at the synapse with neuronal postsynaptic afferents. These afferents belong to nerve fibers from the cranial nerves VII and IX for taste, or VIII for sound and balance, which directly connect to the CNS. In the visual system, postsynaptic boutons belong to a network of interneurons that bring encoded visual information to retinal ganglion neurons forming the optic nerve (Kandel et al., 2013).

### 1.3.1 The highly efficient ribbon-type sensory synapses

Some sensory modalities require sustained neurotransmitter release for long time periods, accompanied by high sensitivity for stimulus variations. To accomplish this task, vertebrates evolved a proteinaceous organelle that tethers synaptic vesicles and concentrates them at the active zone, boosting vesicle release rates. This structure has been called synaptic body or synaptic ribbon, and it can be found sitting at the active zones of pinealocytes, photoreceptors, and hair cells of the auditory and vestibular systems, of the fish lateral line, and of electroreceptors at the fish ampullae of Lorenzini (Sjöstrand, 1953; De Robertis and Franchi, 1956; Sjostrand, 1958; Smith and Sjöstrand, 1961; Sejnowski and Yodlowski, 1982; Zanazzi and Matthews, 2009). Thanks to a scaffolding protein called RIBEYE, ribbons can adopt a variety of shapes from planar to spherical. So far, RIBEYE has been only found in synaptic ribbons, being their most abundant component (Schmitz et al., 2000; Khimich et al.,

2005; Magupalli et al., 2008; LoGiudice and Matthews, 2009). Ribbons are anchored to the plasma membrane of active zones by the cytomatrix protein bassoon, and associate with cytoskeletal molecules, phosphorylation enzymes, molecular chaperones, and proteins involved in vesicle handling (Kantardzhieva et al., 2012; Jing et al., 2013).

Synaptic ribbons are important for fast, synchronous release (Matthews and Fuchs, 2010). Capacitance measurements recorded from hair cells and photoreceptors have revealed two kinetically different modes of exocytosis: a fast component, with time constant of a few milliseconds; and a slow component, which can sustain constant release rates for up to 150 milliseconds in photoreceptors, or 1-2 s in hair cells (Parsons et al., 1994; von Gersdorff and Matthews, 1994; Mennerick and Matthews, 1996; Moser and Beutner, 2000; Spassova et al., 2004). Fast transmission at these synapses is favored by the expression of L-type  $Ca_v1.3$  or  $Ca_v1.4$  calcium channels, which activate at more negative membrane potentials and have slow inactivation kinetics, and by their clustering of these channels under the ribbon (Kollmar et al., 1997; Bech-Hansen et al., 1998; Strom et al., 1998; Nachman-Clewner et al., 1999; Zenisek et al., 2003; Sidi et al., 2004; Brandt et al., 2005).

Electron microscopy and capacitance measurements of ribbon-containing synapses, have led to a reinterpretation of the synaptic vesicle pool concept. Three pools have been morphologically identified and associated with the two modes of exocytosis (Paillart et al., 2003; Khimich et al., 2005; Nouvian et al., 2006; LoGiudice and Matthews, 2009):

- 1) The pool of vesicles tethered to the base of the ribbon and docked to the plasma membrane. This pool has been interpreted as the RRP, since the membrane area provided by these vesicles correlates with capacitance changes during the initial fast round of exocytosis. This pool could be complemented by docked vesicles sitting on the plasma membrane, but not tethered to the ribbon.
- 2) The remaining pool of ribbon-associated vesicles. Once the RRP is depleted, this pool could repopulate docking positions, explaining the slow phase of exocytosis. However, it is not clear if these vesicles slide down the ribbon to reach the plasma membrane, or they could fuse before release in what is called compound exocytosis. These two options for ribbon function are known as the conveyor belt and the safety belt hypothesis, respectively (Parsons and Sterling, 2003). It is also uncertain whether some of the vesicles in this pool could move down fast enough to participate in fast exocytosis.
- 3) Free cytosolic vesicles that upon prolonged exocytosis refill the ribbon, being

considered as a reserve pool. These vesicles move freely in the cytoplasm as synapsin, the protein that tethers reserve pool vesicles to the actin cytoskeleton in conventional synapses, is not present (Favre et al., 1986; Mandell et al., 1990; Holt et al., 2004). It is not clear if these highly mobile vesicles simply collide with the ribbon, or are rather delivered to it by a controlled mechanism.

### 1.3.2 Ribbon synapses in the auditory system

#### 1.3.2.1 The hearing process

In mammals, sound stimuli first reach the animal through the outer ear. This is composed of a funnel-shaped structure called the pinna, which collects the air vibrations, and an ear canal that conveys them to the middle ear. At this point, the tympanic membrane converts air vibrations into mechanical movements that are received and amplified by a complex of three ossicles aligned one after the other, the malleus, incus and stapes. The latter transfers the fine movements to a membrane-covered opening called the oval window. This is the entrance to the auditory part of the inner ear, a snail-shaped bony cavity also known as the cochlea. Inside the cochlea three cavities separated by membranes run along in a spiral. The upper cavity is called the *scala vestibuli*, the lower one *scala tympani*, and the middle one *scala media*. The *scala vestibuli* and *scala tympani* are filled with a solution called *perilymph*, containing 140 mM Na<sup>+</sup> and 4-6 mM K<sup>+</sup> (Wangemann, 2006). Mechanical deflections in the membrane of the oval window are transferred to the fluid *perilymph*, inducing vibrations of the **basilar membrane**, a pseudo-resonant structure that separates the *scala media* and *tympani*. Changes in stiffness and width allow the basilar membrane to preferentially vibrate with high-frequency sounds at the cochlea base, and with low frequency sounds at the cochlea apex, with a gradient of vibration between these two points. This topographic representation of tone frequency is called tonotopy (Rubel, 1984; Bear et al., 2006).

Sitting on the basilar membrane from base to apex and facing the inner space of the *scala media* is the **organ of Corti** (Figure 1.3). This is an epithelial structure that during development gives rise to two types of polarized presynaptic cells (Fekete, 1996). The inner hair cells (**IHCs**), responsible for transduction of sound-elicited waves of the basilar membrane into an electric signal; and the outer hair cells (**OHCs**), an electromotile cell type that is controlled by efferents from the superior olivary complex in the brainstem, and whose contractions increase basilar membrane vibration to further amplify low-intensity sound stimuli (Cooper and Guinan, 2006). The organ of Corti is composed of one row of IHCs

and three rows of OHCs separated by the tunnel of Corti, which is lined up by the slender pillar cells. Additionally, IHCs and OHCs are surrounded by supporting cells (Bear et al., 2006). The organ of Corti is bathed by *endolymph*, a solution filling the scala media, rich in  $K^+$  (157 mM) and low in  $Na^+$  (1.3 mM) (Wangemann, 2006).

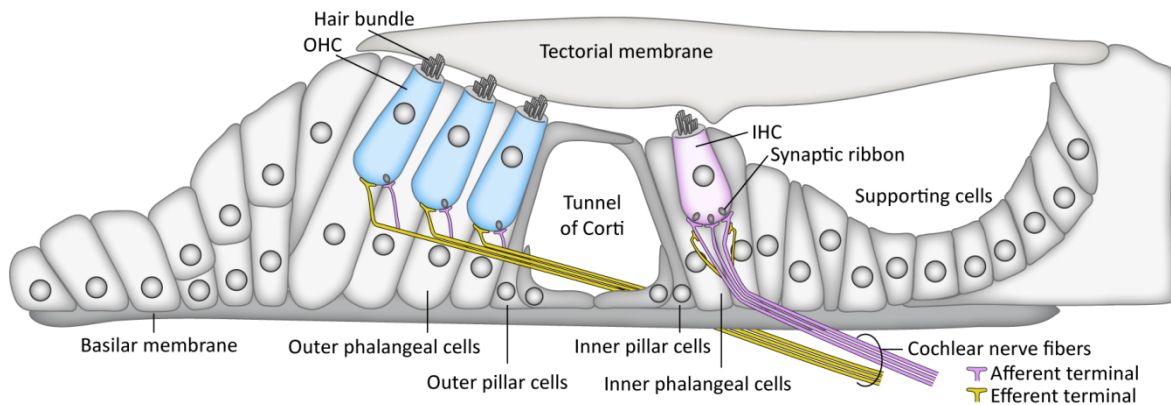


**Figure 1.3 Structure of the organ of Corti.**

The organ of Corti is a specialized sensory epithelium sitting on the basilar membrane of the cochlea. It contains two types of hair cells: the inner hair cells (IHCs, purple), which are responsible for sound encoding and make synapses with afferents of the spiral ganglion neurons. The outer hair cells (OHCs, blue), which use electromotile activity for signal amplification and are controlled by the brainstem through efferent innervation. One row of IHCs and three rows of OHCs run along the organ of Corti. Supporting cells provide the stability and flexibility required for proper hearing function (e.g. pillar and phalangeal cells). The sensory transduction process starts at the apical stereocilia bundle of IHCs, which is deflected against the tectorial membrane at every vibration of the basilar membrane. This leads to cationic influx currents, cell depolarization and synaptic vesicle release at the active zones, located at the IHC base. Fast and synchronous exocytosis of synaptic vesicles is facilitated by synaptic ribbons sitting on the active zones.

Besides the cochlea, the inner ear is also composed by the vestibular labyrinth, divided in the otolith organs (sacule and utricle) for gravity detection, and the semicircular canals, to sense head rotation. These structures are made of bony chambers and tubes carpeted with a sensory epithelium containing hair cells for stimuli transduction, similar to the cochlear IHCs and OHCs (Bear et al., 2006).

Hair cells of the auditory and vestibular systems are similar in anatomy and function to those at the fish lateral line. A particular anatomical feature of all hair cells is the absence of a synaptic terminal, meaning that synaptic active zones are directly located at the cell soma (**somatic active zones**). As a result, synaptic vesicles intermix in the cytoplasmic volume with other organelles involved in constitutive membrane trafficking. With a polarized morphology, hair cells develop at their apical pole the **hair bundle**, a collection of actin-filled stereocilia organized in several rows of increasing heights (Furness and

Hackney, 2001). Right below the apical membrane, a dense mesh of actin filaments, called **cuticular plate**, anchors the rootlets of each stereocilia actin core providing them with support (DeRosier and Tilney, 1989). Stereocilia from adjacent rows are connected by filamentous structures named 'tip links' (Corey, 2009). In the organ of Corti, IHCs and OHCs stereocilia are in close contact with an acellular gel-like structure composed of collagen and glycoproteins called the **tectorial membrane** (Goodyear and Richardson, 2002).

### 1.3.2.2 The transduction process at IHCs

The arrival of a sound stimulus induces vibration of the basilar membrane, which is further amplified by force generated by the OHCs. This vibration leads to movements of the fluid surrounding the IHC's hair bundle, resulting in bundle deflection in the direction of the tallest stereocilia (Fridberger et al., 2006). The whole bundle moves as a unit thanks to the tip links. Deflection opens **mechanoelectric transduction (MET) channels** located at the tip of each stereocilia, helped also by the force imposed by the tip links (Beurg et al., 2009). An inward current of  $K^+$  (and in less extent  $Ca^{2+}$ ) enters the MET channels causing membrane depolarization and concomitant activation of voltage-gated calcium channels at the basal pole of the IHCs, where synaptic ribbons are located, triggering the release of **glutamate-filled synaptic vesicles** (Moser et al., 2006).

Each hair cell can form 10 – 30 synapses with afferents from spiral ganglion neurons of the auditory nerve. Each afferent receives information from one active zone, normally occupied by one ribbon (Fuchs et al., 2003). Hair cells can release synaptic vesicles at rates several orders of magnitude higher than conventional synapses for long time periods, earning the name of indefatigable (Griesinger et al., 2005). At sustained depolarization, estimations in frog saccular hair cells report the release of around ~10,000 vesicles/second per cell (~500 vesicles/second per ribbon), and in mouse 28,000 vesicles/second per IHC (Parsons et al., 1994; Moser and Beutner, 2000). Such high rates of synaptic activity likely rely on synaptic ribbon function and tight coupling of synaptic vesicle release with  $Ca^{2+}$  influx at the active zone (Fuchs et al., 2003; Goutman and Glowatzki, 2007).

The molecules involved in synaptic vesicle exocytosis in IHC ribbon synapses are not clear. In mouse IHCs, it was found that immature cells express the calcium sensors synaptotagmin 1 (Syt 1), Syt 2 and Syt 7 to drive spontaneous  $Ca^{2+}$ -dependent vesicle release. With the increase in vesicle release during maturation (around postnatal day 4), they are replaced by a  $Ca^{2+}$ -binding protein called **otoferlin**, which drives receptor

potential- and  $\text{Ca}^{2+}$ -dependent vesicle release. After hearing onset (postnatal days 10-14) synaptotagmins expression stops (Safieddine and Wenthold, 1999; Beurg et al., 2010). Otoferlin is defective in a type of recessive deafness, DFNB9 (Varga et al., 2003). Moreover, knockout mice are profoundly deaf due to drastic reduction of exocytosis (Roux et al., 2006; Reisinger et al., 2011). Otoferlin has six  $\text{C}_2$  calcium-binding domains, five of which have been confirmed to bind  $\text{Ca}^{2+}$  and phospholipids (Goodyear et al., 2010; Johnson and Chapman, 2010). This line of evidence has led to establish that otoferlin is the exclusive calcium sensor triggering synaptic vesicle exocytosis in mature IHCs (Roux et al., 2006; Pangršič et al., 2012). Additionally, otoferlin also seems to play a role in replenishment of the RRP of vesicles, and could therefore be responsible for the fast replenishment rates seen in IHC, which are superior to other ribbons synapses (Pangršič et al., 2010).

Surprisingly, although *in vitro* experiments show otoferlin binding to the neuronal t-SNARE proteins syntaxin 1 and SNAP-25 (Roux et al., 2006; Ramakrishnan et al., 2009), these proteins are not present in hair cells (Nouvian et al., 2011). Furthermore, other proteins important for synaptic function in neuronal synapses are also absent in IHCs, including synaptobrevin 1 (VAMP1), synaptobrevin 2 (VAMP2), synaptophysin, complexins and synapsin (Favre et al., 1986; Safieddine and Wenthold, 1999; Strenzke et al., 2009; Uthaiiah and Hudspeth, 2010; Nouvian et al., 2011). Given the epithelial origin of IHCs, it is possible that they express other SNARE proteins not yet identified, which would interact with otoferlin during vesicle exocytosis. Importantly, IHCs rely on the **vesicular glutamate receptor 3 (VGLUT3)** for vesicle neurotransmitter refilling (Ruel et al., 2008; Seal et al., 2008), in comparison to VGLUT1 and VGLUT2 used in conventional glutamatergic synapses (Bellocchio et al., 2000; Fremeau et al., 2001).

### 1.3.2.3 Mechanisms of synaptic vesicle recycling in hair cells

A major difficulty in interpreting synaptic vesicle recycling in hair cells is, as explained above, the lack of a synaptic bouton. The development of somatic active zones implies that synaptic vesicles distribute in the entire cytoplasm and intermix with other organelles involved in secretory and constitutive membrane trafficking pathways, including the endoplasmic reticulum (ER), the Golgi apparatus, endosomes of different types, and secretory, transport and endocytic vesicles. Hence, fluid phase tracers or membrane markers will indistinctly label organelles involved in synaptic vesicle recycling and in constitutive endocytosis (e.g. receptor retrieval). To date, two opposing models of synaptic vesicle recycling have been suggested for hair cells: the first one, based on electron

microscopy and membrane capacitance studies, suggests that membranes supplying synaptic vesicle reformation are retrieved at the cell base, in the local area of the active zone (Figure 1.4A); the second model, based on fluorescence microscopy studies, suggests that apical retrieval is the main membrane source for vesicle reformation (Figure 1.4B). Evidence supporting both models is presented below.

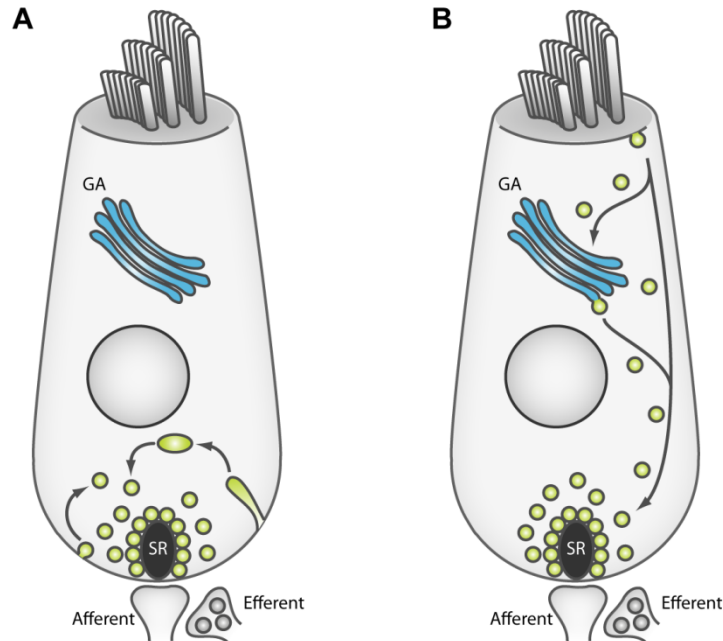


**Figure 1.4 Models of synaptic vesicle recycling in hair cells.**

**A.** The local recycling model proposes that synaptic vesicles are recycled at the cell base, in the vicinity of the ribbon-type active zones. It involves single unit retrieval and the formation of membrane infoldings and cisterns from which vesicles can be recycled. **B.** The apical recycling model suggests that in hair cells membranes are mainly retrieved at the apical pole. Endocytosed organelles are then delivered to the Golgi apparatus (GA), where synaptic vesicles are reformed as precursors for their later delivery to synaptic ribbons (SR).

### Local recycling model

Already in the 80's, Siegel and Brownell (1986) studied membrane recycling in IHCs of chinchillas. Horseradish peroxidase (HRP) was injected in the cochlea of anesthetized animals, in order to trace endocytic events. HRP uptake was revealed by diaminobenzidine (DAB) precipitation, visible in electron microscopy. Labeled organelles were found throughout the IHC cytoplasm. Interestingly, different types of labeled organelles were found in the vicinity of synaptic ribbons: coated and uncoated vesicles and short tubules, also with coated domains. Some of the uncoated vesicles were tethered to the ribbon. In the synaptic area they also found invaginations of the plasma membrane topped with coated pits, from which vesicles seemed to be formed. Coated pits were also seen at the plasma



membrane. These results suggested that mechanisms of membrane recycling take place at the cell base close to synaptic active zones, and that they not only involve vesicle retrieval through CME, but also tubules and membrane infoldings resembling the bulk endocytosis of conventional synapses, from which vesicles could be reformed (Figure 1.4A).

A local model of synaptic vesicle recycling became more evident with studies by Lenzi and collaborators (1999, 2002), making electron tomograms of active zones from frog saccular hair cells. After depolarization with high  $K^+$  (30 to 45 mM, 15 to 30 minutes) they found a striking membrane remodeling process, in which the membrane area equivalent to synaptic vesicles exocytosed during stimulation was now contained in membrane infoldings, and cisterns surrounding the synaptic ribbon. Additionally, they found coated and uncoated vesicles and coated pits on the plasma membrane and on the infoldings. Expecting that infoldings and cisterns give rise to reformed synaptic vesicles, they suggested that this local recycling is responsible for ribbon reloading and a three- to 14-fold increase in vesicle abundance near the active zone. Similar cisterns decorated with several coats were also seen by Neef and collaborators (2014) at active zones of stimulated IHCs.

Capacitance measurements of IHCs combined with application of inhibitory molecules for the endocytic proteins clathrin and dynamin, have associated two kinetically different modes of endocytosis to the organelles described above (Moser and Beutner, 2000; Beutner et al., 2001; Cho et al., 2011; Neef et al., 2014):

- A slow mode, with linear kinetics of capacitance decline. This mode is clathrin- and dynamin-dependent, and probably corresponds to single vesicle retrieval directly from the plasma membrane by CME. It is present after short and long depolarizations.
- A mode with exponential capacitance decay and time constant  $\sim 6$  s. This mode was found to be clathrin- and dynamin-independent. It appears only after release of a number of vesicles equivalent to 3-4 times the RRP. It probably corresponds to bulk membrane retrieval (infoldings).

A third fast mode, with time constant of  $\sim 250$ - $300$  ms and only active at cytosolic  $[Ca^{2+}]$  above  $15 \mu M$  has been also described. By its speed, it was carefully interpreted as kiss-and-run vesicle retrieval, and therefore its morphological correlate is not known.

### **Apical recycling model**

FM dyes are a family of styryl molecules that increase their fluorescence by 100-fold once they partition into membranes. They have been commonly used to track endocytosis in conventional neuronal synapses (Betz et al., 1992; Cochilla et al., 1999; Hoopmann et al., 2012; Kavalali and Jorgensen, 2014). When FM 1-43, the most commonly used FM dye, was applied only to the apical region of OHCs and IHCs it labeled the hair bundles strongly. Within a few seconds labeling appeared in intracellular organelles with tubulo-cisternal morphology located under the cuticular plate (“apical aggregate”), and within 180 seconds, it was also seen in organelles located in the basolateral volume and in organelles located at the cell base, where active zones should be located (“basal aggregate”). All these structures were strongly labeled, and fluorescence accumulated progressively over time (Meyer et al., 2001; Griesinger et al., 2002, 2004, 2005). From these observations Griesinger and collaborators (2002, 2004, 2005) proposed an apical mode of endocytosis supplying synaptic vesicle recycling (Figure 1.4B): first, membrane is taken up from areas surrounding the cuticular plate in a very fast mode of endocytosis (within seconds), likely clathrin-independent. These endocytosed organelles would be equivalent to apical early endosomes described in other types of epithelial cells. Then, early endosomes are delivered to subcuticular organelles like the Golgi apparatus, from which synaptic vesicles are reformed as precursors and delivered to the synaptic ribbons for subsequent rounds of exocytosis.

### **FM dyes permeate MET channels of hair cells**

The apical model has been challenged by a series of studies suggesting that FM 1-43 molecules and similar small FM dyes are small enough to penetrate the MET channels located at the tips of stereocilia (Farris et al., 2004). Electrophysiological studies in cochlear hair cells have found that FM 1-43 is a permeant blocker of the MET channel inward current, probably competing with  $\text{Ca}^{2+}$  for binding sites at the core of the pore. Accordingly, application of high  $\text{Ca}^{2+}$  concentrations or pretreatment with EGTA, known to disrupt the tip links and therefore the gating of the channel, resulted in reduction of FM 1-43 labeling (Gale et al., 2001). Similarly, application of MET channel blockers (e.g. neomycin, gentamicin, streptomycin and amiloride) to hair cells of the fish lateral line also reduced FM 1-43 fluorescence inside (Nishikawa and Sasaki, 1996). Further evidence came from incubation of FM 1-43 upon endocytosis inhibition by low temperature, where labeling was strong and comparable to the RT condition. Finally, FM 1-43 was compared to the larger FM 3-25, both with two hydrophobic tails of 4 and 18 carbons respectively. While FM 1-43 labeled the intracellular compartment within a few minutes, FM 3-25 was seen inside the cell only after

60 minutes, indicating that its large size hinders its MET channel permeation (Meyers et al., 2003). Overall, these studies conclude that intense and fast FM dye uptake by hair cells does not correspond to endocytic processes, but rather to artifactual labeling from molecules permeating the MET channels. Such strong labeling masks the signal coming from truly endocytosed molecules.

### **Towards novel approaches to clarify IHC membrane trafficking pathways**

After the studies described above established that FM 1-43 is not suitable for studying membrane recycling in IHCs, no other study attempted to use endocytosis tracers in hair cell preparations. Hence, it remained unclear which of the models, apical or basal, is the one taking place in physiological conditions.

In order to answer this question, an alternative approach to circumvent FM 1-43 channel permeation was applied by our laboratory using dye photo-oxidation (Kamin et al., 2014). In this method cells are allowed to endocytose a fluorescent molecule and are immediately fixed. By continuous illumination at the corresponding excitation wavelength, fluorophores are induced to produce reactive oxygen species (ROS) that can oxidize a substrate molecule like DAB. Upon oxidation, DAB forms electron-dense precipitates only in endocytic compartments where the fluorophore was concentrated (Henkel et al., 1996). When this technique was applied to IHCs incubated with FM 1-43, molecules that entered the cytoplasm via MET channel permeation gave only a faint precipitate. In contrast, molecules in endocytic organelles produced a dark precipitate. This allowed the selective quantification of endocytosis levels at the apical, nuclear and basal levels of resting (0 mM  $\text{Ca}^{2+}$ , 5 mM  $\text{K}^+$ , 1 min) and stimulated (2 mM  $\text{Ca}^{2+}$ , 65 mM  $\text{K}^+$ , 1 min) IHCs. It was found that although endocytosis was abundant throughout the IHC, high  $\text{K}^+$  stimulation only increased endocytosis levels at the cell base, while they remained constant at the apical and nuclear regions. Tubular structures dominated the top and nuclear regions and endosome- and vesicle-like structures dominated the cell base. Interestingly, after a 5-minute or 30-minute recovery period following stimulation, most of the tubules and endosome-like structures were processes into smaller vesicles. However, vesicles located at the top and nuclear regions were significantly larger than those at the cell base. The latter were statistically equal in size to *bona fide* synaptic vesicles located at surrounding efferents. These results suggested that synaptic vesicle recycling indeed happens at the cell base, supporting the local recycling model, and that constitutive recycling is likely happening at the top and nuclear regions of IHCs (Figure 1.5) (Kamin et al., 2014).

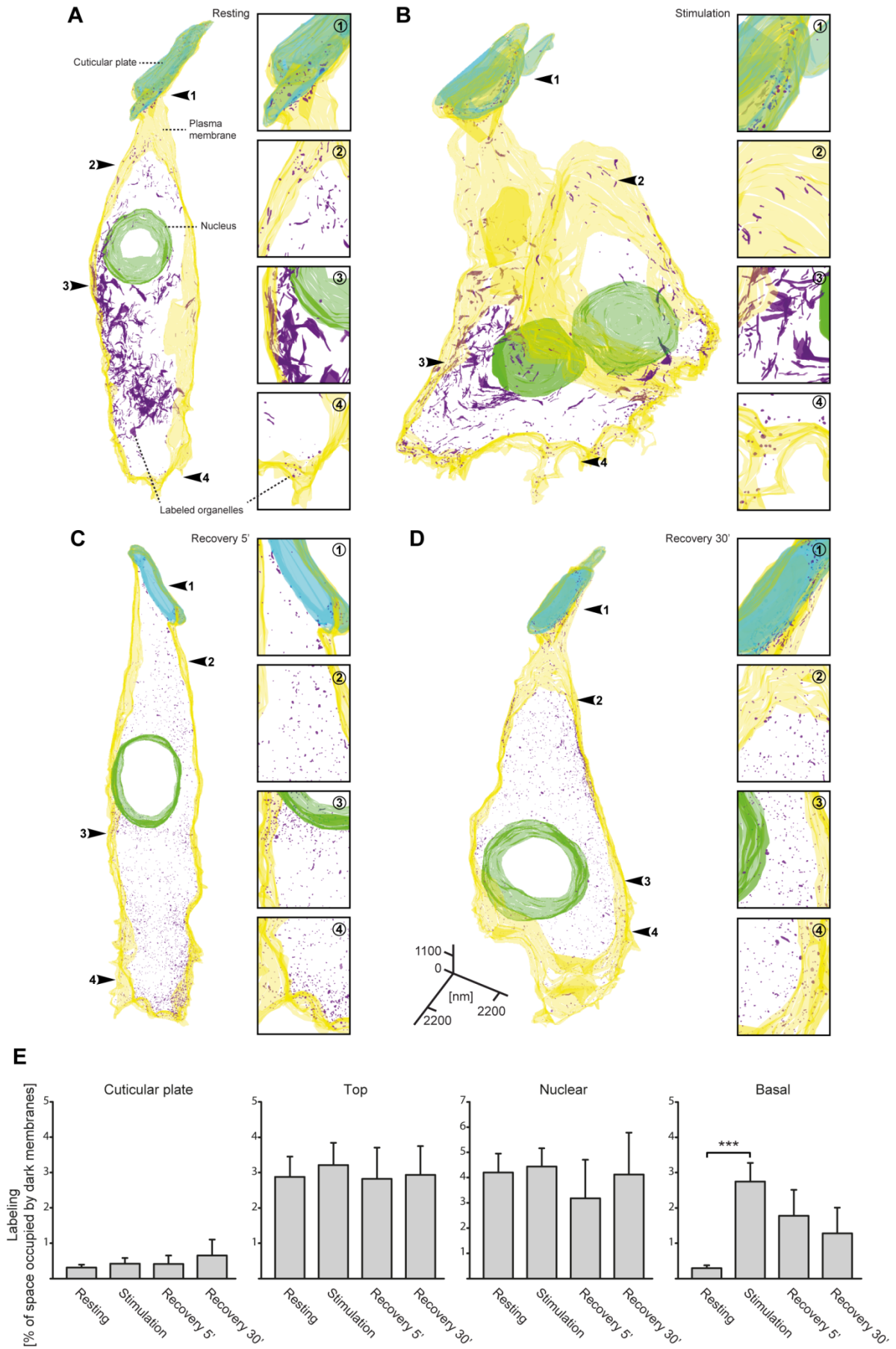


**Figure 1.5 FM 1-43 photo-oxidation supports the local model of synaptic vesicle recycling taking place at the IHC basal level.**

After FM 1-43 labeling and fixation, IHCs were incubated with DAB under constant illumination. This process, called photo-oxidation, created an electron-dense DAB precipitate only in organelles containing endocytosed dye molecules. In contrast, molecules permeating MET channels produced only a faint signal. Electron micrographs of treated cells were used to draw the perimeter of labeled endocytic organelles and render 3D reconstructions of **A.** resting cells, **B.** stimulated cells, and cells recovered after stimulation for **C.** 5 minutes or **D.** 30 minutes. Large tubulo-cisternal structures were found at the top and nuclear levels of resting and stimulated IHCs. The basal level was dominated in both cases by smaller endosome- and vesicle-like structures. After 5 minutes of recovery large labeled organelles were processed into smaller vesicles, still present after 30 minutes. Vesicles at top and nuclear levels were significantly larger than those at the cell base, more similar to *bona fide* synaptic vesicles (not shown) **E.** Quantification of intracellular area percentage occupied by labeled organelles revealed that high  $K^+$  stimulation triggered increases in endocytosis levels only at the cell basal level. These results suggest that local endocytosis and trafficking at the cell base is the synaptic vesicle recycling mechanism used by IHCs (Modified from (Kamin et al., 2014)).

## 1.4 High-resolution STED microscopy for the study of membrane trafficking pathways

Although our study (Kamin et al., 2014) represents a step forward towards the understanding of IHC physiology, further investigations would require the association of recycling organelles with synaptic vesicle markers in a high-resolution microscopy technique. That is the main aim of the project described in this thesis. Transmission electron microscopy (TEM) is the technique that has reached the highest resolution so far (<2 nm in biological samples) (Faas et al., 2012). However, immunolabeling techniques suitable for EM microscopy require laborious procedures that at the end offer poor epitope recognition and low labeling density. Therefore, a fluorescence microscopy technique would be more convenient for the easy sample preparation and high imaging throughput.

A major drawback of light-based microscopy techniques is the diffraction of light when passing through the lenses of a microscope. The German physicist Ernst Abbe postulated (1873) that a beam of light with a wavelength  $\lambda$ , converging to a lens of refractive index  $n$  and aperture angle  $\theta$ , will produce a focal spot with a full width at half maximum (FWHM) given by the formula  $\Delta r = \lambda/2(n\sin\theta)$ , where  $n\sin\theta$  is equivalent to what is nowadays known as the objective numerical aperture (NA) (Hell, 2007). This means that two point sources of light imaged with a conventional fluorescence microscope cannot be told apart if they are closer than approximately 200 to 300 nm, for emission wavelengths in the range of the visual spectrum. In the case of synaptic vesicles and trafficking organelles, typically in the size range of 30 nm to a few hundreds of nm, and densely packed in the cytoplasmic volume,

this is an important difficulty.

In 1994 Stefan Hell and Jan Wichman postulated the principles of what would become the first far-field microscopy technique overcoming Abbe's diffraction barrier: stimulated emission depletion (STED) microscopy (Figure 1.6) (Hell and Wichmann, 1994). Six years later, the first practical demonstration was published, imaging the plasma membrane of *Saccharomyces cerevisiae* and *Escherichia coli* cells (Klar et al., 2000). STED microscopy is based on sample laser scanning, as done in confocal microscopy. However, in this technique an excitation laser is spatially overlapped with a second depletion laser. The front wave of the latter is physically modified with a vortex plate so as to generate a toroid or doughnut shape with zero intensity in the center and maximum intensity at the borders. The wavelength of the depletion laser is chosen to match the red-side tail of the fluorophore's emission spectrum. In the doughnut center, where only the excitation laser is present, fluorophores are allowed to emit photons spontaneously. In contrast, in the outer area where both lasers are present, fluorophores will reach the excited state but the depletion beam will induce them to emit photons at its same red-shifted wavelength. These photons (stimulated emission) can be filtered out to only detect those produced at the doughnut center, resulting in a narrower diffraction-unlimited point spread function (PSF) (Klar et al., 2000; Hell et al., 2004). Abbe's equation is therefore redefined as  $\Delta r \approx \lambda / (2NA\sqrt{1 + I/I_s})$ , where  $I$  is the maximum intensity of the depletion (STED) beam, and  $I_s$  corresponds to the saturation intensity required to reduce fluorescence probability by half. Thereby, higher depletion laser intensities will render narrower imaged areas, increasing the resolution of the microscope (Nägerl et al., 2008; Moneron et al., 2010).

In the past, STED microscopy has fostered important findings related to constitutive trafficking pathways and synaptic function: it was useful to establish the molecular players and steps required for cargo sorting and budding in early endosomes (Barysch, 2009). It validated the role of endosomal sorting in the segregation of plasma membrane proteins from recycled synaptic vesicles (Hoopmann et al., 2010). It revealed that only 40-50% of the SNARE proteins Syntaxin 1 and SNAP-25 are located at putative vesicle release sites, while the rest dispersed on the plasma membrane (Punge et al., 2008). It also helped to establish that synaptotagmin 1 remains clustered on the plasma membrane upon synaptic vesicle exocytosis (Willig et al., 2006). Among other studies, it also helped to put forward a novel hypothesis: the majority of synaptic vesicles found in the synaptic terminal (>80%) do not participate in neurotransmitter release, but rather act as a buffer for proteins involved in

vesicle recycling, keeping them concentrated for their eventual use (Denker et al., 2011b).

Using a commercial STED microscopy setup, like the one I used in this study, resolution can go down to 30-40 nm in biological preparations. The relatively short image acquisition time and the instant delivery of diffraction-unlimited images, without the need for further signal computation, are the main advantages of STED microscopy over other high-resolution microscopy techniques.

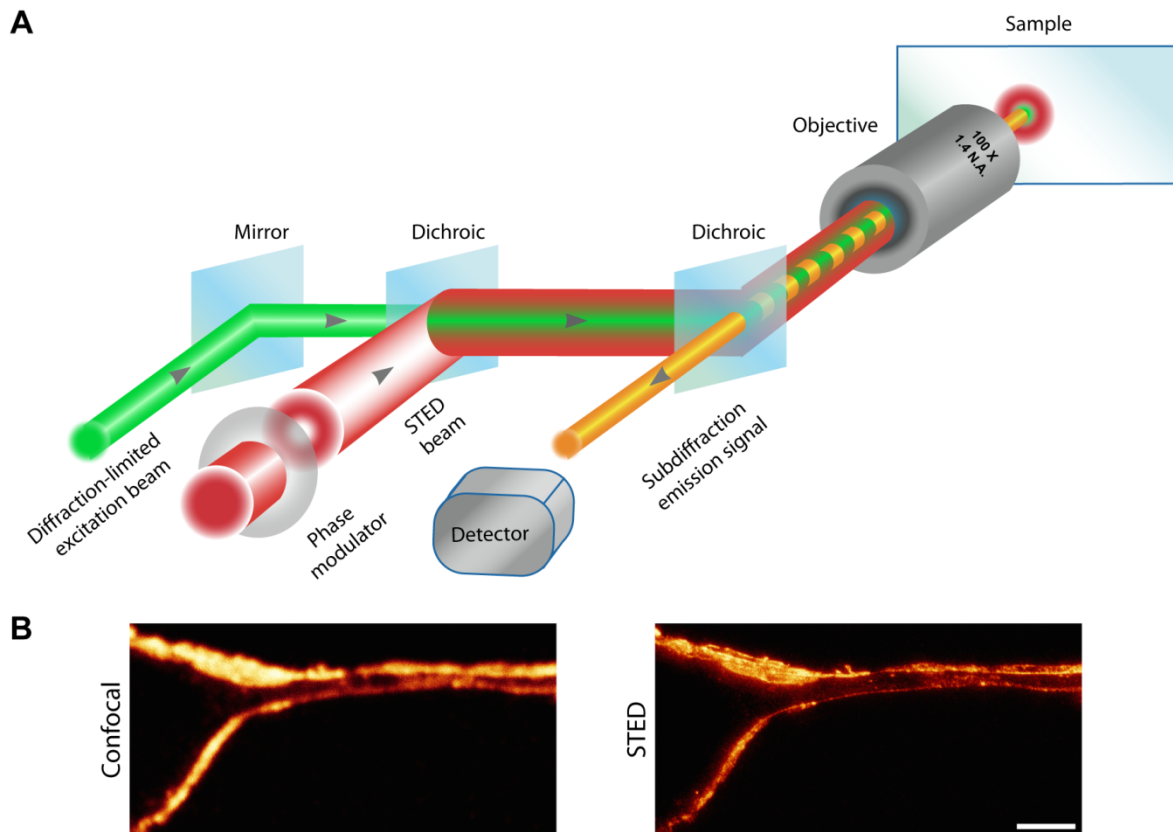


**Figure 1.6 Working principle of high-resolution STED microscopy.**

**A.** Schematic representation of the basic elements in a STED microscope. An excitation beam (green) is spatially overlapped with a depletion beam (red) and scanned over the sample as in conventional confocal microscopy. The depletion beam is modified by a phase modulator to create a zero intensity region in its center, resulting in a toroid or doughnut-shaped front wave. Furthermore, the wavelength of the depletion beam is selected to fall in the red side tail of the fluorophore's emission spectrum. In the sample, the fluorophores located at the center of the depletion doughnut are excited and allowed to emit photons spontaneously (yellow), which are collected by the detection device. In contrast, the excited fluorophores at the borders of the depletion doughnut are stimulated to emit photons in the red-shifted wavelength of the depletion beam, which is filtered out of the detection range. Hence, photons are only collected from a smaller subdiffraction-sized area. **B.** Example images of a neuronal soma and process imaged in confocal (left) and STED microscopy (right). Membrane labeling was performed with the novel endocytosis marker developed in this study (see section 3.2.3). Note that intracellular organelles are only distinguishable in the improved STED image. Scale bar, 2  $\mu\text{m}$ .

### 1.5 Aims of this work

Research on hair cell physiology, development and proteome has been essential for the treatment and prevention of congenital and acquired hearing impairment. In the biological aspect, it has helped to partially understand how an epithelial cell evolved into an extraordinarily efficient synaptic machine. However, despite decades of hair cell research, we still do not know what proteins drive synaptic vesicle fusion in these cells, or how they perform constitutive “housekeeping” processes in parallel to the demanding task of neurotransmission. As mentioned in the introduction, two main models of synaptic vesicle recycling have been proposed using different technical approaches: 1) local recycling at the cell base, with little involvement of other cell regions. 2) Apical recycling, with the participation of the biosynthetic pathways. Proving the validity of these models has been difficult, due to the somatic location of hair cell active zones, and the lack of suitable endocytosis tracers that do not permeate MET channels. Although with our previous study combining dye photo-oxidation and EM we made a safer step in understanding synaptic recycling as a local process (model 1) (Kamin et al., 2014), conclusive data will only come from molecular identification of the recycling organelles and the study of larger cell populations.

The major aim of this project was to develop a novel endocytosis marker for the study of membrane recycling in auditory inner hair cells (IHCs). For this molecule to sort the caveats already presented, it should fulfill a series of requirements:

- It should not permeate MET channels to undoubtedly see endocytic processes.
- It should be suitable for high-resolution fluorescence microscopy in order to study recycling organelles, typically smaller than the diffraction barrier of light (200-300 nm). Fluorescence microscopy is preferred over EM-based approaches, for the easier sample preparation, higher throughput and wider field of view.
- It should be fixable and compatible with immunolabeling procedures, in order to assign synaptic or constitutive molecular identity to endocytic organelles.

Once a successful molecule would be obtained from a pool of tested candidates, its uptake would then be compared with our previous findings using dye photo-oxidation (Kamin et al., 2014). This novel tool should allow, for the first time, to establish the molecular identity of recycling organelles in IHCs, and to determine to what extent the constitutive pathways are involved in the synaptic vesicle recycling process.



If success would be met to this point, a further goal of this project would be to prove the applicability of the novel tool in other neuronal preparations. It could, for example, help to understand yet unanswered aspects of protein organization and synaptic function in the small boutons of hippocampal neurons:

- Are spontaneously released synaptic vesicles identical in protein composition to actively released ones?
- What is the fraction of synaptic vesicle proteins that remains stranded on the neuronal plasma membrane (known as “readily retrievable pool” of vesicles)?
- Are the t-SNARE proteins Syntaxin 1 and SNAP-25 similarly organized on plasma membranes and intracellular organelles?

Additionally, uptake of the novel probe could be also evaluated in other non-neuronal systems, like cultured cells.

Obtaining a fixable endocytosis marker that remains on labeled membranes, even after permeabilization and immunostaining procedures, would not only be an achievement for studying IHCs, but also a valuable tool for describing membrane trafficking in virtually any cell type.



## 2 MATERIALS AND METHODS

### 2.1 Materials

#### 2.1.1 Reagents

**Table 2.1 List of reagents used in this study**

	Product	Catalog Number	Company
Commercial membrane markers	FM 1-43	70020	Biotium, Hayward, CA, USA
	AM 1-43	70024	Biotium
	FM 4-64	70021	Biotium
	FM 4-64FX	F34653	Molecular Probes, Life Technologies, Darmstadt, Germany
	FM 1-84	70047	Biotium
	FM 3-25	70048	Biotium
	5-Dodecanoylaminofluorescein (DCF)	D109	Molecular Probes, Life Technologies
	Di-2-ANEPEQ	D6923	Molecular Probes, Life Technologies
Development of new membrane-binding tools	Transferrin – Alexa 594	T13343	Molecular Probes, Life Technologies
	Insulin human	I2643	Sigma-Aldrich, Munich, Germany
	Atto 647N NHS ester	AD 647N-31	ATTO-TEC GmbH, Siegen, Germany
	Palmitic acid N-hydroxysuccinimide ester	P1162	Sigma-Aldrich
	Cholera Toxin Subunit B (Recombinant), Alexa Fluor® 594 Conjugate	C34777	Molecular Probes, Life Technologies
	Poly-L-hydrobromide 1000-5000 Da (PLL 1-5 kDa)	P0879	Sigma-Aldrich
	Poly-L-hydrobromide 4000-15000 Da (PLL 4-15 kDa)	P6516	Sigma-Aldrich
	Disposable PD-10 desalting column (PD Mini Trap G-10)	17-0851-01	GE Healthcare, Freiburg, Germany

	mCLING		Designed by Prof. Silvio O. Rizzoli. Synthesized by Synaptic Systems, Göttingen, Germany
	Epidermal Growth Factor, Tetramethylrhodamine Conjugate (rhodamine EGF)	E3481	Molecular Probes, Life Technologies
Endocytosis reporters	Low Density Lipoprotein from Human Plasma, Dil complex (Dil LDL)	L3482	Molecular Probes, Life Technologies
	Transferrin From Human Serum, Alexa Fluor 488 Conjugate	T13342	Molecular Probes, Life Technologies
	Transferrin From Human Serum, Alexa Fluor 546 Conjugate	T23364	Molecular Probes, Life Technologies
	Bromophenol blue	B8026	Sigma-Aldrich
mCLING validation	Propidium Iodide	P1304MP	Molecular Probes, Life Technologies
	SynaptopHluorin (VAMP2) construct		Kindly provided by Leon Lagnado, Medical Research Council, Cambridge, United Kingdom
	Dynasore hydrate	D7693	Sigma-Aldrich
	Pitstop 2	ab120687	abcam, Cambridge, UK
	Tetrodotoxin (TTX)	T8024	Sigma-Aldrich
	p-toluensulfonic acid monohydrate	402885	Sigma-Aldrich
Embedding media	2,4,6-Tris[bis(methoxymethyl)amino]-1,3,5-triazine (melamine)	T2059	TCI Europe, Zwijndrecht, Belgium
	EpoFix kit (epoxy resin)	40200029	Struers A/S, Ballerup, Denmark
	Mowiol 4-88 reagent	475904	Merck Millipore, Merck KGaA, Darmstadt, Germany

## 2.1.2 Buffers and solutions

**Table 2.2 List of buffers and solutions used in this study**

Buffer	Composition (concentrations in mM)
Tyrode's buffer for neuronal cultures	124 NaCl, 5 KCl, 2 CaCl <sub>2</sub> , 1 MgCl <sub>2</sub> , 30 glucose, 25 HEPES, pH 7.4
Ringer's buffer for COS7 cells	130 NaCl, 4 KCl, 5 CaCl <sub>2</sub> , 1 MgCl <sub>2</sub> , 48 glucose, 10 HEPES, pH 7.4
Hank's Balanced Salt Solution without calcium ( <b>HBSS without Ca<sup>2+</sup></b> ), for OC dissection and resting condition of IHCs	141.7 NaCl, 5.36 KCl, 1 MgCl <sub>2</sub> , 0.5 MgSO <sub>4</sub> , 3.4 L-Glutamine, 6.3 glucose, 10 HEPES, pH 7.4. 295-300 mOsm
Hank's Balanced Salt Solution with high	135.1 NaCl, 10 KCl, 2 CaCl <sub>2</sub> , 1 MgCl <sub>2</sub> , 0.5 MgSO <sub>4</sub> ,

potassium ( <b>HBSS high K<sup>+</sup> 10mM</b> ), for mild stimulation of IHCs	3.4 L-Glutamine, 6.3 glucose, 10 HEPES, pH 7.4. 295-300 mOsm
Hank's Balanced Salt Solution with high potassium ( <b>HBSS high K<sup>+</sup> 25mM</b> ), for stimulation of IHCs	120.1 NaCl, 25 KCl, 2 CaCl <sub>2</sub> , 1 MgCl <sub>2</sub> , 0.5 MgSO <sub>4</sub> , 3.4 L-Glutamine, 6.3 glucose, 10 HEPES, pH 7.4. 295-300 mOsm
Hank's Balanced Salt Solution with high potassium ( <b>HBSS high K<sup>+</sup> 65mM</b> ), for strong stimulation of IHCs	79.7 NaCl, 65.36 KCl, 2 CaCl <sub>2</sub> , 1 MgCl <sub>2</sub> , 0.5 MgSO <sub>4</sub> , 3.4 L-Glutamine, 6.3 glucose, 10 HEPES, pH 7.4. 295-300 mOsm
Hank's Balanced Salt Solution with calcium ( <b>HBSS with Ca<sup>2+</sup></b> ) for recovery after stimulation of IHCs	139.7 NaCl, 5.36 KCl, 2 CaCl <sub>2</sub> , 1 MgCl <sub>2</sub> , 0.5 MgSO <sub>4</sub> , 3.4 L-Glutamine, 6.3 glucose, 10 HEPES, pH 7.4. 295-300 mOsm
Fluorescence quenching solutions (Figure 3.13)	HBSS with Ca <sup>2+</sup> and HBSS high K <sup>+</sup> 65 mM were supplemented with <b>0.75 mM BPB</b>
Hank's Balanced Salt Solution with high potassium and no calcium (HBSS high K <sup>+</sup> 65mM, without Ca <sup>2+</sup> ), for strong stimulation in absence of calcium, used as control (Figure 3.13.)	81.7 NaCl, 65.36 KCl, 1 MgCl <sub>2</sub> , 0.5 MgSO <sub>4</sub> , 3.4 L-Glutamine, 6.3 glucose, 10 HEPES, pH 7.4. 295-300 mOsm, <b>5 EGTA, 0.75 BPB</b>
Standard <i>Drosophila</i> stimulation buffer	130 NaCl, 36 sucrose, 5 KCl, 2 CaCl <sub>2</sub> , 2 MgCl <sub>2</sub> , 5 HEPES, pH 7.3 (Jan and Jan, 1976)
Yeast minimal medium	0.67 % Difco yeast nitrogen based w/o amino acids (Beckton, Dickison and company), 0.07 % complete supplement mix (MP biomedical) and 2 % sucrose (Roth)
Phosphate buffer saline (PBS)	150 NaCl, 20 Na <sub>2</sub> HPO <sub>4</sub> , pH 7.4
High-salt PBS	500 NaCl, 20 Na <sub>2</sub> HPO <sub>4</sub> , pH 7.4
Permeabilization solution for cultured neurons, mammalian cells and yeast cells	0.1% Triton X-100 and 2.5% bovine serum albumin (BSA) in PBS
Permeabilization solution for organs of Corti and <i>Drosophila</i> preparations	0.5% Triton X-100 and 1.5% bovine serum albumin (BSA) in PBS
Quenching solution (after fixation)	100 NH <sub>4</sub> Cl and 100 Glycine in PBS

### 2.1.3 List of Antibodies

**Table 2.3 List of antibodies used in this study**

Antibody	Catalog number, type	Company/Source
β-tubulin	single-chain recombinant antibody	(Nizak et al., 2003)
Bruchpilot	nc82, mouse monoclonal	Developmental Studies Hybridoma Bank at University of Iowa, IA, USA

## Materials and Methods

Calnexin	ab22595, rabbit polyclonal	abcam, Cambridge, UK
Chromo494-coupled goat anti-Mouse IgG	15032	Active Motif, La Hulpe, Belgium
Chromo494-coupled goat anti-Rabbit IgG	15042	Active Motif
CtBP2 (also recognizing Ribeye A domain)	612044, mouse monoclonal	BD Biosciences, Heidelberg, Germany
Cy2-coupled goat anti-mouse IgG	115-225-146	Dianova GmbH, Hamburg, Germany
Cy2-coupled goat anti-rabbit IgG	111-225-144	Dianova GmbH
GM130	610822, mouse monoclonal	BD Biosciences,
LAMP1	ab24170, rabbit polyclonal	abcam
Otoferlin	ab53233, mouse monoclonal	abcam
Rab3A	610379, mouse monoclonal	BD Biosciences. IHCs.
Rab3A	107 003, rabbit polyclonal	Synaptic Systems, Göttingen, Germany. Hippocampal neurons
Ribeye B domain	192 003, rabbit polyclonal	Synaptic Systems
SNAP-25	111 002, rabbit polyclonal	Synaptic Systems
Synapsin	106 002, rabbit polyclonal	Synaptic Systems
Synaptophysin	G96, rabbit polyclonal raised against synaptophysin purified from rat synaptic vesicles	Kindly provided by Prof. Reinhard Jahn, Max Planck Institute for Biophysical Chemistry, Göttingen, Germany. (Jahn et al., 1985)
Synaptotagmin 1	105 102, rabbit polyclonal	Synaptic Systems
Syntaxin 1	110 011, mouse monoclonal	Synaptic Systems
Syntaxin 6	610636, mouse monoclonal	BD Biosciences
Syntaxin 13	110 131, mouse monoclonal	Synaptic Systems
Syntaxin 16	rabbit polyclonal	Kindly provided by Prof. Reinhard Jahn, Max Planck Institute for Biophysical Chemistry, Göttingen, Germany. Same as 110 162, from Synaptic Systems GmbH, Göttingen, Germany
VAMP2	104 211, mouse monoclonal	Synaptic Systems
VAMP4	136 002, rabbit polyclonal	Synaptic Systems

VGLUT1/2	135 503, rabbit polyclonal	Synaptic Systems
VGLUT3	135 203, rabbit polyclonal	Synaptic Systems
Vti1a	611220, mouse monoclonal	BD Biosciences

## 2.1.4 Microscopes and equipment

**Table 2.4 List of microscopes and equipment used in this study**

Element	Characteristics	Company
Leica SP2 upright confocal microscope	- Water immersion objective (63×, 0.9 NA, HCX APO L U-V-I)	Leica Microsystems GmbH, Wetzlar, Germany
Leica pulsed STED microscopy setup based on a TCS SP5 inverted confocal microscope	- HCX PL APO Oil immersion STED objective (100× 1.4 NA) - HCX PL APO Oil immersion objective (63× 1.4 NA) - Excitation: pulsed diode laser (18 mW, 80 MHz, 640 nm emission, PicoQuant, Germany) - Depletion: pulsed infrared Titanium:Sapphire (Ti:Sa) tunable laser (1W, 80 MHz, 720–1000 nm, Mai Tai Broadband; Spectra-Physics, Santa Clara, CA, USA). - Detection: two ultra-sensitive avalanche photodiodes and high sensitivity, low noise PMTs were used	Leica Microsystems GmbH
Olympus IX 71 inverted epifluorescence microscope	- Oil immersion objective (60× 1.35 NA) - TIRFM oil immersion objective (100× 1.45 NA. - 100 W mercury lamp. - F-View II CCD camera (Soft Imaging System GmbH, Münster, Germany)	Olympus, Hamburg, Germany
Inverted epifluorescence Nikon Eclipse Ti-E microscope	- CFI S Plan Fluor ELWD air objective (40× 0.60 NA) - Plan apochromat oil immersion objective (60×, N.A. 1.4) - HBO-100W Lamp - IXON X3897 Andor Camera	Nikon GmbH, Düsseldorf, Germany
NanoDrop Spectrophotometer	- Model ND1000	Wilmington, DE, USA
Leica Ultramicrotome	- Model EM UC6	Leica Microsystems GmbH

## 2.1.5 Software

**Table 2.5 List of software used in this study**

Software	Application	Provider
LAS AF Version 2.7.3.9723	Image acquisition software for Leica TCS SP5 STED microscope	Leica Microsystems GmbH, Wetzlar, Germany
Leica Confocal Software Version 2.61	Image acquisition software for Leica SP2 confocal microscope	Leica Microsystems GmbH
Cell^P Version 3.4	Image acquisition software for Olympus IX 71 inverted microscope	Olympus Soft Imaging Solutions GmbH, Hamburg, Germany
NiS – Elements AR, Version 4.20	Image acquisition software for Nikon Eclipse Ti-E microscope	Nikon GmbH, Düsseldorf, Germany
ACD/C ChemSketch (Freeware version 12.01)	Generation of chemical structures for mCLING and FM 1-43	Advanced Chemistry Development Inc., Toronto, Canada
PyMol (Version 1.6.0.0)	Graphic rendering of molecular structures for mCLING and FM 1-43	Schrödinger, Portland, OR, USA
SigmaPlot Version 10.0	Statistical analysis, data plotting and graphs generation	Systat Software, Inc., Erkrath, Germany
Matlab Version 7.5.0.342 (R2007b)	Image analysis	The MathWorks Inc., Natick, MA, USA
Huygens Essential 4.4	Image deconvolution	Scientific Volume Imaging B.V., Hilversum, The Netherlands
Image J 1.47v	Image processing and preparation for figures	Wayne Rasband, US National Institutes of Health, <a href="http://rsb.info.nih.gov/ij/">http://rsb.info.nih.gov/ij/</a>
Adobe Photoshop CS6 Version 13.0	Image processing and preparation for figures	Adobe Systems Inc., San Jose, CA, USA
Adobe Illustrator CS6 Version 16.0.0	Figures formatting and graphic design	Adobe Systems Inc., San Jose, CA, USA



## 2.2 Methods

### 2.2.1 Generation of tools for the study of membrane traffic

#### 2.2.1.1 Generation and dialysis of membrane-binding molecules

Alternative fluorescent membrane-binding molecules were generated by coupling proteins to lipid tails and/or fluorescent molecules. For this purpose a standard protocol based on covalent conjugation was applied. Four different reactions were carried out:

- 1) insulin, palmitic acid and the fluorophore Atto 647N bearing an N-Hydroxysuccinimide (NHS) ester group for amine crosslinking;
- 2) transferrin-Alexa 594 and palmitic acid;
- 3) PLL 1-5 kDa and Atto 647N -NHS ester; and
- 4) PLL 4-15 kDa and Atto 647N -NHS ester

Briefly, 1 mg of protein was resuspended in 1 mL PBS solution (pH 7.4) containing 100 mM NaHCO<sub>3</sub> (stock solution at pH 8.6), and later transferred to a small glass bottle. Apart, a solution of 10mg/ml palmitic acid and/or 10mg/ml fluorophore was prepared in dimethylformamide (DMF). 10 µL of this solution were slowly added to the protein solution while stirring and then mixed for 1 hour, protected from the light. The reaction was stopped with 20 µL of 1.5 M hydroxylamine (freshly prepared, pH 8.5) and the solution was stirred for other 5 minutes. The obtained mixture was loaded in a PD-10 desalting column, previously washed and loaded with PBS (pH 6.5). 5 fractions of approximately 500 µL were collected for later application to biological samples or dialyzed when necessary. PLL 1-5 kDa and PLL 4-15 kDa conjugated to Atto 647N were dialyzed against HBSS buffer without Ca<sup>2+</sup> through 3500 MW-exclusion and 6000-8000 MW-exclusion membranes, respectively. The final products were aliquoted and stored at -80°C.

#### 2.2.1.2 mCLING generation and concentration estimation

The design of mCLING as an oligopeptide containing seven lysine molecules, conjugated to a palmitic group and a molecule of the fluorophore Atto 647N, was an original idea of Prof. Silvio Rizzoli. Synthesis of the mCLING molecule was carried out by Synaptic Systems GmbH, Göttingen, Germany. To determine the concentration of the mCLING stock solution, fluorescence intensity of a dilution series was measured with a spectrophotometer (NanoDrop ND1000). Concentration values were calculated from a linear regression curve

obtained from fluorescence intensity values of increasing concentrations of an Atto 647N-conjugated oligonucleotide (1:1 ratio Atto 647N:oligonucleotide, Eurofins MWG Operon, Ebersberg, Germany).

### 2.2.2 Experiments performed with cultured mammalian cells

#### 2.2.2.1 Preparation of coverslips for cell culture seeding

18 mm diameter coverslips (thickness Nr. 1: 0,13 - 0,16 mm; Menzel Gläser, Braunschweig, Germany) were thoroughly washed before use:

- Incubation in 1M HCl overnight followed by 5 washes with Milli-Q-purified water
- Wash with 1M NaOH for 1-2 hours followed by 5 or more washes with Milli-Q-purified water until reaching a neutral pH
- Wash and storage in 100% ethanol

Coverslips were flamed, placed on 12-well plates and coated with a PLL solution (0.1 mg/mL) for 1 hour. Excess of PLL was washed 3 times with distilled water. Plates were sterilized with UV light under a laminar flow hood and stored at 4°C until their use for cell culture.

#### 2.2.2.2 Endocytosis assays in COS7 cells

COS7 cells (fibroblast-like cell line from monkey kidney) were cultured in Dulbbeco's modified Eagle medium (DMEM with 4.5 g/L glucose; Lonza, Cologne, Germany) supplemented with 10% fetal calf serum (FCS; PAA Laboratories, Clöbe, Germany), 4 mM glutamine (Lonza) and 100 units/ml penicillin and streptomycin (Lonza).

One day before the experimental procedure, cells were briefly washed with PBS and treated with trypsin EDTA (Gibco, Life technologies, Darmstadt, Germany) for 5 minutes at 37°C. After collection and wash, cells were resuspended in supplemented DMEM medium, plated on PLL-coated coverslips, and kept at 37°C and 5% CO<sub>2</sub> culture conditions. Before performing the endocytosis assays, cells were washed with pre-warmed Ringer's buffer, and then incubated for 5 minutes at 37°C with different membrane and/or endocytosis markers dissolved in pre-warmed Ringer's buffer. A list of markers used and their concentrations is presented below:

- 0.2-0.4 µM mCLING,
- 5 µM FM 1-43,

- 5  $\mu$ M AM 1-43,
- 5  $\mu$ M FM 4-64FX,
- 25  $\mu$ g/ml Alexa 546-Transferrin,
- 0.4 ng/ml tetramethylrhodamine-EGF,
- or 15  $\mu$ g/ml DiI-LDL

When necessary, membrane/endocytosis labeling was followed by fixation with 4% PFA + 0.2% glutaraldehyde for 20 minutes on ice and 20 minutes at RT. Excess of aldehyde fixatives was quenched during 30 min at RT using quenching buffer (100 mM  $\text{NH}_4\text{Cl}$  and 100 mM glycine solution in PBS). Permeabilization was carried out in 3 rounds of 5 minutes with a 0.1% Triton X-100 + 2.5% BSA solution in PBS. Primary antibodies were incubated for 1 hour in permeabilization solution followed by 3 washes of 5 minutes with permeabilization solution. Secondary antibodies were incubated for 1 hour in permeabilization solution. After immunostaining, coverslips were washed 3 times for 5 minutes with high-salt PBS and 2 times for 5 minutes with standard PBS. Coverslips were mounted on glass slides using Mowiol as embedding medium.

For pictures in Figures 3.5, 3.7 and 3.8A, cells were imaged in live, fixed, or fixed and permeabilized conditions, in an Olympus IX 71 inverted microscope (60 $\times$  1.35 NA oil immersion objective, or 100 $\times$  1.45 NA TIRFM oil immersion objective) equipped with an F-View II CCD camera (Soft Imaging System GmbH, Münster, Germany).

For studying the effects of mCLING on membrane trafficking pathways, cells were first incubated for 5 minutes with mCLING and Alexa 546-Transferrin at 37 $^\circ\text{C}$ , washed with Ringer's buffer and incubated again at 37 $^\circ\text{C}$  for 20 minutes in Ringer's buffer. Cells were fixed and quenched as described above. For figures 3.6 and 3.8B-C, images were acquired in the confocal mode of a Leica TCS SP5 STED microscope using an HCX PL APO 63 $\times$  1.4 NA oil immersion objective.

### 2.2.2.3 mCLING toxicity assay in COS7 cells

A cell viability assay was performed to assess the concentration-dependent toxicity of mCLING labeling. COS7 cells were directly plated on a 24-well plastic plate. For the assay wells were first washed with pre-warmed Ringer's buffer, incubated in Ringer's buffer containing increasing concentrations of mCLING (in  $\mu\text{M}$ : 0, 0.21, 0.42, 0.85, 1.7, 3.4, 6.8) for 5 minutes, washed, and incubated in Ringer's buffer containing propidium iodide (Sigma). Cells were imaged after 5 minutes in an inverted epifluorescence Nikon Eclipse Ti-E

microscope (CFI S Plan Fluor ELWD 40× 0.60 NA air objective). Propidium iodide was imaged using the Cy3 filter set (excitation: 545/25, dichroic mirror: 565, barrier filters: 605/70 BP). Imaging of mCLING was performed with the Cy5 filter set (excitation: 620/60, dichroic mirror: 660, barrier filter: 700/75 BP).

### **2.2.2.4 Culture methods for rat hippocampal neurons**

The cultured hippocampal neurons were obtained from dissociated hippocampi of newborn rats (modified from (Banker and Cowan, 1977; Beaudoin et al., 2012)). Dissection procedures and culture methods were performed by our technical assistant Christina Schäffer. Briefly, brains were extracted from the skulls of P2 rat pups, and the hippocampi were isolated under a dissection microscope. The tissue was washed several times with HBSS (Invitrogen) to remove tissue debris and thereafter incubated for 1h in enzyme solution (10 ml DMEM, 2 mg cysteine, 100 mM CaCl<sub>2</sub>, 50 mM EDTA, and 25 units Papain sterile bubbled with carbogen for 10 minutes and sterile filtered). Neurons were washed thoroughly with HBSS and incubated for 15 min in inactivating solution (2 mg Albumin, 2 mg Trypsin-Inhibitor in 10 ml of FCS containing DMEM medium) followed by mechanical dissociation. The coverslips on which neurons were seeded were prepared as explained in section 2.2.2.1 but PLL coating was done at higher concentration (1mg/ml) overnight. Neurons were seeded in plating medium (Eagle's Minimum Essential Medium, MEM, supplemented with 10% horse serum, 3.3 mM glucose, and 2 mM glutamine) and incubated for 1–4 hours at 37°C in a 5% CO<sub>2</sub> humidified atmosphere to allow adhesion to the substrate. After adhesion the medium was changed to Neurobasal-A medium containing: 500 ml Neurobasal-A (Gibco, Life technologies, Darmstadt, Germany), 10 ml B27 supplement (Gibco, Life Technologies), and 5 ml Glutamax I stock. To avoid glial proliferation 5-fluoro-2'-deoxyuridine (FUDR) was added to the culture after 2 DIV. The neurons were kept in culture at 37°C and 5% CO<sub>2</sub> for 14 days before use.

### **2.2.2.5 Neuronal transfection with Synaptophluorin construct**

To study the effects of mCLING on synaptic vesicle recycling, neurons were transfected with a plasmid carrying Synaptophluorin (VAMP2-pHluorin, see (Miesenböck et al., 1998; Sankaranarayanan and Ryan, 2000; Granseth et al., 2006)). The synaptophluorin insert (kindly provided by Dr. Leon Lagnado, University of Sussex, UK) was subcloned into a pEGFP-N1 plasmid (CMV promoter, Clontech, Mountain View, CA, USA) by PCR by inclusion of a KpnI restriction site in the forward primer (AAT-GGTACC-GCCGGTCGCCACC) and a NotI

restriction site in the reverse primer (AAT-GCGGCCGC-TTTAACCGGTTTTGTATAG). Ligation was confirmed by sequencing. Transfection was carried out using the calcium phosphate-based ProFection Mammalian transfection system (E1200; Promega, Madison, WI, USA). Briefly, coverslips with neuronal cultures were transferred to a 12-well plate containing fresh DMEM (5 mL 1M MgCl<sub>2</sub> and 2.5 mL 1M HEPES in 500 mL DMEM). The transfection reaction solution was prepared according to the amount of coverslips to be transfected, with the following amounts per well: 3.2 µL 2M CaCl<sub>2</sub>, 2 µg plasmidic DNA, Nuclease-free water to a final volume of 25 µL. This solution was mixed with 25 µL/well of HEPES-buffered saline and precipitates were allowed to form for 15-30 minutes at RT. 50µL of the transfection solution were applied drop-wise to every well and incubated for 15-30 minutes at 37°C. Wells were washed 3 times with fresh DMEM and kept in the last wash for 15 minutes at 37°C. Coverslips were finally replaced to the original plate with the old medium and kept at 37°C 5% CO<sub>2</sub> until imaging was performed.

### **2.2.2.6 SynaptopHluorin experiments in neuronal hippocampal cultures**

To test the innocuity of mCLING to neuronal cells and assess its possible effect on synaptic vesicle recycling, a fluorescent assay reporting synaptic vesicle release was designed. 8 days after SynaptopHluorin transfection coverslips with cultured neurons were placed in a stimulation chamber, labeled with 0.2 µM mCLING for 5 minutes and washed with Tyrode's buffer. Spontaneous network activity was blocked after mCLING labeling using a solution containing 10 µM CNQX and 1 µM AP5 in Tyrode's buffer. Neurons were stimulated with the same instruments described in section 2.2.2.7. 100-mA shocks were delivered initially in a short stimulus (60 AP, 3 seconds at 20 Hz) and 40 seconds later in a long stimulus (600 AP, 30 seconds at 20 Hz). Control neurons were directly treated with CNQX and AP5 and imaged in absence of mCLING. Imaging was performed in the same Nikon setup described in section 2.2.2.3. SynaptopHluorin was imaged using the 60X oil immersion objective (plan apochromat, N.A. 1.4) and the filter set for EGFP (excitation: 470/40, dichroic mirror: 495, barrier filter: 525/50 BP).

### **2.2.2.7 mCLING applications to cultured rat hippocampal neurons**

In order to label the recycling organelles and/or the plasma membrane of cultured hippocampal neurons, these were incubated in Tyrode's buffer containing mCLING (0.68 µM). Three different types of labeling were performed:

- Selective labeling of the actively released pool of synaptic vesicles: neurons were

prelabeled with mCLING for 5 minutes and then stimulated with 600 APs (30 seconds, 20 Hz) in presence of mCLING. For electric stimulation a custom-made chamber holding two platinum electrodes was fixed on top of the cells culture. 100 mA shock stimuli were delivered using an A385 stimulus isolator and an A310 Accupulser stimulator (both from World Precision Instruments, Sarasota, FL, USA).

- Selective labeling of the spontaneously released pool of synaptic vesicles: neurons were incubated in tetrodotoxin (1  $\mu$ M) for 15 minutes in presence of mCLING.
- Surface labeling of the neuronal plasma membrane: cells were preincubated in cold mCLING-free buffer for 5 minutes on ice. Keeping the cells on ice, an mCLING solution was added and further incubated for 5 minutes.

After mCLING labeling neurons were fixed, permeabilized and immunostained, as described above for COS7 cells. After immunostaining, coverslips were mounted on glass slides using Mowiol as embedding medium. The following primary antibodies were used: VGLUT1/2, synaptophysin, synaptotagmin 1, VAMP2, synapsin, syntaxin 13, Vti1a, VAMP4, Rab3a, syntaxin, and SNAP-25. Chromeo494-coupled goat secondary antibodies were used accordingly.

### 2.2.2.8 Preparation of Mowiol embedding medium

24 g of glycerol and 9.6 g Mowiol 4-88 reagent were mixed with 62.4 mL distilled water and 9.6 mL 1M Tris buffer in a glass beaker. The mixture was stirred for 5 to 7 days and occasionally heated at 40-50°C to help Mowiol dissolving. The mixture was let to settle and only the supernatant was aliquoted. Aliquots were kept at -20°C for long-term storage and at 4°C for daily use.

### 2.2.3 Dissection and uses of the mouse organ of Corti

#### 2.2.3.1 Animals

Wild-type mice (*Mus musculus*) from the substrains C57BL/6N and C57Bl/6J were obtained from the animal facility of the University Medical Center Göttingen or from Charles River Laboratories (Sulzfeld, Germany). Otoferlin knockout mice (*Otof*<sup>-/-</sup>, described in (Reisinger et al., 2011)) were kindly provided by Dr. Ellen Reisinger (Molecular Biology of Cochlear Neurotransmission Group, Department of Otolaryngology, University Medical Center Göttingen, Germany). Animals were handled according to the specifications of the University of Göttingen and of the State of Lower Saxony (Landesamt für Verbraucherschutz, LAVES,

Braunschweig, Germany).

### 2.2.3.2 Dissection of the organ of Corti (OC)

Male or female mice at ages between postnatal days 14 to 18 (P14-P18) were used for organ of Corti dissection. At this age mice can already hear (hearing onset occurs at P10) and their cochlear structure is still soft enough for an easy dissection. Animals were sacrificed by decapitation. After a sagittal cut of the head's skin, this was removed up to the snout. The head was divided through the sagittal plane in two halves and preserved in ice-cold HBSS without  $\text{Ca}^{2+}$  until further dissection. The brain was removed to uncover the vestibular and cochlear organs, and these were detached from the temporal bone by gently pulling them out. The bony walls of the cochlea and the *stria vascularis* were carefully opened up to expose the organ of Corti. Using fine forceps, the apical turn of the organ of Corti was pulled out while breaking up the central column of the *modiolus* to release it. The dissected organs of Corti were used for experimental procedures within 5 to 10 minutes after dissection.

### 2.2.3.3 Testing commercial fluorescent dyes in living IHCs

Experiments were done as indicated in (Kamin et al., 2014). For dye labeling and imaging of IHCs at low temperature, I constructed a customized chamber suitable for imaging in an upright confocal microscope: the lid of a plastic petri dish was filled with the gel from a freezing pad, covered and sealed with PARAFILM, and topped with a 25-mm coverslip (Figure 2.1). After dissection the apical turn of the OC was incubated for 5 minutes in ice-cold HBSS without  $\text{Ca}^{2+}$ , and placed on a previously cooled imaging chamber containing HBSS without  $\text{Ca}^{2+}$ . The OC was clamped to the chamber's coverslip using a metal harp with nylon strings. IHCs were then incubated with different fluorescent dyes from the FM family (FM 1-43, AM 1-43, FM 4-64, FM 4-64FX and FM 1-84) at a final concentration of 10  $\mu\text{M}$  in HBSS without  $\text{Ca}^{2+}$ . Other membrane-binding dyes like dodecanoylaminofluorescein (DCF, 188  $\mu\text{M}$ ) and Di-2-ANEPEQ (JPW 1114, 100  $\mu\text{M}$ ) were also tested. IHCs were imaged along their longitudinal axis using the 63 $\times$  water immersion objective of a Leica SP2 upright confocal microscope. FM dyes, DCF and Di-2-ANEPEQ were excited with the 488 nm line of an argon laser and their emission was detected in the range of 500-700 nm with a PMT.

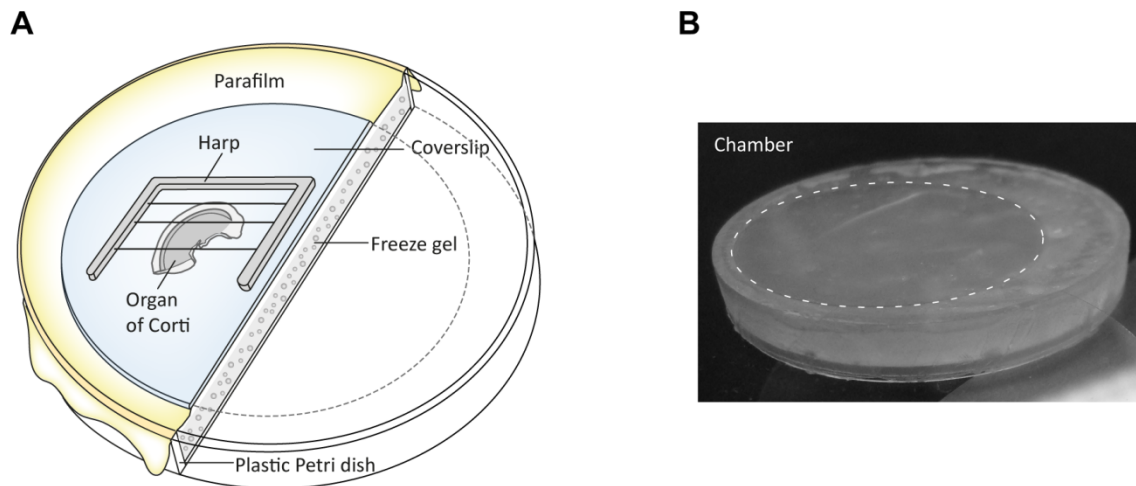


**Figure 2.1 Customized chamber for IHC imaging at low temperature.**

This chamber was designed to keep the OCs at low temperature while being imaged under the upright confocal microscope. This assay was important to study membrane labeling under inhibition of endocytosis by low temperature. **A.** The lid of a plastic Petri is filled with freeze gel and covered with a layer of PARAFILM. This chamber is kept at  $-20^{\circ}\text{C}$  for storage and at  $4^{\circ}\text{C}$  shortly before the experiment. Before imaging, a coverslip is placed on the PARAFILM-covered surface on top of which the dissected organ of Corti is placed, kept in place by a metallic harp. The organ of Corti is covered with the required buffer. **B.** Image of the assembled chamber.

#### 2.2.3.4 mCLING labeling and immunostaining of OCs

The apical turn of the organ of Corti was dissected and directly placed in a Petri dish filled with ice-cold HBSS without  $\text{Ca}^{2+}$ . Plasma membrane and endocytic events were labeled by incubating the OC in  $1.7\ \mu\text{M}$  mCLING. Incubation times were always of 3 minutes to ensure adequate probe penetration into the tissue. Fast transfer and good preservation of OCs through the different incubation steps was ensured by using 24-well plates and a fire-polished glass pipette (See Figure 2.2). Three main stimulation conditions were applied at  $37^{\circ}\text{C}$ :

- Resting condition: the OC was incubated in HBSS without  $\text{Ca}^{2+}$  for 3 minutes in presence of mCLING.
- Strong stimulation condition: the OC was first incubated for 2 minutes in HBSS without  $\text{Ca}^{2+}$  + mCLING and then transferred to a well containing HBSS high  $\text{K}^{+}$  (65 mM) + mCLING for 1 minute. The same treatment was applied at milder stimulation conditions of 10 and 25 mM  $\text{K}^{+}$ .
- Recovery after stimulation: after a strong stimulation treatment (65 mM  $\text{K}^{+}$ ), excess of mCLING was washed off from the OC using HBSS with  $\text{Ca}^{2+}$  and then incubated for 5 minutes in dye-free HBSS with  $\text{Ca}^{2+}$ .



All solutions were carbogen-charged for 30 minutes and pre-warmed at 37°C before the experiments. After labeling, samples were rapidly washed with HBSS without Ca<sup>2+</sup>, fixed in 4% PFA + 0.2% glutaraldehyde for 30 minutes on ice followed by 30 minutes at RT, and quenched in 100 mM NH<sub>4</sub>Cl and 100 mM glycine in PBS for 30 minutes. Afterwards OCs were permeabilized in 3 rounds of 10 minutes with 0.5% Triton X-100 and 1.5% BSA in PBS, and incubated for 1 hour with primary antibody(ies) (diluted in permeabilization solution). After primary antibody incubation, 3 washes of 10 minutes with permeabilization solution were performed. Secondary antibodies were also incubated for 1 hour. Finally, organs were washed with high salt PBS (3 times for 10 minutes) and standard PBS (2 times for 10 minutes), followed by embedding in plastic resin (see section 2.2.5.1).

The primary antibodies used on IHCs in this study included different organellar markers: VGLUT3, Rab3, otoferlin, calnexin, GM130, syntaxin 6, syntaxin 16, Vti1a and LAMP1. As secondary antibodies Chromeo494-coupled goat anti-Rabbit IgG and Chromeo494-coupled goat anti-Mouse IgG were used accordingly. Chromeo494 is a long Stokes shift dye that allows two-color STED imaging with only one depletion laser line when combined with Atto 647N (present in mCLING).

For identifying the synaptic ribbon (Figure 3.16) primary antibodies against CtBP2 (also recognizing Ribeye A domain) or Ribeye B domain, were combined with secondary antibodies Cy2-coupled goat anti-mouse IgG or goat anti-rabbit IgG. Ribbons were imaged in the confocal mode of the Leica STED setup described above using a He-Ne laser (488 nm) for excitation, and a very narrow detection window to be able to differentiate its signal from that one of Chromeo494 (495-520 nm).

mCLING-labeled and immunostained samples were embedded in melamine resin, cut into 200nm-thick sections and later on imaged in two-color STED microscopy using the Leica TCS SP5 STED microscope described in the Materials section. For images shown in Figure 3.21, samples were cut into 50 nm-thick sections and imaged in the Olympus IX 71 epifluorescence inverted microscope described in the Materials section.

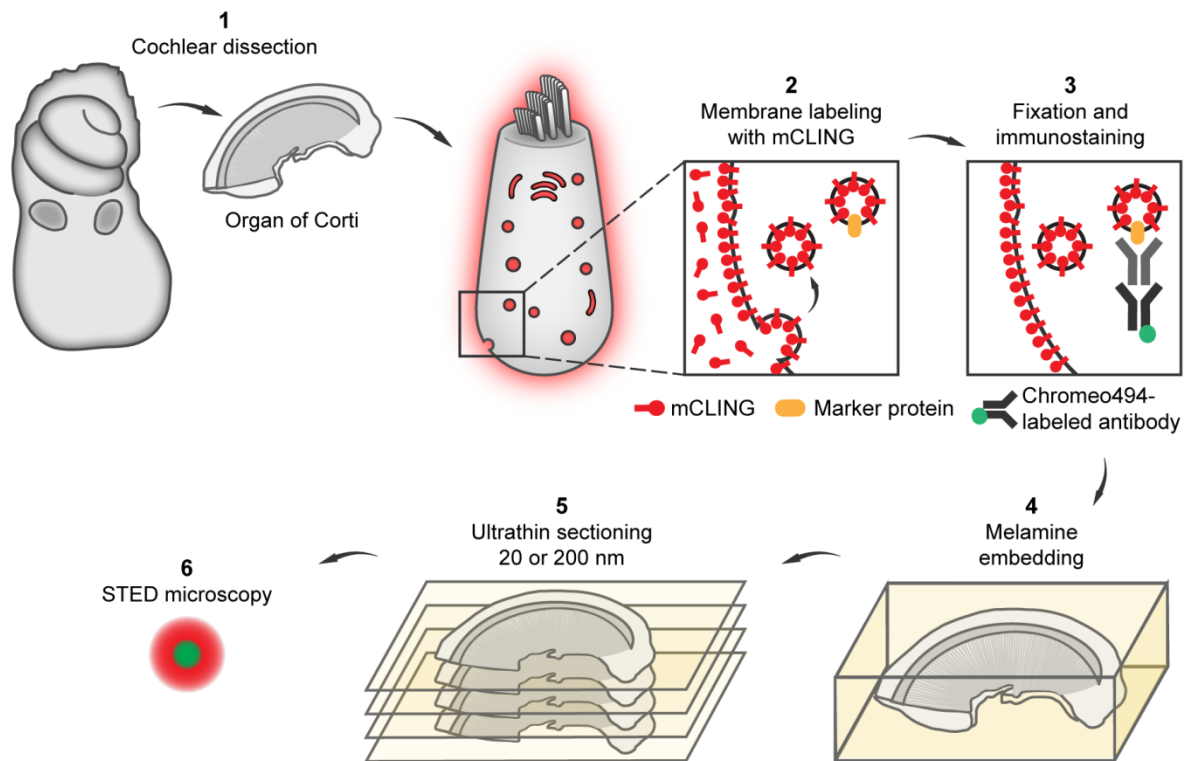


**Figure 2.2 Experimental workflow for the membrane labeling, immunostaining and plastic embedding of OCs**

The bony labyrinth and cochlea were dissected out of the mouse skull. The apical turn of the organ of Corti was carefully dissected out (1), and incubated with mCLING at different stimulation conditions to label IHCs plasma membrane and membrane uptake processes (2). After labeling, OCs were fixed and immunostained for different organellar protein markers (3). In order to obtain improved Z-resolution, OCs were embedded in a plastic resin (melamine, 4) and sliced with a microtome (5) for later imaging in two-color STED microscopy (6). The final outcome of this procedure is high-resolution images of endocytosed organelles and plasma membranes, with information on organellar identity and protein distribution for correlation analyses.

### 2.2.3.5 Vesicle release estimation by cell surface quenching of mCLING in IHCs

In the previous sections mCLING uptake was used to reveal endocytosed organelles and the cell plasma membrane. An assay to study the opposite process, mCLING release upon  $K^+$  stimulation, was designed. Given the non-washability of mCLING from plasma membranes, bromophenol blue (BPB) was used as surface fluorescence quencher to obtain a better signal of stimulation-dependent fluorescence loss.

After a round of mCLING labeling ( $1.7 \mu\text{M}$ ) in strong stimulation conditions at  $37^\circ\text{C}$ , i.e. 2 min in HBSS without  $\text{Ca}^{2+}$  and 1 min in HBSS with  $65 \text{ mM } K^+$ , the OC was placed in an imaging chamber containing mCLING-free HBSS with  $\text{Ca}^{2+}$  and  $0.75 \text{ mM}$  Bromophenol blue

(BPB) for recovery during 5 minutes. BPB quenched the mCLING on the cell surface, enabling the live imaging of endocytic organelles. IHCs were stimulated for a second time by replacing the solution with HBSS with 65 mM K<sup>+</sup> and 0.75 mM BPB for 1 minute. For the control group, the second stimulation was performed in absence of Ca<sup>2+</sup>, in presence of 0.75 mM BPB and 5 mM EGTA. Live imaging was performed using the water immersion objective (HCX APO L U-V-I ,63×, 0.9 NA) from the Leica SP2 upright confocal microscope described in the Materials section.

### 2.2.3.6 Application of endocytosis inhibitors to IHCs

OCs were incubated for 5 minutes in HBSS without Ca<sup>2+</sup>. Subsequently, OCs were kept for 25 minutes in a 30 μM pitstop 2 or 100 μM dynasore solution in HBSS without Ca<sup>2+</sup>. Afterwards OCs were treated with the strong stimulation protocol described in section 2.2.3.4: first a two-minute incubation in a 1.7 μM mCLING HBSS without Ca<sup>2+</sup> plus inhibitor (same concentrations), and then a one-minute stimulation in HBSS High K<sup>+</sup> with 1.7 μM CLPF plus inhibitor (same concentrations). The entire procedure was performed at 37°C in the well of a plastic plate continuously supplied with carbogen to keep pH levels stable. Fixation, quenching and immunostaining for VGLUT3 were performed as described above. Quantification of endocytosis levels was compared to control IHCs, treated with the same buffers and incubation periods, in absence of the inhibitors. 500x dynasore and 500x pitstop 2 stock solutions were prepared in 100% DMSO and stored at -20°C.

### 2.2.3.7 Experiments with otoferlin knockout (*Otof*<sup>-/-</sup>) mice

*Otof*<sup>-/-</sup> mice were kindly provided by Dr. Ellen Reisinger (Molecular Biology of Cochlear Neurotransmission Group, Department of Otolaryngology, University Medical Center Göttingen) and described in (Reisinger et al., 2011). These knockout mice were generated by homologous recombination with a target plasmid to excise exons 14 and 15 of the otoferlin wild type gene. The deletion of this gene region leads to a frame shift and incomplete translation of the otoferlin protein. The recombinant sequence included a neomycin selection cassette flanked by floxP sequences. The targeting vector was electroporated into 129ola embryonic stem cell colonies, which were then selected with G418 and ganciclovir. The positive clones, confirmed by Southern blot, were injected into mouse blastocysts to generate chimeric mice. Their heterozygous offspring was bred with cre-recombinase-expressing mice, leading to excision of the neomycin cassette. Deletion of the neomycin cassette was confirmed by PCR and absence of otoferlin from inner hair cells was confirmed

by immunostaining. OCs obtained from P14-P18 *Otof*<sup>-/-</sup> mice were treated under the strong stimulation condition (65 mM K<sup>+</sup>), fixed and immunostained for VGLUT3, in the same way described in section 2.2.3.4. Endocytosis levels in *Otof*<sup>-/-</sup> IHCs were compared to values found in IHCs from wild-type animals.

### **2.2.4 mCLING application on the larval neuromuscular junction (NMJ) of *Drosophila***

#### **2.2.4.1 Dissection of *Drosophila* larvae and mCLING labeling**

Third instar wildtype larvae were immobilized on Sylgard-coated plastic Petri dishes. Using fine scissors, larvae were dorsally opened along the middle line of the sagittal plane. Internal organs were removed and the skin sides pinned down to expose the ventral muscles. The preparation was preincubated during 2 minutes with 1.7 μM mCLING in standard *Drosophila* buffer (Jan and Jan, 1976). Next the preparation was electrically stimulated with 160 APs (20 Hz for 8 seconds) in *Drosophila* buffer (Jan and Jan, 1976) and in presence of mCLING (same concentration). 100 mA shock stimuli were delivered using an A385 stimulus isolator and an A310 Accupulser stimulator (both from World Precision Instruments, Sarasota, FL, USA). The preparation was immediately fixed and immunostained in the same way as for OCs (section 2.2.3.4). Active zones at the NMJs were identified by immunostaining with primary antibodies against Bruchpilot and Cy-3 labeled secondary antibodies. These preparations were embedded in melamine and cut into 200 nm sections with a Leica ultramicrotome (Leica Microsystems GmbH) for later imaging in the Leica TCS SP5 STED microscope described in section 2.2.5.2.

### **2.2.5 Sample embedding, sectioning and imaging**

#### **2.2.5.1 Melamine preparation, embedding and sectioning**

Embedding procedures of cells and tissues were performed as described previously (Punge et al., 2008). Melamine resin was freshly prepared the same day of the experiment. The following recipe was used to embed up to 7 samples. First 48 mg of resin catalyzer (p-toluensulfonic acid monohydrate) were thoroughly dissolved in 0.576 ml distilled water in a 15-mL conical tube. Next 1.344 g of melamine (2,4,6-Tris[bis(methoxymethyl)amino]-1,3,5-triazine) were added to the solution and thoroughly mixed until all melamine was covered by the solution. The tube was agitated on a horizontal shaker at 250 rpm for 2 hours or until the melamine was completely dissolved (transparent homogeneous appearance). The two

reagents were kept dry and clean from other substances at 4°C to avoid coloration or polymerization defects in the final melamine product. After mCLING labeling and immunostaining, the OC or the *Drosophila* larva was placed on an 18-mm glass coverslip. I found out that at this point it is important to place the OC with the tectorial membrane facing down to the coverslip for better IHC preservation. A BEEM capsule (Beem Inc., West Chester, PA, USA), whose bottom had previously been cut, was placed with the opening down, surrounding the preparation. 200 µl of freshly prepared melamine were slowly poured inside the BEEM capsule, covering the tissue completely. The mounted sample was placed in a box containing silica beads for removing the environmental water, and left overnight at room temperature to allow penetration of melamine into the tissue. The box with the samples inside was transferred to an oven at 40°C for 24 hours. The BEEM capsule was filled to the top with Epoxy resin (Epo Fix kit) and then heated up at 60°C for 48 hours. The melamine around the OC or larval tissue was trimmed away with a razor blade and samples were again incubated at 60°C for 48 hours, for complete hardening. Melamine blocks were cut into thin sections with a Leica ultramicrotome. Sections were dried on a coverslip and embedded in Mowiol for two-color STED or epifluorescence imaging.

### 2.2.5.2 STED and confocal microscopy

A Leica TCS SP5 STED microscope equipped with a HCX PL APO 100× 1.4 NA oil STED objective and operated with the Leica LAS AF imaging software was used for performing one-color or two-color STED microscopy (Leica Microsystems GmbH). Atto 647N (present in mCLING) was excited with a pulsed diode laser (PDL 800-D, PicoQuant, Berlin, Germany) emitting at 640 nm and its fluorescence signal was detected with an avalanche photodiode (APD). Chromeo494, a long stokes shift dye, was used for the second STED channel. Chromeo was excited also with a PDL emitting at 531 nm, and detected with an APD. Both Atto 647N and Chromeo494 were depleted with a STED beam generated by a pulsed infrared titanium:sapphire (Ti:sa) tunable laser (1W, 80 MHz, 720–1000 nm) set at 750 nm (Mai Tai Broadband, Spectra-Physics, Santa Clara, CA, USA). This microscope was also used for combined STED/confocal or only confocal microscopy images. Excitation of the different dyes in confocal mode was performed with: a Helium-Neon laser emitting at 633 nm for mCLING; the 488 nm line of an argon laser for FM 1-43 and Cy2 (in secondary antibodies indicating the position of IHCs and *Drosophila* NMJs active zones); and a Helium-Neon laser emitting at 543 nm for LDL-Dil and Trasferrin-Alexa 546. An acousto-optical tunable filter (AOTF) was used to adjust the fluorescence detection window for each of these dyes.

Detection devices included low noise PMTs.

### 2.2.5.3 Thin-section imaging

Sample preparation and embedding was performed as for the 200-nm sections. Samples were cut into 20-nm thick sections using a Leica ultramicrotome (Leica Microsystems GmbH). Sections were imaged using an epifluorescence microscope from Olympus (IX71; Hamburg, Germany), with a 100× 1.45 NA TIRFM oil immersion objective (Olympus) and an F-View II CCD camera (1,376 × 1,032 pixels, pixel size of 6.45 × 6.45 μm; Olympus). FITC and RFP filter sets were used to image Cy2- and Cy3-labeled secondary antibodies, respectively. A Cy5 filter set was used for imaging mCLING (AHF, Tübingen, Germany).

### 2.2.6 Experiments with microorganisms

#### 2.2.6.1 mCLING validation on yeast cells

*Saccharomyces cerevisiae* cells from the strain BY4742 were grown in yeast nitrogen base (YNB) medium overnight at 30°C. Before the experiments, glass coverslips were coated with PLL as explained in section 2.2.2.1. A cell suspension was poured on top of a PLL-coated coverslip and allowed to precipitate on it for 10 minutes. Excess of medium was removed and a solution of either 20 μM FM 4-64 (Biotium) or 0.4 μM mCLING in YNB medium was applied on top of the immobilized cells for 20 minutes. Some of the coverslips were later on fixed, or fixed and immunostained in the same way as for COS7 cells (section 2.2.2.2). Imaging was performed in the same Olympus microscope described in the previous section using a 100× 1.45 NA TIRFM oil immersion objective combined with an optovar lens of 1.6× magnification.

#### 2.2.6.2 mCLING validation in bacteria

For membrane staining of cells from the species *Escherichia coli*, a cell suspension was first pelleted by centrifugation (5 minutes, 4500 rpm) and resuspended either in a 5 μM FM 1-43 (Biotium) or 0.4 μM mCLING solution (diluted in Lysogeny Broth, LB, medium). Cells incubated in FM 1-43 were directly immobilized for 10 minutes on a PLL-coated coverslip. Cells labeled with mCLING were pelleted again, resuspended in dye-free LB medium and also immobilized on PLL-coated coverslips. The coverslips were mounted on glass slides using Mowiol. FM 1-43 and mCLING staining were imaged in the confocal and the STED mode, respectively, of the Leica TCS SP5 STED microscope described above.

## 2.2.7 Data analysis

### 2.2.7.1 Image analysis and processing

The analysis of the data presented in this study was entirely performed using custom-made Matlab routines (The Mathworks Inc., Natick, MA, USA), all written by Silvio O. Rizzoli. Four main types of analysis were performed, with variations according to the analysis needs.

**Type 1 analysis.** This was a fluorescence intensity-based analysis applied on tif files generated by the Cell<sup>^</sup>P, Leica Confocal, or the Leica LAS AF software. A MatLab routine was used to determine the average fluorescence intensity of the pixels contained in a square (for IHCs) or hand-drawn ROI (for COS7 cells). The mean values were compared among the different treatments. Figure 3.1, Figure 3.4, Figure 3.6, Figure 3.7 and Figure 3.27 contain data analyzed with this routine.

**Type 2 analysis.** For calculating endocytosis levels (Figure 3.12, Figure 3.14 and Figure 3.15) raw STED images from transversal cuts of mCLING-labeled IHCs were analyzed using a custom-made MatLab routine. First, the area occupied by the IHCs was defined by hand drawing the cell perimeter, helped by the mCLING signal from the plasma membrane. From this area the percentage occupied by intracellular mCLING-labeled organelles was calculated. mCLING-labeled organelles were defined as groups of pixels with fluorescence intensities above the mean mCLING background value. A similar routine was used in Figure 3.13 taking into account the mCLING intensity levels, rather than the area occupied. Another variation was used to establish the percentage of signal located on the plasma membrane, from the total signal found in synaptic boutons and axonal processes (Figure 3.24).

**Type 3 analysis.** To evaluate the presence of various proteins within mCLING-labeled organelles (Figure 3.17, Figure 3.18, Figure 3.19, Figure 3.20 and Figure 3.21), two-color STED or epifluorescence images taken from transversal cuts of mCLING-labeled and immunostained IHCs were analyzed. The self-written MatLab routine was used to calculate Pearson's correlation coefficients between the mCLING and the immunostaining signals, within line scans (20 pixels long, 2 pixels wide, with a pixel size equivalent to 25.2 x 25.2 nm) drawn specifically across mCLING labeled organelles.

**Type 4 analysis.** This analysis was used to obtain averaged STED pictures of IHC active zones (Figure 3.16). For this purpose at least 20 regions of interest (5x5  $\mu\text{m}^2$ ) centered on synaptic ribbons were selected for each condition. The self-written MatLab routine stacked

two of these areas and rotated them using the overlapped ribbons as rotation axis until perfect overlap between the images was found. To determine the cytoplasmic side of mCLING-labeled plasma membrane, the analysis was also based on a VGLUT3 image of the same region. Once the highest correlation between the images was found, the next area was added to the stack and processed until all the ROIs were aligned. A final image of the average fluorescence intensities was then generated from the stack of individual images. Similar routines were used to identify and average the neuronal organelles (Figure 3.23) or SNARE clusters (Figure 3.25). The complete MatLab script for this type of analysis can be found in the Appendix section at the end of this thesis.

### **2.2.7.2 Statistical analysis**

All the histogram bars presented in this study correspond to mean values  $\pm$  standard error of the mean (SEM), unless otherwise indicated in the figure legends. The student's t-test (unpaired) was calculated using either the statistical package of MatLab (The Mathworks Inc.) or the in-built statistical function of Sigma Plot (Systat Software, Inc.). P values are indicated in the figure legends. No blinding was used for data analysis, as each data set could be easily recognized.

### **2.2.7.3 Data presentation**

For presentation purposes the STED images presented in sections 3.3 and 3.4 were deconvolved using Huygens Essential 4.4, from Scientific Volume Imaging (Hilversum, The Netherlands). The deconvolution procedure run by this software is based on a Maximum Likelihood Estimation (CMLE) algorithm. The in-built deconvolution functions of the software were adapted to the imaging parameters of the STED microscope described above.



## 3 RESULTS

---

### 3.1 Testing commercial membrane markers in IHCs

#### 3.1.1 FM dyes, their analogs and fluid phase markers fail to label endocytosis in IHCs

As mentioned in the Introduction, the initial motivation to develop a customized membrane/endocytosis marker was the interest to study synaptic vesicle recycling and membrane trafficking in the auditory IHCs. Up to know this issue has been elusive due to the permeation of commonly used dyes through mechanoelectric transduction (MET) channels located at the hair bundle of these cells (Nishikawa and Sasaki, 1996; Gale et al., 2001; Meyers et al., 2003). Hence, incubation with these dyes results in a very strong cytoplasmic labeling (due to dye molecules permeating the MET channels) that masks the fluorescent signal contributed by truly endocytosed dye molecules. The first step in this project was to revisit the application of such dyes in our own working conditions and setups. Preliminary work was performed in a previous PhD project carried out in our laboratory (Kamin, 2011). Dr. Dirk Kamin applied a series of commercial dyes on the mouse organ of Corti (OC), the sensory epithelium that hosts IHCs, to evaluate their diffusion properties into such structure and their permeation into the IHCs. A list of the dyes he used can be found in Table 3.1.

The first group included dyes from the FM family. These are styryl molecules that reversibly bind to membranes and have been widely used in the last two decades to study synaptic vesicle recycling in synaptic boutons (Betz et al., 1992; Hoopmann et al., 2012). Dr. Kamin found that except for FM 3-25, all other dyes from the FM family that were evaluated produced a strong and fast staining of the IHC cytoplasm, being much stronger than the intensity found in the surrounding cells (e.g. pillar and supporting cells). By its characteristics, this labeling is difficult to reconcile with an endocytosis-dependent pathway and suggests that the dye molecules rather reach the interior of the IHCs by permeating their MET channels. The same results were obtained using other small membrane-binding molecules like DCF and Di-2-ANEPEQ. The first conclusion of these results is that dyes in the size range of the 450-550 Daltons are small enough to pass through the MET channels. The

second conclusion is that a long and highly hydrophobic molecule like FM 3-25, with two octadecyl chains, is retained in the outermost regions of the tissue and therefore does not diffuse freely into the OC. In his study, Dr. Kamin also found that soluble compounds like calcein or fluorescein-coupled dextrans could successfully reach the fluid space around the IHCs without permeating them, but would not be taken up into endocytic organelles. Being calcein a relatively small molecule (622 Da), it was concluded that membrane binding is important for MET channels permeation, and efficient endocytic uptake (Kamin et al., 2014).

**Table 3.1 List of commercial dyes tested on IHCs**

	Dye	Molecular Weight
<b>FM family of styryl dyes</b>	FM 1-43	451
	AM 1-43 (fixable version of FM 1-43)	454
	FM 4-64	448
	FM 4-64FX (fixable version of FM 4-64)	448
	FM 1-84	478
	FM 3-25	843
<b>Membrane-binding probes</b>	5-Dodecanoylaminofluorescein (DCF)	530
	Di-2-ANEPEQ (also known as JPW1114)	549
<b>Fluid phase markers</b>	Calcein	622
	3000 Da Dextran - Fluorescein	~1500-3000 (range of sizes obtained through a viscosity-based purification)

To strengthen these results and prove that this fluorescence signal is mainly generated by artifactual labeling of the cytoplasm and in a less extent by dye endocytosis, I tested the probes that showed IHCs permeation (FM 1-43, AM 1-43, FM 4-64, FM 4-64FX, FM 1-84, DCF and Di-2-ANEPEQ) at low temperature, at which endocytic processes should be inhibited. I found that at such conditions all FM dyes permeated IHCs (Figure 3.1A), in a similar fashion that at RT and comparable to a previous study reporting FM 1-43 permeation at 4°C in bullfrog saccular hair cells (Meyers et al., 2003). The same strong labeling was also seen for DCF and Di-2-ANEPEQ (Figure 3.1B). Quantification of the fluorescence intensity levels for RT and low temperature incubations showed no significant difference in the amount of labeling, confirming that IHC staining cannot be exclusively explained by endocytic processes (Figure 3.1C).

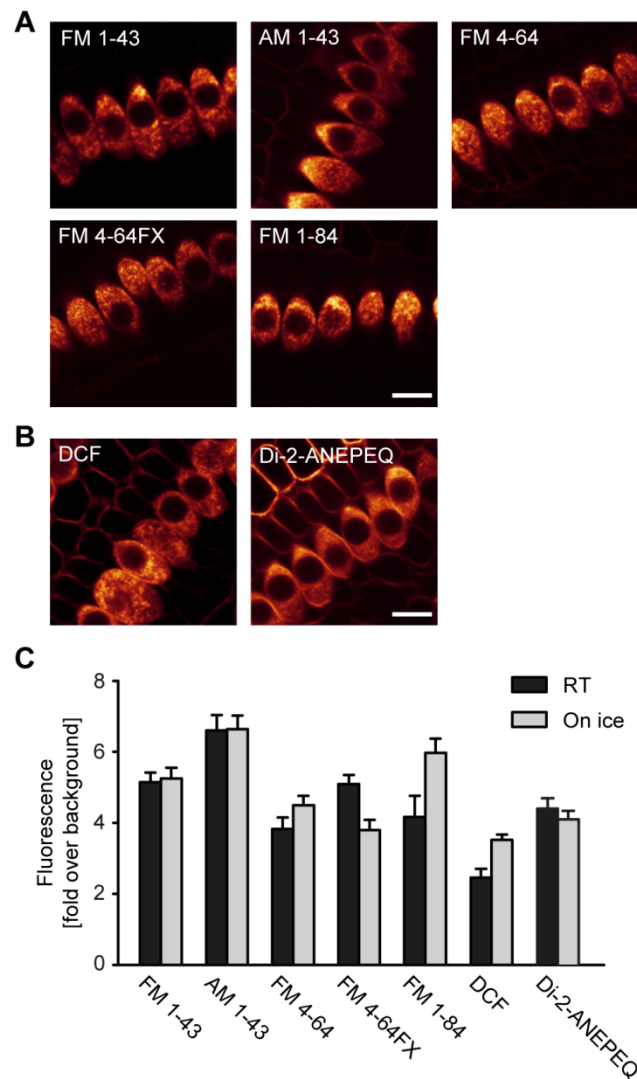


**Figure 3.1 Commercial membrane markers label IHCs in an endocytosis-independent process.**

**A.** Dyes from the FM family different in size and structure (450-480 Da) were incubated on IHCs at low temperature to inhibit endocytosis. Strong IHC labeling suggests permeation of the dyes through MET channels. Scale bar, 10  $\mu$ m. **B.** Two membrane-binding probes, DCF and the voltage sensor Di-2-ANEPEQ, labeled the cytoplasm of IHCs in a similar fashion to FM dyes. Scale bar, 10  $\mu$ m. **C.** Analysis of fluorescence intensity for dyes that gave a strong labeling inside IHCs. ROIs were selected from the cell cytoplasm, avoiding the nuclear area. Fluorescence values are expressed as fold over background. The black bars represent experiments performed at RT. The gray bars represent experiments performed at low temperature (2-4°C). Data analysis was performed using the following numbers of IHCs per condition. FM 1-43: 26 at RT, 19 on ice; AM 1-43: 20, 16; FM 4-64: 13, 23; FM 4-64FX: 8, 20; FM 1-84: 7, 27; DCF: 8, 15; Di-2-ANEPEQ: 30, 35.

From these results I concluded that none of the commonly used commercial dyes tested here is suitable for assessing endocytosis in IHCs, and that a better approach requires the design of customized membrane-binding fluorescent tools.

I then set out to target the different parameters that would define a suitable endocytosis

marker for IHCs. In section 3.2 I will describe the steps that led me to successfully develop such marker, mainly based on the implementation of membrane labeling and uptake assays in cultured mammalian cells. In section 3.3 I will show how the obtained marker was applied to the study of membrane trafficking in IHCs.

## 3.2 Design, synthesis and evaluation of novel membrane-binding probes

### 3.2.1 Requirements for the generation of suitable membrane probes to study IHCs

Based on the results described in the previous section and the aims of this study, a newly designed membrane-binding probe applicable to IHCs should meet the following requirements:

- Size/structure: it has been proposed that permeant blockers of open MET channels of hair cells fulfill two requirements: electrochemical interaction with the channel pore via partially charged amine groups, and a molecular radius below the diameter of the MET channel pore at its narrowest point, estimated in  $12.5 \pm 0.8 \text{ \AA}$ . Molecules interacting with the channel but that exceeded such diameter blocked cation currents but did not permeate into cells (Farris et al., 2004). From what was seen in the previous section, one could expect that molecules with sizes above 600-700 Da and that still reach the surface of IHCs, have a radius large enough to hinder open MET channel permeation, independent of their electrochemical interaction with the channel.
- Binding: interaction with the plasma membrane seems to be important for efficient uptake of the probe into endocytic compartments. In this study lipid tails and charge-based attachment were explored.
- Tissue penetration: as seen for FM 3-25, penetration of the probe into a complex tissue like the OC is necessary to ensure that first, the probe reaches the surrounding space of the IHCs, and second, that it has the opportunity to be taken up along with all endocytic events.
- Fixability: as described in the Introduction (section 1.3.2.3), different organelles have been involved in SV recycling in IHCs. However, these assumptions were made based on morphological descriptions in EM micrographs (Siegel and Brownell, 1986; Spicer et al., 2007) or by anatomical location using fluorescence images (Griesinger et al., 2002, 2004, 2005). The best way to identify recycling SVs would be to use a tool that not only labels them during endocytosis, but that also allows their later identification by immunolabeling. This implies that such tool should be fixable to remain in the originally labeled structures, even after permeabilization procedures.

- STED-suitable fluorescence: up to know high-resolution images of the SV recycling process in IHCs are only available in electron microscopy and electron tomography (Siegel and Brownell, 1986; Lenzi et al., 2002; Kamin et al., 2014). Lenzi and collaborators (2002) provided important information about the plasma membrane remodeling upon stimulation-triggered vesicle release, although they did not use an endocytosis tracer. Siegel and Brownell used HRP as tracer, but its penetration requires long incubation times that still do not ensure the labeling of all recycling organelles. From our own work (Kamin et al., 2014), we established dye-photo-oxidation EM of IHCs to distinguish FM 1-43 labeling contained in endocytosed organelles from the signal of cytoplasmic dye that permeated MET channels. However, combining this technique with immunolabeling EM techniques would be very laborious, and even this solution would difficulty multiple labeling for different proteins. Additionally, EM procedures require long sample preparation times. A fluorescence high-resolution technique like STED microscopy would overcome these difficulties while providing detailed images of subdiffraction-sized organelles like SVs and organelles of the endosomal trafficking pathway. STED microscopy requires dyes that are stable under increasing intensities of the depletion laser, have high quantum yield for enabling detection of the typically narrow detection areas and suitable fluorescence lifetimes that allow reasonable lengths of excitation-depletion cycles. One of the best dyes recommended for the STED setup used in this study is, for example, Atto 647N (Atto-Tech GmbH).

These requirements should make the probe also valid for endocytosis studies in other tissue preparations and cultured cells, as it will be shown along the Results section of this study.

### 3.2.2 Strategies for probe design

As it will be seen along this section, refinement of the ideal probe properties was achieved along the experimental path. The initial strategy I started out with was to generate novel membrane-binding probes fulfilling the above mentioned requirements by conjugation of different elements into one molecule:

- Fixable component: molecules ranging from short peptides to large proteins could be used as substrates for amine crosslinking by aldehyde fixatives.
- Membrane-binding component: lipid tails can be added to ensure partition of the molecule into the cell plasma membrane. Positively charged molecules could also

offer membrane binding capacity due to their interaction with negative charges present on the plasma membrane.

- Fluorescent component: fluorescent molecules are available in different modification variants, like NHS ester groups for amine-specific crosslinking, or maleimide groups for reaction with sulfhydryl groups of proteins.

### 3.2.2.1 Lessons from protein-based probes

For a first exploration of membrane binding and fixability properties two chimeric membrane-binding molecules were synthesized:

- Insulin-palmitoyl-Atto 647N (IPA): coupling of human insulin, palmitic acid and the dye Atto 647N-NHS ester. Estimated size 6.9 kDa.
- Transferrin-palmitoyl-Alexa 594 (TfPA): coupling of human transferrin-Alexa 594 with palmitic acid. Estimated size 80.6 kDa.

Additionally, the B subunit of cholera toxin (CTB) conjugated to Alexa 594 (CTBA) was included in the experimental setup. While the cholera toxin A subunit is responsible for the pathogenic effects such as efflux of chloride ions and H<sub>2</sub>O release to the intestinal lumen via its catalytic activity on ADP-ribosylation, the B subunit facilitates the internalization of the toxin into cells of the host (Sanchez and Holmgren, 2011). CTB binds to the plasma membrane by recognition of the pentasaccharide chain of GM1 gangliosides (Eidels et al., 1983). Although initial studies proposed an exclusive caveolar endocytosis pathway for CTB (Tran et al., 1987), more recent studies propose also uptake by clathrin-dependent, and caveolin- and clathrin- independent mechanisms (Torgersen et al., 2001). Thus, CTB has been used as endocytosis tracer to study early endosome sorting and budding (Barysch et al., 2009). At neutral pH the CTB subunit (11.4 kDa) can also exist as pentamers (57 kDa), ranging in size between IPA and TfPA.

Cultured hippocampal neurons were incubated for 5 minutes with IPA, TfPA or CTBA and fixed for 30 minutes with a 4% PFA solution. After quenching with 100 mM NH<sub>4</sub>Cl, coverslips were placed on glass slides using Mowiol for embedding. Considering that the reaction performed to produce IPA and TfPA results in bulk labeling of the proteins with a variable number of fluorophore copies per molecule, it was difficult to determine the final concentration of the products in the output solution. IPA, TfPA and CTBA were diluted in Tyrode's buffer at different concentrations and evaluated under epifluorescence microscopy to establish a concentration giving appropriate fluorescence intensity.

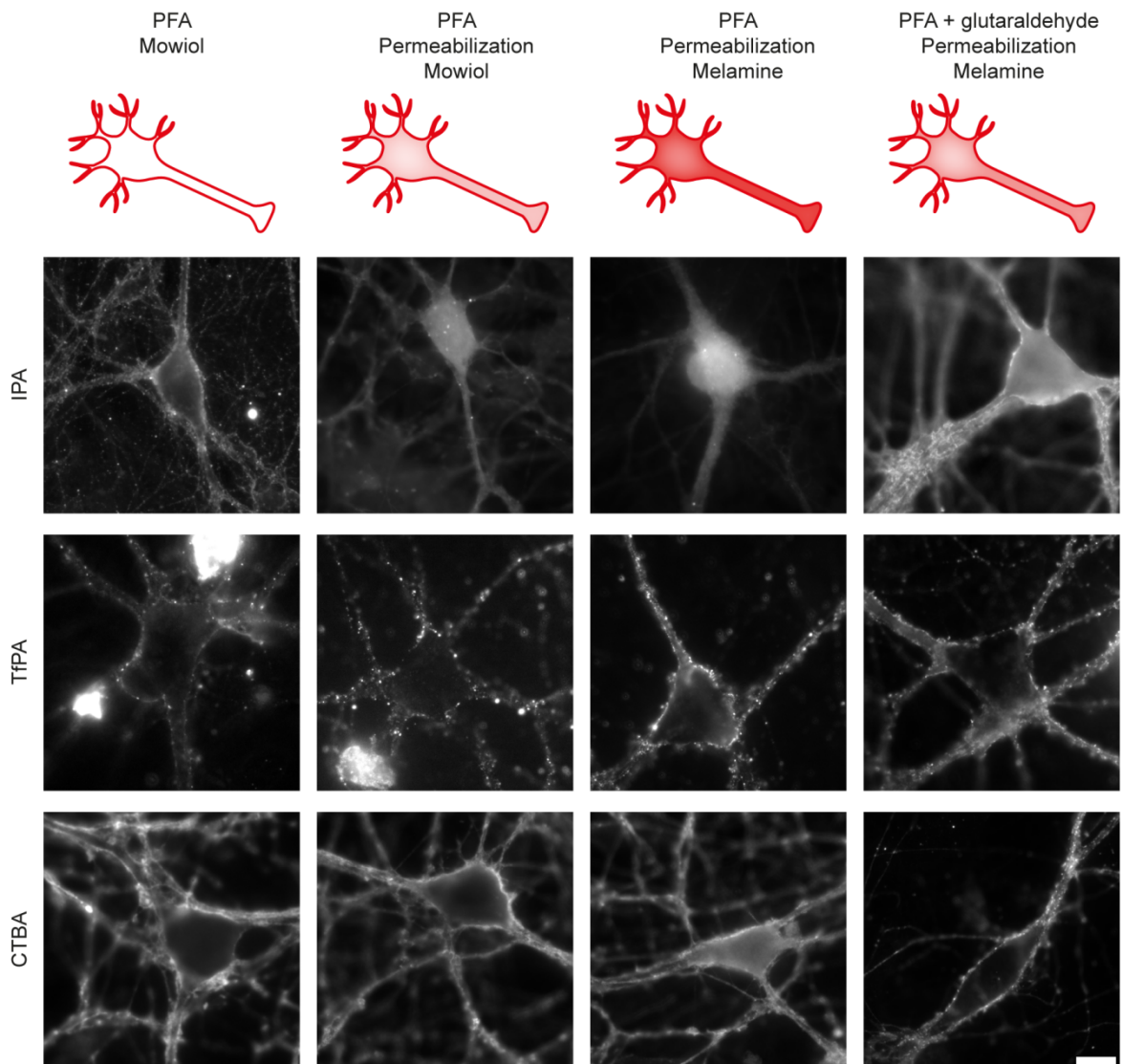


**Figure 3.2 Differences in fixability and labeling distribution among protein-based membrane-binding probes.**

Insulin and transferrin molecules conjugated to fluorescent and lipid molecules (IPA and TfPA, respectively), were compared to the fluorescently labeled cholera toxin B subunit (CTBA) in a membrane labeling assay. Probe incubations were performed on neuronal rat hippocampal cultures. Homogeneity of membrane labeling was found to be size-dependent and preserved upon fixation and embedding in Mowiol. Permeabilization, as used in immunostaining procedures, detached unfixed probe molecules and mobilized them into the cell interior. This effect was worsened by embedding with melamine resin after permeabilization. Improving fixation with glutaraldehyde helped to keep the probes bound to membranes. Scale bar, 10  $\mu\text{m}$ .

While IPA and CTBA gave a homogenous labeling of neuronal membranes, TfPA gave a dotted discontinuous labeling pattern (Figure 3.2, first column). This could be explained by the larger size of TfPA, which seems to precipitate on the cellular membranes forming protein clusters. These results already suggest the inconvenience of TfPA for homogeneously reporting all endocytic events happening at the cell surface.



It is also important to highlight that IPA and TfPA were normally found on the plasma membrane of the intact cells, and only rarely in endocytosed structures. This would suggest that their relatively large sizes, when compared to dyes from the FM family, might hamper their uptake, being this lower than the non-conjugated native molecules.

When fixation was followed by a permeabilization procedure (0.1% Triton X-100 plus 2.5% BSA, 1.5 hours) and Mowiol embedding, IPA was found inside the cell soma and processes, indicating very poor fixability. TfPA and CTBA remained on the membranes (Figure 3.2, second column).

As explained in the Methods section, the OC is a complex and thick tissue that would be difficult to study in detail under STED microscopy. For obtaining detailed images of recycling organelles, resin embedding followed by thin sectioning is a good option. Melamine is a non-fluorescent water-baser resin that offers good sample preservation. When labeled, fixed and permeabilized neurons were embedded in melamine instead of Mowiol, the probe molecules were mobilized into the cell somas and processes, with stronger effects again on IPA (Figure 3.2, third column). This effect was largely reduced by including a post-fixation step with 2.5% glutaraldehyde after the permeabilization, and before the Melamine embedding (Figure 3.2, fourth column).

Important aspects of probe-membrane interaction can be deduced from these results:

- Large probes like TfPA (80.6 kDa) have difficulties to homogeneously distribute along plasma membranes, reducing their ability to report endocytic events.
- Although IPA has a smaller size (6.9 kDa) and offers a continuous membrane labeling, it was not properly fixed. CTBA was better preserved on membranes, but after melamine embedding its staining appeared less continuous and punctuated. Deficient fixation of these molecules is probably due to concealing of amine groups by the protein's tertiary and quaternary structures (in the case of CTBA), leaving only a few accessible groups for aldehyde crosslinking.
- Permeabilization washes off probe molecules that are not properly fixed, and relocalizes them in structures or compartments that were not labeled initially (e.g. cytoplasm).
- Resin diffusion into cells and its polymerization impose additional factors for probe mobilization from membranes, which can be partly compensated for by using more efficient fixation protocols (e.g. using glutaraldehyde).

The main conclusion of these experiments is that **fixability** and **probe size** are pivotal aspects for the successful labeling of cell membranes and its preservation for further sample processing (e.g. immunostaining).

### 3.2.2.2 PLLs conjugated to Atto 647N fail to fix on membranes

For the next step towards achieving an ideal probe for IHCs labeling, I generated two new probes based on commercial PLL homopolymers, which should offer abundant and freely available amine groups for aldehyde crosslinking. PLLs were coupled to Atto 647N by an NHS ester group. Membrane binding was expected to be facilitated by the binding of positive charges of the polymer chains to negative charges of the plasma membrane (Jacobson and Branton, 1977). Sigma-Aldrich offers PLLs in different size ranges, from which 1-5 kDa and 4-15 kDa were selected. Their relatively small size should account for OC penetration, and interaction with membranes for their endocytic uptake.

To analyze the capability of these dyes as endocytosis markers, OCs were incubated at RT with PLL-Atto 647N conjugates and imaged under an upright confocal microscope. Surprisingly, 1-5 kDa PLL-Atto 647N labeling was very similar to that seen with FM dyes. IHCs cytoplasm was strongly labeled, with much higher fluorescence levels than the surrounding cells. 4-15 kDa PLL-Atto 647N gave a dimmer staining than its smaller counterpart, with fluorescent signal inside IHCs but also with clearly labeled plasma membranes not only from IHCs but also from the synaptic boutons at their base, and other cells types like pillar cells (Figure 3.3 A left panels).

The main explanation for the strong labeling with 1-5 kDa PLL-Atto 647N is that smaller PLL species (below 1 kDa) could be present in the mixture as conjugates and permeate the MET channels. According to the manufacturer's specifications, provided PLL mixtures are purified through a viscosity-based selection procedure that does not ensure a sharp cut off of molecular sizes. To solve this difficulty I proceeded dialyzing the PLL-Atto 647N conjugates with a 3.5 kDa exclusion membrane for the 1-5 kDa variant and a 6-8 kDa exclusion membrane for the 4-15 kDa one. When dialysis products were applied to OCs, the 1-5 kDa PLL-Atto 647N (now from 3.5 kDa up) gave a similar staining to the undialyzed 4-15 variant although stronger. The dialyzed 4-15 variant (now from 6 kDa up) gave a very weak staining, indicating that molecules larger than 6 kDa have difficulties to penetrate into the OC, making impossible the labeling of endocytosis at IHCs and giving a very weak inhomogeneous signal (Figure 3.3 A middle panels).

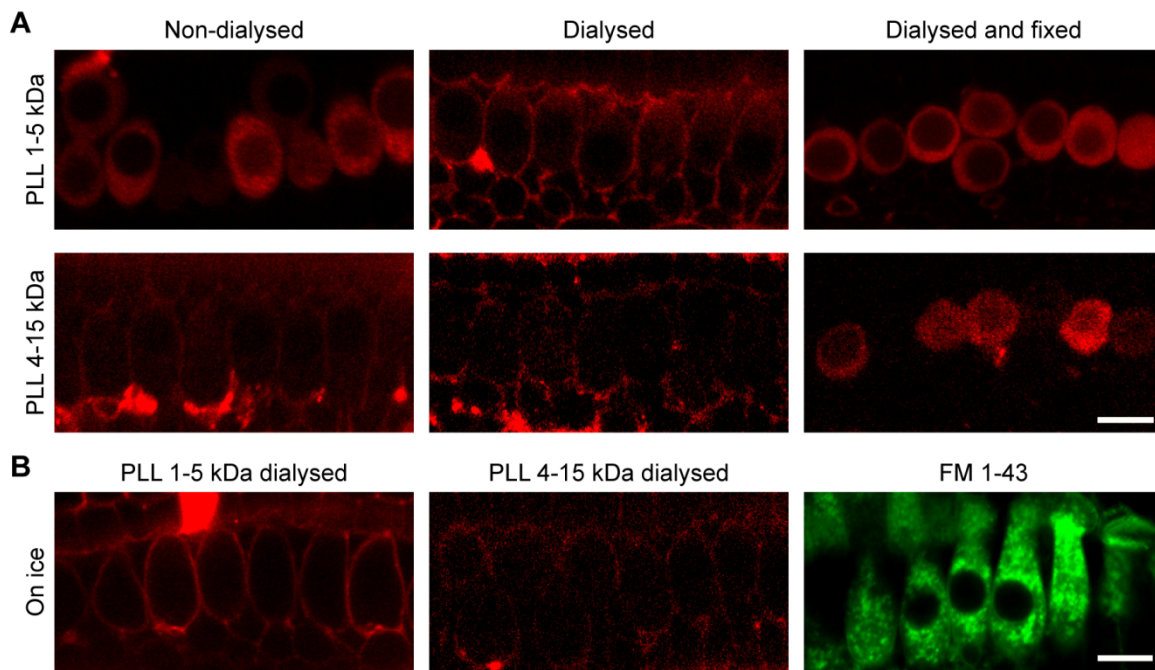


**Figure 3.3 PLL molecules conjugated to Atto 647N do not fix to membranes.**

**A.** Commercial 1-5 kDa and 4-15 kDa PLL mixtures contain small polymer species that permeate IHC MET channels. **Left panels**, OCs incubated at RT with Atto 647N-conjugated PLLs and imaged under confocal microscopy. The 1-5 kDa mixture labels IHCs in a similar way to FM dyes. **Middle panels**, Atto 647N-PLL mixtures were dialyzed and evaluated on IHCs showing a moderate labeling pattern. **Right panels**, OCs were fixed with a PFA/glutaraldehyde solution after labeling with dialyzed products. The strong labeling of IHCs suggest that Atto 647N-PLLs conjugates cannot be properly fixed **B.** OCs were incubated with dialyzed products and imaged at low temperature conditions. The lack of labeling inside IHCs indicates no permeation of MET channels and real endocytic nature of fluorescence seen in the middle panels of A. IHCs incubated with FM 1-43 at low temperature are presented for comparison. Scale bars, 10  $\mu$ m.

When OCs were incubated with dialyzed products and later fixed with a 4% PFA + 0.2% glutaraldehyde solution, very strong labeling was seen in IHCs cytoplasm for both the small and the large PLL variants (Figure 3.3A right panels). The most feasible explanation for these results is that PLL molecules are not as fixable as thought initially, probably due to preferential cis-crosslinking of amino groups of the same molecule over trans-crosslinking with proteins at the membrane. Moreover, in the conjugation protocol I used it is difficult to control the amount of Atto 647N molecules that covalently bind to the amine groups of the PLL molecule, likely making many of those groups unavailable for aldehyde fixation. Another factor that would add up to the strong post-fixation staining is the fact that the readily exposed membrane region of IHCs, the hair bundle, preferentially concentrated a large amount of PLL-Atto 647 conjugates, making them difficult to fix and prone to migrate into the cells during fixation. It is not clear however why the dye concentration happens exclusively inside IHCs.

Interestingly, incubations of living IHCs with dialyzed Atto 647N-conjugated PLLs at low temperature showed that the probes stay at the plasma membranes with no labeling inside IHCs (Figure 3.3B). This indicates that fluorescent signals seen inside IHCs at RT (Figure 3.3A middle panel) was endocytosis-dependent.

The presented data suggest that the product obtained from dialyzing 1-5 kDa PLL Atto 647N conjugates could be used as endocytosis tracer in IHC live experiments, but it cannot be used for fixation and immunostaining assays. Moreover, I can conclude that using labeled lysine polymers is a valid direction towards the generation of the ideal endocytosis marker. However, their fixability and penetration need to be improved by: ensuring conjugation of one polymer molecule with only one fluorophore molecule; improving their membrane binding capacity by adding a lipid tail; and reducing their size to a range between 1 and 6 kDa.

### **3.2.3 mCLING, a novel membrane-binding fluorescent probe**

#### **3.2.3.1 Design and validation of mCLING**

Taking into account the results of the previous section, a new molecule was designed that contained a seven-lysine polymer for easing aldehyde fixation, one palmitoyl tail for binding to cell membranes, and one molecule of the fluorescent dye Atto 647N conjugated to a cysteine residue through a maleimide group. This molecule was called mCLING (membrane-binding fluorophore-Cysteine-Lysine-Palmitoyl Group). Its structure was suggested by my supervisor, Prof. Silvio O. Rizzoli, and its synthesis was carried out in the laboratories of Synaptic Systems GmbH, Göttingen, Germany. mCLING has a molecular weight of 2056 Da, including the Atto 647N moiety, being 4 to 5 times larger than FM 1-43 (Figure 3.4A). A great advantage of its modular design is that mCLING fluorescence properties can be easily adjusted to the experimenter's needs, by replacing the Atto 647N molecule with any fluorophore available with a maleimide group.

A series of experiments were conducted in order to validate mCLING as a probe that readily labels endocytosed organelles and is innocuous for the cells. One important step in the establishment of a labeling protocol with mCLING was the determination of a working concentration. To this end, the lyophilized conjugation product was resuspended in PBS and its concentration was established using a fluorescence vs concentration linear regression curve. The latter was obtained from a dilution series of an Atto 647N-conjugated DNA oligomer solution of known concentration labeling ration (1 dye molecule : 1 oligomer

molecule). Concentrations between 0.2 and 0.4  $\mu\text{M}$  mCLING were found to offer sufficiently strong signal for fluorescence microscopy when tested in cultured cells.

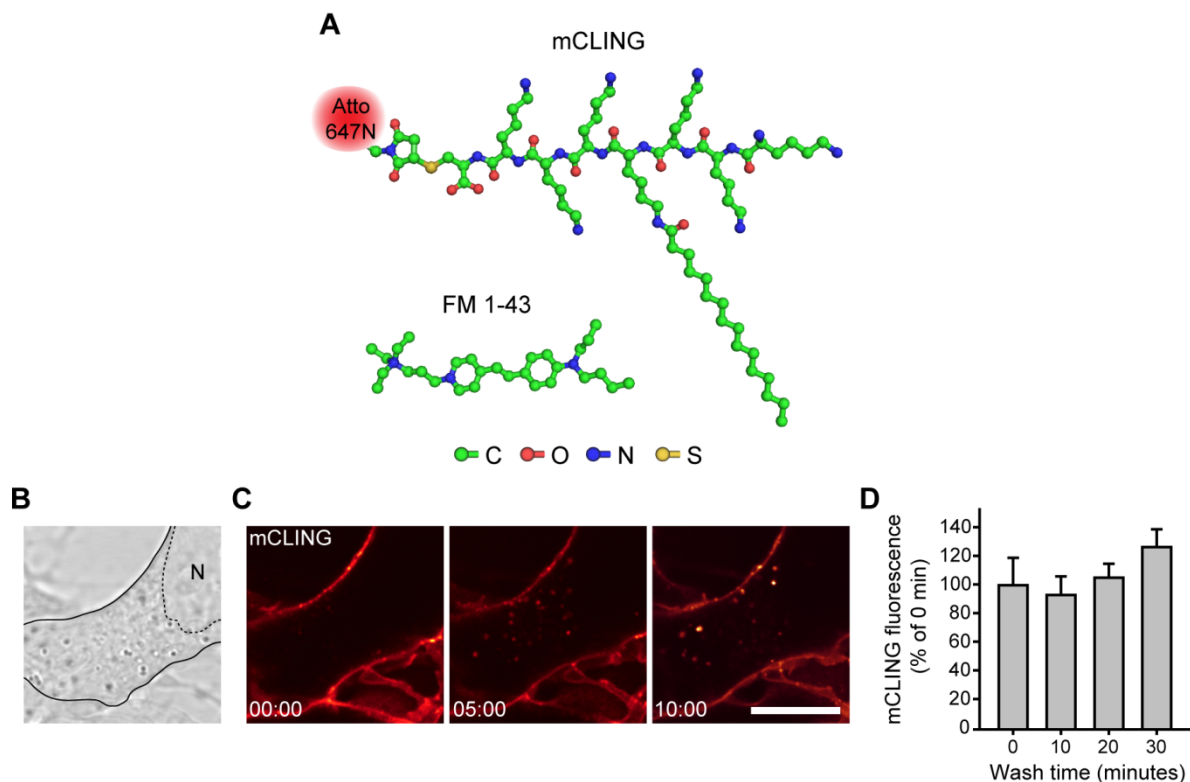


**Figure 3.4 mCLING, a novel probe that successfully labels endocytosis.**

**A.** mCLING molecular structure. In this study the core components were coupled via a maleimide group to an Atto 647N molecule, but this could be exchanged by other fluorophores with maleimide modifications. The structure of the styryl dye FM 1-43 is presented for comparison. **B.** Outline of a cultured COS7 cell in bright-field microscopy (solid line). N marks the nucleus (dashed outline). **C.** The cell in B. was incubated with 0.2  $\mu\text{M}$  mCLING in Ringer's buffer. mCLING homogeneously labeled the plasmalemma and was taken up into endocytic organelles. Confocal images were taken immediately after applying the probe to the cells (left panel), at 5 minutes after application (middle panel) and at 10 minutes after application (right panel). Scale bar, 10  $\mu\text{m}$ . **D.** mCLING wash-off kinetics. COS7 cells were incubated with 0.2  $\mu\text{M}$  mCLING for 5 minutes, and then washed for different time periods. Bars represent mean fluorescence intensity normalized to first imaging point  $\pm$  SEM. 24 to 28 cells were evaluated for every incubation time point. Note that mCLING is only slowly washed-off the membranes.

mCLING was then applied to living COS7 cells and imaged under confocal microscopy. Plasma membrane labeling was homogeneous, probably due to its relatively small size. A few minutes after incubation onset, round bright organelles were seen freely moving inside the cells, indicating successful mCLING uptake along with endocytic events (Figure 3.4B). In contrast to styryl dyes of the FM family, mCLING is not washable and stays on plasma membranes of living cells, even after 30 minutes of incubation (Figure 3.4C). These results confirm that mCLING is a suitable tool for tracing endocytosis in cultured cells.

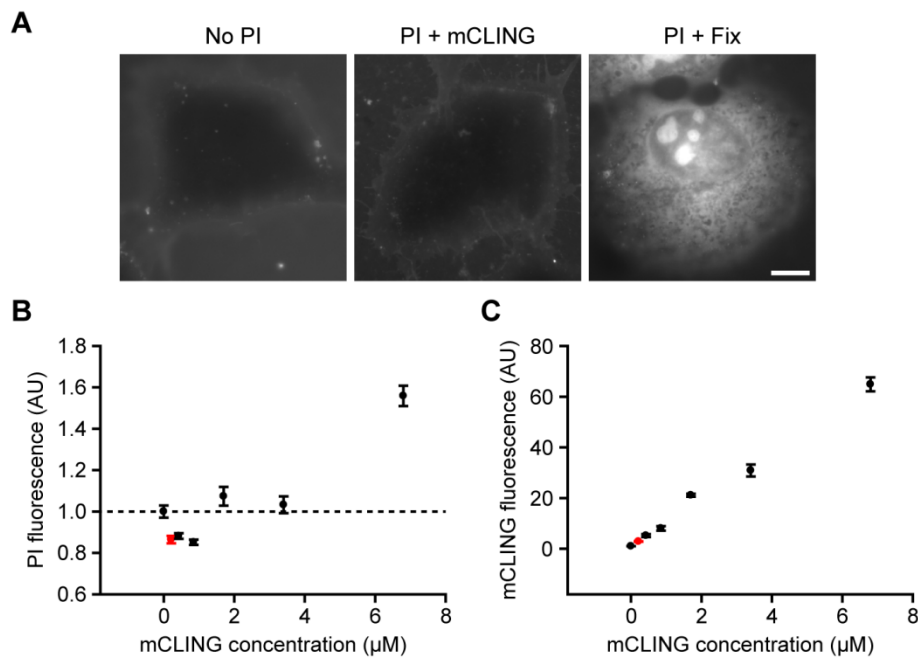


**Figure 3.5 mCLING is not toxic for cells at working concentrations for membrane labeling.**

**A.** PI-based viability assay. Background fluorescence intensity in a control cell (no PI, **left panel**) is shown for comparison. Intact cells have low PI fluorescence values, comparable to those at control situation; a 0.2  $\mu\text{M}$  mCLING-treated cell is shown as example of a viable cell (**middle panel**). Cells with disrupted membranes will allow PI to penetrate, showing high PI fluorescent values due to its binding to nucleic acids in the nucleus and cytoplasm; to represent this situation membrane pores for PI diffusion were induced in the plasma membrane of cells by aldehyde fixation (**right panel**). Scale bar, 10  $\mu\text{m}$ . **B.** mCLING toxicity was evaluated based on a PI viability assay. COS7 cells were labeled with different amounts of mCLING (in  $\mu\text{M}$ : 0, 0.21, 0.42, 0.85, 1.7, 3.4, 6.8), washed and then incubated with PI. After treatment, cells were imaged in an epifluorescence Nikon microscope. Quantification of the average PI fluorescence was normalized to the control treatment (no mCLING), as a function of mCLING fluorescence. PI fluorescence only increases above the cellular autofluorescence when mCLING surpasses 5  $\mu\text{M}$ . The red dot indicates the concentration of mCLING I used in cellular experiments (0.2  $\mu\text{M}$ ). Data are plotted as normalized mean fluorescence  $\pm$  SEM. **C.** Plot of mCLING fluorescence, in the same experiment. Data are plotted as mean fluorescence  $\pm$  SEM.

As next step, a cell viability assay based on nuclear staining with the DNA-intercalating agent propidium iodide (PI) was established to determine at what concentration mCLING becomes harmful for the cells, and what range of concentrations can be considered for future applications, e.g. endocytosis tracing in complex tissues (Figure 3.5A). COS7 cells were incubated in increasing concentrations of mCLING, washed and subsequently incubated with PI. As expected, high concentrations of mCLING caused cell damage and membrane lysis, due to a “detergent” effect exerted by its palmitoyl tail. While working concentrations (between 0.2 and 0.4  $\mu\text{M}$ ) did not have a negative impact on the cells, evidenced by PI fluorescence values comparable to control conditions (no mCLING). A concentration of 6.8  $\mu\text{M}$  was found to significantly increase PI fluorescence (Figure 3.5B, C).

With the PI assay I confirmed that low concentrations of mCLING do not affect the plasma membrane integrity. This assay, however, does not provide information on the effects of mCLING on cell physiology and the general membrane trafficking dynamics. To address this issue I performed an assay to evaluate the effects of mCLING on endosomal trafficking using transferrin as a marker. Transferrin is a protein important for iron systemic distribution and delivery to cells. The transferrin receptor is constitutively endocytosed via CME, and delivered to early/sorting endosomes. When a retrieved receptor is bound to diferric transferrin, loaded iron is released from transferrin by the lower pH of the endosome compartment. Then the receptor still bound to transferrin is recycled back to the plasma membrane (Maxfield and McGraw, 2004; Leonard et al., 2008).

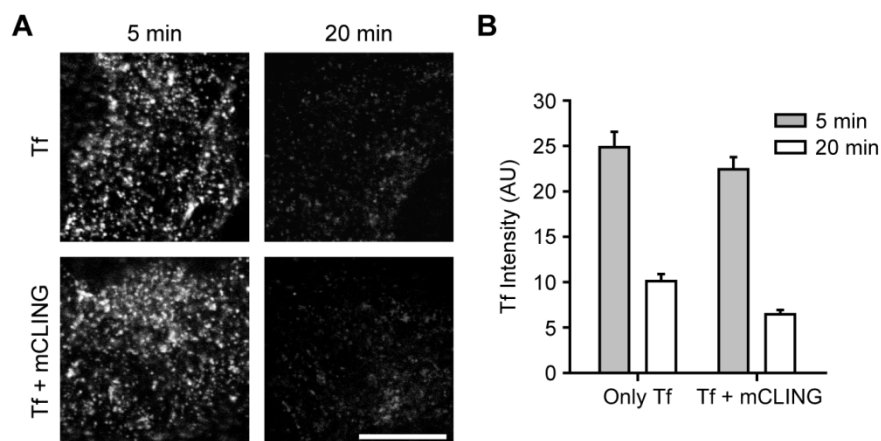


**Figure 3.6 mCLING does not affect endosomal traffic in COS7 cells.**

**A.** COS7 cells were incubated with Alexa 546-Transferrin in presence or absence of mCLING for 5 minutes to allow their uptake. Alternatively, incubation was followed by a 20-minute period at 37°C to allow receptor recycling. The images in the **upper panels** show that in control cells transferrin is endocytosed within 5 minutes. If incubated for further 20 minutes (in absence of transferrin) the endocytosed transferrin can be recycled back to the plasma membrane and washed off as evidenced by the reduction in fluorescence. The **lower panels** show that uptake and recycling are unaltered when mCLING is added during the initial 5-minute incubation period. Scale bar, 10  $\mu$ m. **B.** Quantification of Alexa 546-transferrin fluorescence levels after uptake (5 minutes, gray bars) or after traffic-dependent release (20 minutes, white bars) in mCLING-treated and untreated cells. Note that both transferrin uptake and release are normal in presence of mCLING, when compared to control cells. Error bars represent mean fluorescence intensity  $\pm$  SEM for 40 to 44 cells per condition.

In this assay COS7 cells were simultaneously incubated with mCLING and Alexa 546-Transferrin at 37°C, to allow their uptake by endocytosis. Control cells were only incubated with Alexa 546-Transferrin. After 5 minutes, cells were washed with Ringer's buffer and fixed directly (4% PFA plus 0.2% glutaraldehyde) to assess the levels of transferrin uptake. Alternatively, the 5-minute incubation period was followed by a 20-minute incubation in mCLING- and transferrin-free Ringer's buffer at 37°C, wash and fixation. During those 20

minutes, transferrin receptors are expected to be recycled back to the plasma membrane releasing Alexa 546-transferrin molecules that can be then washed off. A comparison of the average Alexa 546 fluorescence intensity levels shows that mCLING does not affect transferrin uptake or its recycling towards the plasma membrane. These results confirm that mCLING does not have negative effects on cellular processes of membrane traffic (Figure 3.6).

### **3.2.3.2 mCLING is superior in fixability to commercially available probes**

Additional validation of mCLING as endocytosis marker required its comparison to customarily used membrane probes. Here I used FM dyes as reference to evaluate mCLING uptake and fixability. As shown in Table 3.1, fixable versions of FM dyes are also available in the market. They typically carry an extra amine group in their polar head to offer a crosslinking target for aldehyde fixatives.

Living COS7 cells were simultaneously incubated with mCLING and FM 1-43 and imaged with conventional fluorescence microscopy. The labeling pattern of mCLING was identical to that of FM 1-43, seen by good localization of both fluorescence signals in endocytosed organelles (Figure 3.7A). This observation confirms that mCLING indeed reports endocytosis and that it can be introduced to target the same endocytic processes studied before with FM dyes.



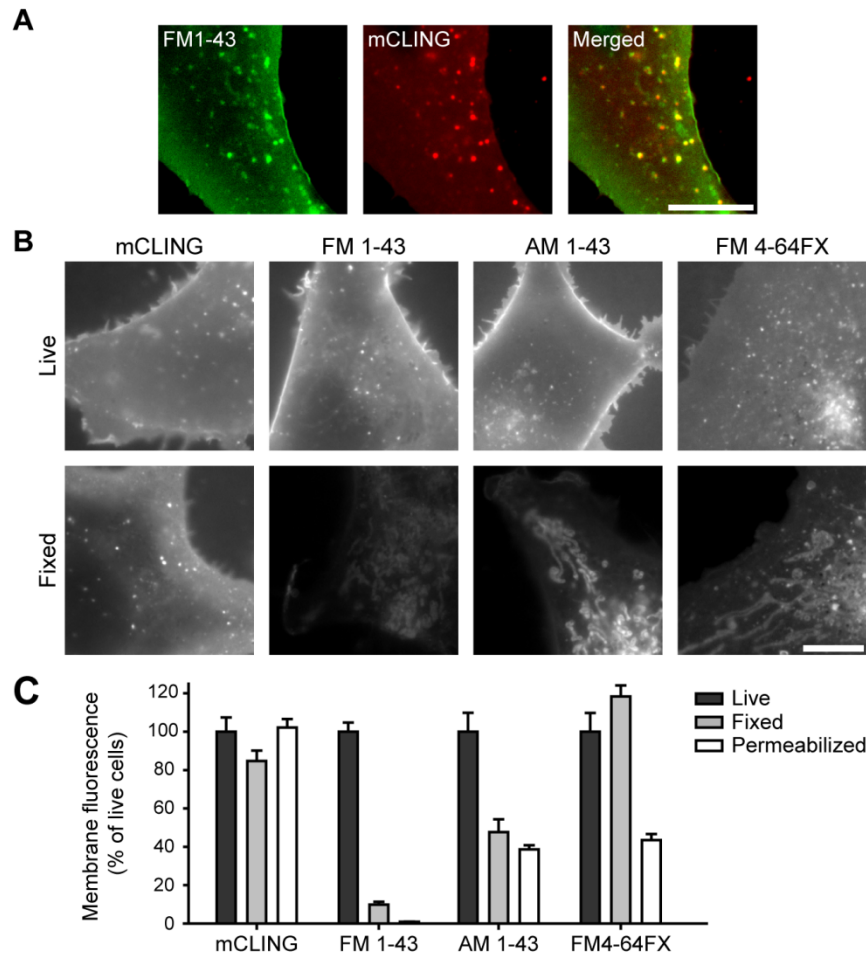


**Figure 3.7 In contrast to fixable FM dyes, mCLING labeling is preserved after permeabilization.**

**A.** Epifluorescence imaging of living COS7 cells co-incubated for 5 minutes with 5  $\mu$ M FM 1-43 and 0.2  $\mu$ M mCLING. Intracellular organelles containing both fluorescent signals confirm mCLING uptake by similar endocytic processes as for FM 1-43. Scale bar, 10  $\mu$ m. **B.** Comparison between live (upper panels) and fixed (lower panels) COS7 cells, incubated with mCLING, FM 1-43, AM 1-43, and FM 4-64FX. Endocytosis and labeling of membranes was similar for all dyes in living cells. During fixation FM dyes were disengaged from the membranes and mobilized into organelles resembling mitochondria. In contrast, mCLING remained attached to the original cellular membranes that it labeled in living cells. Scale bars, 10  $\mu$ m. **C.** Evaluation of the same four dyes by quantification of their fluorescence intensity in living, fixed, or fixed and permeabilized cells. Error bars represent mean fluorescence intensity normalized to the live values  $\pm$  SEM from 21 to 37 cells per condition.

mCLING labeling in living cells was comparable to that of AM 1-43 (fixable version of FM 1-43) and FM 4-64FX (fixable version of FM 4-64). Plasma membrane was homogeneously labeled and endocytosed organelles were seen inside the cells. However, once the cells were fixed the advantage of mCLING was evident. While mCLING remained bound to membranes and inside organelles, FM dyes were mobilized from their original locations and ended up concentrated in structures resembling mitochondria (Figure 3.7B).

In order to confirm this observation fluorescence levels were quantified in live, fixed or fixed and permeabilized cells for the different dyes. Areas around the nucleus, where the artifactual mitochondrial staining was present, were avoided and only membranes and organelles at the cell periphery were taken into account. mCLING labeling was preserved even after fixation and permeabilization, which goes in line with the slow wash-off kinetics described in Figure 3.4D. In contrast, FM dye labeling was strongly affected. FM 1-43 was almost completely lost after fixation and permeabilization. AM 1-43 fluorescence was reduced by more than 50% already after fixation. FM 4-64FX labeling, although preserved in membranes and organelles after fixation, was also inside mitochondria-like structures, and reduced to ~50% after permeabilization (Figure 3.7C). Hence, although fixable FM dyes were better preserved than FM 1-43 upon fixation, their labeling is not reliable and they still cannot be combined with immunostaining procedures.

These results suggest that first, one amine moiety (as in AM 1-43 and FM 4-64FX) is not enough to provide optimal fixability, and second, that efficient fixability indeed requires the combination of several amine groups with a strong membrane binding capacity as in the mCLING structure. Therefore, I conclude that mCLING is likely the only available membrane-binding probe that is optimally fixable and therefore compatible with later immunostaining.

### **3.2.3.3 mCLING is taken up into organelles involved in ligand trafficking**

An important requirement for a general endocytosis marker is that its structure and interaction with the plasma membrane do not hinder its uptake by any of the naturally occurring endocytic events. Hence, mCLING uptake was further characterized to assess whether it can be endocytosed along with receptor ligands commonly used as endocytosis and endosomal trafficking markers.

Transferrin (Tf), low-density lipoprotein (LDL) and Epidermal Growth Factor (EGF) were selected as receptor ligands due to their wide use in endocytosis research and their essential role in cell function. Upon receptor binding, all three ligands are endocytosed by CME. However, EGF can be also endocytosed by alternative dynamin-dependent pathways not completely understood. Within a few minutes (3 to 6) after uptake ligands are delivered by the endocytic vesicles to the early endosomal compartments (Leonard et al., 2008; Barysch et al., 2009; Henriksen et al., 2013).

Fluorescently labeled variants of these three ligands, Alexa546-Tf, DiI-LDL, and

tetramethylrhodamine EGF (TMR-EGF), were incubated in combination with mCLING on COS7 cells for 5 minutes at 37°C. Epifluorescence imaging of living cells showed that essentially all organelles labeled with any of the three markers colocalized with mCLING signal. Moreover, some of the mCLING-labeled organelles did not carry the ligand signal, confirming that mCLING labels different endocytic processes (Figure 3.8A). In another set of experiments, cells were fixed (4% PFA and 0.2% glutaraldehyde) after the initial 5-minute labeling period and imaged under confocal microscopy. Images revealed similar results to the live condition, with most ligand-labeled organelles carrying mCLING as well (Figure 3.8B). These results confirm that mCLING can be used along with the standard protocols used for ligand labeling. Finally, cells labeled with either EGF or Tf in combination with mCLING were fixed, permeabilized (0.5% Triton-X 100 and 2.5% BSA) and immunostained for the endosomal marker Syntaxin 6 (Sx 6). Confocal microscopy images revealed organelles bearing the three signals from ligand, mCLING and Sx 6, confirming that mCLING remains bound to membranes even after permeabilization (Figure 3.8C). Due to its poor fixability, LDL signal was lost after permeabilization and therefore could not be included in this last assay.

In summary, mCLING is indistinctly retrieved from the plasma membrane by different endocytic processes normally occurring in a healthy cell. Furthermore, I confirmed that, due to its fixability, mCLING has a marked potential in studies requiring determination of the molecular identity of recycling organelles.

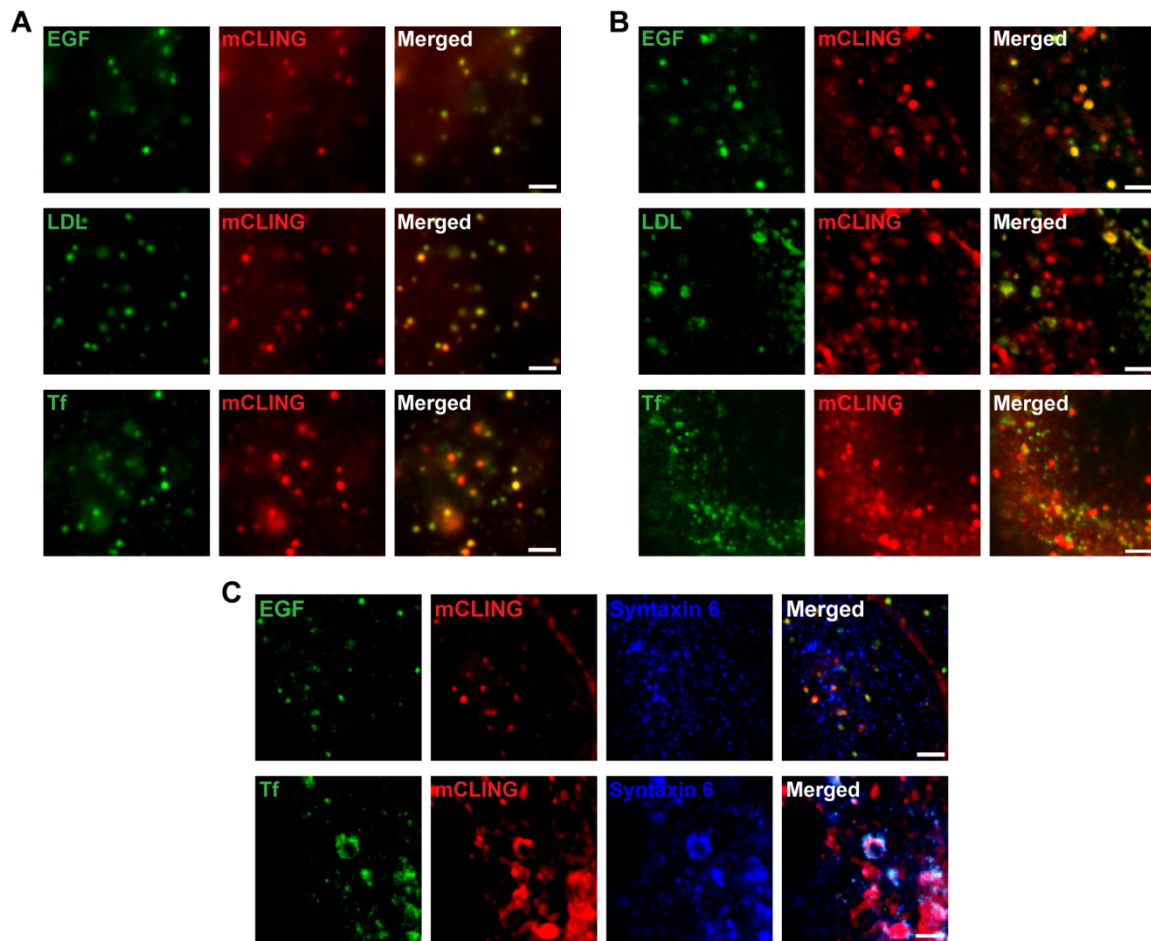


**Figure 3.8 mCLING labels endocytic organelles involved in ligand trafficking.**

**A.** COS7 cells were incubated during 5 minutes at 37°C with fluorescently-labeled Tf, LDL or EGF in presence of mCLING. Afterwards, living cells were imaged with a conventional epifluorescence microscope. Colocalization with mCLING is observed for all tested ligands. **B.** The correlation of mCLING with the ligands is also evident in fixed cells. Images were acquired in confocal microscopy. **C.** mCLING fixability was tested by permeabilization and immunostaining after fixation. Cells labeled with mCLING and transferrin or EGF were stained for the endosomal SNARE protein Syntaxin 6. Note the correlation of mCLING not only with the ligand labeling but also with the endosomal marker. (LDL was not used due to its poor signal after permeabilization). Scale bars, 2  $\mu$ m.

## 3.3 mCLING elucidates membrane trafficking pathways in IHCs

### 3.3.1 Challenges in the study of endocytic events in IHCs

To this point, the evidence collected in cultured cells confirms that mCLING outstands when compared to the traditionally used membrane-binding probes. mCLING is a non-toxic fixable endocytosis marker that offers a new way to look at the nature of recycling organelles.

The next obvious challenge for mCLING labeling was its application to complex tissues, where probe diffusion and penetration can be easily limited. As already in section 3.1.1 I explained that mCLING design was first called for by the difficulty of studying synaptic vesicle recycling in the auditory inner hair cells (IHCs), which are embedded in the very specialized and complex epithelium called the Organ of Corti (OC).

The study of membrane trafficking pathways in IHCs is not only challenged by the presence of mechanotransduction channels (MET) that allow the passage of small dye molecules (see section 3.1.1 and 3.2.1). The anatomy of IHCs also difficulties the separate study of synaptic vesicle recycling from the constitutive (housekeeping) membrane trafficking pathways (e.g. ER-to-Golgi transport, receptor endocytosis and endosomal trafficking). Most neurotransmitter-releasing cells, like neurons of the central and peripheral nervous systems or photoreceptors in the retina, enclose the processes of SV release and recycling in a compartment called nerve terminal or presynaptic bouton. Usually those boutons are anatomically separated from the cell soma and connected to it by a conveying process called fiber or axon (Heuser and Reese, 1973; Schaeffer and Raviola, 1978; Südhof, 2004; Bear et al., 2006). In contrast, IHCs managed to evolve an extremely efficient synaptic machinery in the “premises” of the cell soma, without developing a synaptic bouton. Thus, the specialized ribbon-type active zones that characterize IHCs can be found from the plasma membrane surrounding the cell nucleus to the cell base (Smith and Sjöstrand, 1961; Uthaiyah and Hudspeth, 2010). A practical implication is that once a general endocytosis marker is applied, it is difficult to know whether it has been taken up by a compartment of the synaptic machinery, or one of a constitutive pathway, as they share the same cytoplasmic volume.

Therefore, the study of membrane trafficking in IHCs requires the use of a relatively large probe that does not permeate the MET channels at the IHC stereocilia bundle, and that is

fixable to allow molecular identification of endocytosed structures by later immunolabeling.

### 3.3.2 mCLING does not permeate the MET channels of IHCs

mCLING penetration into the organ of Corti and its permeation through MET channels of IHCs were evaluated. The apical turn of the organ of Corti dissected from 14-18 day old wild type mice (substrains C57BL/6N, C57Bl/6J) was incubated with a 1.7  $\mu\text{M}$  solution of mCLING in HBSS without  $\text{Ca}^{2+}$ . Organs were imaged under an upright confocal microscope, focusing on the IHCs. The apical stereocilia bundle, which is the most exposed membrane of IHCs, was strongly labeled by mCLING (Figure 3.9, in red). However, and unlike FM 1-43 (green insets), mCLING did not rapidly and diffusely stain the cytoplasmic compartment of IHCs. In contrast to FM 1-43 labeling, which is dense from the top to the base of the cells, mCLING labeled only a few organelles inside the cells, visible at the top, nuclear and basal cellular levels. Moreover, mCLING was also seen to reach the IHC plasma membrane from the bottom side of the organ of Corti, evidenced by the labeling of synaptic efferent and afferent terminals located at the base of IHCs. These results indicate that mCLING does not pass through the apical channels of IHCs and that it seems to be taken up into endocytosed organelles.

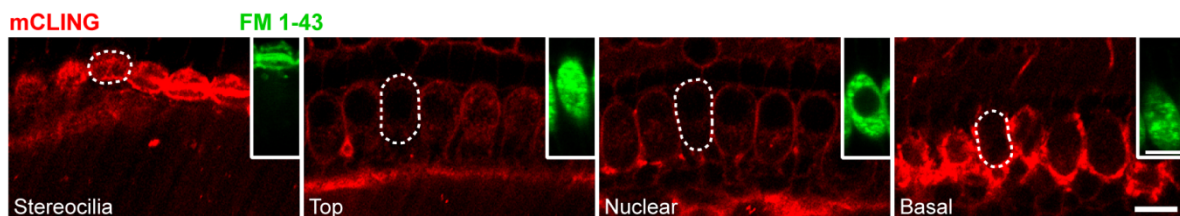


**Figure 3.9 mCLING does not permeate the MET channels of living IHCs.**

The apical turn of the mouse organ of Corti was incubated for 3 minutes with mCLING (1.7  $\mu\text{M}$ ) and imaged under confocal microscopy. Images at four different cell levels of a row of living IHCs were acquired: at the stereocilia bundle, at the cell top (supranuclear compartment), at the nuclear level, and at the basal level (infranuclear compartment). Although mCLING was found inside the cells, its labeling was not as diffuse and strong as for FM 1-43 (green, insets), suggesting that the mCLING-labeled structures are presumably endocytic organelles. Contrary to FM 1-43, mCLING does not seem to penetrate the MET channels of IHCs. The dashed line in every panel shows the profile of one IHC at the four different imaged planes. Scale bars, 10  $\mu\text{m}$ .

### 3.3.3 mCLING labeling and sample processing for the study of recycling organelles in IHCs at nano-resolution

The images shown in Figure 3.9 strongly suggest that with mCLING a novel endocytosis marker that fulfills the requirement of IHCs has been found. However, achieving a detailed

study on membrane recycling organelles in IHCs meets other limitations:

- The organ of Corti is a thick and complex tissue, where IHCs are surrounded by cells of other types (e.g. pillar cells and supporting cells), and covered on the apical side by the tectorial membrane. Although confocal microscopy has been useful to study the general labeling pattern of IHCs, endocytosis processes at smaller scales would be difficult to see.
- The accumulation of mCLING at the plasma membrane gives a strong fluorescence signal that could mask the weaker signal coming from small endocytosed organelles, even in confocal imaging.
- Electron microscopy studies have associated several types of organelles to synaptic vesicle recycling in IHCs: synaptic vesicles of 31 nm average diameter, larger clathrin-coated vesicles of 54 nm average diameter, and large cisternae of around 100 to 200 nm that resemble bulk endocytosis (Lenzi et al., 2002; Kamin et al., 2014; Neef et al., 2014). Additionally, other structures that are presumably involved in constitutive membrane recycling include tubular structures with profiles of a few tens of nanometers distributed at the cell top and nuclear levels, as well as vesicles endocytosed right below the cuticular plate with sizes below 100 nm (Kachar et al., 1997; Spicer et al., 1999; Kamin et al., 2014). The small size of these structures, many times far below the Abbe's diffraction barrier of light (200-300 nm), requires the implementation of a high-resolution fluorescence microscopy method.

These three difficulties were addressed by the implementation of an adapted protocol for sample preparation and imaging, described in the Methods section (2.2.5.1 and 2.2.5.2). A way to simplify the study of the organ of Corti and circumvent the first and second problems described above was to embed the mCLING-labeled organ of Corti in a water-based resin called melamine. When prepared, melamine resin is liquid and transparent, which is convenient for sample embedding and deep tissue penetration. After heating it up in steps of increasing temperature, melamine hardens and can be cut into sections as thin as 20 to 200 nm with a conventional ultramicrotome. These sections offer a clearer view of single organelles and bring the advantage of avoiding scattering background fluorescence from other planes of the sample, or bleaching fluorophores in the areas adjacent to the focal plane. Hence, different volumes of the cells can be imaged independently with increased detail. Additionally, melamine is non-fluorescent and due to its hydrophilic properties does not require sample dehydration, therefore offering good ultrastructure preservation (Punge

et al., 2008; Punge, 2009).

For studying organelles with sizes below the sub-diffraction limit, presented above as the third limitation, I relied on our laboratory expertise implementing high-resolution stimulated emission depletion (STED) microscopy to different biological preparations. Our laboratory has successfully used STED to study endosomal and synaptic vesicle trafficking in cultured cells and neurons (Barysch et al., 2009; Hoopmann et al., 2010; Opazo et al., 2010). As explained in the Introduction (section 1.4), in this technique the sample is illuminated with an excitation beam and a doughnut-shaped depletion beam spatially overlapped. As a result, in the doughnut center, where only the excitation light is present, photons will be collected as in conventional fluorescence microscopy. However, in the doughnut border, where both beams coincide, fluorophores will be excited and then stimulated by the depletion beam to emit photons at longer wavelengths than usual, far from the fluorescence detection window (Klar et al., 2000). In this way, the effective excitation volume is modulated to achieve resolutions 16-fold higher in the planar axis than its confocal counterparts (Hoopmann et al., 2010). Moreover, STED microscopy is convenient over other high-resolution light microscopy techniques, because it instantly delivers sub-diffraction images without relying on further computational processing (Klar et al., 2000; Hell, 2007).

One limitation of commercial STED setups, like the one I used for this study, is that resolution improvement is only achieved in the X-Y plane, while in the axial direction resolution is similar to that of conventional light microscopy (500-600 nm). Fortunately, this drawback is compensated for by the sectioning of the melamine embedded samples. Altogether, while STED microscopy provides lateral high-resolved images, melamine sectioning offers increased axial resolution, which can actually be modulated by the cutting thickness (See Figure 2.2).

Since one of the main objectives of this study is to characterize synaptic vesicle recycling in IHCs, an adequate stimulation protocol was necessary. Previous studies have used  $K^+$  solutions at concentrations ranging from 30 to 80 mM with stimulation periods between 10 and 30 minutes. We estimated that such incubation times are typically long and not comparable with the physiological situation. In a previous electron microscopy study we found that incubation of the OC in a 65 mM  $K^+$  solution for 1 minute, was enough to trigger important membrane recycling processes in IHCs (Kamin et al., 2014). With the present study I would like to not only confirm those results by high-resolution fluorescence microscopy, but also extend them with information on the molecular/organelar identity of



the recycling structures.

I proceeded incubating OCs with 1.7  $\mu\text{M}$  mCLING for 1 minute. OCs were then fixed, embedded in melamine, and cut into 200 nm sections. When these sections were studied under epifluorescence microscopy, I found that mCLING penetration was poor, sometimes getting trapped in extracellular structures like the tectorial membrane (Figure 3.10A), or reaching only the membrane surrounding the hair bundle at the cell top, or the cell base with its neighboring afferents (Figure 3.10B). Extending the incubation period to 2-3 minutes ensured good mCLING penetration and endocytic uptake, as seen in the following results sections. When stimulation was required, high  $\text{K}^+$  was applied only in the last minute.

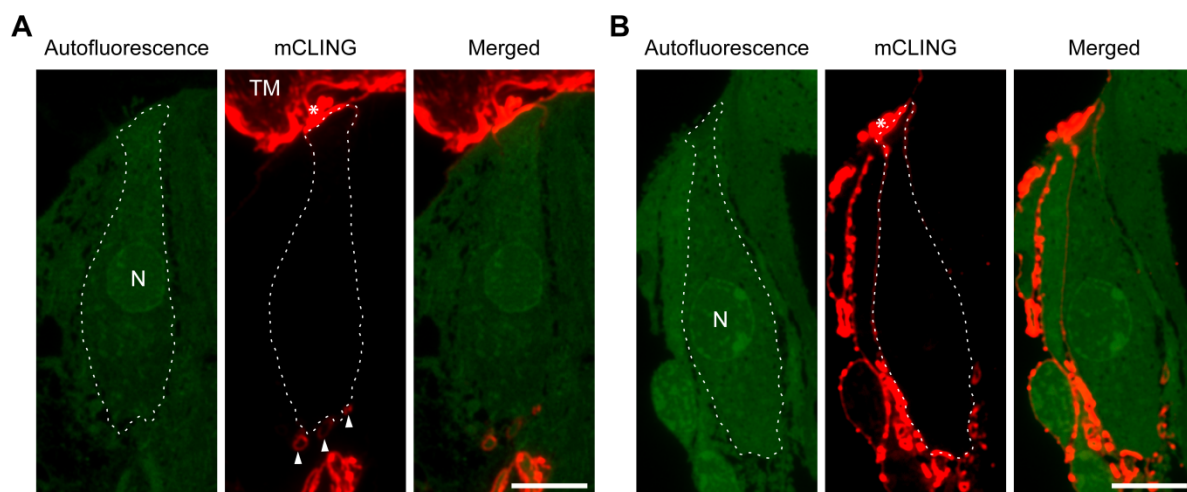


**Figure 3.10 A 1-minute incubation period is not long enough for mCLING to penetrate into OCs and label IHCs homogeneously.**

Organs of Corti were incubated with 1.7  $\mu\text{M}$  mCLING solution for 1 minute, fixed with 4% PFA and 0.2% glutaraldehyde, embedded in melamine resin and cut into 200 nm thick sections. Sections were imaged in epifluorescence microscopy. mCLING is shown in red. An autofluorescence picture (FITC channel in green) is presented as aid to determine the IHCs outline. **A.** pictures an example in which mCLING is retained by the tectorial membrane (TM), reaching only the hair bundle at the IHC apical pole (white asterisk). At the cell base mCLING labeled some of the synaptic terminals (white arrowheads), confirming that it can also diffuse from the OC bottom. **B.** shows a case in which mCLING had better penetration into the OC but could not be taken up by endocytosis, evidenced by the absence of labeled organelles inside the IHC. These pictures also prove that even when mCLING reaches the hair bundle, it does not permeate the MET channels, since no apical staining is present.

### 3.3.4 mCLING uptake is endocytosis-dependent and therefore inhibited by low temperature

A final test was performed to verify that mCLING labeling inside IHCs, as seen in Figure 3.9, is indeed occurring via probe uptake through endocytic events. Using the improved labeling

protocol, OCs were incubated during 3 minutes with 1.7  $\mu\text{M}$  mCLING in HBSS without  $\text{Ca}^{2+}$ , either at physiological temperature (37°C) or on ice (2-4°C). After fixation and melamine embedding, OCs were cut into 200 nm sections and imaged.

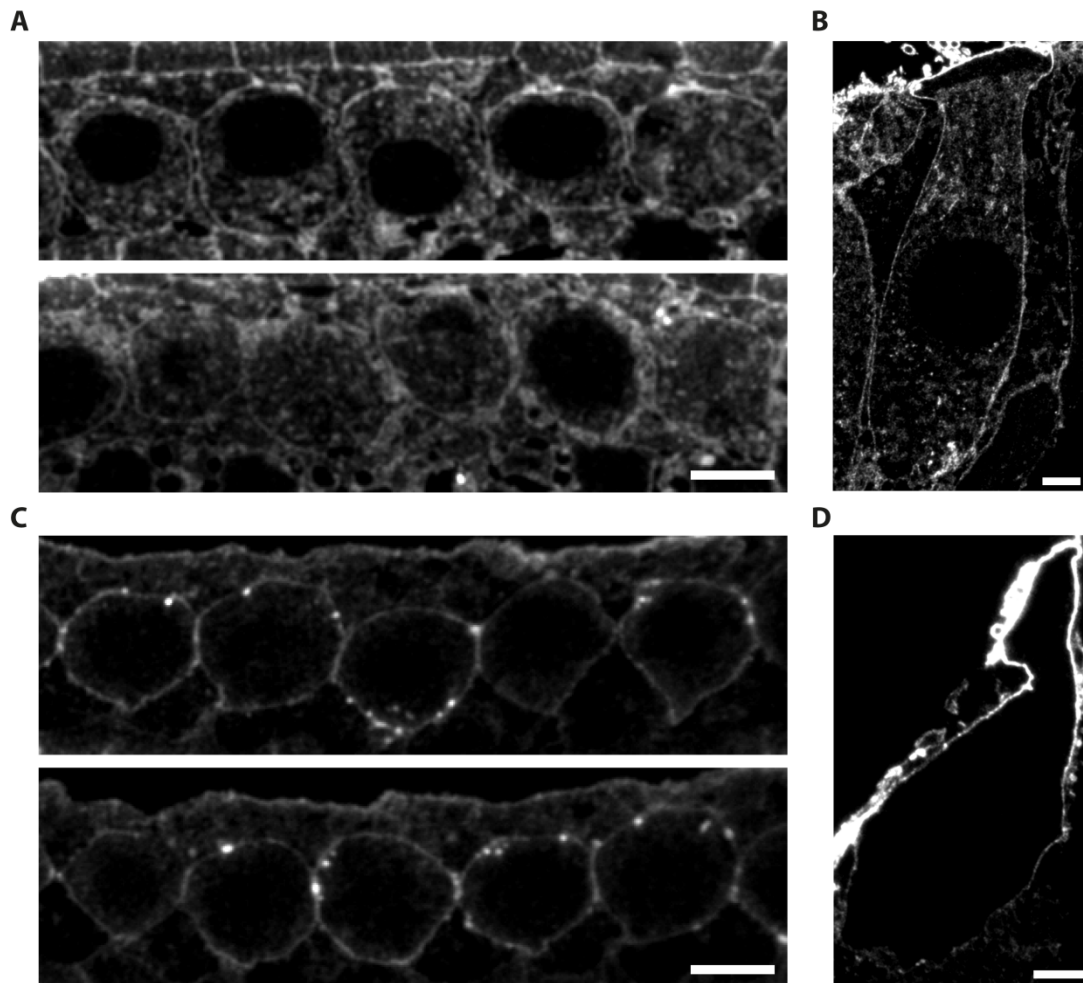


**Figure 3.11 mCLING uptake into IHCs is endocytosis-dependent and therefore inhibited by low temperature.**

OCs were labeled for 3 minutes with 1.7  $\mu\text{M}$  mCLING, fixed, embedded and sectioned. **A-B.** When incubated at 37°C, mCLING is found in abundant structures, homogeneously distributed throughout the IHCs. Transversal cuts were imaged in epifluorescence microscopy (A) and longitudinal cuts were imaged with STED microscopy for comparison (B). **C-D.** Incubation on ice (2-4°C) inhibited mCLING uptake, being only visible on the plasma membrane of all cell types. A few organelles seem to be stuck in the initial steps of endocytosis (C). Similar results were seen by STED microscopy (D). Scale bars: 5  $\mu\text{m}$  in A. and C.; 2  $\mu\text{m}$  in B. and D.

In cells incubated at 37°C abundant organelles were seen inside the cells, evident in transversal cuts imaged in epifluorescence microscopy (Figure 3.11A), or in longitudinal cuts imaged with STED microscopy (Figure 3.11B). Labeled structures were distributed from top to base, sparing only the nuclear volume. On the contrary, most of the cells incubated on ice had mCLING exclusively on the plasma membrane, with a few exceptions showing labeled organelles trapped in the initial steps of endocytosis and apparently still

bound to the plasma membrane (Figure 3.11 C). A longitudinal section imaged in STED microscopy confirms these results, depicting a cell with visible labeling only at the plasma membrane (Figure 3.11D). These results contrast with the strong FM dye uptake at low temperature (Figure 3.1).

These results ratify that once mCLING penetrates the OC and reaches the plasma membrane of IHCs, it is taken up by endocytic events. Moreover, the absence of label at low temperatures confirms that mCLING does not permeate the MET channels at the apical stereocilia bundle. Interestingly, mCLING not only reports endocytosis in IHCs but also in the surrounding supporting cells, at slightly lower levels.

### **3.3.5 mCLING reveals that stimulation-induced synaptic vesicle recycling occurs at the IHC base**

As mentioned in the introduction, one of the most intriguing questions in the IHC field is the localization of membrane retrieval hotspots that could supply SV recycling. So far two possibilities have been derived from different technical approaches. On one hand, several EM studies have shown important processes of membrane recycling happening at the cell base upon stimulation, close to the synaptic active zones, suggesting a local recycling (Siegel and Brownell, 1986; Spicer et al., 1999, 2007; Lenzi et al., 2002; Kamin et al., 2014). On the other hand, studies using fluorescence imaging of FM 1-43 proposed a pathway starting with endocytosis at the apical pole of the cell, followed by membrane sorting in organelles at the cell top, like the Golgi apparatus or the ER, from where SVs are reformed and delivered to the active zones. (Griesinger et al., 2002, 2004, 2005). However, the already exposed concerns about the use of FM dyes in IHCs make this last model controversial. With the use of mCLING I expect to solve the long-standing question about the origin of recycling SVs in IHCs.

Another unanswered question in IHC's physiology is the nature of the tubular structures often described by EM in the literature, and sometimes proposed as source of SV reformation (Siegel and Brownell, 1986; Spicer et al., 2007). Their identity has been difficult to define because, as explained at the beginning of section 3.3, constitutive membrane recycling and synaptic vesicle recycling occur in the same cellular volume in IHCs. Therefore, mCLING is a potential tool to dissect the morphology and physiology of both constitutive and synaptic recycling, and to elucidate which of those are the tubules more related to.

In a first approach to answer these questions, transversal melamine sections of mCLING-labeled IHCs were imaged to study the morphology and distribution of recycling organelles. With the aim to discriminate between constitutive- and synaptic-related events, different labeling strategies were used:

- Resting condition: intended to evaluate only constitutive membrane recycling. OCs were incubated for **3** minutes at 37°C in HBSS without Ca<sup>2+</sup> containing 1.7 μM mCLING. After incubation, OCs were briefly washed in mCLING-free buffer and directly fixed in 4% PFA and 0.2% glutaraldehyde. Embedding and sectioning were performed as described before.
- Stimulation condition: intended to evaluate constitutive membrane recycling and synaptic vesicle recycling. OCs were incubated for **2** minutes at 37°C in HBSS without Ca<sup>2+</sup> containing 1.7 μM mCLING. OCs were immediately transferred to HBSS high K<sup>+</sup> (65 mM) with 1.7 μM mCLING for **1** minute, to stimulate synaptic vesicle exocytosis. After incubation OCs were briefly washed in mCLING-free HBSS without Ca<sup>2+</sup> and directly fixed in 4% PFA and 0.2% glutaraldehyde. Embedding and sectioning were performed as described before.
- Recovery condition: intended to follow how the endocytosed structures containing mCLING are later processed by the different trafficking pathways. The same protocol used in the stimulation condition was applied but after high K<sup>+</sup> and before fixation the OC was incubated for **5** minutes at 37°C in mCLING-free HBSS with Ca<sup>2+</sup>. This buffer has only 5 mM K<sup>+</sup> and allows the cells to recover after strong SV release before they are fixed. Embedding and sectioning were also performed.

One of the first features I found when imaging melamine sections in high-resolution STED microscopy, was that the staining of the plasma membrane was not always uniform. It has been previously reported that during the fixation procedure some of the membrane phospholipids are solubilized by aldehyde fixatives, and removed by detergents when combined with immunostaining (Doggenweiler and Zambrano, 1981). Extracted phospholipids can leave behind pores that in sections look as discontinuities of the membrane. Such level of detail was not possible with conventional confocal microscopy. Evidence of these pores was already shown in Figure 3.5A, right panel, where fixed cells were easily permeated by PI. Similarly, discontinuous membranes were also seen in fixed and permeabilized cultured hippocampal neurons (see section 3.4).

STED images from IHC transversal sections revealed abundant endocytosed structures in

both resting and stimulated conditions. This indicates that constitutive membrane traffic is relatively strong in IHCs (Figure 3.12A). The top and nuclear levels were dominated by large and elongated structures resembling tubules, with the presence of large and small round structures. In contrast, the cell base contained mainly small round vesicle-like structures and larger endosome-like ones of different sizes and shapes (from round to elongated). Stimulated cells seemed to have more endocytosed structures at the cell base than resting ones (Figure 3.12A). In the recovery condition, the sizes of the tubular structures at the cell top and nucleus, as well as the organelles seen at the cell base were reduced, likely due to processes of budding and vesicle reformation. This is also supported by a more homogeneous size and distribution of labeled organelles. These observations go in line with previous results obtained in our laboratory using FM 1-43 photo-oxidation combined with EM to track recycling organelles in IHCs (Kamin et al., 2014), as well as with other EM studies (Siegel and Brownell, 1986; Lenzi et al., 1999, 2002; Kamin et al., 2014).

A MatLab script (written by Silvio O. Rizzoli) was used to quantify the percentage of area occupied by mCLING labeled organelles from the total area delimited by the plasma membrane in transversal sections. The analysis was divided in the aforementioned cellular levels (top, nuclear and basal) among the three different treatments. While endocytic uptake at the top and nuclear levels of the IHC seemed to be not affected by synaptic stimulation, it was greatly increased by more than two-fold at the basal level, when compared to the resting condition (Figure 3.12C). In the recovery condition the area occupied by mCLING-labeled organelles was reduced, probably due to two reasons: the breaking up of endosome-like structures and tubules into small vesicles that are more difficult to detect by the analysis, and the recycling of labeled organelles back to the plasma membrane.

Important aspects of IHC physiology can be derived from these results: first, even in resting conditions IHCs seem to have a very active membrane recycling activity, when compared, for example, with cultured COS7 cells incubated with mCLING for a longer period (5 minutes, Figure 3.4C and Figure 3.7B). Second, that synaptic vesicle recycling seems to occur only in the basal region of the IHCs, and not at the top and nuclear regions as it was suggested before (Griesinger et al., 2002, 2004, 2005). Third, it is likely that the abundant membrane uptake at the IHC top and nuclear levels represents constitutive trafficking.

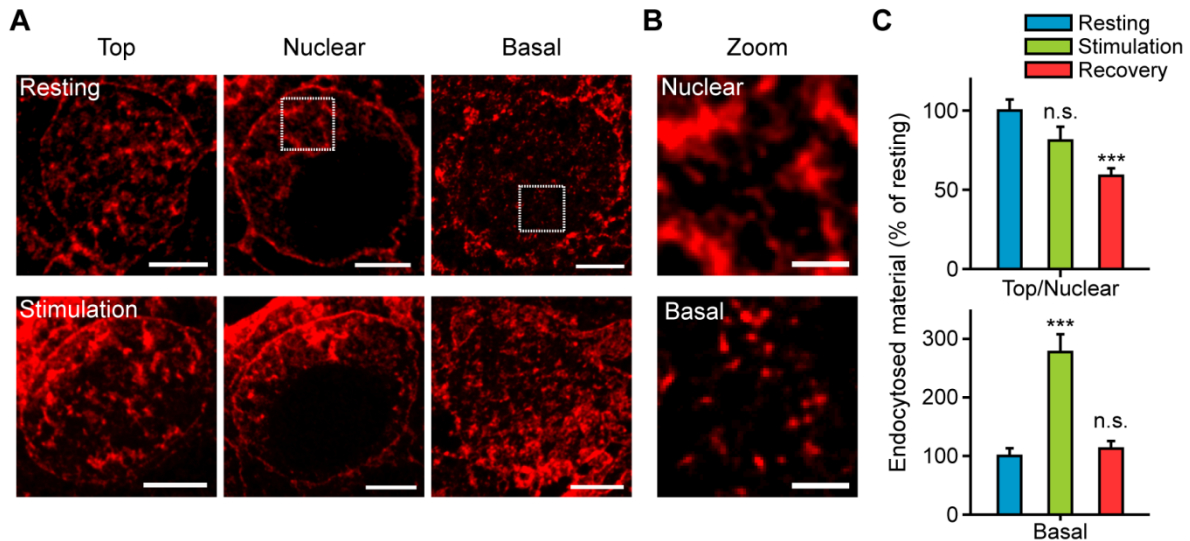


**Figure 3.12 mCLING reveals recycling organelles in IHCs.**

**A.** When incubated at 37°C, mCLING was found in organelles of different shapes and sizes in both resting (top panels) and stimulated cells (lower panels). While the top and nuclear levels were dominated by tubular and round structures, the basal level was populated mostly by round organelles including vesicle-like ones. Stimulation increased mCLING staining mostly at the base of the cell. Scale bars, 2  $\mu$ m. **B.** Zoom-ups corresponding to the dashed line squares depicted in **A**. The upper panel shows typical tubular-like structures found at the cell top and nuclear levels, while the lower panel shows the more homogeneous profile of the cell base. Scale bars, 500 nm. **C.** Endocytosis levels were quantified as the area occupied by mCLING-labeled organelles. Stimulation increases mCLING endocytosis only in the basal region of the cells. The bars show mean % normalized to the resting condition  $\pm$  SEM, from 27, 22 and 57 cell top and nuclear regions (resting, stimulation and recovery, respectively), and from 25, 28 and 27 cell bases (resting, stimulation and recovery, respectively). n.s., no significant difference (t-test,  $P > 0.05$ ). \*\*\*, significant difference (t-test,  $P \leq 0.001$ ).

### 3.3.6 mCLING unloading reports SV exocytosis at the IHC base

If synaptic vesicle recycling is indeed a local process occurring at the basal pole of the IHC, it would be logic to think that synaptic vesicle exocytosis is also happening in that cell region. This idea would be supported by the fact that in hair cells the active zones are distributed from the lower nuclear level down to the cell bottom. This assumption was confirmed by a recent study using VGLUT1-pHluorin as SV exocytosis indicator and specific localization of synaptic ribbons with a fluorescently-labeled peptide. SV exocytosis induced by  $Ca^{2+}$  influx was found to preferentially occur at the IHC active zones (Neef et al., 2014).

One possible way to confirm that observation was to look at mCLING unloading in living IHCs cells. FM dyes have been often used in the past in loading-unloading experiments to reveal synaptic vesicle recycling in conventional synapses (Betz et al., 1992). First, cells are stimulated in presence of the dye to induce its uptake. Due to FM dyes washability, a dye-

free solution can be perfused to wash off dye molecules from the plasma membrane to better reveal labeled SVs. Release of those SVs can be seen as reduction in fluorescence after a second stimulus.

Since mCLING binds more strongly to membranes than FM dyes (Figure 3.4D), a different method for eliminating membrane fluorescence was necessary. Bromophenol blue (BPB) is a membrane-impermeant molecule that has been used in the past to quench cell surface fluorescence from molecules like FM 1-43, FM 3-25, GFP and synaptopHluorin, thus helping in the study of SV recycling (Harata et al., 2006b; Li et al., 2009; Wilhelm et al., 2010). I established an assay using BPB to visualize SV exocytosis in IHCs. Briefly, SVs were loaded with mCLING by a first round of stimulation with 65 mM K<sup>+</sup> for 1 minute. Then cells were allowed to recover for 5 minutes in HBSS with Ca<sup>2+</sup> and 0.75 mM BPB, which quenched the fluorescence of the Atto 647N moiety in mCLING molecules at the plasma membrane. A second stimulus was applied to induce exocytosis of SVs, among them mCLING-labeled ones. Once these vesicles fuse and get exposed to the medium, the mCLING molecules associated to their membranes are also quenched (Figure 3.13A). By looking for areas where fluorescence levels declined after the second stimulation one could estimate where SV release took place. This assay is based on the fact that only synaptic vesicles are responsive to K<sup>+</sup> stimulation, while the organelles involved in constitutive trafficking pathways are unaffected.

While establishing this assay I observed that high concentrations of BPB (>1.5 - 2 mM) interfere with proper illumination of the sample and efficient detection of fluorescence. I found that 0.75 mM BPB was the most convenient concentration that efficiently quenched Atto 647N fluorescence from membranes and still allowed the imaging routine. Concentrations below 0.5 mM would not quench fluorescence significantly. Long illumination exposures of cells in presence of BPB seemed to be toxic. Therefore, laser light was strictly used for image acquisition and not for finding the imaging area.

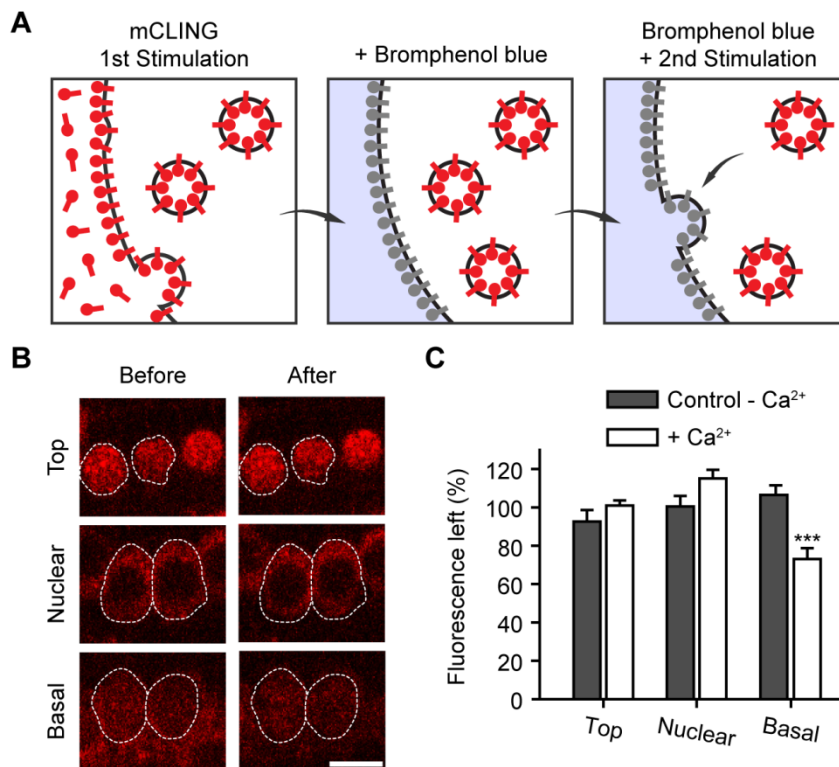


**Figure 3.13 mCLING unloading, evidenced by BPB fluorescence quenching, locates SV exocytosis exclusively at the IHC basal level.**

**A.** Experimental principle for mCLING loading and unloading using BPB as fluorescence quencher. IHCs were stimulated in presence of mCLING (65 mM KCl, 1 minute), labeling recycling organelles. Cells were then incubated in a recovery solution (HBSS with Ca<sup>2+</sup>) for 5 minutes and BPB was added to quench the Atto 647N fluorescent molecules exposed at the plasma membrane (shown as gray molecules). A second round of stimulation in the presence of BPB (65 mM KCl, 1 minute) causes the exocytosis of labeled organelles, whose fluorescence is also quenched. **B.** Typical fluorescence images of top, nuclear and basal regions of IHCs treated with BPB, before (left panels) or after the second round of stimulation (right panels). Fluorescence reduction due to SV exocytosis is apparent only at the cell bases. Scale bar, 10  $\mu$ m. **C.** Quantification of fluorescence intensity values at top, nuclear and basal levels, expressed as percentage of remaining fluorescence after the second round of stimulation (white bars). As a control, SV exocytosis was blocked by removal of Ca<sup>2+</sup> during the second stimulus (gray bars). All measurements are normalized to their initial, before stimulation, intensity values. A significant decrease is only obtained for the basal level of the cells (t-test,  $P < 0.001$ ; 2-6 independent experiments were performed, with 8-15 IHCs analyzed in each experiment).

mCLING fluorescence coming from intracellular organelles was detected in all cell areas (top, nuclear and basal) after applying BPB to the solution. After the second stimulus (in presence of BPB), fluorescence appeared to be unchanged at the cell top and nuclear levels, while being reduced at the basal level (Figure 3.13B). A quantification of the fluorescence intensities confirmed this observation (Figure 3.13C, white bars). In control cells, where the second stimulation was performed in the absence of Ca<sup>2+</sup> to inhibit exocytosis, no significant changes in fluorescence were detected at any level (Figure 3.13C, gray bars). This confirms that the reduction in fluorescence seen at the base of treated IHCs is directly related to SV



exocytosis. The results of this section again support the idea that SV recycling (exo- and endocytosis) is preferentially located at the IHC base, while the membrane recycling processes at the cell top and nuclear levels are unrelated to the synaptic function.

### **3.3.7 Endocytic processes reported by mCLING are dynamin- and clathrin-dependent**

In Figure 3.11 I showed that incubation of IHCs with mCLING at low temperatures resulted in inhibition of its uptake. This important outcome suggests the potential of mCLING as marker for endocytic activity levels. Hence, I used mCLING to study the effects of inhibiting two important molecules previously involved in conventional endocytosis (see Introduction), and also in SV recycling at conventional synapses (Brodin et al., 2000): clathrin and dynamin.

In order to inhibit clathrin-mediated endocytosis I used pitstop 2, a small molecule (473 Da) that binds to the terminal domain of the clathrin heavy chain and hinders its association with other proteins like amphiphysin, AP180 and Synpatojanin1, resulting in inhibition of clathrin coat formation (von Kleist and Haucke, 2011; von Kleist et al., 2011). To inhibit dynamin activity I used dynasore, another small molecule (322 Da) that permeates the plasma membrane and acts as a noncompetitive inhibitor of the GTPase activity of dynamin (Macia et al., 2006; Newton et al., 2006). Dynasore has been used to inhibit synaptic vesicle recycling in conventional synapses (Chung et al., 2010; Hoopmann et al., 2010; Watanabe et al., 2013) and in cells containing ribbon-type synapses like photoreceptors (Van Hook and Thoreson, 2012; Wahl et al., 2013) and IHCs (Duncker et al., 2013).

To study the effects of clathrin and dynamin inhibition in stimulated IHCs, OCs were treated during 25 minutes with either pitstop 2 (30  $\mu$ M) or dynasore (100  $\mu$ M) in HBSS without  $\text{Ca}^{2+}$ . Afterwards an stimulation protocol was applied as described before: 2 minutes in HBSS without  $\text{Ca}^{2+}$  with 1.7  $\mu$ M mCLING, in presence of the inhibitor (same concentration), followed by 1 minute HBSS high  $\text{K}^{+}$  (65 mM) with mCLING and the inhibitor (same concentrations). OCs were washed, fixed and immunostained for the standard vesicular marker of IHCs, the Vesicular Glutamate Transporter 3 (VGLUT3). OCs were embedded in melamine and cut into 200 nm sections. Control cells were incubated with mCLING using the same protocol and buffers, but in absence of the inhibitors.

STED images of treated cells show that pitstop 2 reduced the amount of endocytosed organelles throughout the IHC. The tubular structures normally seen at the cell top and

nuclear levels were reduced in number. At the cell base very few structures were visible (Figure 3.14A). The same quantification analysis used in Figure 3.12C was applied to determine the area occupied by mCLING-labeled structures, reporting a reduction of endocytosis down to ~33% at the cell top/nuclear levels when compared to untreated stimulated cells. Endocytosis levels at the cell base went down to ~7% (Figure 3.14B).

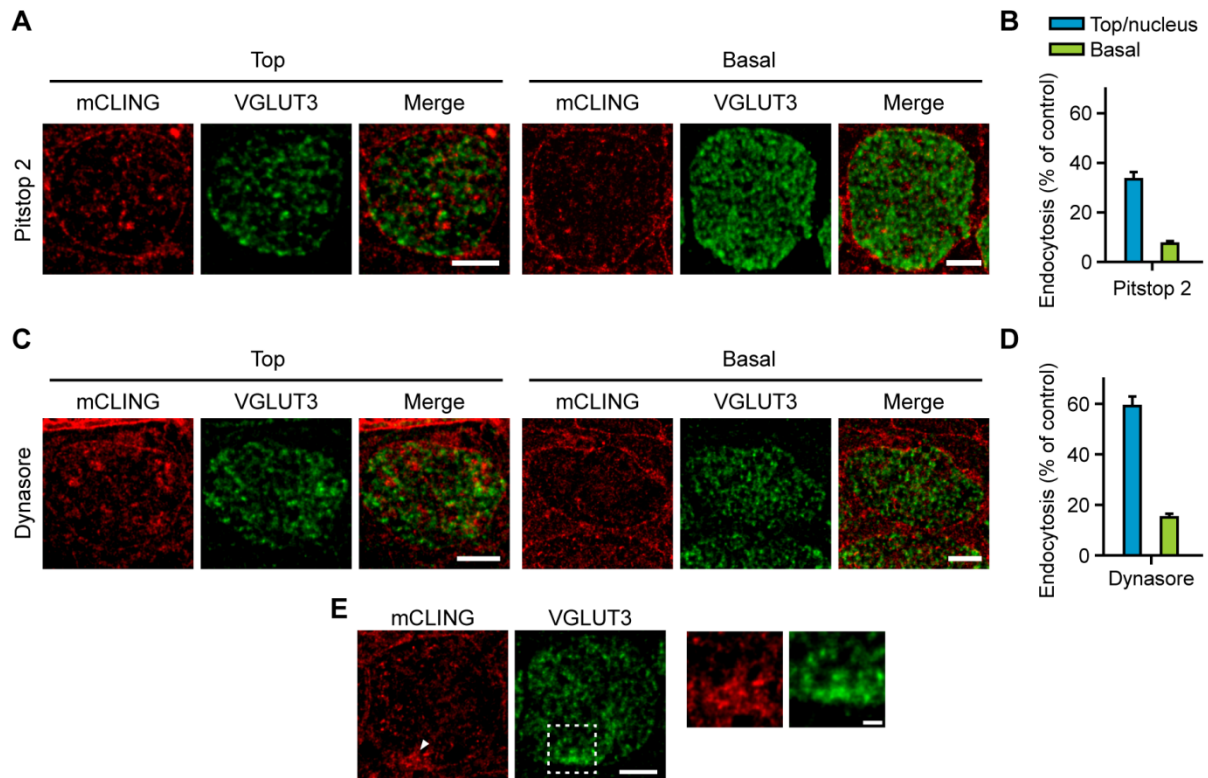


**Figure 3.14 Effects of clathrin and dynamin inhibition visualized by mCLING labeling in IHCs.**

**A.** IHCs were incubated with the clathrin inhibitor pitstop 2 (30  $\mu$ M) for 25 minutes, and were then stimulated using 65 mM KCl, for 1 minute in buffer containing mCLING. Endocytosed organelles were less abundant than in untreated cells (see Figure 3.12 for reference). Scale bars, 2  $\mu$ m. **B.** The amount of mCLING endocytosis at the top/nuclear and basal levels of pitstop 2 treated cells was compared to the corresponding values in control cells. Error bars represent mean percentage  $\pm$  SEM from 63 cell top/nuclear areas and 52 cell bases treated with pitstop 2. **C.** IHCs were incubated with the dynamin inhibitor dynasore (100  $\mu$ M) for 25 minutes and stimulated as described for pitstop 2. Here endocytosis was also reduced at all cell levels. Scale bars, 2  $\mu$ m. **D.** Quantification of mCLING endocytosis in dynasore treated cells compared to control cells. Error bars represent mean percentage  $\pm$  SEM from 54 cell top/nuclear areas and 100 cell bases treated with dynasore. In general, clathrin and dynamin inhibition had stronger effects at the cell base of IHCs. **E.** Example of a dynasore-treated cell presenting mCLING-labeled structures accumulated at the cell base plasma membrane (white arrowhead). Right panels show a zoom in of the depicted area (white dashed-line square). Scale bars, 2  $\mu$ m and 500 nm, respectively.

Dynasore had the same effects on endocytosis as pitstop 2, with reduced amount of mCLING-labeled structures at all cellular levels (Figure 3.14C). Endocytosis levels were

reduced to 59% at the cell top/nuclear levels, and to 15% at the cell base (Figure 3.14D). Interestingly, while most of the dynasore-treated IHCs had reduced amount of organelles, a few cells presented large clumps of mCLING-labeled structures retained at the plasma membrane of the cell bottom (Figure 3.14E).

These results show that inhibition of both, clathrin and dynamin, had stronger effects at the cell basal level than at the top and nuclear levels. Considering the data previously presented, I could suggest that these two proteins have an important role in SV recycling. The molecular mechanisms supporting the remaining endocytosis at the upper levels remain unclear, as they seem to be more clathrin- and dynamin-independent.

### **3.3.8 Impairment of synaptic vesicle exocytosis reduces mCLING-reported endocytosis**

The high rates of SV release found in IHCs have to be compensated by equally efficient mechanisms of membrane retrieval. The equilibrium between both processes is important to guarantee availability of synaptic vesicles and their proteins for future rounds of exocytosis, as well as to keep a constant surface area of the cell. One interesting question is if the impairment of SV release has also an impact in the levels of endocytosis. To answer this question I applied mCLING to OCs dissected from animals lacking the protein otoferlin, involved in SV exocytosis and priming (Roux et al., 2006; Pangršič et al., 2010). Otoferlin knockout mice (*Otof*<sup>-/-</sup>) have pronounced hearing impairment due to a drastic reduction of exocytosis levels (Roux et al., 2006).

OCs from *Otof*<sup>-/-</sup> mice were incubated with mCLING in the same stimulation conditions described before (section 3.3.5). OCs were subsequently fixed, immunostained for VGLUT3, embedded in melamine and cut into 200 nm sections. STED images show an important reduction of endocytosed organelles, in a similar way to the inhibition of clathrin and dynamin (Figure 3.15A). When compared to wild type animals, endocytosis was reduced to ~32% at the cells top/nuclear levels, and to ~8% at the cell base (Figure 3.15B).

These data are consistent with the model of basal synaptic recycling, suggesting that an impairment in SV release entails reduction in compensatory endocytic processes. It is not clear, however, how the reduction on SV recycling would affect endocytosis at the top and nuclear levels of the IHCs. Overall, these experiments demonstrate that mCLING indeed reports endocytic membrane uptake and that it can be easily used for its quantification.

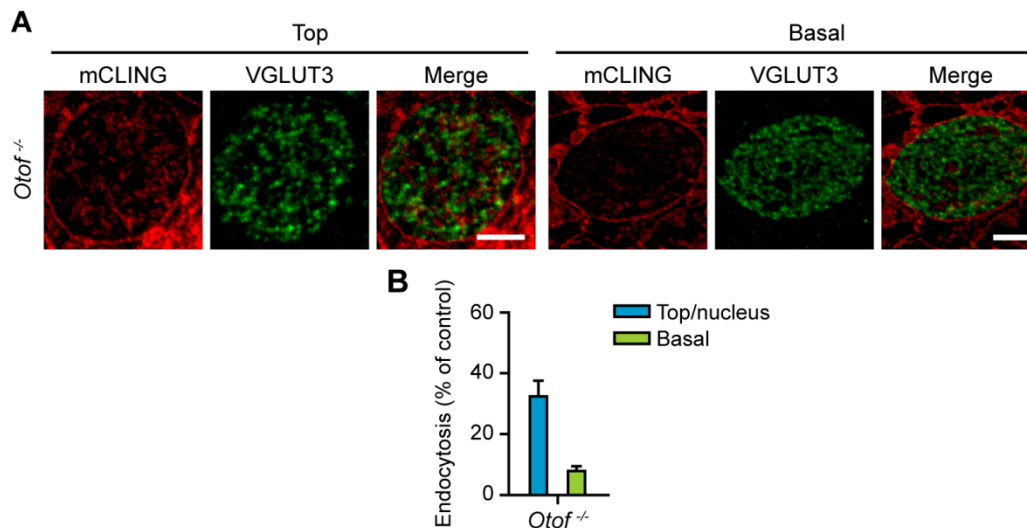


**Figure 3.15 Impaired SV exocytosis by deletion of the protein otoferlin is accompanied by reduced levels of endocytosis in IHCs.**

**A.** IHCs from otoferlin-deficient animals (*Otof*<sup>-/-</sup>), in which exocytosis is completely abolished, were stimulated in the presence of mCLING. Endocytosis was reduced, especially at the base of the cell. Scale bars, 2  $\mu$ m. **B.** The amount of endocytosis was compared to that in wildtype cells at the top/nuclear levels and at the basal level of *Otof*<sup>-/-</sup>. Error bars represent mean percentage  $\pm$  SEM from 28 cell top/nuclear areas and 26 cell bases. Values are presented as percentage of the wildtype condition.

### 3.3.9 Membrane recycling at the active zones of IHCs

The evidence accumulated in the last sections confirms that SVs are not only released but also recycled in the basal region of the IHCs. My next objective was to test the ability of mCLING, combined with high-resolution STED microscopy, to dissect the membrane trafficking processes occurring right at the vicinity of the active zone. Although electron microscopy and tomography studies already proposed membrane infoldings and cisterns as SV recycling intermediates (Siegel and Brownell, 1986; Lenzi et al., 2002), vesicle reformation from those organelles has not been studied in fluorescence microscopy, and the temporal dynamics of the whole process are not yet clear.

Due to the already exposed difficulty to perform high-resolution live imaging in a thick tissue, I attempted to describe the process of SV recycling by fixing IHCs after mCLING labeling along with different levels of stimulation (10, 25 and 65 mM K<sup>+</sup>). These were compared to the resting and recovered (after 65 mM K<sup>+</sup>) conditions. Active zones were identified by immunostaining against Ribeye, the most abundant protein of the synaptic ribbon, responsible for its structure (Schmitz et al., 2000; Khimich et al., 2005; Magupalli et al., 2008). mCLING labeling was imaged with STED microscopy and ribeye with confocal microscopy from 200 nm melamine sections.

mCLING-labeled organelles were studied in a region limited by the plasma membrane approximately 3.6  $\mu\text{m}$  wide with center at the synaptic ribbon, and 1.8  $\mu\text{m}$  deep into the cytoplasm. Resting cells (no  $\text{Ca}^{2+}$ ) contained sparse round organelles of heterogeneous sizes. After a mild stimulation with 10 mM  $\text{K}^+$ , endosome-like structures appeared around the ribbon, sometimes making contact with it. The number and size of these structures increased with 25 mM  $\text{K}^+$  accompanied by the appearance of membrane infoldings. After 65 mM  $\text{K}^+$  the labeled structures were even more abundant,  $41 \pm 4.2\%$  ( $n = 4$  independent experiments) of those being infoldings still connected to the plasma membrane. After 5 minutes of recovery following the 65 mM  $\text{K}^+$  stimulation, the infoldings and endosome-like organelles disappeared, to be replaced by a more diffuse, punctate labeling characteristic of small organelles (Figure 3.16A). To confirm that the formation of infoldings and large endosome-like organelles is a wide spread feature among stimulated active zones, I used a MatLab routine to calculate average intensity images of 20-31 active zones for each treatment (See section 2.2.7.1 for a description of this analysis). In the average images the same general trend was found: low labeling density at resting conditions, followed by gradual increase of objects density and fluorescence intensity as the stimulation grew stronger. After recovery, labeling is again homogeneous but brighter than the resting condition as result of stimulation-dependent mCLING uptake (Figure 3.16B).

The previous results can be summarized in a series of events: first, stimulation triggers the formation of membrane infoldings around the synaptic ribbon. Eventually those infoldings detach from the plasma membrane and give rise to endosome-like structures (cisterns), which finally are broken up into reformed SVs. The latter appear to diffuse and intermix with other organelles. To determine if those reformed SVs are recruited again to the synaptic ribbon, I performed a 65 mM  $\text{K}^+$  stimulation, followed by a recovery period and a second round of stimulation. As a result, a dense layer of mCLING-labeled organelles formed around the ribbons. These organelles were smaller than the infoldings and cisterns, and sometimes they appeared to make contact with the ribbon. These results are confirmed in an average picture of several active zones (Figure 3.16C).

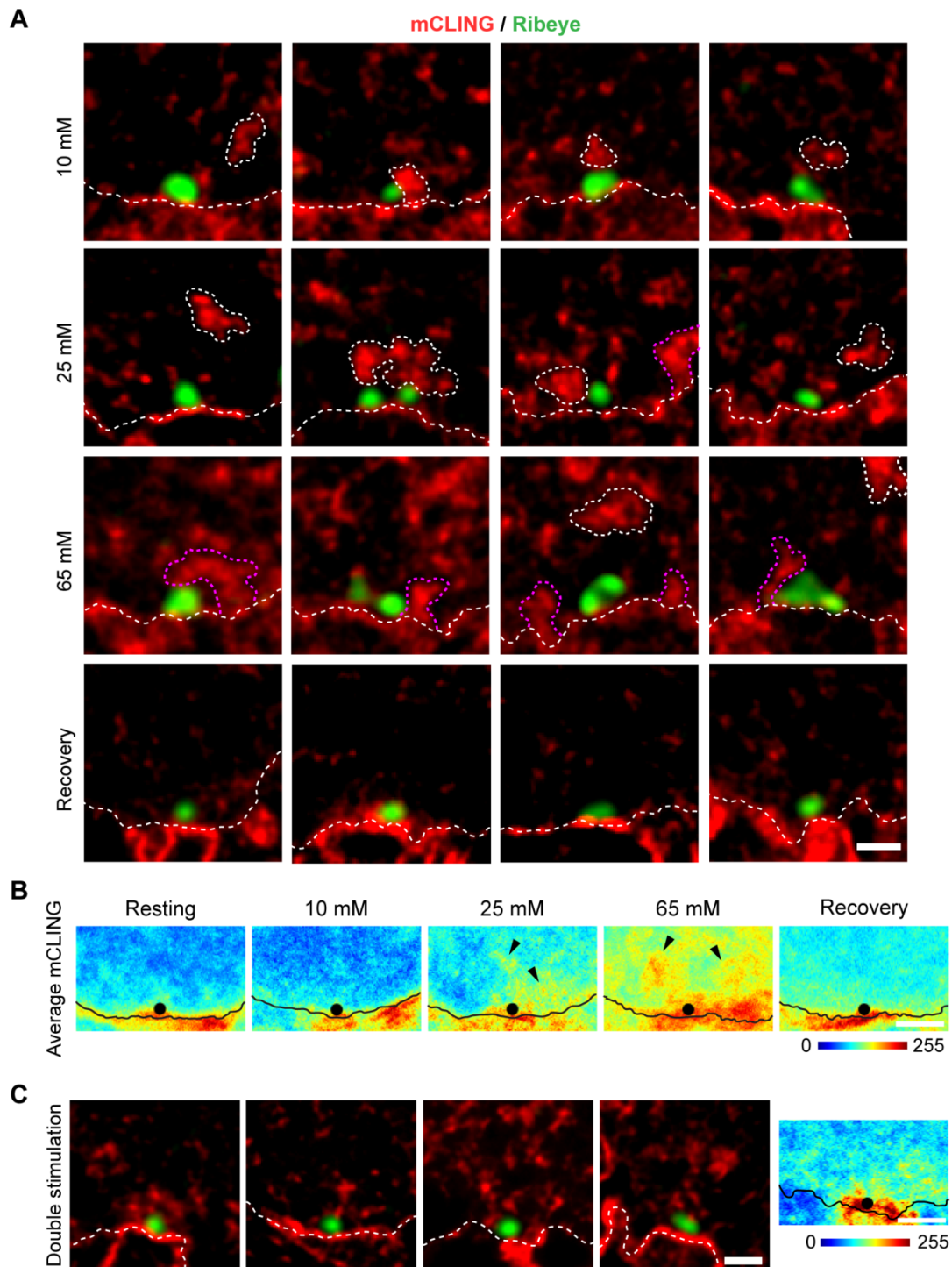


**Figure 3.16 mCLING reveals the morphology of the organelles that locally recycle SVs at the IHCs active zone.**

**A.** mCLING uptake (red) was evaluated at the area surrounding the synaptic ribbon (ribeye immunostaining, green) of IHCs. The different panels show organelles appearing in stimulated cells (depolarization for 1 minute with 10, 25 or 65 mM KCl), and after recovery from 65 mM KCl depolarization (5 minutes in  $\text{Ca}^{2+}$ -containing buffer). Endocytic intermediates form during stimulation and disappear during recovery, leaving behind smaller, synaptic vesicle-like organelles (bottom row). mCLING-labeled and internalized organelles are indicated by the dashed white lines. The plasma membrane is indicated by a similar white dashed line. Structures that appear to be connected to the plasma membrane (infoldings) are indicated by the dashed pink lines. Scale bar, 500 nm. **B.** Pseudocolor representation of average fluorescence images

obtained from 20-31 individual ribbon synapses in all conditions. Note the increase in average fluorescence and density around the ribbon upon stimulation (black arrowheads), and its redistribution after the recovery period. Scale bar, 1  $\mu\text{m}$ . **C.** Active zones subjected to two rounds of stimulation (65 mM KCl, 1 min each), separated by a 5-minute recovery period. The double-stimulated cells have, as expected, a denser cloud of labeled organelles around the ribbon (compare with bottom row of cells in panel A). This is confirmed by an average picture of 10 ribbons (right panel).

### 3.3.10 Organelles recycling at the basal levels of IHCs colocalize with vesicular markers

The main advantage of using mCLING as endocytosis marker is that the organellar identity of recycling membranes can be determined by immunolabeling. This becomes useful to establish if the abundant membrane recycling occurring at the IHC base is indeed related to SV markers. In this context, I combined mCLING labeling under stimulation conditions (65 mM K<sup>+</sup>, 1 minute) with labeling against three important proteins involved in synaptic function: VGLUT3, a typical SVs marker in IHCs, responsible for their refilling with glutamate and whose impairment and absence have been involved in deafness (Ruel et al., 2008; Seal et al., 2008); Rab3, a small GTPase that recruits synaptic vesicles to the active zone in conventional synapses (Geppert et al., 1994a; Geppert and Südhof, 1998), and that has been found to co-precipitate with ribeye in sensory synapses, having a potential role in the attachment of SVs to the ribbon (Uthaiiah and Hudspeth, 2010); finally, otoferlin, the Ca<sup>2+</sup> sensor involved in SV exocytosis and priming, previously described in section 3.3.8. After immunostaining, samples were embedded in melamine, cut into 200 nm sections and imaged under two-color STED microscopy. For quantifying the level of colocalization between mCLING and protein signal, Pearson's correlation values were calculated from ROIs of 20×2 pixels located across mCLING-labeled organelles.

VGLUT3 staining was abundant and present in vesicle-like organelles throughout the IHCs. Although this marker was excluded from the tubular structures at the cell top and nuclear levels, it colocalized with the organelles endocytosed at the cell base. These results are supported by negative Pearson's correlation values at the top and nuclear levels, and positive values at the cell base (Figure 3.17A, D). Similar results were obtained for Rab3, which also showed better correlation with organelles at the cell base (Figure 3.17B, D).

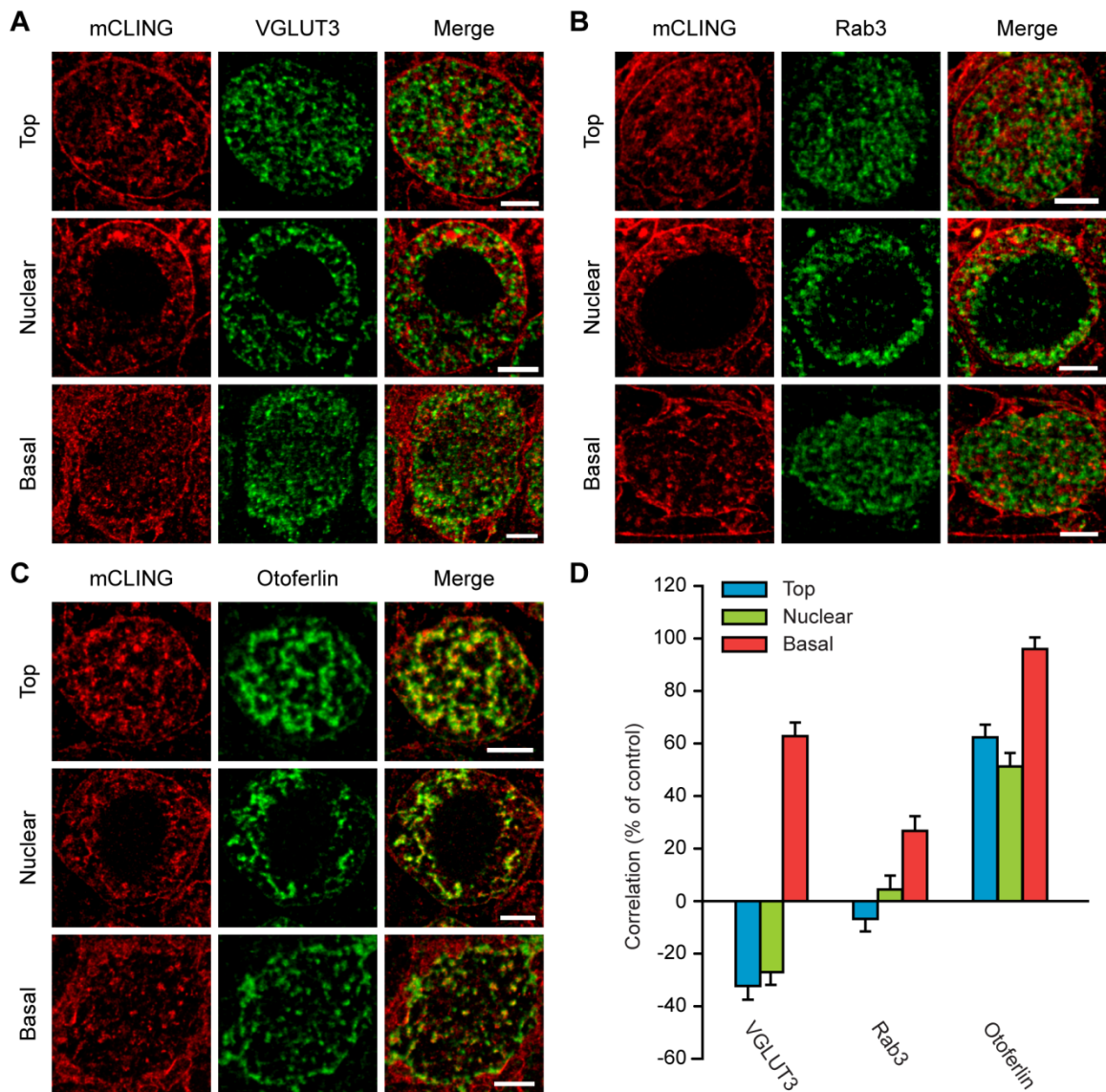


**Figure 3.17 mCLING-labeled organelles at the cell base show better colocalization with SV markers than those at the top and nuclear levels**

OCs were labeled with mCLING at stimulating conditions and then immunostained for SV markers. Samples were imaged using two-color STED. **A.** VGLUT3, the main SV marker in IHCs. **B.** Rab3, a second synaptic vesicle marker. **C.** Otoferlin, a  $\text{Ca}^{2+}$  sensing protein. Scale bars, 2  $\mu\text{m}$ . **D.** Pearson's correlation coefficients were determined for each protein at top, nuclear and basal levels. Coefficients are expressed as percent of the maximum expected correlation (% of control), obtained from VGLUT3 immunostained cells, incubated with two secondary antibodies, each coupled to either Atto 647N or Chromeo494. Error bars represent mean correlation coefficient  $\pm$  SEM (from 66 to 161 mCLING-labeled organelles, from 17 to 48 cells for each marker protein).

Otoferlin staining was abundant at all cell levels and present in organelles of different shapes and sizes. An important feature found from the melamine sections, which is not evident in confocal microscopy of whole cells, is that at the cell top this protein is mostly present in intracellular organelles; at the nuclear level it starts appearing also at the plasma



membrane, with an increasing gradient towards the cell bottom. Surprisingly, otoferlin was present not only in basal mCLING-labeled organelles, but also in the tubular structures at the cell top and nuclear levels. Correlation values were positive for all levels, but still higher at the cell base (Figure 3.17C, D). Interestingly, otoferlin labeling had the highest correlation values among all proteins tested (including also the ones used in the two following sections).

These results demonstrate that, even though synaptic vesicles are present in large numbers across the IHC, only those located at the cell base are released upon membrane depolarization and therefore recycled. Additionally, these results open new questions about the role of otoferlin in IHC physiology, since this is the first study showing the broad presence of otoferlin in endocytic organelles.

### **3.3.11 Tubular structures at the top and nuclear levels of IHCs have an endosomal nature**

After confirming the basal location of SV recycling, I moved to the other pole of the IHC and focused on the nature of the tubular structures endocytosed at the top and nuclear levels. I set out to determine the organellar identity of those tubules by combining mCLING labeling with immunostaining against two organelles sharing the same location: the ER, identified by its luminal chaperone calnexin (Danilczyk et al., 2000); and the Golgi apparatus, identified by the cis-Golgi-network organizer GM130 (Nakamura et al., 1995).

Calnexin labeling was homogeneous throughout IHCs. Despite its sparse distribution, it always excluded mCLING labeling (Figure 3.18A), reflected in negative correlation values at all cell levels (Figure 3.18C). In contrast, GM130 was only present at a reduced volume of the supranuclear compartment, in accordance to previous EM descriptions locating the Golgi apparatus exclusively in this cell region (Siegel and Brownell, 1986; Spicer et al., 1999, 2007). GM130 poorly colocalized with mCLING-labeled structures (Figure 3.18B, C). From these results, I conclude that the tubular organelles are not related to ER or the cis-Golgi network, and that these organelles do not recycle on the time scale evaluated in this study (3 minutes).

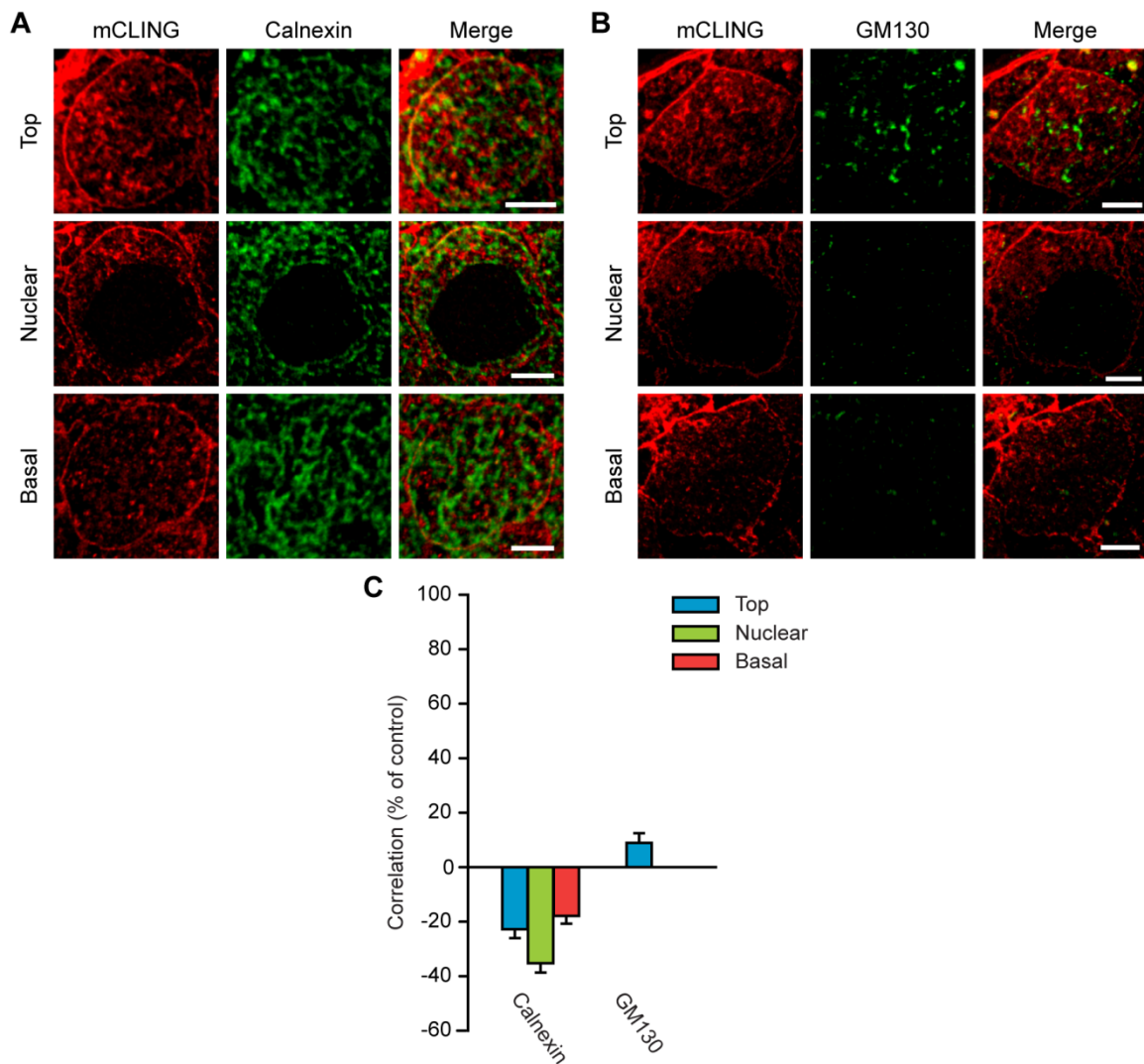


### Figure 3.18 Tubular structures at top and nuclear level are not related to ER or cis-Golgi

After labeling OCs with mCLING at stimulating conditions (65 mM K<sup>+</sup>), these were immunostained for ER and Golgi markers, given the location of these organelles at the IHC top. **A.** Calnexin, a common ER marker active as chaperone in its lumen **B.** GM130, a resident protein of the cis-Golgi network. Scale bars, 2  $\mu$ m. **C.** Pearson's correlation coefficients between each protein and mCLING were determined at the cell levels where the proteins were present. Calnexin anticorrelated with mCLING. GM130 had low correlation. Coefficients are expressed as percent of the maximum expected correlation (% of control) (See Figure 3.17). Error bars represent mean correlation coefficient  $\pm$  SEM (from 211 to 414 mCLING-labeled organelles, from 44 to 84 cells for each marker protein).

Having ruled out an ER or Golgi identity, I next tested two SNARE proteins implicated in the retrograde traffic between early/recycling endosomes and the trans-Golgi-network, Syntaxin 6 (Sx 6) and Syntaxin 16 (Sx 16) (Mallard et al., 2002; Brandhorst et al., 2006; Jahn and Scheller, 2006). Both proteins were found in tubule-like structures and round organelles, mainly at the cell top and nuclear levels. At the cell base the staining was poor and only present in round structures (Figure 3.19A, B). Colocalization with mCLING was strong at the top and nuclear levels, confirmed by positive Pearson's correlation values

(Figure 3.19C). For comparison, the SNARE protein Vti1a, which has been implicated in homotypic fusion between early endosomes (Brandhorst et al., 2006), was also tested. Vti1a distribution was similar to that of Sx 6 and Sx 16, present at the supranuclear level, and almost absent at the cell base. In contrast to Sx 6 and Sx 16, Vti1a had low correlation values with mCLING (Figure 3.19C).

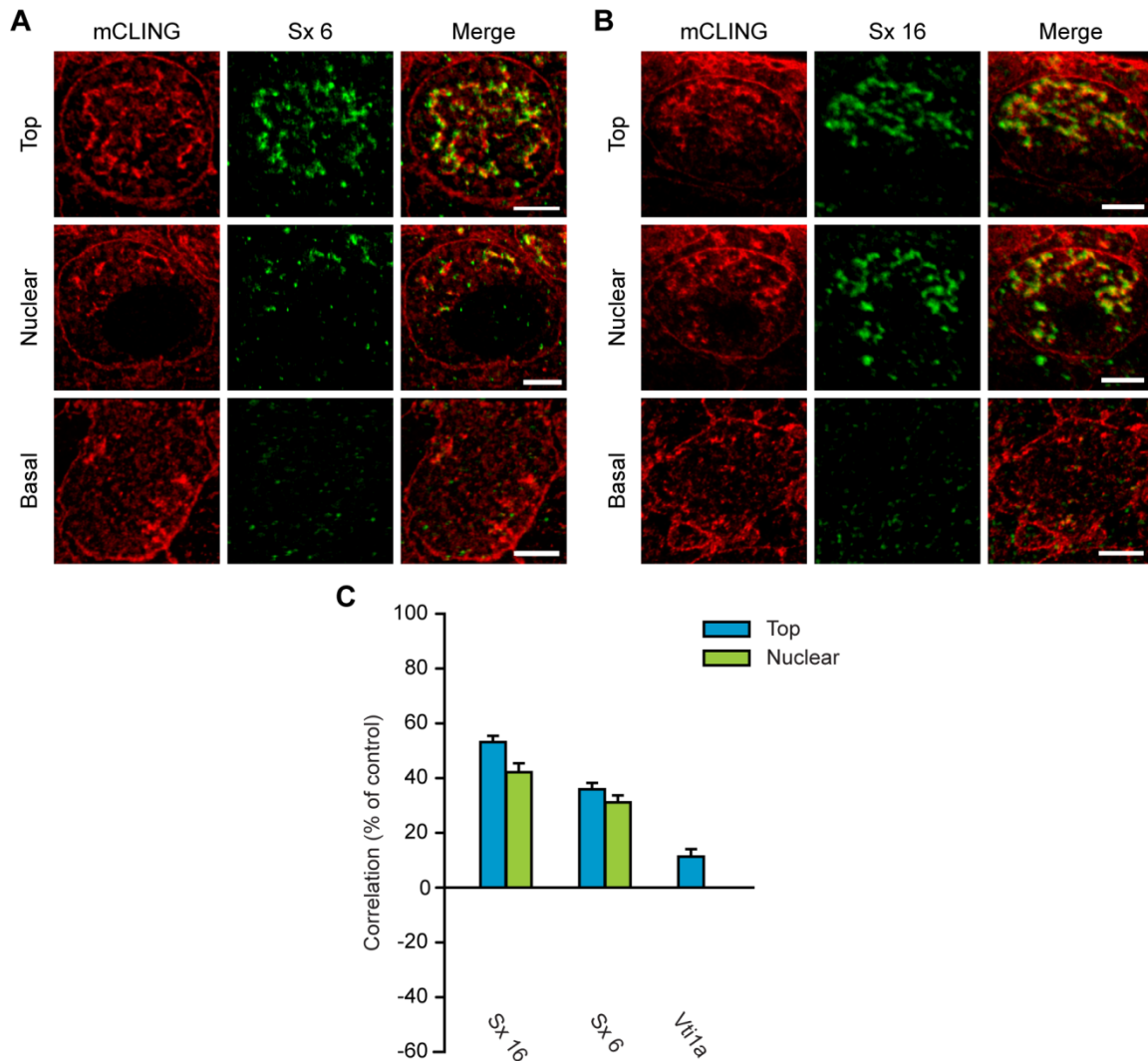


**Figure 3.19 The tubular organelles endocytosed at the IHC top and nuclear levels have endosomal identity**

OCs labeled with mCLING at stimulating conditions (65 mM K<sup>+</sup>) were immunostained for three SNARE proteins. **A.** Syntaxin 6, and early endosome marker also implied in transport toward TGN. **B.** Syntaxin 16, implicated in transport from early/recycling endosomes to the TGN. Scale bars, 2  $\mu$ m. **C.** Pearson's correlation coefficients between Sx 6, Sx 16 and Vti1a, an early endosome marker, and mCLING were determined at top and nuclear levels depending on the location of each protein. While Sx 6 and Sx 16 had good correlation with mCLING, Vti1a had low correlation. Coefficients are expressed as percent of the maximum expected correlation (% of control) (See Figure 3.17). Error bars represent mean correlation coefficient  $\pm$  SEM (from 313-626 mCLING-labeled organelles, from 12-89 cells for each protein).

The previous results indicate that the studied tubules participate in constitutive endosomal

traffic at a stage posterior to early endosomes, with its main location at the upper half of the IHCs.

### **3.3.12 mCLING-labeled organelles surrounding the cuticular plate participate in constitutive traffic to lysosomes**

A collection of mCLING-labeled organelles was always seen in the area surrounding the cuticular plate. Very active processes of endocytosis in a ring of cytoplasm surrounding the IHC cuticular plate have been described before (Kachar et al., 1997). Electron micrographs revealed abundant coated and uncoated vesicles in the pericuticular region, and mitochondria, microtubules and lysosomes in the subcuticular cytoplasm. All these organelles could be implicated in constitutive exchange of material between the IHC and the endolymph (Kachar et al., 1997; Spicer et al., 1999).

To study the nature of this local recycling I focused on the lysosome membrane associated protein 1 (LAMP1), a glycoprotein responsible for selective fusion in late endosomes and lysosomes (Chen et al., 1985; Dunster et al., 2002). After mCLING labeling and immunostaining for LAMP1, 200 nm melamine sections were imaged with two-color STED microscopy. In agreement to previous fluorescence microscopy studies (Goodyear et al., 2010), LAMP1 signal was found mainly located in the upper part of the IHC apical region, underlying the cuticular plate. Some of the mCLING-labeled organelles found at this region also contained LAMP1 (Figure 3.20A, and inset). Pearson's correlation values between LAMP1 and mCLING labeling were relatively high at the subcuticular area, contrasted by poor correlation everywhere else (Figure 3.20B). An important conclusion of these data is that newly endocytosed material is delivered towards late endosomes and lysosomal compartments within a relatively short period (around 3 minutes). These findings not only support the existence of a very active local recycling process taking place right around the cuticular plate, but also add up to the idea that IHCs reserve their apical region for constitutive membrane trafficking pathways.

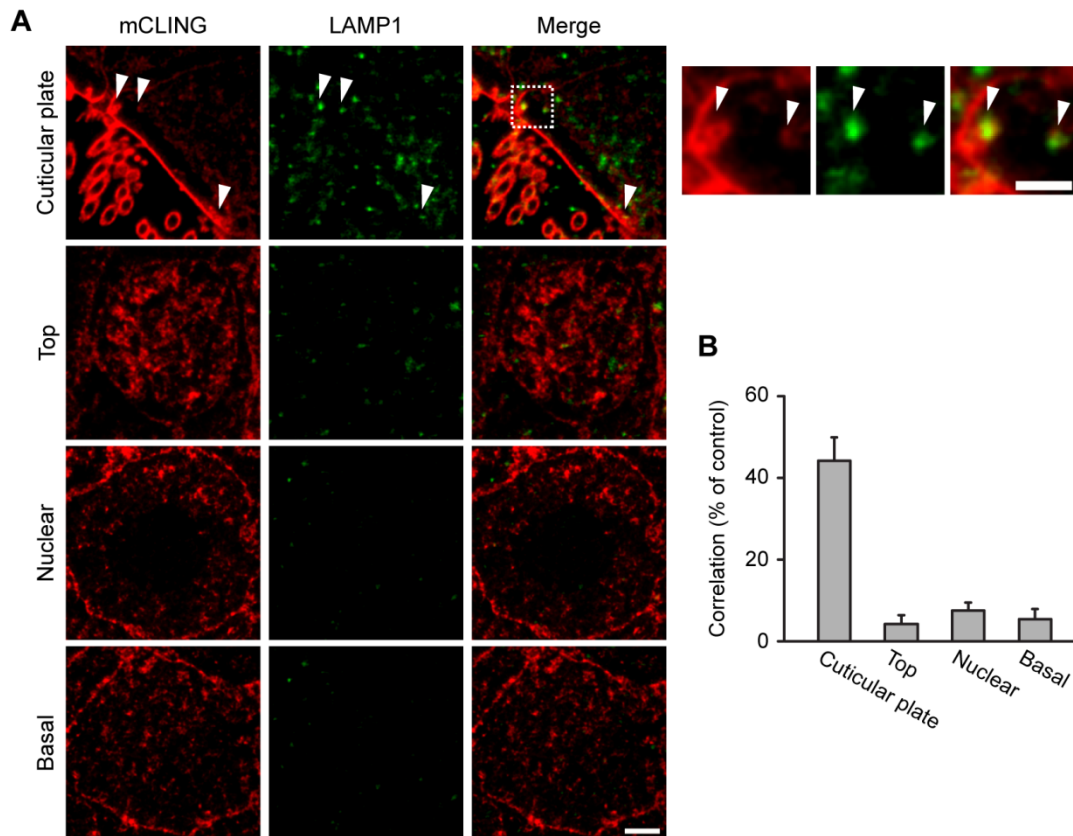


**Figure 3.20 mCLING-labeled organelles surrounding the cuticular plate contain the late endosome/lysosome marker LAMP1**

**A.** IHCs were labeled with mCLING, fixed and immunostained for the late endosome/lysosome marker LAMP1. Melamine sections were imaged in two-color STED microscopy. LAMP1 was abundant in the cytoplasmic volume that surrounds the cuticular plate, where it colocalized with some of the mCLING-labeled organelles (arrowheads). In other cell regions LAMP1 was not abundant and did not colocalize with the mCLING signal. Scale bar, 1  $\mu\text{m}$ , zoom-up 0.5  $\mu\text{m}$ . **B.** Pearson's correlation coefficients for LAMP1 and mCLING were calculated as for Figure 3.17. Note correlation at the level of the cuticular plate. 125-403 organelles were analyzed for each cellular region, from two independent experiments.

### 3.3.13 Functional separation of constitutive and synaptic recycling in IHCs is confirmed by multi-color epifluorescence imaging

Taking into account the evidence presented so far, I can conclude that IHCs compensate for the lack of a synaptic bouton by functionally and spatially separating the housekeeping trafficking pathways from the synaptic function. Accordingly, the organelles involved in the constitutive membrane trafficking pathways (e.g. the tubular type of endosomes characterized here, late endosomes/lysosomes and Golgi apparatus) were found to reside mainly at the upper half of the IHC. Conversely, SVs undergoing exocytosis and the intermediate structures involved in their recycling were exclusively located at the basal half of the cell.

In order to strengthen this hypothesis, a multi-color analysis simultaneously showing endocytosed organelles and markers for both, constitutive and synaptic function, would be necessary. The main difficulty to image such experiment in high-resolution STED microscopy was the limitation of our setup to only two colors. To circumvent this drawback an inexpensive solution was found: melamine blocks containing treated OCs were cut into 20-nm thick sections and imaged under a conventional epifluorescence microscope (instead of the 200-nm sections used so far for STED microscopy). In this way, high-resolution was achieved by physically reducing the axial dimension of the sample. The improved Z-resolution (25 to 30-fold higher than for a confocal microscope) allowed me to perform correlation analyses between the few copies of primary antibodies contained in the ultrathin slices.

OCs were labeled with mCLING at stimulation conditions (65 mM K<sup>+</sup>, 1 minute) and immunostained for two of the already used proteins in different combinations: VGLUT3 and otoferlin, VGLUT3 and syntaxin 6, otoferlin and syntaxin 16, and finally syntaxin 6 and syntaxin 16. When the two synaptic-related proteins VGLUT3 and otoferlin were labeled, triple colocalization with mCLING was only found at the basal level of the IHCs. In contrast, combination of VGLUT3 with the constitutive marker syntaxin 6 showed no coincidence of their signals at endocytic organelles, at any cell level. As expected, syntaxin 6 and syntaxin 16 colocalized with endocytosed organelles at the cell top and nuclear levels. Finally, otoferlin was found to colocalize with syntaxin 16 and mCLING at the cell top and nuclear levels, given its broad distribution (Figure 3.21A). Pearson's correlation values were calculated for the two immunostaining signals only in mCLING-labeled organelles. The obtained values go in agreement with the previous observations (Figure 3.21B).

Overall, multi-color imaging confirmed that the top and nuclear levels of IHCs are dedicated to support constitutive membrane trafficking, while the cell base is mainly responsible for sustaining the synaptic function.

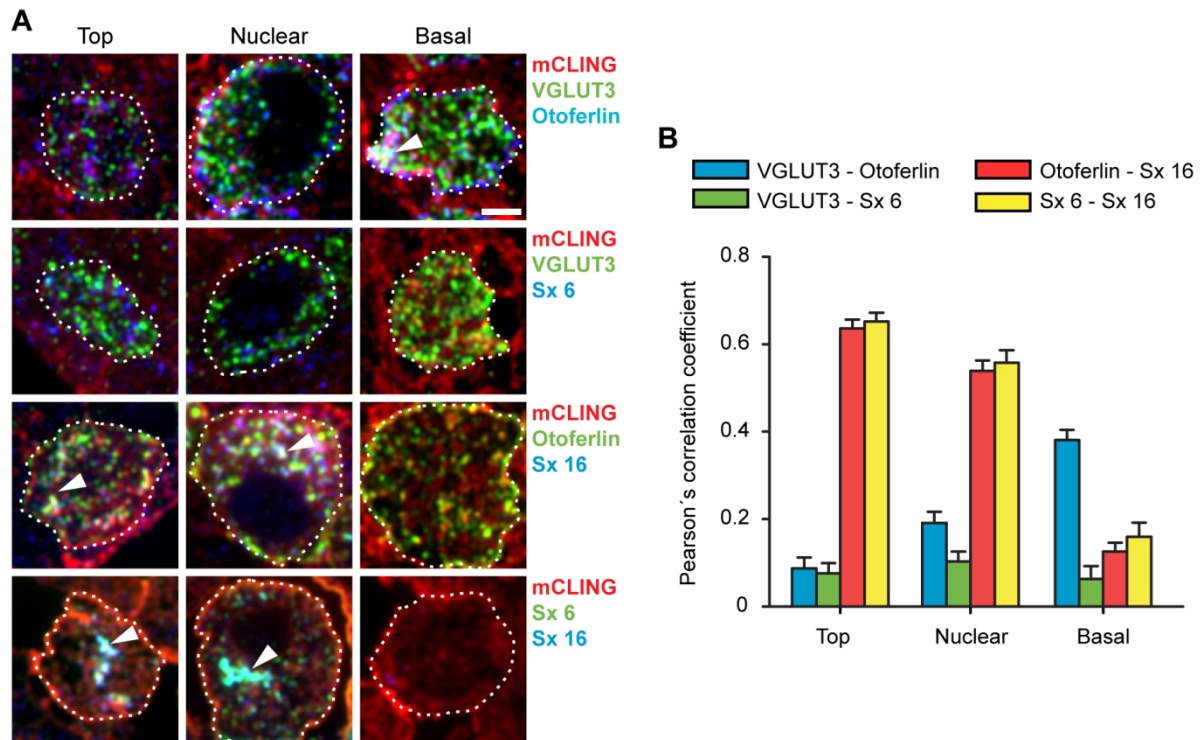


**Figure 3.21 Separation of constitutive and synaptic recycling pathways is confirmed by multi-color imaging**

**A.** After mCLING labeling under stimulation conditions, OCs were immunostained for VGLUT3 and otoferlin (first row of panels), for VGLUT3 and syntaxin 6 (second row), for otoferlin and syntaxin 16 (third row), and finally for syntaxin 6 and syntaxin 16 (fourth row). Samples were embedded in melamine, cut into 20-nm sections and imaged using a conventional epifluorescence microscope. Dashed white lines indicate the cell plasma membrane at every level. Note that synaptic markers (VGLUT3 and otoferlin) co-localize with mCLING only at the basal region (arrowheads), while VGLUT3 and syntaxin 6 do not co-localize at any cell level. The wide spread otoferlin co-localizes with syntaxin 16 at the top and nuclear levels. The two constitutive markers syntaxin 6 and syntaxin 16 also colocalize at those levels (arrowheads). Syntaxin 6 and syntaxin 16 were not abundant at the basal level. Scale bar, 2  $\mu$ m. **B.** Pearson's correlation coefficients for the two immunostained proteins were selectively calculated on mCLING-labeled organelles. The values confirm the colocalizations seen in A. Otoferlin and syntaxin 6 or syntaxin 16 correlate in the mCLING-labeled organelles at the top and nuclear levels. VGLUT3 correlates best with otoferlin at the basal level. At least 100 organelles were analyzed for each condition, at each cellular level.

### 3.4 Studies on synaptic vesicle recycling and protein distribution in hippocampal neurons using mCLING

As presented in the Introduction and the Results sections, mCLING was initially designed as a tool to answer the long-standing questions regarding the location of SV recycling in IHCs. I hope that the presented work convinced the reader that mCLING not only answered these questions successfully, but also offered new insights into the functional adaptations that IHCs underwent to perform efficient membrane traffic. As to now, mCLING was tested in large cells, relatively easy to image and where membrane recycling processes were not spatially constrained. The next objective was to test mCLING uptake in smaller cellular compartments. For this purpose, I moved to the synaptic boutons of hippocampal neurons, a preparation that despite its intense investigation still hosts controversial debates about synaptic vesicle recycling and protein organization.

Uptake into endocytic vesicles largely relies on the ability of a marker to distribute along the plasma membrane (see section 3.2). This becomes even more important in preparations where all events occur in a restricted membrane region, as is the case for the presynaptic terminal. Incubation of neurons with 0.4 – 0.68  $\mu\text{M}$  mCLING showed homogeneous labeling of the neuronal plasma membrane, not only in the cell soma, but also in the thin processes (Figure 3.22A). After showing that mCLING does not affect the plasma membrane integrity of COS7 cells at the concentrations required for appropriate membrane labeling and uptake (Figure 3.5), and that it does not disturb the recycling of organelles back to the plasma membrane (Figure 3.6), I complemented these assays with an experiment to evaluate the effect of mCLING on synaptic vesicle recycling in cultured hippocampal neurons. To this end, neurons were transfected with a VAMP2-pHluorin (synaptopHluorin) construct (see Figure 1.2). After 5 minutes of mCLING application, neurons were stimulated with a train of 60 action potentials (AP), and 40 seconds later with a train of 600 AP, while being imaged for pHluorin signal (See Methods sections 2.2.2.5 and 2.2.2.6). Fluorescence traces show that mCLING did not affect the amount of released synaptic vesicles or the kinetics of their recycling (Figure 3.22B). No significant differences in mean SV release were found between mCLING-treated and untreated cells (Figure 3.22C). The presented data confirm that mCLING does not have negative effects on the synaptic physiology of cultured neurons.



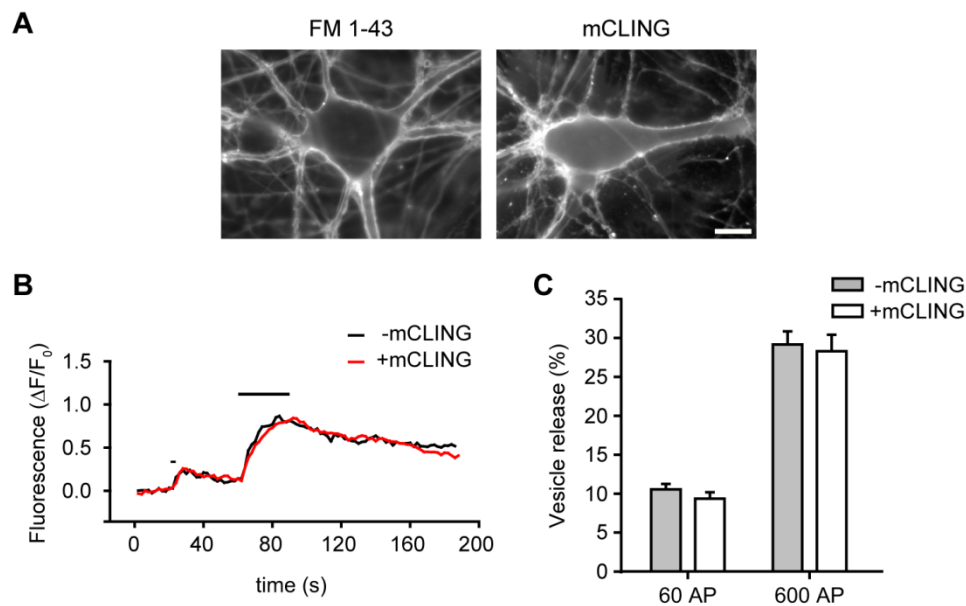


**Figure 3.22 mCLING does not affect synaptic vesicle recycling in hippocampal neurons.**

**A.** mCLING (0.68  $\mu$ M) labels the plasma membrane of hippocampal neurons in a similar fashion as FM 1-43, typically used to study SV recycling in these cells. **B.** Cultured hippocampal neurons were transfected with synaptotHluorin (Sankaranarayanan and Ryan, 2000). After 8 DIV, neurons were incubated for 5 minutes with mCLING and then stimulated at 20 Hz for 3 seconds (60 action potentials, AP), followed by a longer stimulus (30 seconds, 600 AP), with an interval of 40 seconds. SV exocytosis is seen as increases in synaptotHluorin fluorescence. The concomitant endocytosis is seen as fluorescence decay. Typical traces for a control cell (black) and a mCLING-labeled cell (red) are shown. The two stimulations are represented by the black bars over the traces. **C.** The mean amount of vesicles exocytosed after every stimulus is presented as normalized % of the total pool of vesicles. The latter was obtained by adding ammonium chloride at the end of the experiment to make all synaptotHluorin molecules visible. Exocytosis levels were comparable between mCLING-treated and untreated cells. Error bars represent mean percentage  $\pm$  SEM. Control neurons: 6 experiments, 138 boutons analyzed. mCLING treated neurons: 5 experiments, 103 boutons analyzed.

In the following three sections I will show the use of mCLING to study yet unanswered aspects of synaptic function. These experiments were performed in collaboration with my colleague Sven Truckenbrodt.

### 3.4.1 Actively and spontaneously released synaptic vesicles differ in protein composition

As explained in the Introduction, a topic of ongoing debate in the synaptic field is the nature of the spontaneously released synaptic vesicles. A first possibility is that they belong to the same pool of vesicles that normally serve stimulus-dependent neurotransmitter release, and are therefore recorded as fortuitous fusion events of readily releasable vesicles that are already primed (Groemer and Klingauf, 2007; Hua et al., 2010; Wilhelm et al., 2010; Loy et al., 2014). Another possibility is that spontaneously and actively-recycling vesicles actually

belong to different pools that diverge not only in their release (Sara et al., 2005; Mathew et al., 2008; Fredj and Burrone, 2009) but also in their retrieval mechanisms (Chung et al., 2010; Hua et al., 2011b). Furthermore, it has been proposed that spontaneously and actively-released synaptic vesicles differ in their molecular composition (Hua et al., 2011b; Ramirez et al., 2012) (Figure 3.23A).

The molecular composition of spontaneously recycled vesicles has been mainly studied by overexpressing fluorescently-tagged or truncated versions of synaptic and endosomal proteins (Hua et al., 2011b; Ramirez et al., 2012). The use of mCLING as fixable endocytosis marker offers the perfect alternative to look at endogenously expressed vesicular proteins without interfering with the normal synaptic physiology. For this purpose, we selectively labeled spontaneously or actively released synaptic vesicles and studied their molecular composition by subsequent immunostaining against different markers for SVs and proteins involved in constitutive trafficking. Actively released vesicles were labeled by incubating neurons in mCLING (0.68  $\mu$ M) during the delivery of electric stimulation at 20 Hz, for 30 seconds. After a recovery period of 5 minutes, neurons were fixed (4% PFA and 0.2% glutaraldehyde). Spontaneously released synaptic vesicles were labeled by incubating the neurons with mCLING for 15 minutes in presence of tetrodotoxin (TTX), a blocker of voltage-activated Na<sup>+</sup> channels used to stop the network electric activity to only allow spontaneous vesicle release (Wilhelm et al., 2010). After this treatment, cells were directly fixed. Separate immunostainings for five synaptic proteins (VGLUT1/2, synaptophysin, VAMP2, synaptotagmin 1 and synapsin) and three endosomal proteins (syntaxin 13, Vti1a and VAMP4) were performed. Neurons were embedded in melamine and sectioned at 40 to 50 nm for two-color STED imaging.

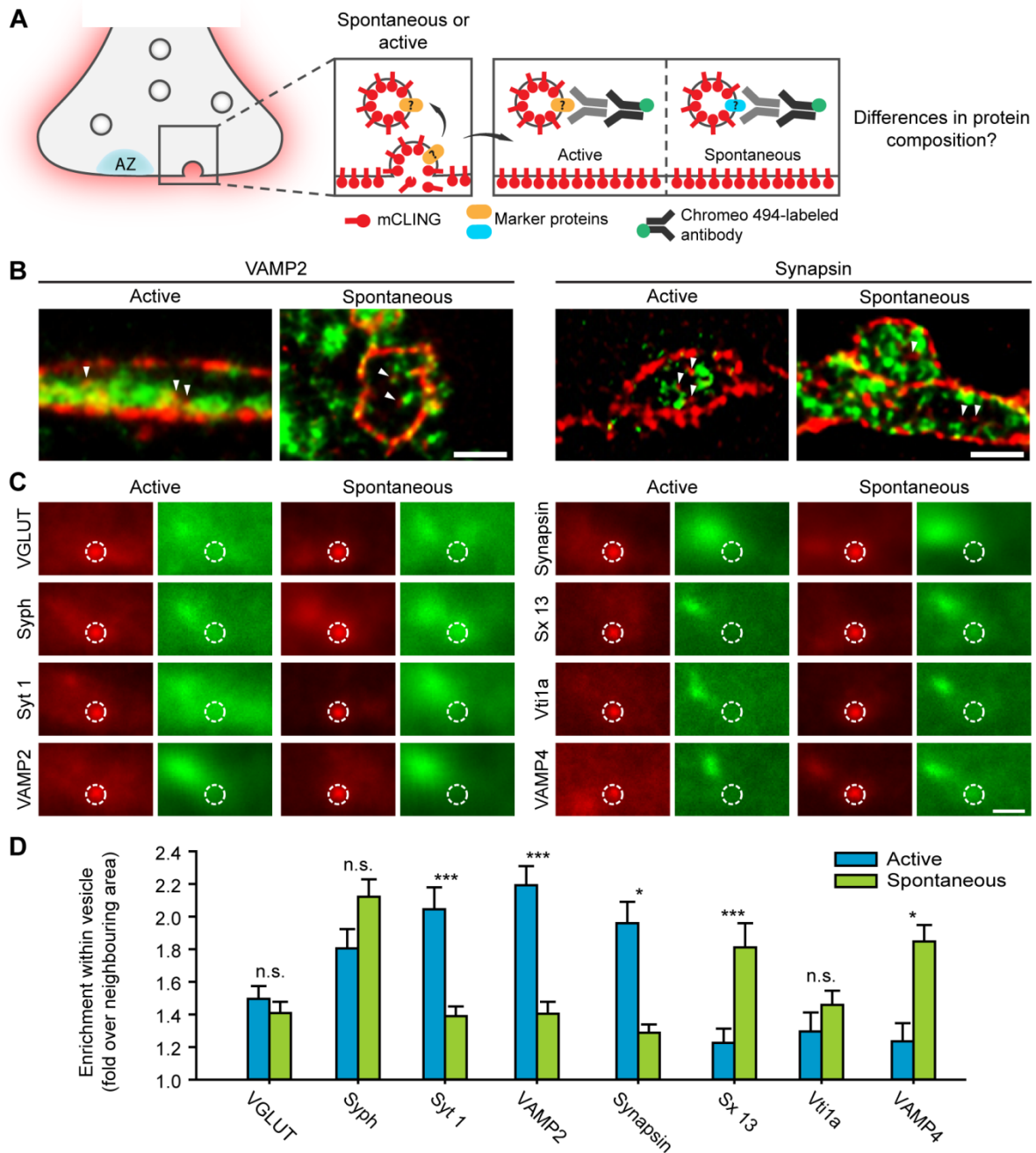


**Figure 3.23 mCLING reveals differences in molecular composition between actively and spontaneously released SVs**

**A.** Experimental principle: neurons were incubated with mCLING in presence of either electrical stimulation or TTX, to label actively or spontaneously recycled SVs respectively. Neurons were then fixed, immunostained, embedded in melamine and cut into 40-50 nm thick sections. Two-color STED microscopy of those sections was employed to estimate differences in molecular composition between the two types of recycling vesicles. **B.** Representative images for mCLING (red) and two proteins (green) of actively and spontaneously labeled synaptic boutons. Scale bar, 500 nm. **C.** A group of vesicles for every protein labeling and condition were stacked, aligned and averaged to determine the presence of the evaluated proteins in mCLING-labeled vesicles. Images in red show the average mCLING signal; green images show the corresponding average immunostaining signal. Dashed circles indicate the position of the average SV. Note that some, but not all proteins, coincide with the location of the average SV. The protein cloud at the upper left area of the green images corresponds to other mCLING-labeled and unlabeled vesicles in the surrounding area. Scale bar, 500 nm. **D.** Enrichment within mCLING-labeled vesicles was

calculated for all proteins, based on the basal fluorescence in the vicinity. The bars show means  $\pm$  SEM from 100-500 mCLING-labeled vesicles. n.s., no significant difference (t-test,  $P > 0.05$ ). \*, significant difference (t-test,  $P \leq 0.05$ ). \*\*, significant difference (t-test,  $P \leq 0.01$ ). \*\*\*, significant difference (t-test,  $P \leq 0.001$ ).

mCLING-labeled vesicles were visible inside synaptic boutons in both, inhibited and stimulated conditions. Immunostaining for synaptic and non-synaptic proteins was indeed also present inside boutons. As explained in section 3.3.5, plasma membranes appear discontinuous in these images due to lipid extraction during the fixation and permeabilization procedures (Figure 3.23B). mCLING and immunostaining images were analyzed to establish the presence of the different proteins in spontaneously and actively released synaptic vesicles. To this end, at least 100 SVs for every condition and every protein were overlapped and rotated until finding perfect matching between structures and membranes, in a similar analysis to the one used in Figure 3.16B, to generate average images for both the mCLING and the immunostaining channel. The average images give an idea of how abundant every protein is in the evaluated vesicles (Figure 3.23C). Using these average images, the levels of protein enrichment inside vesicles, normalized to background levels, were calculated. This analysis discloses quantitative differences in protein composition between the two pools. Spontaneously released vesicles had higher levels of the endosomal proteins syntaxin 13 and VAMP4, and significantly lower levels for the synaptic vesicle proteins synaptotagmin 1, VAMP2 (Synaptobrevin 2) and synapsin. Nevertheless, other synaptic vesicle proteins like the glutamate transporter VGLUT1/2 and synaptophysin were found in comparable levels. These results indicate that spontaneously and actively released synaptic vesicles are indeed two different organelle populations.

### **3.4.2 mCLING surface labeling for the study of membrane-associated proteins**

A readily retrievable pool of presorted and preassembled synaptic vesicle proteins has been suggested to remain stranded on the plasma membrane. Upon stimulation, this pool could drive a first wave of endocytosis upon stimulation, in order to compensate for the time that requires to create clathrin coats on recently exocytosed membranes (Sankaranarayanan and Ryan, 2000; Gandhi and Stevens, 2003; Fernández-Alfonso et al., 2006; Wienisch and Klingauf, 2006). This hypothesis would imply that in order to regenerate synaptic vesicles from this pool of molecules, the relative abundance of every protein should reflect that of the average synaptic vesicle. However, a variety of studies replicating pHluorin fusion for different synaptic proteins have reached varying values for the fraction of molecules

remaining at the membrane: ~2% for VGLUT1 (Balaji and Ryan, 2007), ~8% for synaptophysin (Granseth et al., 2006), ~10-24% for synaptobrevin (Sankaranarayanan and Ryan, 2000; Granseth et al., 2006) and ~22% for synaptotagmin (Fernández-Alfonso et al., 2006). These differences would suggest that the stranded pool is rather the result of varying post-exocytosis retrieval efficiencies among the different synaptic vesicle proteins. With the aim to study this question by an overexpression-independent method, we used mCLING labeling of the plasma membrane as reference point to discern between native immunostained proteins residing at intracellular organelles and those associated to the cell surface. Moreover, we included in the analysis Rab3 and synapsin, two cytoplasmic proteins that transiently associate with synaptic vesicles and therefore cannot be coupled to pHluorin.

First, cultured hippocampal neurons were labeled with mCLING for 5 minutes at low temperature (2-4°C), to selectively label the plasmalemma and estimate the amount of proteins present on it at resting conditions. Neurons were subsequently fixed (4% PFA and 0.2% glutaraldehyde) and immunostained for the synaptic proteins VGLUT1/2, synaptophysin, synaptotagmin 1, VAMP2, synapsin and Rab3 (Figure 3.24A). After immunostaining, cells were embedded in melamine, cut into 40-50 nm sections and imaged by two-color STED microscopy. Using a customized MatLab routine (by Silvio O. Rizzoli), the amount of protein signal contained in the plasma membrane was measured and compared to the total amount of protein found in the axons (see examples in Figure 3.24B). To avoid the quantification of proteins contained in docked synaptic vesicles, only the protein signal coming from the brighter core of the plasma membrane was taken into account. The results show that the fraction of proteins present in the plasma membrane ranged between ~12 and ~22% for all proteins, indicating that relatively high amounts may be participating in fast compensatory recycling of synaptic vesicles (Figure 3.24C). Although these results still report certain variability in membrane-associated protein levels across the evaluated candidates, this difference is narrower than that reported by pHluorin-based assays. This speaks for the high-throughput and fidelity of mCLING labeling coupled to immunostaining.

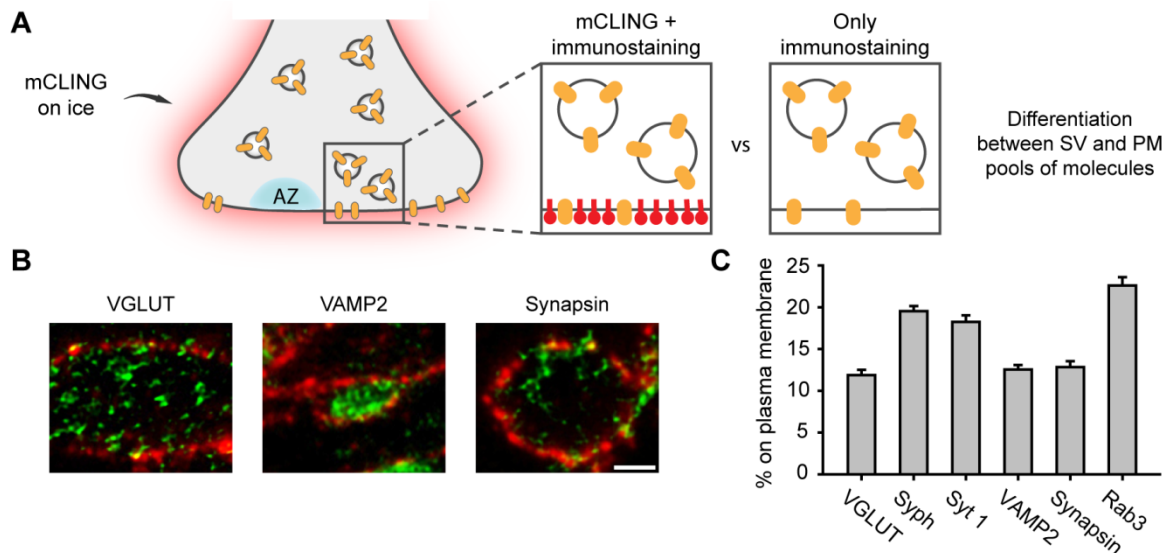


**Figure 3.24 mCLING labeling allows the distinction between the organelle- and the membrane-associated fractions of synaptic vesicle proteins.**

**A.** Experimental scheme: in contrast to conventional immunostaining procedures, where it is impossible to recognize the pool of proteins associated to the plasma membrane (right panel), surface staining at low temperature provides a reference point to easily identify them (left panel). **B.** Typical example pictures of boutons and axonal membranes labeled with mCLING (red) and containing the intracellular and surface fractions of immunostained proteins (green). Scale bar, 500 nm. **C.** Quantitative analysis of the percentage of protein associated with the plasma membrane from the total amount of protein. The bars show means  $\pm$  SEM from 99 to 270 mCLING-labeled membrane areas.

### 3.4.3 Organization of t-SNARE proteins on the plasma membrane and organelles

The diversity of membrane fusion processes taking place in a cell are largely mediated by SNARE proteins (Jahn and Scheller, 2006). In the case of synaptic vesicle release, for example, the t-SNAREs syntaxin 1 and SNAP-25 form a complex with the v-SNARE synaptobrevin, that upon  $\text{Ca}^{2+}$  influx leads to membrane fusion. Several studies based on diffraction-limited and -unlimited microscopy methods have proposed that syntaxin 1 (Lang et al., 2001; Sieber et al., 2006, 2007; Bar-On et al., 2012; Pertsinidis et al., 2013) and SNAP-25 (Halemani et al., 2010; Rickman et al., 2010) form protein clusters on the axonal plasmalemma or the plasma membrane of neuroendocrine cells (PC12 cells), serving as membrane domains where synaptic vesicle fusion would preferentially happen. In contrast, no information is available on how these proteins are organized in axonal organelles. As explained in the previous section, the difficulty to distinguish the plasmalemma and the membranes of intracellular organelles in immunostained preparations makes impossible to assign the labeled molecules to one or another. We combined mCLING labeling with

immunostaining against syntaxin 1 and SNAP-25 to address this question.

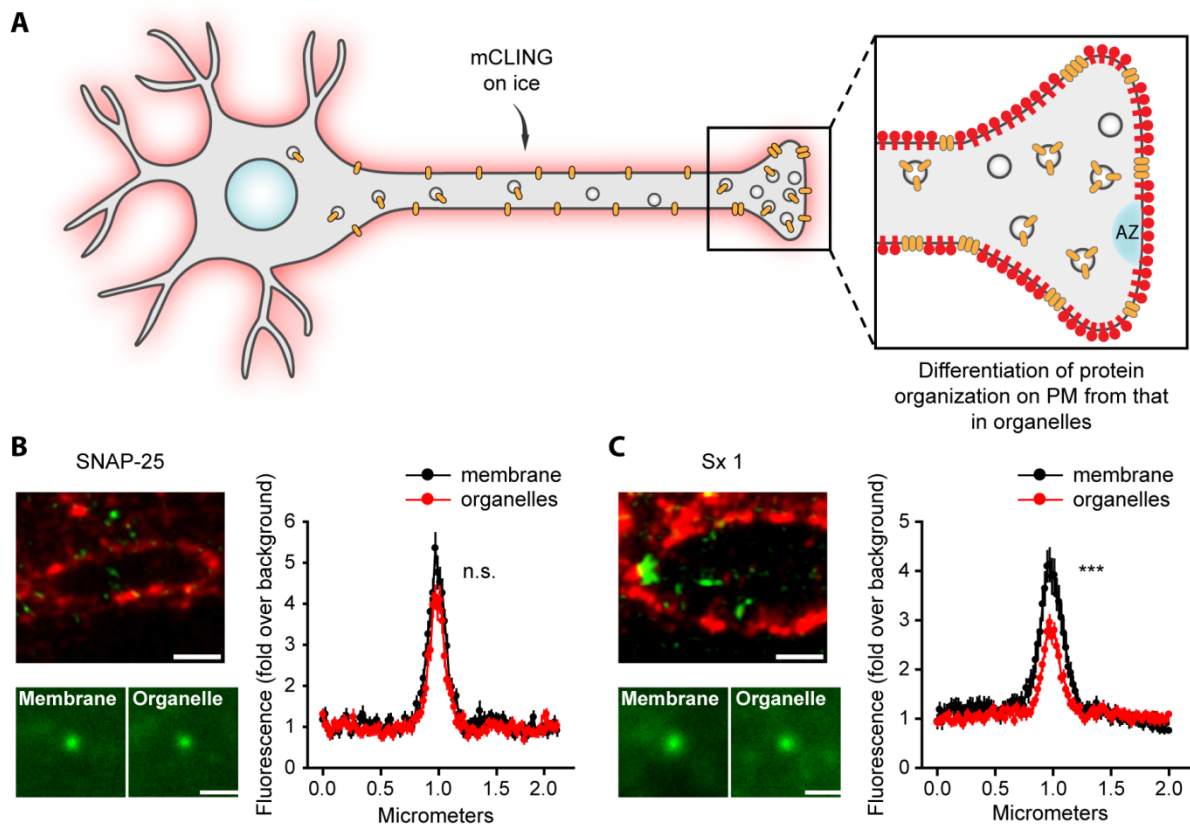


**Figure 3.25 Analysis of membrane-associated protein clusters at high resolution using mCLING**

**A.** Experimental principle: in the same way as in Figure 3.24, mCLING labeling performed at low temperature allows for the selective labeling of the plasma membrane. Combined with immunostaining against proteins of interest, this approach can be used to compare protein cluster located on the plasma membrane with those on organellar membranes. **B.-C.** Top left panels show example two-color STED images of mCLING membrane labeling (red) and immunostaining (green) against the two SNARE proteins of interest, SNAP-25 (**B**) and syntaxin 1 (**Sx 1**, **C**). Scale bars, 500 nm. The bottom left panels show average images from 88-90 SNAP-25 protein clusters, or 115-133 syntaxin 1 protein clusters, selected either from the plasma membrane or from the intracellular organellar signal. Scale bar, 500 nm. Right panels show average line scans through the protein clusters. Graphs show means  $\pm$  SEM, from the same organelles. n.s., no significant difference in intensity between the peaks of the two distributions (t-test,  $P > 0.05$ ). \*\*\*, significant difference (t-test,  $P \leq 0.001$ ).

The same methodological approach used in the last section was adopted here. Cultured hippocampal neurons were labeled with mCLING at low temperature, to ensure surface-only staining (Figure 3.25A), and were immunostained, embedded, cut into 40-50 nm sections and imaged in two-color STED microscopy. This procedure allowed the visual separation between protein molecules associated to the plasma membrane and those inside the cell (as example see Figure 3.25B and C, left upper panels). Using a customized MatLab routine (by Silvio O. Rizzoli), several protein clusters identified in the immunostaining channels were

stacked, aligned by their center of mass and averaged (Figure 3.25B and C, left lower panels). The average size of the clusters was calculated by measuring fluorescence intensity distribution in line scans positioned across the selected clusters. The results show that clusters of SNAP-25 in the plasma membrane have comparable sizes to those found on the organelles (Figure 3.25B, right panel). On the other hand, syntaxin 1 clusters found on the plasma membrane were larger and brighter than their counterparts sitting on the organelles (Figure 3.25C, right panel).



## 3.5 Application of mCLING to other biological preparations

### 3.5.1 mCLING uptake in stimulated neuromuscular junctions of the *Drosophila* larva

Wanting to prove that mCLING can work in a wide range of applications, another conventional synapse was explored, the larval *Drosophila* neuromuscular junction (NMJ). Relying on the release of large amounts of neurotransmitter to keep up with constant muscle contraction, neuromuscular junctions represent an efficient and constantly functional synaptic vesicle recycling machinery. Although this synapse has been extensively studied (see for review (Rizzoli and Betz, 2005)), details on the morphology and location of stimulation-dependent endocytic processes could be further studied with a membrane marker like mCLING.

Preliminary experiments in the third instar *Drosophila* larva NMJ were carried out. Larvae were dissected to expose the ventral muscles and pinned down to a silicone surface. Once open, the preparation was preincubated with a 1.7  $\mu\text{M}$  mCLING solution during 2 minutes and electrically stimulated thereafter with 160 APs (20 Hz for 8 seconds) in presence of mCLING (same concentration). The preparation was immediately fixed in the same way as for the organ of Corti, and immunostained against the active zone organizing protein Bruchpilot (Kittel et al., 2006). mCLING not only labeled the intricate structure of the subsynaptic reticulum, but it also reached the plasma membrane of the presynaptic bouton. mCLING (red) was taken up into round and elongated endocytic structures, some of them apparently still connected to the plasma membrane. Many of the endocytosed structures were found surrounding the active zones (green) (Figure 3.26A, B).

The image shown in Figure 3.26 confirms that mCLING easily diffuses into complex tissue preparations and that combined with immunostaining against the active zones, has a strong potential in the study of synaptic vesicle recycling.

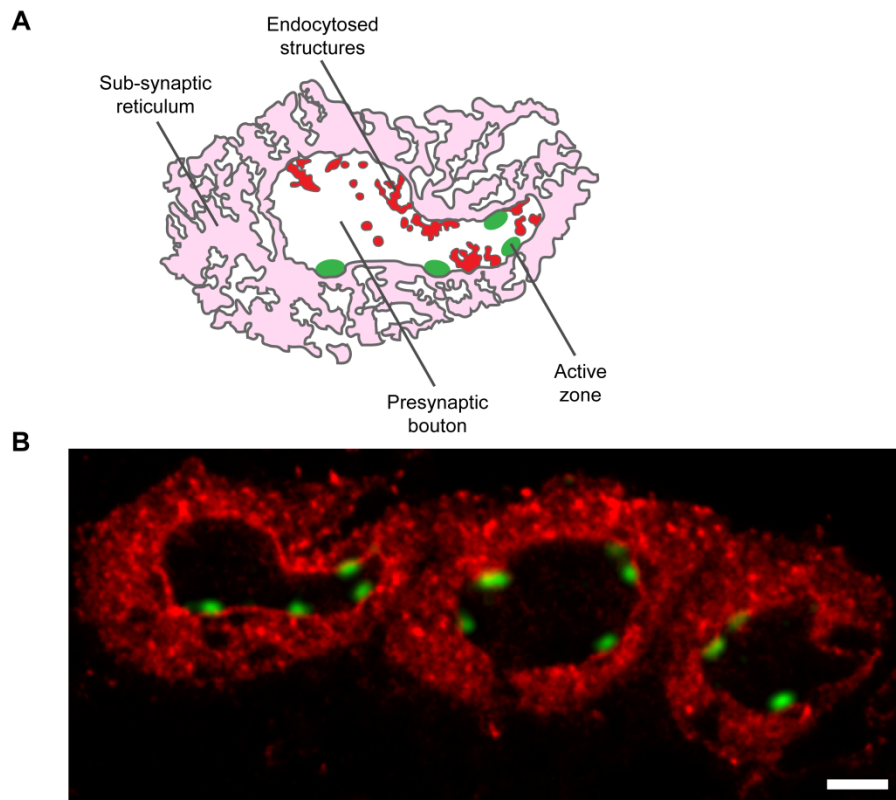


**Figure 3.26 mCLING uptake in the *Drosophila* larva neuromuscular junction.**

**A.** Schematic representation of a single mCLING-labeled presynaptic bouton of the *Drosophila* larva NMJ, taking as example the first one on the left depicted in B. **B.** The preparation was electrically stimulated in presence of mCLING, was fixed and immunostained for the active zone protein Bruchpilot, using the nc82 antibody. Note the presence of mCLING uptake within the synapse, representing endocytosis, as in IHCs. Scale bar, 1  $\mu\text{m}$ . Sample preparation, processing and imaging of the example shown in B. was performed by Goran Kokik, student at the MSc/PhD Molecular Biology Program (Göttingen), under my supervision.

### 3.5.2 Membrane labeling in microorganisms with mCLING

#### 3.5.2.1 mCLING can be used to study membrane uptake in yeast cells

With the advent of FM styryl dyes as fluorescent plasma membrane markers, the red-shifted FM 4-64 was established as a routine endocytosis marker in *Saccharomyces cerevisiae* yeast cells (Vida and Emr, 1995). Being yeast cells a typical biological model for the study of membrane recycling and cell cycle, FM 4-64 became a key tool to study the sites of membrane uptake, the organelles involved in membrane trafficking between the plasma membrane and the vacuole, and the cell functional state. Accordingly, FM 4-64 uptake is a standard test to compare the endocytosis efficiency between cells expressing mutant versions of traffic-related proteins (see for example (Rieder et al., 1996; Tuo et al., 2013)).

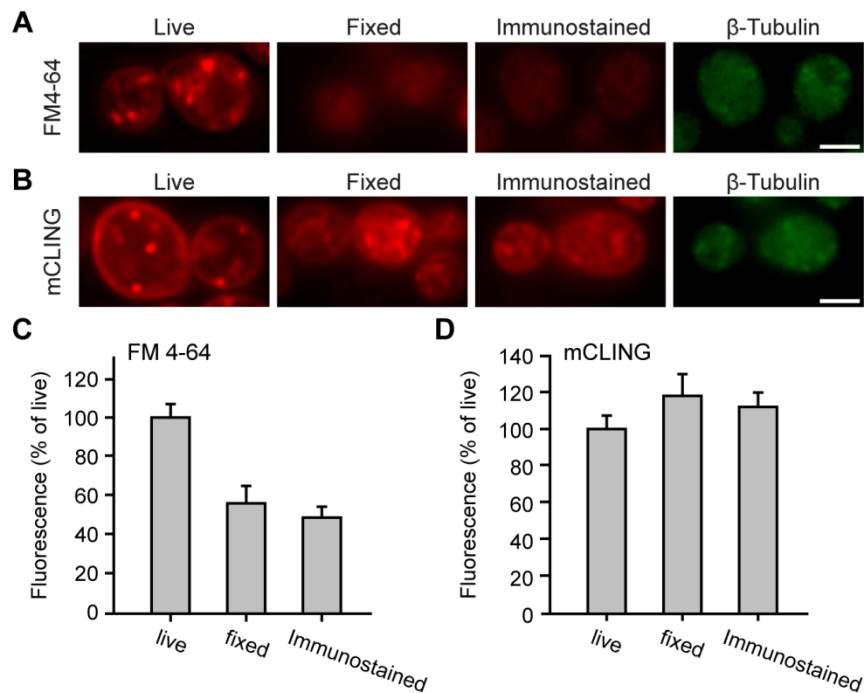


**Figure 3.27 mCLING is taken up in endocytic compartments in yeast cells.**

**A.** *S. cerevisiae* yeast cells from the strain BY4742 were incubated with FM 4-64 for 20 minutes at room temperature and imaged with an epifluorescence microscope in different conditions: live (left panel), after fixation for 30 minutes with 4% PFA + 0.2% glutaraldehyde (middle panel), or after permeabilization and immunostaining for tubulin, using an anti-tubulin single-chain recombinant antibody (Nizak et al., 2003) (right panels). FM 4-64 labels endocytic organelles in living cells, but is lost after fixation and permeabilization. Scale bar, 2  $\mu$ m. **B.** Cells were incubated with mCLING and processed in the same way as for FM 4-64. mCLING labeled endocytosis in the same way as the FM dye, but did not come off membranes after fixation, nor after permeabilization. Scale bar, 2  $\mu$ m. **C.** Quantification of FM 4-64 fluorescence levels confirms its detachment from membranes after fixation and permeabilization. Bars represent mean fluorescence  $\pm$  SEM from 17 to 24 fields of yeast from every condition. Values are represented as percentage of the live condition. **D.** The same quantification for mCLING confirms its fixability, even after immunostaining. The analysis included 24 to 31 fields of yeast cells for each condition.

Using *S. cerevisiae* cells (strain BY4742) I compared mCLING and FM 4-64 in their uptake, fixability and stability after permeabilization. Cells were immobilized on PLL coated coverslips and incubated for 20 minutes with either 20  $\mu$ M FM 4-64 or 0.4  $\mu$ M mCLING. Cells were imaged in epifluorescence microscopy live, fixed, or fixed and immunostained. FM 4-64 labeled endocytic organelles in living yeast cells, as described before. However, its fluorescence was strongly reduced after fixation and permeabilization, giving a very diffuse and poor labeling inside the cells (Figure 3.27A). mCLING also labeled membranes and endocytic structures in living cells, in a very similar pattern to FM 4-64. After fixation and permeabilization, the advantage of mCLING fixability was evident, since the plasma membrane and labeled organelles were still distinguishable with fluorescence intensities

similar to the living condition (Figure 3.27B). These observations were validated by a quantitative analysis evaluating the percentage of fluorescence loss at the different conditions (Figure 3.27C, D).

These results confirm that mCLING is compatible with live imaging of endocytic processes in yeast, offering an extra advantage of fixing the cells and looking at protein distribution by combination with immunostaining.

### **3.5.2.2 High-resolution imaging of *Escherichia coli* membranes with mCLING**

In the past, the labeling of plasma membranes in different gram-negative bacterial species has been important to, for example, discover cell division defects and ampicillin resistance in mutant cells of *Escherichia coli* (Uehara et al., 2009); to identify membrane-associated proteins as virulence factors in *Pseudomonas aeruginosa* (Luckett et al., 2012); or to discover important determinants for *Vibrio cholerae* biofilms formation (Houot and Watnick, 2008). Membrane labeling has also allowed the visualization of chromosomal distribution in the gram-positive *Staphylococcus aureus* (Yu et al., 2010). What all these examples have in common is the use of the brightest member of the FM dyes family, FM 1-43. They also highlight the importance of simple membrane labeling procedures in the study of human pathogens.

Given the already proved convenience of mCLING over FM dyes, I concluded this study by comparing the membrane labeling capacity of mCLING to that of FM 1-43 in cells of the species *E. coli*. In a fast and simple procedure, cells were incubated with either mCLING or FM 1-43 for 5 minutes. After a brief wash and immobilization on PLL coated coverslips cells were ready to be imaged. Since the fluorescent properties of FM 1-43 are not compatible with STED microscopy, its labeling was imaged with conventional confocal microscopy. In contrast, the conjugation of mCLING with the more stable dye Atto 647N allowed, as shown along this study, its imaging with the high-resolution technique. Both dyes labeled the plasma membrane of the bacteria, with no apparent interference from the cell wall encapsulating the plasma membrane. While confocal images of FM 1-43 appeared more homogeneous in distribution and intensity (Figure 3.28A), the STED images of mCLING revealed areas and dots of higher label intensity, in particular at the cell centers and places of division (Figure 3.28B).

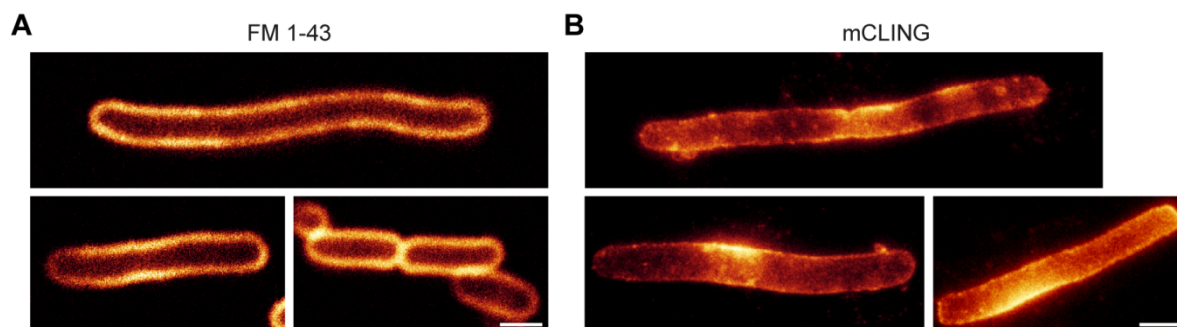


**Figure 3.28 High-resolution imaging of mCLING-labeled membranes of *E. coli* cells.**

**A.** *E. coli* bacteria were incubated with FM 1-43 for 5 minutes, washed and imaged using a confocal microscope. Scale bar, 1  $\mu\text{m}$ . **B.** Alternatively, cells were incubated with mCLING in the same way as with FM 1-43, and were imaged using STED microscopy. Note the improved resolution and detail in membrane labeling pattern in these images. Although both dyes give an inhomogeneous labeling, mCLING could better show brighter areas in the central regions. This particular feature remains to be studied. Scale bar, 1  $\mu\text{m}$ .



## 4 DISCUSSION

---

With the advent of electron microscopy as the first high-resolution microscopy technique, it became clear that the plasma membrane not only constitutes a barrier (Robertson, 1960), but also an exchange platform between a cell and its environment (Fawcett, 1965; Heuser and Reese, 1973; Anderson et al., 1977; Heuser et al., 1979). Another great step in the understanding of subcellular composition came with the development of immunostaining procedures (Marrack, 1934; Coons et al., 1941; Coon et al., 1942). Moreover, the generation of fluorescent lipid-soluble molecules made possible to label membranes in living cells and follow physiological processes like organellar trafficking (Klausner and Wolf, 1980; Struck and Pagano, 1980; Spiegel et al., 1984; Honig and Hume, 1986). Combinations of these approaches have been devised to better understand endocytosis and membrane recycling. Photo-oxidation, for example, allows the transformation of an endocytosed fluorescent signal into an electro-dense precipitate (Sandell and Masland, 1988; Henkel et al., 1996; Gaffield and Betz, 2006). Labeling of antibodies with metallic particles paved the way to immunoelectron microscopy (immuno-EM), for the study of organelle molecular composition at high-resolution (Singer, 1959; Faulk and Taylor, 1971). Furthermore, photo-oxidation and immuno-EM have been combined in an effort to establish the molecular identity of recycling organelles (Malatesta et al., 2013). This last approach, however, has several drawbacks: very low throughput due to laborious sample preparation and extensive imaging time; very low labeling density typical of immuno-EM procedures; and labeling of several proteins at a time limited by the use of metallic particles of different sizes.

The main aim of this study was to establish a simpler, more efficient and more reliable method for the molecular characterization of trafficking organelles. The main motivation for developing such method is the discovery of differences in composition and therefore function among membrane-bound compartments making up, for example, diverse routes of endosomal trafficking or varying types of synaptic vesicles. These results go against that old premise among electron microscopy studies claiming that organelles that are morphologically indistinguishable should accomplish the same function. Surprisingly, in spite of decades of microscopy advances, the molecular study of trafficking organelles has been difficult until now. Although a wide offer of fixable membrane-binding fluorescent

molecules has been put in the market to address this question, none of them can be satisfactorily fixed. Moreover, their fluorescent properties are not compatible with the lately developed high-resolution fluorescence microscopy techniques.

With this background in mind, the main strategy implemented was to design a fixable, fluorescent membrane-binding molecule that would allow the recognition of plasma membranes and endocytic organelles, and that could be combined with the identification of molecular markers by immunolabeling. Since molecular interactions and protein distributions deduced by colocalization under diffraction-limited confocal microscopy can be inaccurate or misleading, I went for a high-resolution microscopy technique as a better way to understand the complexity of subcellular processes (Saka and Rizzoli, 2012). Stimulated Emission Depletion (STED) microscopy offers advantages over other far-field optical nanoscopy techniques (Hell, 2007), like instant delivery of diffraction-unlimited images without the need of further computation and relatively fast imaging times, with a resolution ranging from 40 to 100 nm in our own setup.

The newly developed probe was applicable not only to cultured or isolated cells, but also to complex tissues. Indeed, the initial motivation of this study was the understanding of synaptic vesicle recycling in a cell type difficult to approach, the inner hair cell (IHC) of the mammalian inner ear. In the following sections I will discuss on the process of generating the ideal membrane-labeling probe and its successful application to a wide variety of biological preparations, with more detail on how the new probe solved long-standing questions related to IHC physiology.



## 4.1 The correct recipe for a fixable membrane probe

I first approached the development of a novel membrane-binding tool by understanding the requirements of IHC labeling, as the initial focus of this study. As presented in sections 3.1.1 and 3.2.1, there are two main difficulties imposed by the biology of IHCs for understanding their membrane trafficking processes. First, the presence of mechanoelectric transduction (MET) channels at their apical pole that allow the permeation of small molecules, like the typically used fluorescent membrane probes, giving an artifactual non-endocytic intracellular labeling (Nishikawa and Sasaki, 1996; Gale et al., 2001; Meyers et al., 2003). Second, the lack of a synaptic bouton that physically separates synaptic vesicle recycling from other constitutive membrane trafficking pathways, making difficult their isolated study (Siegel and Brownell, 1986; Lenzi et al., 1999).

In order to solve the first issue I revisited data obtained previously in our laboratory indicating that, at least at room temperature, commonly used membrane/endocytosis markers, including styryl dyes from the FM family, entered IHCs through their MET channels (Kamin, 2011). By applying these dyes at low temperature (2-4°C) to inhibit endocytic processes, I found that they still penetrated the IHCs, confirming an endocytosis-independent labeling mechanism (Figure 3.1). The previous results were pooled together in a publication (Kamin et al., 2014) that not only confirmed previous data on MET channels dye permeation (Nishikawa and Sasaki, 1996; Gale et al., 2001; Meyers et al., 2003), but also expanded it to other probes. These results highlighted the need of finding a proper marker for IHCs endocytosis, whose study was hampered since the last publication on this issue using FM dyes almost a decade ago (Griesinger et al., 2005).

I next generated molecules that combined a protein source of amine groups, a lipidic tail and/or a fluorescent component, which would respectively allow aldehyde fixation, membrane binding and fluorescence microscopy imaging. When tested on cultured neurons, I found that large molecules (e.g. based on transferrin, ~80 kDa) did not distribute homogeneously on the plasma membrane and were not taken up into endocytic structures. Smaller molecules (e.g. based on insulin, ~6.9 kDa) could better distribute on membranes, but could not be efficiently fixed, probably due to concealing of their amine groups by the tridimensional structure of the proteins (Figure 3.2). On the other hand, however, molecules bearing abundant amine groups but not lipidic tails (e.g. fluorescently labeled PLLs) had poor fixability, probably due to preferential crosslinking between their own groups than with the proteins at the membranes (Figure 3.3). **These results indicated that the ideal**

**fixable membrane-labeling probe should have a few amine groups easily accessible by aldehyde fixatives, a lipidic component that could help to strong binding and stability on membranes, and finally, it should only have a few kDa in mass for a better distribution and uptake.** Moreover, we concluded that the lipidic component also contributes to endocytic uptake, since hydrophilic molecules in the fluid phase were not easily taken up, although it should not be too large to avoid trapping at membranous structures surrounding tissues (e.g. FM 3-25 with two tails of 18 carbons) (Kamin et al., 2014). In the context of IHC labeling, application of FM dyes and fluorescently labeled PLLs to organs of Corti suggested that the ideal size of the probe should be between 0.7 and 6 kDa to compensate between MET channel permeation and efficient tissue penetration. Finally, I found that post-labeling procedures like permeabilization (required for later immunostaining) and plastic embedding worsened the fixability of all tested probes, improving only by the combination of PFA with a better fixative like glutaraldehyde.

### 4.2 mCLING labels endocytosis and stays on membranes upon fixation and permeabilization

mCLING was developed as the outcome of the exploratory phase described in the previous section. With seven amine groups provided by a lysine polypeptide, a hexadecanoic hydrophobic tail (palmitoyl-) and an exchangeable fluorophore (Atto 647N in this study), mCLING is a ~2 kDa molecule that homogeneously distributes on plasma membranes and is efficiently taken up into endocytic organelles (Figure 3.4). When compared to non-fixable and fixable dyes from the FM family, this novel molecule was superior in fixability, even after permeabilization (Figure 3.7). Surprisingly, whereas mCLING stayed on plasma membranes and endocytosed organelles after fixation and detergent treatment, fixable FM dyes like AM1-43 and FM 4-64FX detached from those membranes and ended up collected in mitochondria-like structures. Taking into account that FM fixable dyes are coupled to only one amine group, claimed by the manufacturers to confer fixability, these observations confirmed that appropriate fixability of a molecule requires at least several amine groups, and that fixation procedures based only on PFA are not sufficient to keep these molecules in place. In order to further confirm these results I searched for previous publications in which uptake of fixable FM dyes was combined with only fixation or fixation and immunostaining (Wegner et al., 2008; Sousa et al., 2009; Fuenzalida et al., 2011; Mlcochova et al., 2013). Remarkably, FM dye labeling ranged between diffuse, diffuse combined with punctae, and mitochondrial-like, instead of just punctated as it would be expected from endocytic uptake

of either single large organelles or in batch as in synaptic active zones. Interestingly, in one of these publications macrophages were labeled with either FM 4-64FX or CellMask (commercial name for another amphipathic membrane-binding molecule) and fixed, with both dyes giving a mitochondrial-like staining (Mlcochova et al., 2013). Even though the manufacturer declares that CellMask is suitable for fixation but not for permeabilization, the images show that only fixation already removes the molecule from the plasma membrane. This analysis evidences that artifactual labeling as a result of poor fixability has been continuously underestimated by researchers and product developers.

Further experiments showed that in contrast to FM dyes, mCLING is not washable, probably due to a more stable inclusion in the membrane provided by its 16-carbon long tail, compared to the two shorter tails each of 2 or 4 carbons present in FM 4-64 and FM 1-43, respectively. mCLING was also found to be innocuous for the cells at the concentrations required for cell labeling and imaging (0.2-0.4  $\mu$ M). This was concluded from the preserved membrane integrity and normal ligand-receptor endocytosis and trafficking in mCLING-treated cells (Figure 3.5 and Figure 3.6). Additionally, mCLING was taken up indistinctly by different endocytic processes, as evidenced by its colocalization with ligands like transferrin, EGF and LDL. mCLING stability after immunostaining also allowed to confirm its colocalization with the endosomal marker Syntaxin 6 (Figure 3.8). Altogether, mCLING promises to be a suitable pan-endocytosis marker with no toxic effects and probably the only one available that is compatible with immunostaining, perfectly fitting with the requirements for the molecular characterization of recycling organelles.

## 4.3 Membrane trafficking in IHCs

### 4.3.1 Technical improvements for the application of mCLING to the organ of Corti

Application of mCLING to organs of Corti demonstrated that it does not permeate the MET channels at the apical pole of IHCs. Whereas FM dyes strongly and homogeneously labeled IHCs cytoplasm, mCLING labeling was not as strong, revealing the plasma membrane and some organelles inside the cells (Figure 3.9). Importantly, mCLING also labeled membranes and organelles of other cell types in a comparable intensity, which was not the case for FM dyes, whose labeling was much stronger in outer and inner hair cells. Incubation of mCLING at low temperature to inhibit endocytosis showed the lack of the dye from the cytoplasmic region, or even the arrest of endocytic processes, confirming that mCLING uptake by IHCs is

solely dependent on endocytosis (Figure 3.10).

One major difficulty in the use of mCLING for the study of IHCs was the compact and complex structure of the organ of Corti. A physical barrier for mCLING diffusion into the tissue was imposed by the tectorial membrane. Due to its mesh-like structure and composition, the tectorial membrane worked as a trap for mCLING molecules. Although good dissections were important for IHC preservation, they also implicated a tighter contact of the cells with the tectorial membrane, reducing the space gap for mCLING passage. Diffusion of mCLING into the organ of Corti also took place from the side of the basilar membrane. I found that mCLING at a concentration of 1.7  $\mu\text{M}$  (still in the non-toxic range of mCLING concentration) required 2 to 3 minutes to reach the IHCs homogeneously and be taken up. Labeling protocols were adjusted accordingly in order to stimulate synaptic vesicle recycling only in the last one of the 3 minutes of mCLING incubation.

A second difficulty was the access to IHCs for high-resolution imaging when using the whole tissue. This issue was addressed by embedding the organ of Corti in a polymer resin called melamine, which was later on cut at convenient thicknesses between 20 to 200 nm. This method eased the access to the mCLING-labeled subdiffraction-sized organelles contained in the IHCs. Additionally, slicing provided an increased imaging resolution in the Z-axis, complementing the improved resolution in the X-Y plane provided by STED microscopy. In contrast to other resins, melamine embedding does not require tissue dehydration due to its hydrophilic nature, resulting in better tissue preservation. Resin embedding and sectioning is becoming a handy method to complement high-resolution microscopy techniques, as it allows a more precise study of protein distributions. Melamine can be applied not only in tissues but also in cultured cells, e.g. neurons, for estimating protein localization on synaptic vesicles (Opazo et al., 2010), or to render tridimensional cell reconstructions (Punge et al., 2008). The more hydrophobic EPON resin has been also used to obtain thin tissue sections that can be later on treated for immunofluorescence labeling, as it was done in the mouse retina to study the molecular composition of ribbon synapses at photoreceptor active zones (Wahl et al., 2013).

An important concern among scientist is the reduced accessibility to high-resolution microscopy techniques due to their extremely high cost. In this study I showed that just by sectioning the melamine-embedded samples into ultrathin sections of 20 nm, a normal epifluorescence microscope can be converted into a high-resolution one, since only a few copies of the fluorescently labeled antibodies can be captured in such reduced volume

(Figure 3.21). Even though the resolution in the X-Y plane remains the same (200-300 nm), the improved Z-resolution still allows a good estimation of protein presence on mCLING-labeled organelles. Although one could think that the fluorescent signal contained in 20-nm sections is not enough to be detected, only imaging exposure times required adjustment, but not concentrations of mCLING or secondary antibodies.

### 4.3.2 Endocytosis in IHCs

mCLING labeling revealed an intense endocytic activity in IHCs. A significant part of this membrane turnover is likely related to constitutive membrane trafficking pathways, since abundant mCLING-labeled structures were already seen in non-stimulated cells. Interestingly, the labeled structures had a wide variability in morphology and size. Starting at the cell top and nuclear levels, long tubular structures seem to form a complex alternated by large round endosome- and small vesicle-like structures. At the cell base, the large and long tubular structures were not present, leaving only endosome- and vesicle-like organelles (Figure 3.12). These results are in agreement with a previous study performed in our laboratory, in which FM 1-43 labeling in IHCs was followed by photo-conversion and EM processing in order to discern between the truly endocytosed dye molecules, and those that permeated the MET channels (Kamin et al., 2014). Electron-dense signal was also found in tubular and round structures with similar distributions to the mCLING-labeled ones seen in this study (See Figure 1.5). Our results are also similar to those obtained by Siegel and Brownell (1986), who studied horseradish peroxidase (HRP) uptake by IHCs in anesthetized animals, later revealed by DAB oxidation and EM processing. After incubations for 15-30 minutes, they found that at the cytoplasmic region surrounding the active zones, the HRP was taken up into coated and uncoated vesicles and short tubules, which could correspond to the endosome-like structures seen with mCLING. At the apical pole they also observed large quantities of tracer bound to short tubular structures, vacuoles, vesicles and sometimes cisterns of the trans-Golgi network.

Siegel and Brownell proposed that all endocytic events in IHCs, constitutive and synaptic, happen at the basal pole, followed by upwards transport, based on the preferential labeling of basal structures in incubations as short as 3 minutes. Taking my results into account (Figure 3.3), I could think of this assumption as a misinterpretation of the poor diffusion of HRP into the organ of Corti, that due to its large size (~44 kDa), could not reach the top of the cells to report apical uptake in such a short period. It is surprising that they did not report the long tubular structures at the apical and nuclear levels that we see with mCLING

(Figure 3.12) and FM 1-43 photo-oxidation (Kamin et al., 2014). One explanation could be that even after 15-30 minutes, HRP does not manage to homogeneously label the IHC surface, reporting only very few endocytic events. Moreover, due to those long incubation periods, it is likely that a large proportion of the vesicles they observed were the remnants of the originally endocytosed structures after their processing by the trafficking/recycling machinery, therefore underestimating the presence of larger, tubular endocytic intermediates. This assumption is based on our previous observations of fast post-endocytic processing (within 5 minutes) of membrane intermediates into smaller structures (Kamin et al., 2014). The small size of mCLING has therefore a technical advantage over larger tracers like HRP.

Whereas both our previous study (Kamin et al., 2014) and the one from Siegel and Brownell(1986) could only analyze a few cells due to the technical challenges associated to EM, mCLING labeling combined with STED microscopy allowed me to image tens of cells per organ of Corti in a relatively short time. This adds to the reproducibility and reliability of the method developed in this study.

### **4.3.3 Synaptic vesicle recycling in IHCs**

#### **4.3.3.1 Synaptic-related membrane trafficking occurs at the IHC base**

mCLING was first envisioned to establish the origin of the membranes that supply synaptic vesicle recycling in IHCs. As mentioned above, Siegel and Brownell (1986) pointed to local recycling processes taking place in the area surrounding the ribbon type active zones at the cell base. Similar results were obtained by Lenzi and collaborators (2002), who described a strong membrane remodeling process in the vicinity of stimulated synaptic ribbons. A converse view proposed that apical endocytosis is the most important membrane source for vesicle reformation, based on FM 1-43 uptake and imaging (Griesinger et al., 2002, 2005). This latter theory, however, was challenged by a series of publications suggesting that FM 1-43 permeates the MET channels of different types of hair cells, resulting in a misleading labeling that is not endocytosis-dependent (Nishikawa and Sasaki, 1996; Gale et al., 2001; Meyers et al., 2003). Since then, no further study intended to trace endocytosis in hair cells. I aimed to solve this apical-basal recycling duality by quantifying the amount of mCLING endocytosed at the different IHC levels (top, nuclear and basal) in resting and stimulated conditions. I determined that compensatory endocytosis following synaptic vesicle release exclusively occurs at the cell base (Figure 3.12). Accordingly, experiments

using stimulated mCLING loading followed by stimulated unloading confirmed that mCLING-labeled synaptic vesicles are only exocytosed at the cell base (Figure 3.13). These results agree with depolarization-evoked increases of VGLUT1-pHluorin signal preferentially localized at the IHC active zones (Neef et al., 2014), and refute the apical-endocytosis model of synaptic vesicle retrieval (Griesinger et al., 2002, 2005).

Overall, it appeared clear that the IHC basal pole is dedicated to the membrane recycling processes associated with synaptic function. This assertion was further confirmed by correlation analysis between mCLING labeling and immunostaining against proteins associated to synaptic vesicles, like the glutamate transporter VGLUT3 and the exocytosis regulator Rab3. In accordance with the previous results, though IHCs are completely filled with synaptic vesicles from the cell top to the bottom, only the vesicles at the cell base were found to contain mCLING signal, meaning that only those participate in neurotransmitter release and are recycled back into the cell (Figure 3.17A, B, D). The role of the non-releasing vesicles remains unknown. Due to their proximity to the Golgi-apparatus could be possible that the vesicles located at the top and nuclear levels are the youngest and future releasing ones. Although otoferlin, the calcium sensor that triggers synaptic vesicle exocytosis in IHCs, was found in endocytic organelles throughout the cell, its correlation with mCLING signal was still higher at the cell base (Figure 3.17C, D). The function of otoferlin will be further discussed in section 4.3.3.3. The fact that the organelles endocytosed at the cell top and nuclear levels did not contain synaptic vesicle markers, indicates that they are implicated in other modalities of membrane trafficking related to cell constitutive function. In section 4.3.4 this hypothesis is discussed in more detail.

#### **4.3.3.2 Dynamin and clathrin as molecular players of synaptic vesicle recycling**

Up to now, two modes of endocytosis have been postulated to sustain synaptic vesicle retrieval in conventional synapses at physiological stimulation conditions, CME and kiss-and-run. Whereas strong evidence among electron microscopy and electrophysiological studies support the existence of CME, kiss-and-run remains a controversial topic in the field, mostly sustained by the temporal and energetic advantages that it could theoretically contribute to synaptic physiology (Harata et al., 2006a; Wu et al., 2007; Smith et al., 2008). Hence, CME is likely the main mechanisms responsible for vesicle reformation in conventional neuronal boutons (Granseth et al., 2006). Its relevance has been also validated in ribbon type synapses by the presence of clathrin coated pits and coated vesicles in the

vicinity of active zones in hair cells (Siegel and Brownell, 1986; Lenzi et al., 2002), photoreceptors (Rea et al., 2004; Wu et al., 2007; Fuchs et al., 2014) and bipolar cells (Logiudice et al., 2009), and by capacitance measurements of pharmacologically treated synapses (Neef et al., 2014). Moreover, the presence of dynamin at active zones (Wahl et al., 2013; Fuchs et al., 2014), the reduction of endocytosis rates after perturbing dynamin function by molecular blockers (Jockusch et al., 2005; Logiudice et al., 2009; Van Hook and Thoreson, 2012; Neef et al., 2014), and the visual and hearing impairments in a dynamin-1 mutant (Boumil et al., 2010), support the role of CME and perhaps other dynamin-dependent mechanisms in the highly active ribbon synapse. Here, I studied the role of clathrin and dynamin in IHC endocytosis by inhibiting the formation of clathrin coats with the molecule pitstop 2, or by blocking the GTPase activity of dynamin with dynasore. Quantification of mCLING uptake levels in treated cells showed an overall reduction of endocytosis throughout the IHC. Especially, endocytosis at the cell base, which seems to correspond to synaptic vesicle recycling, was more dependent on these two molecules than the endocytosis at the cell top and nuclear levels (Figure 3.14). Interestingly, in some of the dynasore-treated cells membrane clumps sitting on the cell base plasma membrane were found. Similar structures have been described before by EM imaging of neuronal synaptic terminals from dynamin knockout mice (Milosevic et al., 2011; Ferguson and De Camilli, 2012).

It was surprising that dynasore, which should affect other dynamin-dependent endocytosis mechanisms besides CME, had milder effects than pitstop 2. This opened the question on whether the remaining endocytosis was the result of incomplete dynamin inhibition or the activity of other dynamin- and clathrin-independent modes of endocytosis. To evaluate the first possibility I also used Dyngo-4a, a more potent hydroxylated derivative of dynasore that has been replacing it in the last years (Howes et al., 2010; Harper et al., 2011; McCluskey et al., 2013; Neef et al., 2014). Although an apparent reduction of endocytosis was observed, Dyngo-4a gave a strong autofluorescent signal in the far-red range of the spectrum, making the imaging of mCLING impossible (640 nm excitation, data not shown). In the last years, dynasore and dyngo-4a became standard tools to perturb synaptic function at conventional (Newton et al., 2006; Hosoi et al., 2009; Chung et al., 2010; Harper et al., 2011) and ribbon type synapses (Jockusch et al., 2005; Logiudice et al., 2009; Van Hook and Thoreson, 2012; Wahl et al., 2013; Neef et al., 2014). However, a recent study reporting off-target effects on other cellular processes (Park et al., 2013) calls for a careful interpretation when using these two drugs. Alternative approaches to study dynamin and



CME function in IHCs could include characterization of mutant protein versions (Neef et al., 2014) and the use of peptides interfering with protein-protein interactions (Jockusch et al., 2005).

In summary, the results of this and previous studies confirm the relevance of dynamin and CME in IHC synaptic vesicle recycling.

#### 4.3.3.3 A local model for synaptic vesicle recycling

Local membrane uptake in areas surrounding ribbon-type active zones has been reported in hair cells (Siegel and Brownell, 1986; Lenzi et al., 1999, 2002), retinal bipolar neurons (Logiudice et al., 2009) and photoreceptors (Fuchs et al., 2014), using electron microscopy techniques. I wanted to establish whether mCLING uptake, combined with STED microscopy, could also report such endocytosis processes in high detail. In this way, I could narrow down the location of the synaptic recycling processes seen at the IHC base. By looking at the morphology and distribution of mCLING-labeled organelles found in the vicinity of IHC synaptic ribbons, I concluded that synaptic vesicle recycling is indeed a local, multistep process. First, stimulation triggers synaptic vesicle exocytosis, which is compensated by the formation of membrane infoldings arising from the plasmalemma surrounding the synaptic ribbon. Eventually, the infoldings detach from the plasma membrane and give rise to large endosome-like structures (cisterns) of irregular shapes. Finally, in the recovery period after stimulation, infoldings and cisterns disappear leaving behind abundant vesicle-like structures that homogeneously distribute in the cytoplasm, probably intermixing with other vesicles. This simplified model suggests the requirement of endocytic intermediates for synaptic vesicle reformation. However, taking into account previous publications using capacitance measurements, fluorescence and electron microscopy, and the results from this study, it seems that synaptic vesicle recycling follows a more complex dynamic (summarized in Figure 4.1).

**Synaptic vesicle recycling not always recruits endosomal intermediates.** In this study I found that membrane infoldings were small and uncommon in cells stimulated at mild conditions (10 mM K<sup>+</sup>). In contrast, infoldings were larger and frequent upon stronger stimulations (25 and 65 mM K<sup>+</sup>). These observations indicate that the presence, abundance and size of endocytic intermediates (i.e. infoldings and cisterns) correlate with the strength of stimulation (Figure 3.16A, B). Moreover, EM studies have shown coated pits and coated vesicles directly forming at the plasma membrane neighboring the ribbon, indicating that

single unit retrieval by CME is also happening in parallel to the formation of membrane infoldings (Siegel and Brownell, 1986; Lenzi et al., 1999, 2002). Capacitance measurements have also uncovered two types of endocytosis following membrane depolarization in IHCs: a slow one with linear decay kinetics of membrane retrieval, which is dynamin- and clathrin-dependent, likely retrieving single vesicle units via CME; and a faster one, with exponential decay kinetics, time constant of  $\sim 6$  s, and probably corresponding to retrieval in the shape of membrane infoldings that does not require clathrin or dynamin (Moser and Beutner, 2000; Beutner et al., 2001; Neef et al., 2014). It was found that brief stimulation releasing the equivalent to one RRP was ensued only by the slow linear component, while stimulations releasing three to four RRP evoked both, the linear and the exponential component. Interestingly, the amplitude of the exponential capacitance drop correlated with the amount of exocytosis (Neef et al., 2014), corresponding to my observations of denser and more abundant infoldings and cisterns as the  $K^+$  concentration increases. An explanation reconciling all the aforementioned observations would be that mild stimulations only recruit CME for single unit retrieval, while stronger stimuli induce, additionally, membrane retrieval in larger structures resembling bulk endocytosis (Neef et al., 2014). An even faster mode of endocytosis has also been found, with  $\sim 250$ - $300$  ms time constant and only active at cytosolic  $[Ca^{2+}]$  above  $15 \mu M$ . Its molecular players and physiological significance are poorly studied, and it has been cautiously interpreted as a kiss-and-run mode of vesicle retrieval (Moser and Beutner, 2000; Beutner et al., 2001; Cho et al., 2011; Neef et al., 2014).

Similarly, slow (10 s time constant) and fast (1-2 s time constant) independent modes of endocytosis have been also measured in goldfish retinal bipolar cells (von Gersdorff and Matthews, 1994; Neves and Lagnado, 1999; Heidelberger et al., 2002). These modes differ, however, from those in hair cells in some important aspects: here both depend on dynamin, while only the slow one does on clathrin (Jockusch et al., 2005); brief stimuli releasing only the RRP are followed by the fast instead of the slow component (Neves et al., 2001); finally, the fast mode seems to retrieve single vesicle units in a clathrin-independent manner and not in bulk (Jockusch et al., 2005), as it could be hypothesized for hair cells.

**Bulk endocytosis appears to have an important role in ribbon synapse function.** Membrane uptake into large membrane-bound structures after synaptic vesicle release is not exclusive of hair cells (this study; (Siegel and Brownell, 1986; Lenzi et al., 2002). Structures resembling bulk endocytosis have been described among ribbon-type synapses,

albeit differences in their general morphology. While in this study I found elongated infoldings and irregularly shaped cisterns for IHCs, large, round endosome-like structures were seen in goldfish retinal bipolar cells using FM dyes and dextran labeling (Holt et al., 2003; Coggins et al., 2007), or ferritin uptake EM imaging (Paillart et al., 2003). Similar round structures were found containing the tracer HRP in chick photoreceptors, either bound to the plasma membrane or already free into the cytoplasm (Cooper and McLaughlin, 1983). A more complex structure was revealed in mouse photoreceptors by EM, where large multivesicular clusters originated from the plasma membrane, although their nature might be different to conventional bulk endocytosis (Fuchs et al., 2014). The relevance of bulk endocytosis in ribbon synapses at physiological conditions is not yet clear. Assuming that the exponential mode of endocytosis in IHCs corresponds to bulk retrieval, this mode would be already triggered by 200-ms depolarizations releasing 3 to 4 RRP (Neef et al., 2014), or by mild  $K^+$  stimulations (10 mM) lasting one minute, as found in this study (Figure 3.16). Although it is difficult to say if such treatments applied *ex vivo* are comparable to the intensity of real sound stimuli, bulk endocytosis was also seen in IHCs of anesthetized animals, stimulated with a tone-burst and monitored for cochlear viability throughout HRP perfusion (Siegel and Brownell, 1986). In the case of mouse photoreceptors, prolonged activity was simulated by keeping the animals in a dark environment for at least 3 hours. This situation, comparable to the physiological experience, triggered the formation of the aforementioned multivesicular clusters (Fuchs et al., 2014). In goldfish bipolar cells, bulk endocytosis has been more difficult to relate to a physiological condition, since it is not clearly related to the slow or fast modes of endocytosis (Holt et al., 2003; Jockusch et al., 2005), although it has been seen in cells firing spontaneously in presence of  $Ca^{2+}$  (Paillart et al., 2003).

Little is known about the molecules responsible for bulk membrane retrieval. In neuronal terminals, dynamin I dephosphorylation by calcineurin seems important for bulk retrieval activation, whilst syndapin and dynamin GTPase activity could be involved in membrane curvature and fission, respectively (Andersson et al., 2008; Clayton and Cousin, 2009; Clayton et al., 2009). In neuromuscular junctions, actin has been implicated in the initiation of bulk membrane retrieval, and together with dynamin in its maturation into cisternae (Nguyen et al., 2012). In ribbon synapses the only evidence comes from retinal bipolar cells, where actin polymerization was required for bulk endocytosis (Holt et al., 2003). As for IHCs, I found dynamin inhibition affecting endocytosis in general, but its direct effect on bulk retrieval was difficult to determine. Moreover, Neef and collaborators (2014) found

that mutation or inhibition of dynamin did not affect the exponential mode of endocytosis, thought to correspond to bulk retrieval.

Although the physiological significance of bulk endocytosis is still debated in conventional synapses due to its dependence on strong stimulation (Richards et al., 2000; de Lange et al., 2003; Rizzoli and Betz, 2005; Wu and Wu, 2007; Clayton et al., 2008), this kind of membrane retrieval could have a significant role in the normal function of ribbon-type synapses. With graded receptors potentials, instead of action potentials, regulating constant vesicle release and the presence of a ribbon favoring high rates of exocytosis, these synapses can offer a more favorable environment for emergence of bulk endocytosis.

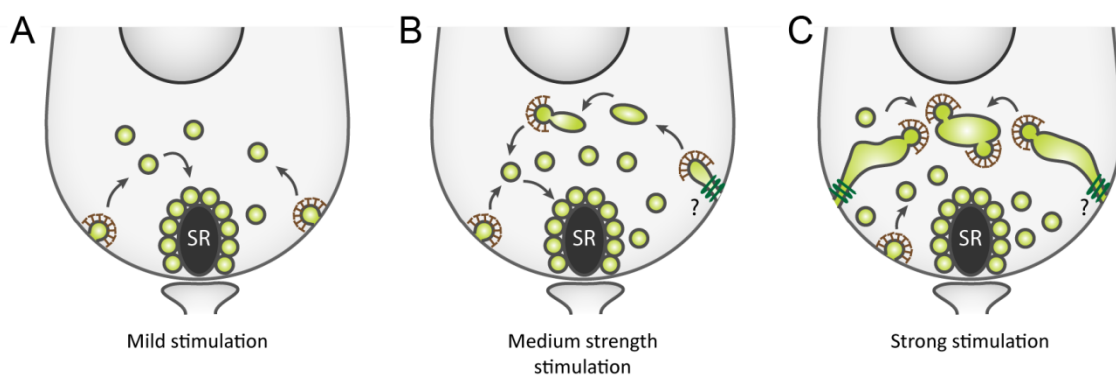


**Figure 4.1 Local model of synaptic vesicle recycling in hair cells.**

Based on the results of this study and the data presented in previous publications (Siegel and Brownell, 1986; Lenzi et al., 1999, 2002; Kamin et al., 2014; Neef et al., 2014), it is possible to conclude that synaptic vesicle recycling in hair cells is a local process taking place in the vicinity of the ribbon-type active zones. **A.** At mild stimulation conditions, triggering only the release of 1-2 times the RRP, compensatory endocytosis retrieves single vesicle units from the plasma membrane with the help of clathrin coat formation. **B.** At stronger stimulation conditions, releasing the equivalent to 3-4 times the RRP, membrane infoldings arise from the areas surrounding the synaptic ribbon (SR). This mode of endocytosis would be similar to the bulk endocytosis described in conventional synapses. Membrane infoldings seem to give rise to cisterns, from which synaptic vesicles can be reformed. CME of single vesicle units continues in parallel to bulk retrieval. **C.** Stronger stimulations will result in the generation of even larger infolding and cisterns. In this study dynamin was found to be important for the general synaptic vesicle recycling process. However, it is not clear if it only participates in the fission of clathrin coated vesicles, or also in the scission of membrane infolding from the plasma membrane.

**Local recycling seems to facilitate synaptic vesicle reformation and recruitment to the ribbon.** Three aspects are particular among ribbon synapses: a large amount of synaptic vesicles, up to 600,000 in the saccular hair cell cytoplasm (Lenzi et al., 1999), and up to 900,000 per goldfish retinal bipolar cell terminal (von Gersdorff et al., 1996; Holt et al., 2004); the lack of synapsin (Favre et al., 1986; Mandell et al., 1990); and as a consequence, high synaptic vesicle mobility (Holt et al., 2004). These three points have led to the

hypothesis that collision of diffusing vesicles with the synaptic ribbon would be sufficient for its replenishment after exocytosis (Parsons and Sterling, 2003; Holt et al., 2004). Conversely, a local recycling model would suggest that ribbon reloading relies on fast vesicle reformation directly from exocytosed membranes. This alternative is supported by a 14-fold increase in vesicle abundance around the synaptic ribbon, the presence of tracer-labeled vesicles tethered to the ribbon, the appearance of membrane infoldings and cisterns around the active zone upon stimulation, and dye uptake specifically around synaptic ribbons (Siegel and Brownell, 1986; Lenzi et al., 1999, 2002; Logiudice et al., 2009; Neef et al., 2014). Furthermore, it has been proposed that the exocytic activity of a ribbon determines the abundance and distribution of vesicles and cisterns in a “sphere of influence” with 350nm radius around the active zone (Kantardzhieva et al., 2013). The results obtained in this study based on mCLING uptake can be associated with the local recycling model: abundant membrane retrieval into infoldings and cisterns in the vicinity of the ribbon, their efficient processing into synaptic vesicles within a few minutes (Figure 3.16A, B), and the apparent delivery of mCLING-labeled reformed vesicles back to the ribbon (Figure 3.16C). Here, mCLING was pivotal for the study of local recycling: its non-washability allowed the labeling of infoldings still open to the exterior. This would be impossible with washable molecules like FM dyes or the fluid phase markers HRP, which would be lost through the organelle’s opening.

Local recycling would likely require a specialized molecular microenvironment surrounding the active zone, grouping important molecular players necessary for vesicle retrieval, reformation and tethering to the ribbon to fuel and speed up synaptic activity. This is true for mouse photoreceptors, where clathrin, dynamin, syndapin and amphiphysin preferentially locate close to the active zone (Wahl et al., 2013; Fuchs et al., 2014). In hair cells, the  $Ca^{2+}$  sensor otoferlin has been proposed to couple exo- and endocytosis based on its recruitment to the plasma membrane, its role in vesicle exocytosis, replenishment of the RRP, and its interaction with the adaptor protein AP2 (Roux et al., 2006; Pangršič et al., 2010, 2012; Levic et al., 2011; Duncker et al., 2013). My results go in line with this idea, since otoferlin better correlated with the organelles endocytosed at the IHC base (Figure 3.17C, D). In the case of otoferlin knockout cells, the reduction in endocytosis could be attributed to impaired exocytosis, but also to a need of otoferlin for proper membrane retrieval at this synapse (Figure 3.15).

In the future, mCLING labeling could help to clarify yet open questions about local recycling.

mCLING could be used, for example, to study the role of synaptic ribbons in recruiting the recycling machinery, since it is known that their detachment from the plasma membrane results in disorganization of active zones and impaired vesicle replenishment (Frank et al., 2010). Moreover, mCLING labeling combined with immunostaining in otoferlin knockout mice, could be used to establish if this protein recruits other proteins involved in clathrin coat formation, as it has been shown for synaptotagmin in conventional synapses (Haucke and De Camilli, 1999; Poskanzer et al., 2003).

**The role of otoferlin in IHC physiology.** In this study I could show, for the first time, a remarkable abundance of otoferlin in endocytic compartments. Surprisingly, this protein was dominant not only in organelles recycling at the cell base, where it is supposed to act, but also in those at the upper IHC levels. There are two possible explanations for this finding: 1) uptake of otoferlin at top and nuclear levels is a passive, unspecific event, due to its enrichment at the plasma membrane; 2) besides playing an important role in synaptic vesicle priming and release, otoferlin is also involved in other mechanisms of membrane trafficking. The second option has been already considered, in view of otoferlin expression in different areas of the brain (cerebellum, hippocampus and cortex) and its interaction with proteins involved in endosomal traffic and CME (Schug et al., 2006; Heidrych et al., 2008; Zak et al., 2011). The interaction of otoferlin with myosin VI seems to be important for organelle targeting and delivery from the trans-Golgi network towards the basolateral region of IHCs (Heidrych et al., 2009; Roux et al., 2009). Additionally, otoferlin could participate in CME via its interaction with AP2 (Duncker et al., 2013). These claims, however, are partially based on colocalization analyses from diffraction-limited confocal pictures. Further confirmation could be obtained by two-color STED imaging of otoferlin and its possible interaction partners in ultrathin melamine sections.

**Synaptic vesicle reformation is an efficient process.** Using long and strong stimulation (30 minutes, 45 mM K<sup>+</sup>), Lenzi and collaborators (2002) proposed that processing of cisterns into synaptic vesicles, but not clathrin uncoating or SNARE complexes formation, is a rate limiting factor for vesicle reformation in hair cells. In this study I could show that the endocytic intermediates formed in response to one-minute stimulation were efficiently broken into smaller organelles within 5 minutes, indicating that in a more physiological condition, vesicle reformation is not rate-limiting (Figure 3.16A). Since shorter recovery incubations were not tested, it is not clear whether this recycling could actually be faster. Evidence for very fast bulk endosome processing into vesicles has been found, for example,

in the snake neuromuscular junction (~10 seconds), but its molecular bases are not clear (Teng et al., 2007).

Based on the finding of coated pits on top of membrane invagination, and coated vesicles in their proximity (Siegel and Brownell, 1986; Lenzi et al., 2002), clathrin-mediated budding is thought to be the mechanisms whereby vesicles reform. Similar clathrin coats have been seen decorating membrane infoldings and bulk endosomes in conventional synapses (Teng and Wilkinson, 2000). Vesicle reformation could be accelerated by coating from different points of the endosomal intermediate, as seen with EM in stimulated IHCs (Neef et al., 2014). It is not clear, however, if the clathrin coated vesicles become ready-to-release synaptic vesicles, since the former are significantly larger, ~53 nm vs ~30nm average internal diameter (Neef et al., 2014). Moreover, it has not been investigated if vesicles generated from endosomal intermediates would be 'contaminated' with plasma membrane proteins, or if an endosomal sorting mechanism, as the one described in conventional synapses (Hoopmann et al., 2010), would be required in hair cells. The main difficulty to answer those questions is that the molecules participating in synaptic vesicle exocytosis in hair cells remain unknown, as they do not use the conventional neuronal SNAREs Syntaxin 1, SNAP-25 or synaptobrevin (Nouvian et al., 2011).

#### **4.3.4 The constitutive recycling pathway in IHCs**

In comparison to synaptic vesicle recycling, constitutive recycling has been poorly studied in ribbon synapses. In the quest to understand their synaptic function, the compact anatomy of IHCs has been beneficial to elucidate the morphology and location of organelles involved in constitutive traffic, given their relatively close location to the synaptic machinery. Capacitance measurements, however, have only focused on the synaptic component of membrane traffic. The main motivation to study constitutive recycling in IHC is to understand how a cell with somatic active zones can accommodate in the same volume a demanding task, as it is synaptic activity, and still perform other processes required for its proper function. As mentioned in sections 4.3.2 and 4.3.3.1, mCLING revealed abundant membrane uptake in IHCs. After finding that endocytic processes at the IHC base support the synaptic activity, it can be deduced that membrane uptake happening elsewhere is involved in 'housekeeping' constitutive recycling. This assertion was confirmed using mCLING through different technical approaches.

#### 4.3.4.1 The identity of constitutively recycling organelles

In this study I found that constitutive recycling involves endocytic intermediates with a wide range of morphologies and sizes. A remarkable type of organelle was the tubular structures occupying the supranuclear and nuclear cytoplasmic volume (Figure 3.12). These structures were also tracked by FM 1-43 photo-oxidation electron microscopy in a previous study from our laboratory (Figure 1.5)(Kamin et al., 2014). A tridimensional reconstruction showed a more complex morphology, with elongated and sheet-like flattened regions that could actually correspond to a tubulo-cisternal network (Kamin et al., 2014). After a 5-minute recovery period, these structures were processed into smaller vesicle-like organelles significantly larger than *bona fide* synaptic vesicles, suggesting a role independent of synaptic activity (Kamin et al., 2014). Apparently, these tubules were also seen before in an EM study using a modified protocol with primary aldehyde-osmium tetroxide fixation and secondary osmium tetroxide-ferrocyanide fixation (Spicer et al., 1999). This method in particular revealed a cytoplasmic network of tubular structures, spanning from the subcuticular region down to the upper midlevel of the nucleus. This network was called the canalicular reticulum (CR) and was speculated to serve as an exit path for cations entering through the MET channels after a sensory input (Spicer et al., 1999). Based on the morphology and location of the mCLING-labeled tubules, the CR could correspond to the same structures. However, it is unknown whether these tubules represent trafficking organelles, as this EM method was never combined with tracer uptake.

Using immunolabeling for different organellar markers I established that the tubules are not related to the cis-Golgi network or the endoplasmic reticulum (Figure 3.18). Interestingly, they contain the SNARE proteins Syntaxin 6 and Syntaxin 16, which have been involved in the retrograde transport from recycling endosomes towards the trans-Golgi network (Figure 3.19) (Mallard et al., 2002; Brandhorst et al., 2006; Jahn and Scheller, 2006). Vti1a, another SNARE protein involved in homotypic fusion of early endosomes (Brandhorst et al., 2006), was not abundant in these structures. Two main conclusions can be drawn from these results:

- 1) The endoplasmic reticulum and cis-Golgi network do not participate in membrane trafficking on the time scales investigated here (~3 minutes). In agreement, previous reports on the dynamics of plasma membrane-Golgi-ER retrograde traffic suggest time scales of at least 10-15 minutes to 60 minutes to reach the Golgi apparatus, and around 30 additional minutes to reach the ER (Sofer and Futerman, 1996; Johannes



et al., 1997; Barysch et al., 2009; Matsudaira et al., 2013).

- 2) The tubular structures indeed participate in constitutive membrane trafficking, probably as recycling endosomes.

Several questions related to these tubules remain open: how do they become labeled with mCLING in a time frame of only 3 minutes? Do they receive membranes directly from endocytic vesicles, or rather from sorted vesicles budding from early endosomes? What is their function? Membrane traffic studies in polarized epithelial cells have described a structure with recycling endosome properties, called the subapical compartment (SAC). This compartment, located in proximity to the trans-Golgi network, was suggested to play a role in the establishment of cell polarity, by coordinating the delivery of recycled or newly synthesized proteins and lipids to the apical or basolateral membranes (van IJzendoorn and Hoekstra, 1999; Fölsch, 2005; van IJzendoorn, 2006). It could be possible that the tubules described here are part of a structure equivalent to the SAC in IHCs. Future experiments combining mCLING with immunolabeling for proteins related to epithelial recycling endosomes (i.e. Rab11a, Rab11b and Rab25), could help to confirm this hypothesis.

In this study, sample slicing offered an improved view of immunostained proteins that are not only abundant in IHCs, but also in other cell types surrounding them. In this way, it was possible to locate the cis-Golgi network in the supranuclear volume, as described previously by EM (Siegel and Brownell, 1986; Spicer et al., 1999, 2007). In contrast to an infranuclear location suggested before, I found the endoplasmic reticulum distributed throughout the IHC (Siegel and Brownell, 1986; Spicer et al., 1999).

#### **4.3.4.2 Membrane traffic at the cuticular plate**

mCLING labeling revealed a collection of endocytic organelles localized in the IHC apical region, close to the membrane supporting the hair bundle. Some of those organelles had a late endosome/lysosomal identity (Figure 3.20). These results agree with a series of EM studies describing a very active membrane recycling process taking place at the apical membrane of cochlear and saccular hair cells. Coated pits, coated and uncoated vesicles, vacuoles and lysosomes accumulate beneath the plasma membrane, in the space surrounding the cuticular plate (Forge and Richardson, 1993; Kachar et al., 1997; Richardson et al., 1997; Spicer et al., 1999). These results confirm again that apical endocytosis is related to constitutive membrane trafficking pathways, and excludes the possibility that synaptic vesicles could be reformed from the apical membrane, as no

correlation with synaptic vesicle markers was found.

### **4.3.4.3 Molecules driving constitutive membrane uptake**

By applying molecular inhibitors for the endocytic proteins clathrin and dynamin, I found that constitutive recycling is less dependent on these two molecules than synaptic vesicle recycling (Figure 3.14). In accordance, Siegel and Brownell (1986) reported the absence of coated pits and coated vesicles at the plasma membrane of the cell nuclear and supranuclear levels. The alternative molecules supporting the formation and fission of constitutively endocytosed vesicles remain to be studied. In the future, it will be also interesting to study the dependence of IHC apical recycling on the actin cytoskeleton, as it has been shown that endocytosis at the apical pole of polarized cells requires the recruitment of actin filaments to counteract higher membrane tension (Boulant et al., 2011).

### **4.3.5 A membrane recycling model for IHCs**

Based on the findings discussed above, a final model of membrane trafficking pathways in IHCs can be put forward (Figure 4.2). This model proposes that IHCs functionally and spatially separate synaptic vesicle recycling from constitutive membrane trafficking. At the cell base, synaptic vesicles are released upon stimulation and then recycled in the vicinity of the ribbon-type active zones. Simultaneously, the cell top and nuclear levels host the membrane trafficking events related to the constitutive function of the cell.

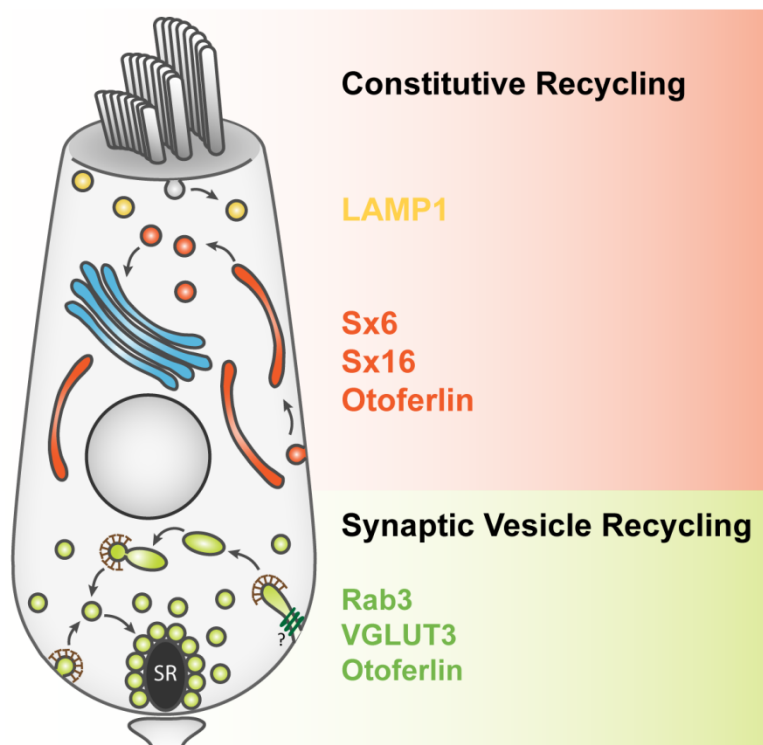


**Figure 4.2 Membrane trafficking pathways in IHCs.**

The data presented here show that in IHCs constitutive membrane trafficking pathways preferentially take place at the cell top and nuclear levels. This was confirmed by the presence of tubulo-cisternal structures containing the protein markers Syntaxin 6 and Syntaxin 16, which likely participate as recycling endosomes in the retrograde transport to the Golgi complex. Apical endocytosis around the cuticular plate was related to constitutive traffic towards late endosome/lysosome compartments, evidenced by LAMP1 labeling. In contrast, synaptic vesicle recycling is preferentially located at the cell basal level and it recruits endocytic intermediates, such as membrane infolding and cisterns, for the reformation of synaptic vesicles. This recycling seems to rely on clathrin and dynamin, although their role is not completely understood. The calcium sensor otoferlin was present in endocytic compartments throughout the IHC, suggesting that this protein might not only be involved in synaptic vesicle exocytosis but also in endocytic processes. Further research on otoferlin will help to better understand IHC physiology.

The data presented in this study proved that the organelles involved in both pathways are functionally separated, despite their intermixing in the cytoplasmic volume. Hence, the participation of organelles related to constitutive function, like the Golgi apparatus, or organelles located at the IHC apical level, are excluded from the synaptic vesicle recycling process (Figure 3.21). The basal model for synaptic vesicle recycling is, at the end, a faster and more energetically economic route than the apical model proposed previously (Griesinger et al., 2002, 2005).

An important implication of the proposed model is that, even in cells with somatic active zones, synaptic vesicle recycling is an exclusive pathway with its own molecular and organellar players. Such model was envisioned before by EM studies describing the

remarkable morphological changes of intracellular organelles from the cell top to the bottom (Siegel and Brownell, 1986; Spicer et al., 1999; Kamin et al., 2014). However, its confirmation was only possible until now, with the development of mCLING and its combination with molecular markers for different organelle types.

### 4.4 New insights into neuronal function

After proving the potential of mCLING to track endocytic organelles in the relatively large cytoplasmic volume of IHCs, a main concern was its ability to reveal membrane uptake in small synaptic boutons. To test this, mCLING was applied to cultured hippocampal neurons, finding no negative effects on plasma membrane integrity or synaptic vesicle recycling (Figure 3.22). Importantly, mCLING was efficiently taken up by recycling synaptic vesicles, allowing the study of their molecular composition by STED microscopy imaging. Moreover, incubations at low temperature (thereby inhibiting endocytosis) facilitated the distinction between immunostained proteins residing on intracellular organelles, and those sitting on the plasma membrane. These technical advantages were used to better understand aspects of the physiology and organization of conventional synapses, described below.

#### 4.4.1 Molecular differences between spontaneously and actively released synaptic vesicles

In this study we combined mCLING labeling of spontaneously and actively released synaptic vesicles with immunostaining against synaptic- and endosomal-related proteins. The results suggest that these two groups of organelles differ in their molecular composition:

- Spontaneously recycling vesicles presented higher levels of endosomal SNARE proteins, like syntaxin 13 and VAMP4.
- The spontaneously released group presented significantly lower levels of three synaptic vesicle proteins, synaptotagmin 1, synapsin and the SNARE protein VAMP2.
- The two groups had similar levels of other synaptic vesicle proteins, like VGLUT1/2 and synaptophysin.

Taken together, our results indicate that quantitative molecular differences between spontaneously and actively released synaptic vesicles not only reside in SNARE proteins, but also on other protein families (Figure 3.23). Additionally, they indicate that spontaneously released organelles might be more related to constitutive trafficking pathways, being “less vesicular” than their actively released counterparts.

Differences in protein make-up between spontaneously and actively released synaptic vesicles were suggested before. Chimeric constructs containing the pH-sensitive protein pHluorin and either VAMP7 or Vti1a, two endosomal SNARE proteins, preferentially located on the spontaneously recycling pool of vesicles (Hua et al., 2011b; Ramirez et al., 2012). Moreover, the involvement of different synaptic proteins in spontaneous release has been indirectly established upon their mutation or knocking down. Thus, the lower levels of synaptotagmin 1 found here for spontaneously recycling vesicles, would agree with previous reports on the independence of spontaneous release rates from synaptotagmin 1 calcium-sensing activity (Geppert et al., 1994b). On the other hand, the low levels of VAMP2 reported here for spontaneously released vesicles are difficult to reconcile with previous findings indicating a 6-fold reduction in spontaneous release in the absence of this protein (Sara et al., 2005).

Even though spontaneous vesicle release has been related to synaptic development, maintenance and strength, the existence of a physiological role for such events is still debated. In the same context, it is difficult to establish whether the presence of glutamate transporters (VGLUT) and synaptophysin is associated to that theoretical function, or is rather the result of inefficient exclusion of protein components during endocytosis. Paradoxically, it has been the presence of transporters and neurotransmitter filling, measured through the concomitant miniature post synaptic currents (mEPSC and mIPSC), the standard tool to characterize spontaneous release (Van der Kloot, 1991; McBain and Dingledine, 1992).

#### **4.4.2 Synaptic vesicle proteins stranded on the plasma membrane**

mCLING surface labeling of isolated hippocampal neurons was combined with immunostaining against synaptic vesicle-associated proteins, in order to establish the percentage of molecules that remains stranded on the plasma membrane at resting conditions. The evaluated proteins included VGLUT1/2, synaptophysin, synaptotagmin 1, VAMP2, synapsin and Rab3.

Overall, the fraction of proteins present in the plasma membrane ranged between ~12 and ~22% of the total amount (Figure 3.24). The relatively low variability among these values contrast with a wider range obtained by different groups using protein-pHluorin coupling: ~2% for VGLUT1, ~8% for synaptophysin, ~10-24% for VAMP2 and ~22% for synaptotagmin (Sankaranarayanan and Ryan, 2000; Fernández-Alfonso et al., 2006;

Granseth et al., 2006; Balaji and Ryan, 2007). Therefore, the mCLING labeling and sample processing protocols used in this study represent a more reliable way to look at protein composition and distribution in synaptic terminals for the following reasons:

- Our method quantifies the endogenously expressed proteins in their native form. In contrast, pHluorin experiments rely on the overexpression of proteins with a large tag at their intravesicular domain (238 aminoacids), likely affecting their targeting, function, clustering and retrieval efficiency from the plasma membrane (Opazo et al., 2010). This is confirmed by similar values for synaptotagmin 1 surface pool of molecules found in this study (~18%) and in a previous report using antibodies against the luminal domain of this protein in resting cells (~19%) (Opazo et al., 2010).
- Immunostaining levels are similar among neurons cultured in the same coverslip. Transfection efficiency is, however, a more variable parameter that could affect the quantification of protein distributions.
- More accurate quantifications can be obtained with high-resolution imaging, in contrast to confocal imaging performed in pHluorin analysis.
- mCLING labeling and immunostaining are easier and more reproducible methods, enabling the study of several proteins in parallel.
- In our study we also analysed cytoplasmic proteins that transiently associate to synaptic vesicles before vesicle release (Rab3 and synapsin). This would have been impossible with pHluorin coupling, since it can only be applied to integral membrane proteins.

Among our results, the abundance of Rab3 (~22%) and synapsin (~13%) on the membrane is surprising, considering their disengagement from the vesicular membrane after exocytosis is accomplished (Fischer von Mollard et al., 1991; Tarelli et al., 1992). Nevertheless, synapsin molecules have been seen before on the plasma membrane by immuno-electron microscopy (Tarelli et al., 1992; Pieribone et al., 1995). This fraction, however, has been difficult to determine due to the difficulties imposed by immuno-EM. Similarly, a fraction of Rab3A molecules was also found on the plasma membrane of small rat brain synapses (Mizoguchi et al., 1990), as well as in the rat NMJ (Mizoguchi et al., 1992).

The results presented here suggest that a relatively large fraction of synaptic vesicle proteins stays on the plasma membrane. It is not clear, however, if these molecules remain together as a vesicular patch, as suggested by STED-microscopy studies (Willig et al., 2006;

Opazo et al., 2010), or if they diffuse and intermix with plasma membrane resident proteins (Sankaranarayanan and Ryan, 2000; Li and Murthy, 2001; Wienisch and Klingauf, 2006). The latter hypothesis, however, is supported by studies using pHluorin expression, which has been shown to impair protein-protein interactions and clustering (Opazo et al., 2010). In the first case, the retrieval of synaptic vesicles as a unit would be facilitated, possibly making vesicle replenishment faster. In the second case, mechanisms of protein organization and clustering would be required either before vesicle retrieval, or by sorting through an endosome (Hoopmann et al., 2010), with expected delays in the recycling processes. The similar percentages found here for all proteins could suggest that their levels on the plasma membrane resemble the stoichiometry of an average synaptic vesicle, supporting their role as a readily retrievable pool of molecules that is eventually endocytosed as a reformed synaptic vesicle.

#### **4.4.3 Differences in protein clustering between SNAP-25 and Syntaxin 1**

In our last approach to hippocampal neurons we studied how the two membrane SNARE proteins, SNAP-25 and syntaxin 1, organize in intracellular organelles and on the plasma membrane. For this, mCLING surface labeling and immunostaining were combined in hippocampal neurons, in the same way as for the previous section. We found that, on average, the size of SNAP-25 clusters on the axolemma was similar to their counterparts from intracellular organelles (Figure 3.25B). In contrast, syntaxin 1 clusters found on the plasma membrane were larger and brighter than the syntaxin 1 staining from organelles (Figure 3.25C), suggesting that this protein forms relatively large molecular assemblies (Sieber et al., 2007; Bar-On et al., 2012) on the plasma membrane, but not on organelles.

Syntaxin 1 clustering depends on homophilic interactions between SNARE motifs, as well as on electrostatic interactions with membrane phosphoinositides (Sieber et al., 2006, 2007; Khuong et al., 2013). Hence, it has been suggested that differences in phosphoinositide composition across organellar and plasma membranes could determine cluster size (Khuong et al., 2013), and therefore explain the results obtained here. SNAP-25 forms less dense and larger clusters than syntaxin 1, with no dependence on its SNARE motifs. Due to its palmitoyl anchoring to the membrane, SNAP-25 diffuses more easily than Syntaxin 1, which contains a C-terminal transmembrane domain, suggesting a less tight control of its cluster size (Halemani et al., 2010; Bar-On et al., 2012). Another important player determining cluster size on intracellular organelles could be cholesterol, as its effect has

been shown before on plasma membranes (Chamberlain et al., 2001; Lang et al., 2001). Overall, the results of this study are in line with the complex mechanisms by which syntaxin 1 forms molecular assemblies, compared to the apparently simple membrane localization of SNAP-25. Further experiments using mCLING labeling could help to study clustering factors for these and other proteins by mutation in their structures or changes in membrane lipid composition.

## 4.5 mCLING uses in other biological preparations

### 4.5.1 Perspectives in *Drosophila* larva neuromuscular junction

When applied to the neuromuscular junction of *Drosophila* larvae, mCLING labeled the subsynaptic reticulum and reached the plasma membrane of the synaptic bouton, allowing its endocytic uptake upon electric stimulation. These results confirmed again that the palmitoyl tail of mCLING does not affect its diffusion into tissues. mCLING was endocytosed into elongated structures arising from different points of the bouton, sometimes in proximity to the active zone. Similar elongated membrane projections, likely corresponding to endocytic intermediates, were previously observed with electron microscopy in the *Drosophila* photoreceptor terminal (Koenig and Ikeda, 1996). In the future, mCLING could be used to study the effects of protein mutations (e.g. in *shibire* flies, carrying a mutant version of dynamin) on the mechanisms of synaptic membrane retrieval.

### 4.5.2 Microorganisms

mCLING was also applied to a simpler organism, the yeast cell. Endocytic events in yeast have been traditionally traced with the styryl dye FM 4-64. *In vivo* labeling was similar between mCLING and FM 4-64. After fixation and permeabilization, however, mCLING remained on endocytic organelles and plasma membranes, but FM 4-64 was removed to a large extent. Yeast cells are an important biological model for the study of membrane trafficking pathways, protein localization and cell division (Schekman, 1985), all of which could benefit from the application of mCLING and its associated high-resolution imaging.

Another microorganism labeled with mCLING was the bacterium *Escherichia coli*. In comparison to a conventional membrane marker like FM 1-43, which only allows confocal imaging, mCLING imaging with STED microscopy gave a superior view on plasma membrane labeling and patterning. This proof-of-principle experiment opens new doors for mCLING use in the labeling of microorganisms, not only as a surface reference for *in vivo* samples,



but probably also in studies following its fixation and combination with proteins markers.

### **4.5.3 Following endocytosis with mCLING in cells with permeable channels**

Due to their small size and elongated molecular structure, FM dyes have been reported to permeate a range of sensory ion channels, including mechanotransduction channels, the capsaicin receptor TRPV1, and the purinergic receptor P2X<sub>2</sub> (Nishikawa and Sasaki, 1996; Gale et al., 2001; Meyers et al., 2003; Farris et al., 2004; Drew and Wood, 2007; Crumling et al., 2009). In neonatal mice injected with AM 1-43, the dye was found 48h later labeling several cell types involved in sensory reception: cochlear and vestibular hair cells, as expected, as well as hair follicles, Merkel cells, spiral afferents of skeletal muscles, nociceptors, enteric neurons, taste receptors in foliate and circumvallate papillae, primary sensory neurons at cranial nerves (trigeminal, geniculate, petrossal, nodose), and dorsal root ganglia neurons (DRG) (Meyers et al., 2003). FM dye permeation was also confirmed by the discovery of unknown mechanoreceptor cells in the sensory Eimer's organ at the nose of talpid moles (Marasco et al., 2006). Furthermore, FM 1-43 and FM 4-64 were shown to enter astrocytes by permeation of an aqueous pore, and once inside they led to an imbalance of Ca<sup>2+</sup> homeostasis (Li et al., 2009).

With this evidence in hand, it is obvious that trafficking studies in any of the aforementioned cell types have been hampered by FM dye permeation through a diversity of ion channels. With the development of mCLING, not only as endocytosis tracer, but also as cell surface marker, new investigations could be pursued to understand endocytosis, membrane traffic and protein distribution in a wide range of sensory/neuronal preparations.

## 5 OUTLOOK

---

In the present study a novel fixable, membrane-binding probe called mCLING (membrane-binding fluorophore-Cysteine-Lysine-Palmitoyl Group) was developed. From the results shown here I conclude that mCLING is currently the only fluorescent probe that allows morphological characterization of subdiffraction-sized endocytic organelles, something that was so far only possible with electron microscopy. Furthermore, combination of mCLING with immunostaining allowed, for the first time, the molecular characterization of recycling organelles in cultured cells and complex tissues. In contrast to conventional immuno-EM methods, the routine mCLING labeling – immunostaining – melamine embedding established here offers higher throughput and easier sample processing.

Overall, the results obtained in this study illustrate the potential of mCLING in studying the organization of membrane proteins, which can be extended to a wide variety of endocytic organelles, cell types and tissues. mCLING incubations at low temperature have the advantage of labeling only the cell surface, while leaving intracellular organelles unlabeled. This is particularly useful to establish parallels for protein distribution between organelles and the plasma membrane, which is not possible in conventional immunostaining protocols. Great work on the distribution and organization of neuronal proteins in the axon or the synapse has been done, based on immunolabeling (Kittel et al., 2006; Willig et al., 2006; Dani et al., 2010; Denker et al., 2011b; Wahl et al., 2013). However, the ability to see the borders of the synaptic boutons would have added much more information, especially in what concerns the spatial distributions of the protein clusters. Therefore, membrane labeling will be an advantage both in synaptic systems, including cultured neurons, and in other cell types. Interesting labeling targets will be receptors and channels. In this line, an additional application of mCLING will be the labeling of isolated organelles, for their molecular characterization *in vitro*. The fact that mCLING is compatible with live imaging (Figure 3.4, Figure 3.7, Figure 3.8 and Figure 3.9) further increases its range of applications.

mCLING applicability is further broadened by its modular design that allows conjugation with any fluorophore containing a maleimide modification, making it adaptable to virtually any confocal or high-resolution microscopy technique. Furthermore, multicolor imaging of 20 nm melamine sections using epifluorescence microscopy (Figure 3.21) is a simple and

inexpensive approach to perform multi-color super-resolution imaging adoptable by any laboratory.

Exactly 20 years ago the seminal work on high-resolution light microscopy was published (Hell and Wichmann, 1994). Since then, numerous technical advances have been achieved, getting us closer to “see” the microscopic universe in high detail. However, the applicability of cutting-edge light microscopy on cellular systems has been hampered by the lack of suitable tools to reveal biological complexity. With the invention of mCLING and the foreseen advances in molecular labeling tools (e.g. nanobodies and aptamers, (Opazo et al., 2012)) the gap between technique and cell biology will be even narrower.

## REFERENCES

---

- Abbe, E. 1873. Beiträge zur Theorie des Mikroskops und der mikroskopischen Wahrnehmung. *Arch. für Mikroskopische Anat.* 9:413–418.
- Akbergenova, Y., and M. Bykhovskaia. 2009. Stimulation-induced formation of the reserve pool of vesicles in *Drosophila* motor boutons. *J. Neurophysiol.* 101:2423–33.
- Alberts, B., A. Johnson, J. Lewis, M. Raff, K. Roberts, and P. Walter eds. . 2008. *Molecular Biology of the Cell*. Fifth edit. Garland Science, Taylor & Francis Group, Abingdon, UK.
- Anderson, R.G., M.S. Brown, and J.L. Goldstein. 1977. Role of the coated endocytic vesicle in the uptake of receptor-bound low density lipoprotein in human fibroblasts. *Cell.* 10:351–64.
- Andersson, F., J. Jakobsson, P. Löw, O. Shupliakov, and L. Brodin. 2008. Perturbation of syndapin/PACSIN impairs synaptic vesicle recycling evoked by intense stimulation. *J. Neurosci.* 28:3925–33.
- Andrews, J., M. Smith, J. Merakovsky, M. Coulson, F. Hannan, and L.E. Kelly. 1996. The stoned locus of *Drosophila melanogaster* produces a dicistronic transcript and encodes two distinct polypeptides. *Genetics.* 143:1699–711.
- Aravanis, a M., J.L. Pyle, and R.W. Tsien. 2003. Single synaptic vesicles fusing transiently and successively without loss of identity. *Nature.* 423:643–7.
- Baba, T., H. Ueda, N. Terada, Y. Fujii, and S. Ohno. 1999. Immunocytochemical Study of Endocytotic Structures Accumulated in HeLa Cells Transformed with a Temperature-sensitive Mutant of Dynamin. *J. Histochem. Cytochem.* 47:637–648.
- Bal, M., J. Leitz, A.L. Reese, D.M.O. Ramirez, M. Durakoglugil, J. Herz, L.M. Monteggia, and E.T. Kavalali. 2013. Reelin Mobilizes a VAMP7-Dependent Synaptic Vesicle Pool and Selectively Augments Spontaneous Neurotransmission. *Neuron.* 80:934–46.
- Balaji, J., and T. a Ryan. 2007. Single-vesicle imaging reveals that synaptic vesicle exocytosis and endocytosis are coupled by a single stochastic mode. *Proc. Natl. Acad. Sci. U. S. A.* 104:20576–81.
- Banker, G.A., and W.M. Cowan. 1977. Rat hippocampal neurons in dispersed cell culture. *Brain Res.* 126:397–42.
- Bar-On, D., S. Wolter, S. van de Linde, M. Heilemann, G. Nudelman, E. Nachliel, M. Gutman, M. Sauer, and U. Ashery. 2012. Super-resolution imaging reveals the internal architecture of nano-sized syntaxin clusters. *J. Biol. Chem.* 287:27158–67.

- Barysch, S. V, S. Aggarwal, R. Jahn, and S.O. Rizzoli. 2009. Sorting in early endosomes reveals connections to docking- and fusion-associated factors. *Proc. Natl. Acad. Sci. U. S. A.* 106:9697–702.
- Bear, M.F., B.W. Connors, and M.A. Paradiso. 2006. Neuroscience: Exploring the Brain. Third Edit. Lippincott Williams & Wilkins, Baltimore.
- Beaudoin, G.M.J., S.-H. Lee, D. Singh, Y. Yuan, Y.-G. Ng, L.F. Reichardt, and J. Arikath. 2012. Culturing pyramidal neurons from the early postnatal mouse hippocampus and cortex. *Nat. Protoc.* 7:1741–54.
- Bech-Hansen, N.T., M.J. Naylor, T. a Maybaum, W.G. Pearce, B. Koop, G. a Fishman, M. Mets, M. a Musarella, and K.M. Boycott. 1998. Loss-of-function mutations in a calcium-channel alpha1-subunit gene in Xp11.23 cause incomplete X-linked congenital stationary night blindness. *Nat. Genet.* 19:264–7.
- Bellocchio, E.E., R.J. Reimer, R.T. Fremeau, and R.H. Edwards. 2000. Uptake of glutamate into synaptic vesicles by an inorganic phosphate transporter. *Science.* 289:957–60.
- Betz, W.J., F. Mao, and G.S. Bewick. 1992. Activity-dependent fluorescent staining and destaining of living vertebrate motor nerve terminals. *J. Neurosci.* 12:363–75.
- Beurg, M., R. Fettiplace, J.-H. Nam, and A.J. Ricci. 2009. Localization of inner hair cell mechanotransducer channels using high-speed calcium imaging. *Nat. Neurosci.* 12:553–8.
- Beurg, M., N. Michalski, S. Safieddine, Y. Bouleau, R. Schneggenburger, E.R. Chapman, C. Petit, and D. Dulon. 2010. Control of exocytosis by synaptotagmins and otoferlin in auditory hair cells. *J. Neurosci.* 30:13281–90.
- Beutner, D., T. Voets, E. Neher, and T. Moser. 2001. Calcium dependence of exocytosis and endocytosis at the cochlear inner hair cell afferent synapse. *Neuron.* 29:681–90.
- Bonifacino, J.S., and R. Rojas. 2006. Retrograde transport from endosomes to the trans-Golgi network. *Nat. Rev. Mol. Cell Biol.* 7:568–79.
- Boulant, S., C. Kural, J.-C. Zeeh, F. Ubelmann, and T. Kirchhausen. 2011. Actin dynamics counteract membrane tension during clathrin-mediated endocytosis. *Nat. Cell Biol.* 13:1124–31.
- Boumil, R.M., V. a Letts, M.C. Roberts, C. Lenz, C.L. Mahaffey, Z.-W. Zhang, T. Moser, and W.N. Frankel. 2010. A missense mutation in a highly conserved alternate exon of dynamin-1 causes epilepsy in fitful mice. *PLoS Genet.* 6:e1001046.
- Brandhorst, D., D. Zwilling, S.O. Rizzoli, U. Lippert, T. Lang, and R. Jahn. 2006. Homotypic fusion of early endosomes: SNAREs do not determine fusion specificity. *Proc. Natl. Acad. Sci. U. S. A.* 103:2701–6.

## References

---

- Brandt, A., D. Khimich, and T. Moser. 2005. Few CaV1.3 channels regulate the exocytosis of a synaptic vesicle at the hair cell ribbon synapse. *J. Neurosci.* 25:11577–85.
- Brodin, L., P. Löw, and O. Shupliakov. 2000. Sequential steps in clathrin-mediated synaptic vesicle endocytosis. *Curr. Opin. Neurobiol.* 10:312–20.
- Bucci, C., R.G. Parton, I.H. Mather, H. Stunnenberg, K. Simons, B. Hoflack, and M. Zerial. 1992. The small GTPase rab5 functions as a regulatory factor in the early endocytic pathway. *Cell.* 70:715–28.
- Del Castillo, J., and B. Katz. 1954. Quantal components of the end-plate potential. *J. Physiol.* 124:560–73.
- Ceccarelli, B., F. Grohovaz, and W.P. Hurlbut. 1979. Freeze-fracture studies of frog neuromuscular junctions during intense release of neurotransmitter. II. Effects of electrical stimulation and high potassium. *J. Cell Biol.* 81:178–92.
- Ceccarelli, B., W.P. Hurlbut, and a Mauro. 1973. Turnover of transmitter and synaptic vesicles at the frog neuromuscular junction. *J. Cell Biol.* 57:499–524.
- Cesca, F., P. Baldelli, F. Valtorta, and F. Benfenati. 2010. The synapsins: key actors of synapse function and plasticity. *Prog. Neurobiol.* 91:313–48.
- Chamberlain, L.H., R.D. Burgoyne, and G.W. Gould. 2001. SNARE proteins are highly enriched in lipid rafts in PC12 cells: implications for the spatial control of exocytosis. *Proc. Natl. Acad. Sci. U. S. A.* 98:5619–24.
- Chaudhary, N., G. a Gomez, M.T. Howes, H.P. Lo, K.-A. McMahon, J. a Rae, N.L. Schieber, M.M. Hill, K. Gaus, A.S. Yap, and R.G. Parton. 2014. Endocytic crosstalk: caveins, caveolins, and caveolae regulate clathrin-independent endocytosis. *PLoS Biol.* 12:e1001832.
- Chen, J.W., T.L. Murphy, M.C. Willingham, I. Pastan, and J.T. August. 1985. Identification of two lysosomal membrane glycoproteins. *J. Cell Biol.* 101:85–95.
- Cho, S., G.-L. Li, and H. von Gersdorff. 2011. Recovery from short-term depression and facilitation is ultrafast and Ca<sup>2+</sup> dependent at auditory hair cell synapses. *J. Neurosci.* 31:5682–92.
- Chung, C., B. Barylko, J. Leitz, X. Liu, and E.T. Kavalali. 2010. Acute dynamin inhibition dissects synaptic vesicle recycling pathways that drive spontaneous and evoked neurotransmission. *J. Neurosci.* 30:1363–76.
- Clayton, E.L., V. Anggono, K.J. Smillie, N. Chau, P.J. Robinson, and M. a Cousin. 2009. The phospho-dependent dynamin-syndapin interaction triggers activity-dependent bulk endocytosis of synaptic vesicles. *J. Neurosci.* 29:7706–17.
- Clayton, E.L., and M. a Cousin. 2009. The molecular physiology of activity-dependent bulk endocytosis of synaptic vesicles. *J. Neurochem.* 111:901–14.

- Clayton, E.L., G.J.O. Evans, and M. a Cousin. 2008. Bulk synaptic vesicle endocytosis is rapidly triggered during strong stimulation. *J. Neurosci.* 28:6627–32.
- Cochilla, A.J., J.K. Angleson, and W.J. Betz. 1999. Monitoring secretory membrane with FM1-43 fluorescence. *Annu. Rev. Neurosci.* 22:1–10.
- Coggins, M.R., C.P. Grabner, W. Almers, and D. Zenisek. 2007. Stimulated exocytosis of endosomes in goldfish retinal bipolar neurons. *J. Physiol.* 584:853–65.
- Collins, B.M., A.J. McCoy, H.M. Kent, P.R. Evans, and D.J. Owen. 2002. Molecular architecture and functional model of the endocytic AP2 complex. *Cell.* 109:523–35.
- Coon, A.H., H.J. Creech, N. Jones, and E. Berliner. 1942. The Demonstration of Pneumococcal Antigen in Tissues by the Use of Fluorescent Antibody. *J. Immunol.* 45:159–170.
- Coons, A.H., H.J. Creech, and R.N. Jones. 1941. Immunological properties of an antibody containing a fluorescent group. *Proc. Soc. Exp. Biol. Med.* 47:200–202.
- Cooper, N.G., and B.J. McLaughlin. 1983. Tracer uptake by photoreceptor synaptic terminals. I. Dark-mediated effects. *J. Ultrastruct. Res.* 84:252–67.
- Cooper, N.P., and J.J. Guinan. 2006. Efferent-mediated control of basilar membrane motion. *J. Physiol.* 576:49–54.
- Corey, D.P. 2009. Cell biology of mechanotransduction in inner-ear hair cells. *F1000 Biol. Rep.* 1:58.
- Cremona, O., and P. De Camilli. 1997. Synaptic vesicle endocytosis. *Curr. Opin. Neurobiol.* 7:323–30.
- Crumling, M.A., M. Tong, K.L. Aschenbach, L.Q. Liu, C.M. Pipitone, and R.K. Duncan. 2009. P2X antagonists inhibit styryl dye entry into hair cells. *Neuroscience.* 161:1144–53.
- Daly, C., M. Sugimori, J.E. Moreira, E.B. Ziff, and R. Llinás. 2000. Synaptophysin regulates clathrin-independent endocytosis of synaptic vesicles. *Proc. Natl. Acad. Sci. U. S. A.* 97:6120–5.
- Dani, A., B. Huang, J. Bergan, C. Dulac, and X. Zhuang. 2010. Superresolution imaging of chemical synapses in the brain. *Neuron.* 68:843–56.
- Danilczyk, U.G., M.F. Cohen-Doyle, and D.B. Williams. 2000. Functional relationship between calreticulin, calnexin, and the endoplasmic reticulum luminal domain of calnexin. *J. Biol. Chem.* 275:13089–97.
- Denker, A., I. Bethani, K. Kröhnert, C. Körber, H. Horstmann, B.G. Wilhelm, S. V Barysch, T. Kuner, E. Neher, and S.O. Rizzoli. 2011a. A small pool of vesicles maintains synaptic activity in vivo. *Proc. Natl. Acad. Sci. U. S. A.* 108:17177–82.

## References

---

- Denker, A., K. Kröhnert, J. Bückers, E. Neher, and S.O. Rizzoli. 2011b. The reserve pool of synaptic vesicles acts as a buffer for proteins involved in synaptic vesicle recycling. *Proc. Natl. Acad. Sci. U. S. A.* 108:17183–8.
- Denker, A., K. Kröhnert, and S.O. Rizzoli. 2009. Revisiting synaptic vesicle pool localization in the *Drosophila* neuromuscular junction. *J. Physiol.* 587:2919–26.
- DeRosier, D.J., and L.G. Tilney. 1989. The structure of the cuticular plate, an in vivo actin gel. *J. Cell Biol.* 109:2853–67.
- Dietzen, D.J., W.R. Hastings, and D.M. Lublin. 1995. Caveolin is palmitoylated on multiple cysteine residues. Palmitoylation is not necessary for localization of caveolin to caveolae. *J. Biol. Chem.* 270:6838–42.
- Diril, M.K., M. Wienisch, N. Jung, J. Klingauf, and V. Haucke. 2006. Stonin 2 is an AP-2-dependent endocytic sorting adaptor for synaptotagmin internalization and recycling. *Dev. Cell.* 10:233–44.
- Doggenweiler, C.F., and F. Zambrano. 1981. Extraction of phospholipids from aldehyde-fixed membranes. *Arch. Biol. Med. Exp. (Santiago).* 14:343–7.
- Doherty, G.J., and H.T. McMahon. 2009. Mechanisms of endocytosis. *Annu. Rev. Biochem.* 78:857–902.
- Drab, M., P. Verkade, M. Elger, M. Kasper, M. Lohn, B. Lauterbach, J. Menne, C. Lindschau, F. Mende, F.C. Luft, a Schedl, H. Haller, and T. V Kurzchalia. 2001. Loss of caveolae, vascular dysfunction, and pulmonary defects in caveolin-1 gene-disrupted mice. *Science.* 293:2449–52.
- Drew, L.J., and J.N. Wood. 2007. FM1-43 is a permeant blocker of mechanosensitive ion channels in sensory neurons and inhibits behavioural responses to mechanical stimuli. *Mol. Pain.* 3:1.
- Duncker, S. V., C. Franz, S. Kuhn, U. Schulte, D. Campanelli, N. Brandt, B. Hirt, B. Fakler, N. Blin, P. Ruth, J. Engel, W. Marcotti, U. Zimmermann, and M. Knipper. 2013. Otoferlin couples to clathrin-mediated endocytosis in mature cochlear inner hair cells. *J. Neurosci.* 33:9508–19.
- Dunster, K., B.H. Toh, and J.W. Sentry. 2002. Early endosomes, late endosomes, and lysosomes display distinct partitioning strategies of inheritance with similarities to Golgi-derived membranes. *Eur. J. Cell Biol.* 81:117–24.
- Edeling, M. a, C. Smith, and D. Owen. 2006. Life of a clathrin coat: insights from clathrin and AP structures. *Nat. Rev. Mol. Cell Biol.* 7:32–44.
- Eidels, L., R.L. Proia, and D.A. Hart. 1983. Membrane receptors for bacterial toxins. *Microbiol. Rev.* 47:596–620.



- Evans, G.J.O., and M. a Cousin. 2007. Activity-dependent control of slow synaptic vesicle endocytosis by cyclin-dependent kinase 5. *J. Neurosci.* 27:401–11.
- Faas, F.G. a, M.C. Avramut, B.M. van den Berg, a M. Mommaas, A.J. Koster, and R.B.G. Ravelli. 2012. Virtual nanoscopy: generation of ultra-large high resolution electron microscopy maps. *J. Cell Biol.* 198:457–69.
- Farris, H.E., C.L. LeBlanc, J. Goswami, and a J. Ricci. 2004. Probing the pore of the auditory hair cell mechanotransducer channel in turtle. *J. Physiol.* 558:769–92.
- Fatt, P., and B. Katz. 1952. Spontaneous subthreshold activity at motor nerve endings. *J. Physiol.* 117:109–28.
- Faulk, W., and G. Taylor. 1971. An immunocolloidal method for the electron microscope. *Immunochemistry.* 8:1081–1083.
- Favre, D., E. Scarfone, G. Di Gioia, P. De Camilli, and D. Dememes. 1986. Presence of synapsin I in afferent and efferent nerve endings of vestibular sensory epithelia. *Brain Res.* 384:379–82.
- Fawcett, D.W. 1965. Surface Specializations of Absorbing Cells. *J. Histochem. Cytochem.* 13:75–91.
- Fekete, D.M. 1996. Cell fate specification in the inner ear. *Curr. Opin. Neurobiol.* 6:533–41.
- Ferguson, S.M., and P. De Camilli. 2012. Dynamin, a membrane-remodelling GTPase. *Nat. Rev. Mol. Cell Biol.* 13:75–88.
- Fernández-Alfonso, T., R. Kwan, and T. a Ryan. 2006. Synaptic vesicles interchange their membrane proteins with a large surface reservoir during recycling. *Neuron.* 51:179–86.
- Fesce, R., F. Grohovaz, F. Valtorta, and J. Meldolesi. 1994. Neurotransmitter release: fusion or “kiss-and-run”? *Trends Cell Biol.* 4:1–4.
- Fischer von Mollard, G., T.C. Südhof, and R. Jahn. 1991. A small GTP-binding protein dissociates from synaptic vesicles during exocytosis. *Nature.* 349:79–81.
- Fölsch, H. 2005. The building blocks for basolateral vesicles in polarized epithelial cells. *Trends Cell Biol.* 15:222–8.
- Ford, M.G.J., I.G. Mills, B.J. Peter, Y. Vallis, G.J.K. Praefcke, P.R. Evans, and H.T. McMahon. 2002. Curvature of clathrin-coated pits driven by epsin. *Nature.* 419:361–6.
- Forge, a, and G. Richardson. 1993. Freeze fracture analysis of apical membranes in cochlear cultures: differences between basal and apical-coil outer hair cells and effects of neomycin. *J. Neurocytol.* 22:854–67.

## References

---

- Frank, T., M. a Rutherford, N. Strenzke, A. Neef, T. Pangršič, D. Khimich, A. Fejtova, A. Fetjova, E.D. Gundelfinger, M.C. Liberman, B. Harke, K.E. Bryan, A. Lee, A. Egner, D. Riedel, and T. Moser. 2010. Bassoon and the synaptic ribbon organize Ca<sup>2+</sup> channels and vesicles to add release sites and promote refilling. *Neuron*. 68:724–38.
- Fredj, N. Ben, and J. Burrone. 2009. A resting pool of vesicles is responsible for spontaneous vesicle fusion at the synapse. *Nat. Neurosci*. 12:751–8.
- Fremeau, R.T., M.D. Troyer, I. Pahner, G.O. Nygaard, C.H. Tran, R.J. Reimer, E.E. Bellocchio, D. Fortin, J. Storm-Mathisen, and R.H. Edwards. 2001. The expression of vesicular glutamate transporters defines two classes of excitatory synapse. *Neuron*. 31:247–60.
- Frick, M., N. a Bright, K. Riento, A. Bray, C. Merrified, and B.J. Nichols. 2007. Coassembly of flotillins induces formation of membrane microdomains, membrane curvature, and vesicle budding. *Curr. Biol*. 17:1151–6.
- Fridberger, A., I. Tomo, M. Ulfendahl, and J. Boutet de Monvel. 2006. Imaging hair cell transduction at the speed of sound: dynamic behavior of mammalian stereocilia. *Proc. Natl. Acad. Sci. U. S. A*. 103:1918–23.
- Fried, R.C., and M.P. Blaustein. 1978. Retrieval and recycling of synaptic vesicle membrane in pinched-off nerve terminals (synaptosomes). *J. Cell Biol*. 78:685–700.
- Fuchs, M., J.H. Brandstätter, and H. Regus-Leidig. 2014. Evidence for a Clathrin-independent mode of endocytosis at a continuously active sensory synapse. *Front. Cell. Neurosci*. 8:1–13.
- Fuchs, P. a, E. Glowatzki, and T. Moser. 2003. The afferent synapse of cochlear hair cells. *Curr. Opin. Neurobiol*. 13:452–458.
- Fuenzalida, L.C., K.L. Keen, and E. Terasawa. 2011. Colocalization of FM1-43, Bassoon, and GnRH-1: GnRH-1 release from cell bodies and their neuroprocesses. *Endocrinology*. 152:4310–21.
- Furness, D.N., and C.M. Hackney. 2001. The Structure and Composition of the Stereociliary Bundle of Vertebrate Hair Cells. *Techniques*. 95–153.
- Futter, C.E., a Pearse, L.J. Hewlett, and C.R. Hopkins. 1996. Multivesicular endosomes containing internalized EGF-EGF receptor complexes mature and then fuse directly with lysosomes. *J. Cell Biol*. 132:1011–23.
- Gaffield, M. a, and W.J. Betz. 2006. Imaging synaptic vesicle exocytosis and endocytosis with FM dyes. *Nat. Protoc*. 1:2916–21.
- Gale, J.E., W. Marcotti, H.J. Kennedy, C.J. Kros, and G.P. Richardson. 2001. FM1-43 dye behaves as a permeant blocker of the hair-cell mechanotransducer channel. *J. Neurosci*. 21:7013–25.

- Gandhi, S.P., and C.F. Stevens. 2003. Three modes of synaptic vesicular recycling revealed by single-vesicle imaging. *Nature*. 423:607–13.
- Geppert, M., V.Y. Bolshakov, S.A. Siegelbaum, K. Takei, P. De Camilli, R.E. Hammer, and T.C. Südhof. 1994a. The role of Rab3A in neurotransmitter release. *Nature*. 369:493–7.
- Geppert, M., Y. Goda, R.E. Hammer, C. Li, T.W. Rosahl, C.F. Stevens, and T.C. Südhof. 1994b. Synaptotagmin I: a major Ca<sup>2+</sup> sensor for transmitter release at a central synapse. *Cell*. 79:717–27.
- Geppert, M., and T.C. Südhof. 1998. RAB3 and synaptotagmin: the yin and yang of synaptic membrane fusion. *Annu. Rev. Neurosci.* 21:75–95.
- Von Gersdorff, H., and G. Matthews. 1994. Dynamics of synaptic vesicle fusion and membrane retrieval in synaptic terminals. *Nature*. 367:735–9.
- Von Gersdorff, H., E. Vardi, G. Matthews, and P. Sterling. 1996. Evidence that vesicles on the synaptic ribbon of retinal bipolar neurons can be rapidly released. *Neuron*. 16:1221–7.
- Godenschwege, T. a, D. Reisch, S. Diegelmann, K. Eberle, N. Funk, M. Heisenberg, V. Hoppe, J. Hoppe, B.R.E. Klagges, J.-R. Martin, E. a Nikitina, G. Putz, R. Reifegerste, N. Reisch, J. Rister, M. Schaupp, H. Scholz, M. Schwärzel, U. Werner, T.D. Zars, S. Buchner, and E. Buchner. 2004. Flies lacking all synapsins are unexpectedly healthy but are impaired in complex behaviour. *Eur. J. Neurosci.* 20:611–22.
- González-Gaitán, M., and H. Jäckle. 1997. Role of *Drosophila* alpha-adaptin in presynaptic vesicle recycling. *Cell*. 88:767–76.
- Goodyear, R.J., P.K. Legan, J.R. Christiansen, B. Xia, J. Korchagina, J.E. Gale, M.E. Warchol, J.T. Corwin, and G.P. Richardson. 2010. Identification of the hair cell soma-1 antigen, HCS-1, as otoferlin. *J. Assoc. Res. Otolaryngol.* 11:573–86.
- Goodyear, R.J., and G.P. Richardson. 2002. Extracellular matrices associated with the apical surfaces of sensory epithelia in the inner ear: molecular and structural diversity. *J. Neurobiol.* 53:212–27.
- Gorvel, J.P., P. Chavrier, M. Zerial, and J. Gruenberg. 1991. Rab5 controls early endosome fusion in vitro. *Cell*. 64:915–25.
- Goutman, J.D., and E. Glowatzki. 2007. Time course and calcium dependence of transmitter release at a single ribbon synapse. *Proc. Natl. Acad. Sci. U. S. A.* 104:16341–6.
- Granseth, B., B. Odermatt, S.J. Royle, and L. Lagnado. 2006. Clathrin-mediated endocytosis is the dominant mechanism of vesicle retrieval at hippocampal synapses. *Neuron*. 51:773–86.

## References

---

- Grass, I., S. Thiel, S. Höning, and V. Haucke. 2004. Recognition of a basic AP-2 binding motif within the C2B domain of synaptotagmin is dependent on multimerization. *J. Biol. Chem.* 279:54872–80.
- Griesinger, C.B., C.D. Richards, and J.F. Ashmore. 2002. FM1-43 reveals membrane recycling in adult inner hair cells of the mammalian cochlea. *J. Neurosci.* 22:3939–52.
- Griesinger, C.B., C.D. Richards, and J.F. Ashmore. 2004. Apical endocytosis in outer hair cells of the mammalian cochlea. *Eur. J. Neurosci.* 20:41–50.
- Griesinger, C.B., C.D. Richards, and J.F. Ashmore. 2005. Fast vesicle replenishment allows indefatigable signalling at the first auditory synapse. *Nature.* 435:212–5.
- Grimmer, S., B. van Deurs, and K. Sandvig. 2002. Membrane ruffling and macropinocytosis in A431 cells require cholesterol. *J. Cell Sci.* 115:2953–62.
- Groemer, T.W., and J. Klingauf. 2007. Synaptic vesicles recycling spontaneously and during activity belong to the same vesicle pool. *Nat. Neurosci.* 10:145–7.
- Gruenberg, J. 2001. The endocytic pathway: a mosaic of domains. *Nat. Rev. Mol. Cell Biol.* 2:721–30.
- Halemani, N.D., I. Bethani, S.O. Rizzoli, and T. Lang. 2010. Structure and dynamics of a two-helix SNARE complex in live cells. *Traffic.* 11:394–404.
- Harata, N.C., A.M. Aravanis, and R.W. Tsien. 2006a. Kiss-and-run and full-collapse fusion as modes of exo-endocytosis in neurosecretion. *J. Neurochem.* 97:1546–70.
- Harata, N.C., S. Choi, J.L. Pyle, A.M. Aravanis, and R.W. Tsien. 2006b. Frequency-dependent kinetics and prevalence of kiss-and-run and reuse at hippocampal synapses studied with novel quenching methods. *Neuron.* 49:243–56.
- Harper, C.B., S. Martin, T.H. Nguyen, S.J. Daniels, N. a Lavidis, M.R. Popoff, G. Hadzic, A. Mariana, N. Chau, A. McCluskey, P.J. Robinson, and F. a Meunier. 2011. Dynamin inhibition blocks botulinum neurotoxin type A endocytosis in neurons and delays botulism. *J. Biol. Chem.* 286:35966–76.
- Haucke, V., and P. De Camilli. 1999. AP-2 recruitment to synaptotagmin stimulated by tyrosine-based endocytic motifs. *Science.* 285:1268–71.
- Haucke, V., M.R. Wenk, E.R. Chapman, K. Farsad, and P. De Camilli. 2000. Dual interaction of synaptotagmin with mu2- and alpha-adaptin facilitates clathrin-coated pit nucleation. *EMBO J.* 19:6011–9.
- Heidelberger, R., Z.-Y. Zhou, and G. Matthews. 2002. Multiple components of membrane retrieval in synaptic terminals revealed by changes in hydrostatic pressure. *J. Neurophysiol.* 88:2509–17.

- Heidrych, P., U. Zimmermann, A. Bress, C.M. Pusch, P. Ruth, M. Pfister, M. Knipper, and N. Blin. 2008. Rab8b GTPase, a protein transport regulator, is an interacting partner of otoferlin, defective in a human autosomal recessive deafness form. *Hum. Mol. Genet.* 17:3814–21.
- Heidrych, P., U. Zimmermann, S. Kuhn, C. Franz, J. Engel, S. V Duncker, B. Hirt, C.M. Pusch, P. Ruth, M. Pfister, W. Marcotti, N. Blin, and M. Knipper. 2009. Otoferlin interacts with myosin VI: implications for maintenance of the basolateral synaptic structure of the inner hair cell. *Hum. Mol. Genet.* 18:2779–90.
- Hell, S.W. 2007. Far-field optical nanoscopy. *Science.* 316:1153–8.
- Hell, S.W., M. Dyba, and S. Jakobs. 2004. Concepts for nanoscale resolution in fluorescence microscopy. *Curr. Opin. Neurobiol.* 14:599–609.
- Hell, S.W., and J. Wichmann. 1994. Breaking the diffraction resolution limit by stimulated emission: stimulated-emission-depletion fluorescence microscopy. *Opt. Lett.* 19:780–2.
- Henkel, a W., J. Lübke, and W.J. Betz. 1996. FM1-43 dye ultrastructural localization in and release from frog motor nerve terminals. *Proc. Natl. Acad. Sci. U. S. A.* 93:1918–23.
- Henley, J.R., E.W. Krueger, B.J. Oswald, and M. a McNiven. 1998. Dynamin-mediated internalization of caveolae. *J. Cell Biol.* 141:85–99.
- Henriksen, L., M.V. Grandal, S.L.J. Knudsen, B. van Deurs, and L.M. Grøvdal. 2013. Internalization mechanisms of the epidermal growth factor receptor after activation with different ligands. *PLoS One.* 8:e58148.
- Heuser, J.E., and T.S. Reese. 1973. Evidence for recycling of synaptic vesicle membrane during transmitter release at the frog neuromuscular junction. *J. Cell Biol.* 57:315–44.
- Heuser, J.E., T.S. Reese, M.J. Dennis, Y. Jan, L. Jan, and L. Evans. 1979. Synaptic vesicle exocytosis captured by quick freezing and correlated with quantal transmitter release. *J. Cell Biol.* 81:275–300.
- Hinshaw, J.E. 2000. Dynamin and its role in membrane fission. *Annu. Rev. Cell Dev. Biol.* 16:483–519.
- Holt, M., A. Cooke, A. Neef, and L. Lagnado. 2004. High mobility of vesicles supports continuous exocytosis at a ribbon synapse. *Curr. Biol.* 14:173–83.
- Holt, M., A. Cooke, M.M. Wu, and L. Lagnado. 2003. Bulk membrane retrieval in the synaptic terminal of retinal bipolar cells. *J. Neurosci.* 23:1329–39.
- Holtzman, E., A.R. Freeman, and L.A. Kashner. 1971. Stimulation-dependent alterations in peroxidase uptake at lobster neuromuscular junctions. *Science.* 173:733–6.

## References

---

- Honig, M.G., and R.I. Hume. 1986. Fluorescent carbocyanine dyes allow living neurons of identified origin to be studied in long-term cultures. *J. Cell Biol.* 103:171–87.
- Van Hook, M.J., and W.B. Thoreson. 2012. Rapid synaptic vesicle endocytosis in cone photoreceptors of salamander retina. *J. Neurosci.* 32:18112–23.
- Hoopmann, P., A. Punge, S. V Barysch, V. Westphal, J. Bückers, F. Opazo, I. Bethani, M. a Lauterbach, S.W. Hell, and S.O. Rizzoli. 2010. Endosomal sorting of readily releasable synaptic vesicles. *Proc. Natl. Acad. Sci. U. S. A.* 107:19055–60.
- Hoopmann, P., S.O. Rizzoli, and W.J. Betz. 2012. Imaging synaptic vesicle recycling by staining and destaining vesicles with FM dyes. *Cold Spring Harb. Protoc.* 2012:77–83.
- Hosoi, N., M. Holt, and T. Sakaba. 2009. Calcium dependence of exo- and endocytotic coupling at a glutamatergic synapse. *Neuron.* 63:216–29.
- Houot, L., and P.I. Watnick. 2008. A novel role for enzyme I of the *Vibrio cholerae* phosphoenolpyruvate phosphotransferase system in regulation of growth in a biofilm. *J. Bacteriol.* 190:311–20.
- Howes, M.T., M. Kirkham, J. Riches, K. Cortese, P.J. Walser, F. Simpson, M.M. Hill, A. Jones, R. Lundmark, M.R. Lindsay, D.J. Hernandez-Deviez, G. Hadzic, A. McCluskey, R. Bashir, L. Liu, P. Pilch, H. McMahon, P.J. Robinson, J.F. Hancock, S. Mayor, and R.G. Parton. 2010. Clathrin-independent carriers form a high capacity endocytic sorting system at the leading edge of migrating cells. *J. Cell Biol.* 190:675–91.
- Hu, Y., L. Qu, and T. Schikorski. 2008. Mean synaptic vesicle size varies among individual excitatory hippocampal synapses. *Synapse.* 62:953–7.
- Hua, Y., R. Sinha, M. Martineau, M. Kahms, and J. Klingauf. 2010. A common origin of synaptic vesicles undergoing evoked and spontaneous fusion. *Nat. Neurosci.* 13:1451–3.
- Hua, Y., R. Sinha, C.S. Thiel, R. Schmidt, J. Hüve, H. Martens, S.W. Hell, A. Egner, and J. Klingauf. 2011a. A readily retrievable pool of synaptic vesicles. *Nat. Neurosci.* 14:833–839.
- Hua, Z., S. Leal-Ortiz, S.M. Foss, C.L. Waites, C.C. Garner, S.M. Voglmaier, and R.H. Edwards. 2011b. v-SNARE composition distinguishes synaptic vesicle pools. *Neuron.* 71:474–87.
- Huang, K.M., L. Gullberg, K.K. Nelson, C.J. Stefan, K. Blumer, and S.K. Lemmon. 1997. Novel functions of clathrin light chains: clathrin heavy chain trimerization is defective in light chain-deficient yeast. *J. Cell Sci.* 110 (Pt 7):899–910.
- Van IJzendoorn, S.C., and D. Hoekstra. 1999. The subapical compartment: a novel sorting centre? *Trends Cell Biol.* 9:144–9.

- Van Ijzendoorn, S.C.D. 2006. Recycling endosomes. *J. Cell Sci.* 119:1679–81.
- Jacobson, B.S., and D. Branton. 1977. Plasma membrane: rapid isolation and exposure of the cytoplasmic surface by use of positively charged beads. *Science.* 195:302–4.
- Jahn, R., and R.H. Scheller. 2006. SNAREs — engines for membrane fusion. *Nat. Rev. Mol. Cell Biol.* 7:631–43.
- Jahn, R., W. Schiebler, C. Ouimet, and P. Greengard. 1985. A 38,000-dalton membrane protein (p38) present in synaptic vesicles. *Proc. Natl. Acad. Sci. U. S. A.* 82:4137–41.
- Jan, L.Y., and Y.N. Jan. 1976. Properties of the larval neuromuscular junction in *Drosophila melanogaster*. *J. Physiol.* 262:189–214.
- Jing, Z., M. a Rutherford, H. Takago, T. Frank, A. Fejtova, D. Khimich, T. Moser, and N. Strenzke. 2013. Disruption of the Presynaptic Cytomatrix Protein Bassoon Degrades Ribbon Anchorage, Multiquantal Release, and Sound Encoding at the Hair Cell Afferent Synapse. *J. Neurosci.* 33:4456–4467.
- Jockusch, W.J., G.J.K. Praefcke, H.T. McMahon, and L. Lagnado. 2005. Clathrin-dependent and clathrin-independent retrieval of synaptic vesicles in retinal bipolar cells. *Neuron.* 46:869–78.
- Johannes, L., D. Tenza, C. Antony, and B. Goud. 1997. Retrograde transport of KDEL-bearing B-fragment of Shiga toxin. *J. Biol. Chem.* 272:19554–61.
- Johnson, C.P., and E.R. Chapman. 2010. Otoferlin is a calcium sensor that directly regulates SNARE-mediated membrane fusion. *J. Cell Biol.* 191:187–97.
- Jovic, M., M. Sharma, J. Rahajeng, and S. Caplan. 2010. The early endosome: a busy sorting station for proteins at the crossroads. *Histol. Histopathol.* 25:99–112.
- Kachar, B., A. Battaglia, and J. Fex. 1997. Compartmentalized vesicular traffic around the hair cell cuticular plate. *Hear. Res.* 107:102–112.
- Kamin, D. 2011. Synaptic vesicle recycling investigated by high-resolution microscopy in a conventional and a sensory synapse. (Dorctoral dissertation). Georg-August-Universität Göttingen, Germany.
- Kamin, D., N.H. Revelo, and S.O. Rizzoli. 2014. FM Dye Photo-Oxidation as a Tool for Monitoring Membrane Recycling in Inner Hair Cells. *PLoS One.* 9:e88353.
- Kandel, E.R., J.H. Schwartz, T.M. Jessell, S.A. Siegelbaum, and A.J. Hudspeth eds. . 2013. Principles of neural science. Fifth edit. The MacGraw Hill Companies, Inc.
- Kantardzhieva, a, M. Peppi, W.S. Lane, and W.F. Sewell. 2012. Protein composition of immunoprecipitated synaptic ribbons. *J. Proteome Res.* 11:1163–74.

## References

---

- Kantardzhieva, A., M.C. Liberman, and W.F. Sewell. 2013. Quantitative analysis of ribbons, vesicles, and cisterns at the cat inner hair cell synapse: correlations with spontaneous rate. *J. Comp. Neurol.* 521:3260–71.
- Katz, B., and R. Miledi. 1969. Spontaneous and evoked activity of motor nerve endings in calcium Ringer. *J. Physiol.* 203:689–706.
- Kavalali, E.T., and E.M. Jorgensen. 2014. Visualizing presynaptic function. *Nat. Neurosci.* 17:10–6.
- Kessels, M.M., J. Dong, W. Leibig, P. Westermann, and B. Qualmann. 2006. Complexes of syndapin II with dynamin II promote vesicle formation at the trans-Golgi network. *J. Cell Sci.* 119:1504–16.
- Khimich, D., R. Nouvian, R. Pujol, S. Tom Dieck, A. Egner, E.D. Gundelfinger, and T. Moser. 2005. Hair cell synaptic ribbons are essential for synchronous auditory signalling. *Nature.* 434:889–94.
- Khuong, T.M., R.L.P. Habets, S. Kuenen, A. Witkowska, J. Kasprovicz, J. Swerts, R. Jahn, G. van den Bogaart, and P. Verstreken. 2013. Synaptic PI(3,4,5)P3 is required for Syntaxin1A clustering and neurotransmitter release. *Neuron.* 77:1097–108.
- Killisch, I., P. Steinlein, K. Römisch, R. Hollinshead, H. Beug, and G. Griffiths. 1992. Characterization of early and late endocytic compartments of the transferrin cycle. Transferrin receptor antibody blocks erythroid differentiation by trapping the receptor in the early endosome. *J. Cell Sci.* 103 (Pt 1):211–32.
- Kirchhausen, T., and T. Toyoda. 1993. Immunoelectron microscopic evidence for the extended conformation of light chains in clathrin trimers. *J. Biol. Chem.* 268:10268–73.
- Kirkham, M., A. Fujita, R. Chadda, S.J. Nixon, T. V Kurzchalia, D.K. Sharma, R.E. Pagano, J.F. Hancock, S. Mayor, and R.G. Parton. 2005. Ultrastructural identification of uncoated caveolin-independent early endocytic vehicles. *J. Cell Biol.* 168:465–76.
- Kittel, R.J., C. Wichmann, T.M. Rasse, W. Fouquet, M. Schmidt, A. Schmid, D. a Wagh, C. Pawlu, R.R. Kellner, K.I. Willig, S.W. Hell, E. Buchner, M. Heckmann, and S.J. Sigrist. 2006. Bruchpilot promotes active zone assembly, Ca<sup>2+</sup> channel clustering, and vesicle release. *Science.* 312:1051–4.
- Klar, T. a, S. Jakobs, M. Dyba, A. Egner, and S.W. Hell. 2000. Fluorescence microscopy with diffraction resolution barrier broken by stimulated emission. *Proc. Natl. Acad. Sci. U. S. A.* 97:8206–10.
- Klausner, R.D., and D.E. Wolf. 1980. Selectivity of fluorescent lipid analogues for lipid domains. *Biochemistry.* 19:6199–203.
- Von Kleist, L., and V. Haucke. 2011. At the Crossroads of Chemistry and Cell Biology: Inhibiting Membrane Traffic by Small Molecules. *Traffic.* 495–504.



- Von Kleist, L., W. Stahlschmidt, H. Bulut, K. Gromova, D. Puchkov, M.J. Robertson, K. a MacGregor, N. Tomilin, N. Tomlin, A. Pechstein, N. Chau, M. Chircop, J. Sakoff, J.P. von Kries, W. Saenger, H.-G. Kräusslich, O. Shupliakov, P.J. Robinson, A. McCluskey, and V. Haucke. 2011. Role of the clathrin terminal domain in regulating coated pit dynamics revealed by small molecule inhibition. *Cell*. 146:471–84.
- Klenchin, V. a, and T.F. Martin. 2000. Priming in exocytosis: attaining fusion-competence after vesicle docking. *Biochimie*. 82:399–407.
- Van der Kloot, W. 1991. The regulation of quantal size. *Prog. Neurobiol.* 36:93–130.
- Koenig, J.H., and K. Ikeda. 1996. Synaptic vesicles have two distinct recycling pathways. *J. Cell Biol.* 135:797–808.
- Koenig, J.H., K. Yamaoka, and K. Ikeda. 1998. Omega images at the active zone may be endocytotic rather than exocytotic: implications for the vesicle hypothesis of transmitter release. *Proc. Natl. Acad. Sci. U. S. A.* 95:12677–82.
- Kollmar, R., L.G. Montgomery, J. Fak, L.J. Henry, and A.J. Hudspeth. 1997. Predominance of the alpha1D subunit in L-type voltage-gated Ca<sup>2+</sup> channels of hair cells in the chicken's cochlea. *Proc. Natl. Acad. Sci. U. S. A.* 94:14883–8.
- Kosaka, T., and K. Ikeda. 1983. Possible temperature-dependent blockage of synaptic vesicle recycling induced by a single gene mutation in *Drosophila*. *J. Neurobiol.* 14:207–25.
- Lang, T., D. Bruns, D. Wenzel, D. Riedel, P. Holroyd, C. Thiele, and R. Jahn. 2001. SNAREs are concentrated in cholesterol-dependent clusters that define docking and fusion sites for exocytosis. *EMBO J.* 20:2202–13.
- De Lange, R.P.J., a D.G. de Roos, and J.G.G. Borst. 2003. Two modes of vesicle recycling in the rat calyx of Held. *J. Neurosci.* 23:10164–73.
- Lemmon, S.K. 2001. Clathrin uncoating: Auxilin comes to life. *Curr. Biol.* 11:R49–52.
- Lenzi, D., J. Crum, M.H. Ellisman, and W.M. Roberts. 2002. Depolarization Redistributes Synaptic Membrane and Creates a Gradient of Vesicles on the Synaptic Body at a Ribbon Synapse. *Neuron*. 36:649–659.
- Lenzi, D., J.W. Runyeon, J. Crum, M.H. Ellisman, and W.M. Roberts. 1999. Synaptic vesicle populations in saccular hair cells reconstructed by electron tomography. *J. Neurosci.* 19:119–32.
- Leonard, D., A. Hayakawa, D. Lawe, D. Lambright, K.D. Bellve, C. Standley, L.M. Lifshitz, K.E. Fogarty, and S. Corvera. 2008. Sorting of EGF and transferrin at the plasma membrane and by cargo-specific signaling to EEA1-enriched endosomes. *J. Cell Sci.* 121:3445–58.

## References

---

- Levic, S., Y. Bouleau, and D. Dulon. 2011. Developmental acquisition of a rapid calcium-regulated vesicle supply allows sustained high rates of exocytosis in auditory hair cells. *PLoS One*. 6:e25714.
- Li, D., K. Héroult, M. Oheim, and N. Ropert. 2009. FM dyes enter via a store-operated calcium channel and modify calcium signaling of cultured astrocytes. *Proc. Natl. Acad. Sci. U. S. A.* 106:21960–5.
- Li, Z., and V.N. Murthy. 2001. Visualizing postendocytic traffic of synaptic vesicles at hippocampal synapses. *Neuron*. 31:593–605.
- Llinás, R., and C. Nicholson. 1975. Calcium role in depolarization-secretion coupling: an aequorin study in squid giant synapse. *Proc. Natl. Acad. Sci. U. S. A.* 72:187–90.
- Llobet, A., J.L. Gallop, J.J.E. Burden, G. Camdere, P. Chandra, Y. Vallis, C.R. Hopkins, L. Lagnado, and H.T. McMahon. 2011. Endophilin drives the fast mode of vesicle retrieval in a ribbon synapse. *J. Neurosci.* 31:8512–9.
- LoGiudice, L., and G. Matthews. 2009. The role of ribbons at sensory synapses. *Neuroscientist*. 15:380–91.
- LoGiudice, L., P. Sterling, and G. Matthews. 2008. Mobility and turnover of vesicles at the synaptic ribbon. *J. Neurosci.* 28:3150–8.
- Logiudice, L., P. Sterling, and G. Matthews. 2009. Vesicle recycling at ribbon synapses in the finely branched axon terminals of mouse retinal bipolar neurons. *Neuroscience*. 164:1546–56.
- Lombardi, D., T. Soldati, M. a Riederer, Y. Goda, M. Zerial, and S.R. Pfeffer. 1993. Rab9 functions in transport between late endosomes and the trans Golgi network. *EMBO J.* 12:677–82.
- Loy, K., O. Welzel, J. Kornhuber, and T.W. Groemer. 2014. Common strength and localization of spontaneous and evoked synaptic vesicle release sites. *Mol. Brain*. 7:23.
- Luckett, J.C. a, O. Darch, C. Watters, M. Abuoun, V. Wright, E. Paredes-Osses, J. Ward, H. Goto, S. Heeb, S. Pommier, K.P. Rumbaugh, M. Cámara, and K.R. Hardie. 2012. A novel virulence strategy for *Pseudomonas aeruginosa* mediated by an autotransporter with arginine-specific aminopeptidase activity. *PLoS Pathog.* 8:e1002854.
- Luzio, J.P., S.R. Gray, and N. a Bright. 2010. Endosome-lysosome fusion. *Biochem. Soc. Trans.* 38:1413–6.
- Macia, E., M. Ehrlich, R. Massol, E. Boucrot, C. Brunner, and T. Kirchhausen. 2006. Dynasore, a cell-permeable inhibitor of dynamin. *Dev. Cell*. 10:839–50.

- Magupalli, V.G., K. Schwarz, K. Alpadi, S. Natarajan, G.M. Seigel, and F. Schmitz. 2008. Multiple RIBEYE-RIBEYE interactions create a dynamic scaffold for the formation of synaptic ribbons. *J. Neurosci.* 28:7954–67.
- Malatesta, M., C. Zancanaro, M. Costanzo, B. Cisterna, and C. Pellicciari. 2013. Simultaneous ultrastructural analysis of fluorochrome-photoconverted diaminobenzidine and gold immunolabelling in cultured cells. *Eur. J. Histochem.* 57:e26:168–171.
- Mallard, F., B.L. Tang, T. Galli, D. Tenza, A. Saint-Pol, X. Yue, C. Antony, W. Hong, B. Goud, and L. Johannes. 2002. Early/recycling endosomes-to-TGN transport involves two SNARE complexes and a Rab6 isoform. *J. Cell Biol.* 156:653–64.
- Mandell, J.W., E. Townes-Anderson, a J. Czernik, R. Cameron, P. Greengard, and P. De Camilli. 1990. Synapsins in the vertebrate retina: absence from ribbon synapses and heterogeneous distribution among conventional synapses. *Neuron.* 5:19–33.
- Marasco, P.D., P.R. Tsuruda, D.M. Bautista, D. Julius, and K.C. Catania. 2006. Neuroanatomical evidence for segregation of nerve fibers conveying light touch and pain sensation in Eimer's organ of the mole. *Proc. Natl. Acad. Sci. U. S. A.* 103:9339–44.
- Marrack, J. 1934. Nature of Antibodies. *Nature.* 133:292–93.
- Mathew, S.S., L. Pozzo-Miller, and J.J. Hablitz. 2008. Kainate modulates presynaptic GABA release from two vesicle pools. *J. Neurosci.* 28:725–31.
- Matsudaira, T., Y. Uchida, K. Tanabe, S. Kon, T. Watanabe, T. Taguchi, and H. Arai. 2013. SMAP2 regulates retrograde transport from recycling endosomes to the Golgi. *PLoS One.* 8:e69145.
- Matthews, G., and P. Fuchs. 2010. The diverse roles of ribbon synapses in sensory neurotransmission. *Nat. Rev. Neurosci.* 11:812–22.
- Maxfield, F.R., and T.E. McGraw. 2004. Endocytic recycling. *Nat. Rev. Mol. Cell Biol.* 5:121–32.
- Mayor, S., J.F. Presley, and F.R. Maxfield. 1993. Sorting of membrane components from endosomes and subsequent recycling to the cell surface occurs by a bulk flow process. *J. Cell Biol.* 121:1257–69.
- McBain, C., and R. Dingledine. 1992. Dual-component miniature excitatory synaptic currents in rat hippocampal CA3 pyramidal neurons. *J. Neurophysiol.* 68:16–27.
- McCluskey, A., J. a Daniel, G. Hadzic, N. Chau, E.L. Clayton, A. Mariana, A. Whiting, N.N. Gorgani, J. Lloyd, A. Quan, L. Moshkanbaryans, S. Krishnan, S. Perera, M. Chircop, L. von Kleist, A.B. McGeachie, M.T. Howes, R.G. Parton, M. Campbell, J. a Sakoff, X. Wang, J.-Y. Sun, M.J. Robertson, F.M. Deane, T.H. Nguyen, F. a Meunier, M. a Cousin,

## References

---

- and P.J. Robinson. 2013. Building a better dynasore: the dyngo compounds potently inhibit dynamin and endocytosis. *Traffic*. 14:1272–89.
- McKinney, R. a, M. Capogna, R. Dürr, B.H. Gähwiler, and S.M. Thompson. 1999. Miniature synaptic events maintain dendritic spines via AMPA receptor activation. *Nat. Neurosci.* 2:44–9.
- McPherson, P.S., E.P. Garcia, V.I. Slepnev, C. David, X. Zhang, D. Grabs, W.S. Sossin, R. Bauerfeind, Y. Nemoto, and P. De Camilli. 1996. A presynaptic inositol-5-phosphatase. *Nature*. 379:353–7.
- McPherson, P.S., K. Takei, S.L. Schmid, and P. De Camilli. 1994. p145, a major Grb2-binding protein in brain, is co-localized with dynamin in nerve terminals where it undergoes activity-dependent dephosphorylation. *J. Biol. Chem.* 269:30132–9.
- Mennerick, S., and G. Matthews. 1996. Ultrafast exocytosis elicited by calcium current in synaptic terminals of retinal bipolar neurons. *Neuron*. 17:1241–9.
- Meyer, J., a F. Mack, and a W. Gummer. 2001. Pronounced infracuticular endocytosis in mammalian outer hair cells. *Hear. Res.* 161:10–22.
- Meyers, J.R., R.B. MacDonald, A. Duggan, D. Lenzi, D.G. Standaert, J.T. Corwin, and D.P. Corey. 2003. Lighting up the senses: FM1-43 loading of sensory cells through nonselective ion channels. *J. Neurosci.* 23:4054–65.
- Miesenböck, G., D.A. De Angelis, and J.E. Rothman. 1998. Visualizing secretion and synaptic transmission with pH-sensitive green fluorescent proteins. *Nature*. 394:192–5.
- Miller, T.M., and J.E. Heuser. 1984. Endocytosis of synaptic vesicle membrane at the frog neuromuscular junction. *J. Cell Biol.* 98:685–98.
- Mills, I.G., a T. Jones, and M.J. Clague. 1999. Regulation of endosome fusion. *Mol. Membr. Biol.* 16:73–9.
- Milosevic, I., S. Giovedi, X. Lou, A. Raimondi, C. Collesi, H. Shen, S. Paradise, E. O’Toole, S. Ferguson, O. Cremona, and P. De Camilli. 2011. Recruitment of endophilin to clathrin-coated pit necks is required for efficient vesicle uncoating after fission. *Neuron*. 72:587–601.
- Mizoguchi, A., M. Arakawa, M. Masutani, A. Tamekane, H. Yamaguchi, N. Minami, Y. Takai, and C. Ide. 1992. Localization of smg p25A/rab3A p25, a small GTP-binding protein, at the active zone of the rat neuromuscular junction. *Biochem. Biophys. Res. Commun.* 186:1345–52.
- Mizoguchi, A., S. Kim, T. Ueda, A. Kikuchi, H. Yorifuji, N. Hirokawa, and Y. Takai. 1990. Localization and subcellular distribution of smg p25A, a ras p21-like GTP-binding protein, in rat brain. *J. Biol. Chem.* 265:11872–9.

- Mlcochova, P., A. Pelchen-Matthews, and M. Marsh. 2013. Organization and regulation of intracellular plasma membrane-connected HIV-1 assembly compartments in macrophages. *BMC Biol.* 11:89.
- Moneron, G., R. Medda, B. Hein, A. Giske, V. Westphal, and S.W. Hell. 2010. Fast STED microscopy with continuous wave fiber lasers. *Opt. Express.* 18:1302–9.
- Monier, S., D.J. Dietzen, W.R. Hastings, D.M. Lublin, and T. V Kurzchalia. 1996. Oligomerization of VIP21-caveolin in vitro is stabilized by long chain fatty acylation or cholesterol. *FEBS Lett.* 388:143–9.
- Morgan, J.R., X. Zhao, M. Womack, K. Prasad, G.J. Augustine, and E.M. Lafer. 1999. A role for the clathrin assembly domain of AP180 in synaptic vesicle endocytosis. *J. Neurosci.* 19:10201–12.
- Moser, T., and D. Beutner. 2000. Kinetics of exocytosis and endocytosis at the cochlear inner hair cell afferent synapse of the mouse. *Proc. Natl. Acad. Sci. U. S. A.* 97:883–8.
- Moser, T., A. Neef, and D. Khimich. 2006. Mechanisms underlying the temporal precision of sound coding at the inner hair cell ribbon synapse. *J. Physiol.* 576:55–62.
- Nachman-Clewner, M., R. St Jules, and E. Townes-Anderson. 1999. L-type calcium channels in the photoreceptor ribbon synapse: localization and role in plasticity. *J. Comp. Neurol.* 415:1–16.
- Nägerl, U.V., K.I. Willig, B. Hein, S.W. Hell, and T. Bonhoeffer. 2008. Live-cell imaging of dendritic spines by STED microscopy. *Proc. Natl. Acad. Sci. U. S. A.* 105:18982–7.
- Nakamura, N., C. Rabouille, R. Watson, T. Nilsson, N. Hui, P. Slusarewicz, T.E. Kreis, and G. Warren. 1995. Characterization of a cis-Golgi matrix protein, GM130. *J. Cell Biol.* 131:1715–26.
- Neef, J., S. Jung, A.B. Wong, K. Reuter, T. Pangrsic, R. Chakrabarti, S. Kügler, C. Lenz, R. Nouvian, R.M. Boumil, W.N. Frankel, C. Wichmann, and T. Moser. 2014. Modes and regulation of endocytic membrane retrieval in mouse auditory hair cells. *J. Neurosci.* 34:705–16.
- Neves, G., a Gomis, and L. Lagnado. 2001. Calcium influx selects the fast mode of endocytosis in the synaptic terminal of retinal bipolar cells. *Proc. Natl. Acad. Sci. U. S. A.* 98:15282–7.
- Neves, G., and L. Lagnado. 1999. The kinetics of exocytosis and endocytosis in the synaptic terminal of goldfish retinal bipolar cells. *J. Physiol.* 515 (Pt 1):181–202.
- Newton, a J., T. Kirchhausen, and V.N. Murthy. 2006. Inhibition of dynamin completely blocks compensatory synaptic vesicle endocytosis. *Proc. Natl. Acad. Sci. U. S. A.* 103:17955–60.

## References

---

- Nguyen, T.H., G. Maucort, R.K.P. Sullivan, M. Schenning, N. a. Lavidis, A. McCluskey, P.J. Robinson, and F. a. Meunier. 2012. Actin- and Dynamin-Dependent Maturation of Bulk Endocytosis Restores Neurotransmission following Synaptic Depletion. *PLoS One*. 7:e36913.
- Nishikawa, S., and F. Sasaki. 1996. Internalization of styryl dye FM1-43 in the hair cells of lateral line organs in *Xenopus* larvae. *J. Histochem. Cytochem.* 44:733–741.
- Nizak, C., S. Martin-Lluesma, S. Moutel, A. Roux, T.E. Kreis, B. Goud, and F. Perez. 2003. Recombinant antibodies against subcellular fractions used to track endogenous Golgi protein dynamics in vivo. *Traffic*. 4:739–53.
- Nouvian, R., D. Beutner, T.D. Parsons, and T. Moser. 2006. Structure and function of the hair cell ribbon synapse. *J. Membr. Biol.* 209:153–65.
- Nouvian, R., J. Neef, A. V Bulankina, E. Reisinger, T. Pangršič, T. Frank, S. Sikorra, N. Brose, T. Binz, and T. Moser. 2011. Exocytosis at the hair cell ribbon synapse apparently operates without neuronal SNARE proteins. *Nat. Neurosci.* 14:411–3.
- Oh, P., D.P. McIntosh, and J.E. Schnitzer. 1998. Dynamin at the neck of caveolae mediates their budding to form transport vesicles by GTP-driven fission from the plasma membrane of endothelium. *J. Cell Biol.* 141:101–14.
- Oparin, A.I. 1957. The origin of life on the earth. Academic Press, New York.
- Opazo, F., M. Levy, M. Byrom, C. Schäfer, C. Geisler, T.W. Groemer, A.D. Ellington, and S.O. Rizzoli. 2012. Aptamers as potential tools for super-resolution microscopy. *Nat. Methods*. 9:938–9.
- Opazo, F., A. Punge, J. Bückers, P. Hoopmann, L. Kastrup, S.W. Hell, and S.O. Rizzoli. 2010. Limited intermixing of synaptic vesicle components upon vesicle recycling. *Traffic*. 11:800–12.
- Paillart, C., J. Li, G. Matthews, and P. Sterling. 2003. Endocytosis and vesicle recycling at a ribbon synapse. *J. Neurosci.* 23:4092–9.
- Palade, G.E., and R.R. Bruns. 1968. Structural modulations of plasmalemmal vesicles. *J. Cell Biol.* 37:633–49.
- Pangršič, T., L. Lasarow, K. Reuter, H. Takago, M. Schwander, D. Riedel, T. Frank, L.M. Tarantino, J.S. Bailey, N. Strenzke, N. Brose, U. Müller, E. Reisinger, and T. Moser. 2010. Hearing requires otoferlin-dependent efficient replenishment of synaptic vesicles in hair cells. *Nat. Neurosci.* 13:869–76.
- Pangršič, T., E. Reisinger, and T. Moser. 2012. Otoferlin: a multi-C(2) domain protein essential for hearing. *Trends Neurosci.* 35:671–80.

- Park, R.J., H. Shen, L. Liu, X. Liu, S.M. Ferguson, and P. De Camilli. 2013. Dynamin triple knockout cells reveal off target effects of commonly used dynamin inhibitors. *J. Cell Sci.* 126:5305–12.
- Parsons, T.D., D. Lenzi, W. Almers, and W.M. Roberts. 1994. Calcium-triggered exocytosis and endocytosis in an isolated presynaptic cell: capacitance measurements in saccular hair cells. *Neuron.* 13:875–83.
- Parsons, T.D., and P. Sterling. 2003. Synaptic ribbon. Conveyor belt or safety belt? *Neuron.* 37:379–82.
- Parton, R.G., M. Hanzal-Bayer, and J.F. Hancock. 2006. Biogenesis of caveolae: a structural model for caveolin-induced domain formation. *J. Cell Sci.* 119:787–96.
- Parton, R.G., and K. Simons. 2007. The multiple faces of caveolae. *Nat. Rev. Mol. Cell Biol.* 8:185–94.
- Parton, R.G., M. Way, N. Zorzi, and E. Stang. 1997. Caveolin-3 associates with developing T-tubules during muscle differentiation. *J. Cell Biol.* 136:137–54.
- Payne, C.K., S. a Jones, C. Chen, and X. Zhuang. 2007. Internalization and trafficking of cell surface proteoglycans and proteoglycan-binding ligands. *Traffic.* 8:389–401.
- Pearse, B.M. 1975. Coated vesicles from pig brain: purification and biochemical characterization. *J. Mol. Biol.* 97:93–8.
- Pertsinidis, A., K. Mukherjee, M. Sharma, Z.P. Pang, S.R. Park, Y. Zhang, A.T. Brunger, T.C. Südhof, and S. Chu. 2013. Ultrahigh-resolution imaging reveals formation of neuronal SNARE/Munc18 complexes in situ. *Proc. Natl. Acad. Sci. U. S. A.* 110:E2812–20.
- Pfeffer, S.R. 2001. Rab GTPases: specifying and deciphering organelle identity and function. *Trends Cell Biol.* 11:487–91.
- Pieribone, V. a, O. Shupliakov, L. Brodin, S. Hilfiker-Rothenfluh, a J. Czernik, and P. Greengard. 1995. Distinct pools of synaptic vesicles in neurotransmitter release. *Nature.* 375:493–7.
- Piper, R.C., and D.J. Katzmann. 2007. Biogenesis and function of multivesicular bodies. *Annu. Rev. Cell Dev. Biol.* 23:519–47.
- Poskanzer, K.E., K.W. Marek, S.T. Sweeney, and G.W. Davis. 2003. Synaptotagmin I is necessary for compensatory synaptic vesicle endocytosis in vivo. *Nature.* 426:559–63.
- Poteryaev, D., S. Datta, K. Ackema, M. Zerial, and A. Spang. 2010. Identification of the switch in early-to-late endosome transition. *Cell.* 141:497–508.

## References

---

- Presley, J.F., S. Mayor, K.W. Dunn, L.S. Johnson, T.E. McGraw, and F.R. Maxfield. 1993. The End2 mutation in CHO cells slows the exit of transferrin receptors from the recycling compartment but bulk membrane recycling is unaffected. *J. Cell Biol.* 122:1231–41.
- Punge, A. 2009. Polymer embedding for ultrathin slicing and optical nanoscopy of thick fluorescent samples. (Doctoral dissertation). Georg-August-Universität Göttingen, Germany.
- Punge, A., S.O. Rizzoli, R. Jahn, J.D. Wildanger, L. Meyer, A. Schönle, L. Kastrup, and S.W. Hell. 2008. 3D reconstruction of high-resolution STED microscope images. *Microsc. Res. Tech.* 71:644–50.
- Purves, D., G.J. Augustine, D. Fitzpatrick, W.C. Hall, A.-S. LaMantia, J.O. McNamara, and S.M. Williams eds. . 2004. Neuroscience. Third edit. Sinauer Associates, Inc., Sunderland, MA, USA.
- Ramakrishnan, N. a, M.J. Drescher, and D.G. Drescher. 2009. Direct interaction of otoferlin with syntaxin 1A, SNAP-25, and the L-type voltage-gated calcium channel Cav1.3. *J. Biol. Chem.* 284:1364–72.
- Ramirez, D.M.O., M. Khvotchev, B. Trauterman, and E.T. Kavalali. 2012. Vti1a identifies a vesicle pool that preferentially recycles at rest and maintains spontaneous neurotransmission. *Neuron.* 73:121–34.
- Razani, B., T.P. Combs, X.B. Wang, P.G. Frank, D.S. Park, R.G. Russell, M. Li, B. Tang, L. a Jelicks, P.E. Scherer, and M.P. Lisanti. 2002. Caveolin-1-deficient mice are lean, resistant to diet-induced obesity, and show hypertriglyceridemia with adipocyte abnormalities. *J. Biol. Chem.* 277:8635–47.
- Rea, R., J. Li, A. Dharia, and E. Levitan. 2004. Streamlined synaptic vesicle cycle in cone photoreceptor terminals. *Neuron.* 41:755–66.
- Reisinger, E., C. Bresee, J. Neef, R. Nair, K. Reuter, A. Bulankina, R. Nouvian, M. Koch, J. Bückers, L. Kastrup, I. Roux, C. Petit, S.W. Hell, N. Brose, J.-S. Rhee, S. Kügler, J. V Brigande, and T. Moser. 2011. Probing the functional equivalence of otoferlin and synaptotagmin 1 in exocytosis. *J. Neurosci.* 31:4886–95.
- Richards, D. a, C. Guatimosim, and W.J. Betz. 2000. Two endocytic recycling routes selectively fill two vesicle pools in frog motor nerve terminals. *Neuron.* 27:551–9.
- Richardson, G.P., A. Forge, C.J. Kros, J. Fleming, S.D. Brown, and K.P. Steel. 1997. Myosin VIIA is required for aminoglycoside accumulation in cochlear hair cells. *J. Neurosci.* 17:9506–19.
- Rickman, C., C.N. Medine, A.R. Dun, D.J. Moulton, O. Mandula, N.D. Halemani, S.O. Rizzoli, L.H. Chamberlain, and R.R. Duncan. 2010. t-SNARE protein conformations patterned by the lipid microenvironment. *J. Biol. Chem.* 285:13535–41.



- Rieder, S.E., L.M. Banta, K. Köhrer, J.M. McCaffery, and S.D. Emr. 1996. Multilamellar endosome-like compartment accumulates in the yeast vps28 vacuolar protein sorting mutant. *Mol. Biol. Cell.* 7:985–99.
- Rink, J., E. Ghigo, Y. Kalaidzidis, and M. Zerial. 2005. Rab conversion as a mechanism of progression from early to late endosomes. *Cell.* 122:735–49.
- Rizzoli, S.O. 2014. Synaptic vesicle recycling: steps and principles. *EMBO J.* 33:788–822.
- Rizzoli, S.O., and W.J. Betz. 2005. Synaptic vesicle pools. *Nat. Rev. Neurosci.* 6:57–69.
- Rizzoli, S.O., and R. Jahn. 2007. Kiss-and-run, collapse and “readily retrievable” vesicles. *Traffic.* 8:1137–44.
- De Robertis, E., and C.M. Franchi. 1956. Electron microscope observations on synaptic vesicles in synapses of the retinal rods and cones. *J. Biophys. Biochem. Cytol.* 2:307–18.
- Robertson, J.D. 1960. The molecular structure and contact relationships of cell membranes. *Prog. Biophys. Mol. Biol.* 10:343–418.
- Roos, J., and R.B. Kelly. 1999. The endocytic machinery in nerve terminals surrounds sites of exocytosis. *Curr. Biol.* 9:1411–4.
- Roux, I., S. Hosie, S.L. Johnson, A. Bahloul, N. Cayet, S. Nouaille, C.J. Kros, C. Petit, and S. Safieddine. 2009. Myosin VI is required for the proper maturation and function of inner hair cell ribbon synapses. *Hum. Mol. Genet.* 18:4615–28.
- Roux, I., S. Safieddine, R. Nouvian, M. Grati, M.-C. Simmler, A. Bahloul, I. Perfettini, M. Le Gall, P. Rostaing, G. Hamard, A. Triller, P. Avan, T. Moser, and C. Petit. 2006. Otoferlin, defective in a human deafness form, is essential for exocytosis at the auditory ribbon synapse. *Cell.* 127:277–89.
- Rubel, E.W. 1984. Ontogeny of auditory system function. *Annu. Rev. Physiol.* 46:213–29.
- Ruel, J., S. Emery, R. Nouvian, T. Bersot, B. Amilhon, J.M. Van Rybroek, G. Rebillard, M. Lenoir, M. Eybalin, B. Delprat, T.A. Sivakumaran, B. Giros, S. El Mestikawy, T. Moser, R.J.H. Smith, M.M. Lesperance, and J.-L. Puel. 2008. Impairment of SLC17A8 encoding vesicular glutamate transporter-3, VGLUT3, underlies nonsyndromic deafness DFNA25 and inner hair cell dysfunction in null mice. *Am. J. Hum. Genet.* 83:278–92.
- Sachse, M., S. Urbé, V. Oorschot, G.J. Strous, and J. Klumperman. 2002. Bilayered clathrin coats on endosomal vacuoles are involved in protein sorting toward lysosomes. *Mol. Biol. Cell.* 13:1313–28.
- Safieddine, S., and R.J. Wenthold. 1999. SNARE complex at the ribbon synapses of cochlear hair cells: analysis of synaptic vesicle- and synaptic membrane-associated proteins. *Eur. J. Neurosci.* 11:803–12.

## References

---

- Saka, S., and S.O. Rizzoli. 2012. Super-resolution imaging prompts re-thinking of cell biology mechanisms. *Bioessays*. 1–10.
- Sanchez, J., and J. Holmgren. 2011. Cholera toxin - a foe & a friend. *Indian J. Med. Res.* 133:153–63.
- Sandell, J.H., and R.H. Masland. 1988. Photoconversion of some fluorescent markers to a diaminobenzidine product. *J. Histochem. Cytochem.* 36:555–559.
- Sankaranarayanan, S., D. De Angelis, J.E. Rothman, and T. a Ryan. 2000. The use of pHluorins for optical measurements of presynaptic activity. *Biophys. J.* 79:2199–208.
- Sankaranarayanan, S., and T. a Ryan. 2000. Real-time measurements of vesicle-SNARE recycling in synapses of the central nervous system. *Nat. Cell Biol.* 2:197–204.
- Sara, Y., T. Virmani, F. Deák, X. Liu, and E.T. Kavalali. 2005. An isolated pool of vesicles recycles at rest and drives spontaneous neurotransmission. *Neuron*. 45:563–73.
- Schaeffer, S.F., and E. Raviola. 1978. Membrane recycling in the cone cell endings of the turtle retina. *J. Cell Biol.* 79:802–25.
- Schekman, R. 1985. Protein localization and membrane traffic in yeast. *Annu. Rev. Cell Biol.* 1:115–43.
- Schikorski, T., and C.F. Stevens. 2001. Morphological correlates of functionally defined synaptic vesicle populations. *Nat. Neurosci.* 4:391–5.
- Schmitz, F., A. Königstorfer, and T.C. Südhof. 2000. RIBEYE, a Component of Synaptic Ribbons. *Neuron*. 28:857–872.
- Schug, N., C. Braig, U. Zimmermann, J. Engel, H. Winter, P. Ruth, N. Blin, M. Pfister, H. Kalbacher, and M. Knipper. 2006. Differential expression of otoferlin in brain, vestibular system, immature and mature cochlea of the rat. *Eur. J. Neurosci.* 24:3372–80.
- Seal, R.P., O. Akil, E. Yi, C.M. Weber, L. Grant, J. Yoo, A. Clause, K. Kandler, J.L. Noebels, E. Glowatzki, L.R. Lustig, and R.H. Edwards. 2008. Sensorineural deafness and seizures in mice lacking vesicular glutamate transporter 3. *Neuron*. 57:263–75.
- Sejnowski, T.J., and M.L. Yodlowski. 1982. A freeze-fracture study of the skate electroreceptor. *J. Neurocytol.* 11:897–912.
- Shupliakov, O., P. Löw, D. Grabs, H. Gad, H. Chen, C. David, K. Takei, P. De Camilli, and L. Brodin. 1997. Synaptic vesicle endocytosis impaired by disruption of dynamin-SH3 domain interactions. *Science*. 276:259–63.

- Sidi, S., E. Busch-Nentwich, R. Friedrich, U. Schoenberger, and T. Nicolson. 2004. *gemin1* encodes a zebrafish L-type calcium channel that localizes at sensory hair cell ribbon synapses. *J. Neurosci.* 24:4213–23.
- Sieber, J.J., K.I. Willig, R. Heintzmann, S.W. Hell, and T. Lang. 2006. The SNARE motif is essential for the formation of syntaxin clusters in the plasma membrane. *Biophys. J.* 90:2843–51.
- Sieber, J.J., K.I. Willig, C. Kutzner, C. Gerding-Reimers, B. Harke, G. Donnert, B. Rammner, C. Eggeling, S.W. Hell, H. Grubmüller, and T. Lang. 2007. Anatomy and dynamics of a supramolecular membrane protein cluster. *Science.* 317:1072–6.
- Siegel, J.H., and W.E. Brownell. 1986. Synaptic and Golgi membrane recycling in cochlear hair cells. *J. Neurocytol.* 15:311–328.
- Singer, S.J. 1959. Preparation of an electron-dense antibody conjugate. *Nature.* 183:1523–4.
- Sipe, D.M., and R.F. Murphy. 1987. High-resolution kinetics of transferrin acidification in BALB/c 3T3 cells: exposure to pH 6 followed by temperature-sensitive alkalization during recycling. *Proc. Natl. Acad. Sci. U. S. A.* 84:7119–23.
- Sjostrand, F.S. 1958. Ultrastructure of retinal rod synapses of the guinea pig eye as revealed by three-dimensional reconstructions from serial sections. *J. Ultrastruct. Res.* 2:122–70.
- Sjöstrand, F.S. 1953. PROGRAM. Proceedings of the Electron Microscope Society of America. The Ultrastructure of the retinal rod synapses of the guinea pig eye. *J. Appl. Phys.* 24:1422.
- Van der Sluijs, P., M. Hull, P. Webster, P. Mâle, B. Goud, and I. Mellman. 1992. The small GTP-binding protein rab4 controls an early sorting event on the endocytic pathway. *Cell.* 70:729–40.
- Smith, C.A., and F.S. Sjöstrand. 1961. A synaptic structure in the hair cells of the guinea pig cochlea. *J. Ultrastruct. Res.* 5:184–192.
- Smith, S.M., R. Renden, and H. von Gersdorff. 2008. Synaptic vesicle endocytosis: fast and slow modes of membrane retrieval. *Trends Neurosci.* 31:559–68.
- Sofer, a, and a H. Futerman. 1996. Rate of retrograde transport of cholera toxin from the plasma membrane to the Golgi apparatus and endoplasmic reticulum decreases during neuronal development. *J. Neurochem.* 67:2134–40.
- Sousa, V.L., S. Bellani, M. Giannandrea, M. Yousuf, F. Valtorta, J. Meldolesi, and E. Chieregatti. 2009. {alpha}-synuclein and its A30P mutant affect actin cytoskeletal structure and dynamics. *Mol. Biol. Cell.* 20:3725–39.

## References

---

- Spassova, M. a., M. Avissar, A.C. Furman, M. a. Crumling, J.C. Saunders, and T.D. Parsons. 2004. Evidence That Rapid Vesicle Replenishment of the Synaptic Ribbon Mediates Recovery from Short-Term Adaptation at the Hair Cell Afferent Synapse. *J. Assoc. Res. Otolaryngol.* 5:376–390.
- Spicer, S.S., C. Qu, N. Smythe, and B.A. Schulte. 2007. Mitochondria-activated cisternae generate the cell specific vesicles in auditory hair cells. *Hear. Res.* 233:40–5.
- Spicer, S.S., G.N. Thomopoulos, and B.A. Schulte. 1999. Novel membranous structures in apical and basal compartments of inner hair cells. *J. Comp. Neurol.* 409:424–37.
- Spiegel, S., S. Kassis, M. Wilchek, and P.H. Fishman. 1984. Direct visualization of redistribution and capping of fluorescent gangliosides on lymphocytes. *J. Cell Biol.* 99:1575–81.
- Strenzke, N., S. Chanda, C. Kopp-Scheinflug, D. Khimich, K. Reim, A. V Bulankina, A. Neef, F. Wolf, N. Brose, M. a Xu-Friedman, and T. Moser. 2009. Complexin-I is required for high-fidelity transmission at the endbulb of Held auditory synapse. *J. Neurosci.* 29:7991–8004.
- Strom, T.M., G. Nyakatura, E. Apfelstedt-Sylla, H. Hellebrand, B. Lorenz, B.H. Weber, K. Wutz, N. Gutwillinger, K. Rüther, B. Drescher, C. Sauer, E. Zrenner, T. Meitinger, a Rosenthal, and a Meindl. 1998. An L-type calcium-channel gene mutated in incomplete X-linked congenital stationary night blindness. *Nat. Genet.* 19:260–3.
- Struck, D.K., and R.E. Pagano. 1980. Insertion of fluorescent phospholipids into the plasma membrane of a mammalian cell. *J. Biol. Chem.* 255:5404–10.
- Südhof, T.C. 2004. The synaptic vesicle cycle. *Annu. Rev. Neurosci.* 27:509–47.
- Südhof, T.C. 2013. A molecular machine for neurotransmitter release: synaptotagmin and beyond. *Nat. Med.* 19:1227–31.
- Südhof, T.C., and J. Rizo. 2011. Synaptic vesicle exocytosis. *Cold Spring Harb. Perspect. Biol.* 3:1–14.
- Sun, J.-Y., X.-S. Wu, and L.-G. Wu. 2002. Single and multiple vesicle fusion induce different rates of endocytosis at a central synapse. *Nature.* 417:555–9.
- Sutton, M. a, A.M. Taylor, H.T. Ito, A. Pham, and E.M. Schuman. 2007. Postsynaptic decoding of neural activity: eEF2 as a biochemical sensor coupling miniature synaptic transmission to local protein synthesis. *Neuron.* 55:648–61.
- Takamori, S., M. Holt, K. Stenius, E. a Lemke, M. Grønborg, D. Riedel, H. Urlaub, S. Schenck, B. Brügger, P. Ringler, S. a Müller, B. Rammner, F. Gräter, J.S. Hub, B.L. De Groot, G. Mieskes, Y. Moriyama, J. Klingauf, H. Grubmüller, J. Heuser, F. Wieland, and R. Jahn. 2006. Molecular anatomy of a trafficking organelle. *Cell.* 127:831–46.

- Takei, K., P.S. McPherson, S.L. Schmid, and P. De Camilli. 1995. Tubular membrane invaginations coated by dynamin rings are induced by GTP-gamma S in nerve terminals. *Nature*. 374:186–90.
- Tarelli, F.T., M. Bossi, R. Fesce, P. Greengard, and F. Valtorta. 1992. Synapsin I partially dissociates from synaptic vesicles during exocytosis induced by electrical stimulation. *Neuron*. 9:1143–1153.
- Teng, H., M.Y. Lin, and R.S. Wilkinson. 2007. Macroendocytosis and endosome processing in snake motor boutons. *J. Physiol*. 582:243–62.
- Teng, H., and R.S. Wilkinson. 2000. Clathrin-mediated endocytosis near active zones in snake motor boutons. *J. Neurosci*. 20:7986–93.
- Torgersen, M.L., G. Skretting, B. van Deurs, and K. Sandvig. 2001. Internalization of cholera toxin by different endocytic mechanisms. *J. Cell Sci*. 114:3737–47.
- Traer, C.J., A.C. Rutherford, K.J. Palmer, T. Wassmer, J. Oakley, N. Attar, J.G. Carlton, J. Kremerskothen, D.J. Stephens, and P.J. Cullen. 2007. SNX4 coordinates endosomal sorting of TfnR with dynein-mediated transport into the endocytic recycling compartment. *Nat. Cell Biol*. 9:1370–80.
- Tran, D., J.L. Carpentier, F. Sawano, P. Gorden, and L. Orci. 1987. Ligands internalized through coated or noncoated invaginations follow a common intracellular pathway. *Proc. Natl. Acad. Sci. U. S. A.* 84:7957–61.
- Trischler, M., W. Stoorvogel, and O. Ullrich. 1999. Biochemical analysis of distinct Rab5- and Rab11-positive endosomes along the transferrin pathway. *J. Cell Sci*. 112 (Pt 2):4773–83.
- Tuo, S., K. Nakashima, and J.R. Pringle. 2013. Role of endocytosis in localization and maintenance of the spatial markers for bud-site selection in yeast. *PLoS One*. 8:e72123.
- Uehara, T., T. Dinh, and T.G. Bernhardt. 2009. LytM-domain factors are required for daughter cell separation and rapid ampicillin-induced lysis in *Escherichia coli*. *J. Bacteriol*. 191:5094–107.
- Ungewickell, E., and D. Branton. 1981. Assembly units of clathrin coats. *Nature*. 289:420–2.
- Uthaiyah, R.C., and a J. Hudspeth. 2010. Molecular anatomy of the hair cell's ribbon synapse. *J. Neurosci*. 30:12387–99.
- Varga, R., P.M. Kelley, B.J. Keats, a Starr, S.M. Leal, E. Cohn, and W.J. Kimberling. 2003. Non-syndromic recessive auditory neuropathy is the result of mutations in the otoferlin (OTOF) gene. *J. Med. Genet*. 40:45–50.

## References

---

- Verhage, M., A.S. Maia, J.J. Plomp, A.B. Brussaard, J.H. Heeroma, H. Vermeer, R.F. Toonen, R.E. Hammer, T.K. van den Berg, M. Missler, H.J. Geuze, and T.C. Südhof. 2000. Synaptic assembly of the brain in the absence of neurotransmitter secretion. *Science*. 287:864–9.
- Vida, T. a, and S.D. Emr. 1995. A new vital stain for visualizing vacuolar membrane dynamics and endocytosis in yeast. *J. Cell Biol.* 128:779–92.
- Vonderheit, A., and A. Helenius. 2005. Rab7 associates with early endosomes to mediate sorting and transport of Semliki forest virus to late endosomes. *PLoS Biol.* 3:e233.
- Wahl, S., R. Katiyar, and F. Schmitz. 2013. A local, periaxonal zone endocytic machinery at photoreceptor synapses in close vicinity to synaptic ribbons. *J. Neurosci.* 33:10278–300.
- Wangemann, P. 2006. Supporting sensory transduction: cochlear fluid homeostasis and the endocochlear potential. *J. Physiol.* 576:11–21.
- Watanabe, S., B.R. Rost, M. Camacho-Pérez, M.W. Davis, B. Söhl-Kielczynski, C. Rosenmund, and E.M. Jorgensen. 2013. Ultrafast endocytosis at mouse hippocampal synapses. *Nature*.
- Wegner, A.M., C. a Nebhan, L. Hu, D. Majumdar, K.M. Meier, A.M. Weaver, and D.J. Webb. 2008. N-wasp and the arp2/3 complex are critical regulators of actin in the development of dendritic spines and synapses. *J. Biol. Chem.* 283:15912–20.
- Wienisch, M., and J. Klingauf. 2006. Vesicular proteins exocytosed and subsequently retrieved by compensatory endocytosis are nonidentical. *Nat. Neurosci.* 9:1019–27.
- Wilhelm, B.G., T.W. Groemer, and S.O. Rizzoli. 2010. The same synaptic vesicles drive active and spontaneous release. *Nat. Neurosci.* 13:1454–6.
- Willig, K.I., S.O. Rizzoli, V. Westphal, R. Jahn, and S.W. Hell. 2006. STED microscopy reveals that synaptotagmin remains clustered after synaptic vesicle exocytosis. *Nature*. 440:935–9.
- Winkler, F.K., and K.K. Stanley. 1983. Clathrin heavy chain, light chain interactions. *EMBO J.* 2:1393–400.
- Wu, L.-G., T. a Ryan, and L. Lagnado. 2007. Modes of vesicle retrieval at ribbon synapses, calyx-type synapses, and small central synapses. *J. Neurosci.* 27:11793–802.
- Wu, W., and L.-G. Wu. 2007. Rapid bulk endocytosis and its kinetics of fission pore closure at a central synapse. *Proc. Natl. Acad. Sci. U. S. A.* 104:10234–9.
- Yamada, E. 1955. The fine structure of the gall bladder epithelium of the mouse. *J. Biophys. Biochem. Cytol.* 1:445–58.

- Yamashiro, D.J., B. Tycko, S.R. Fluss, and F.R. Maxfield. 1984. Segregation of transferrin to a mildly acidic (pH 6.5) para-Golgi compartment in the recycling pathway. *Cell*. 37:789–800.
- Yoshida, Y., M. Kinuta, T. Abe, S. Liang, K. Araki, O. Cremona, G. Di Paolo, Y. Moriyama, T. Yasuda, P. De Camilli, and K. Takei. 2004. The stimulatory action of amphiphysin on dynamin function is dependent on lipid bilayer curvature. *EMBO J*. 23:3483–91.
- Yu, J., S. Bergaya, T. Murata, I.F. Alp, M.P. Bauer, M.I. Lin, M. Drab, T. V Kurzchalia, R. V Stan, and W.C. Sessa. 2006. Direct evidence for the role of caveolin-1 and caveolae in mechanotransduction and remodeling of blood vessels. *J. Clin. Invest*. 116:1284–91.
- Yu, W., S. Herbert, P.L. Graumann, and F. Götz. 2010. Contribution of SMC (structural maintenance of chromosomes) and SpoIIIE to chromosome segregation in *Staphylococci*. *J. Bacteriol*. 192:4067–73.
- Zak, M., M. Pfister, and N. Blin. 2011. The otoferlin interactome in neurosensory hair cells: significance for synaptic vesicle release and trans-Golgi network (Review). *Int. J. Mol. Med*. 28:311–4.
- Zanazzi, G., and G. Matthews. 2009. The molecular architecture of ribbon presynaptic terminals. *Mol. Neurobiol*. 39:130–48.
- Zenisek, D., V. Davila, L. Wan, and W. Almers. 2003. Imaging calcium entry sites and ribbon structures in two presynaptic cells. *J. Neurosci*. 23:2538–48.
- Zhang, B., Y.H. Koh, R.B. Beckstead, V. Budnik, B. Ganetzky, and H.J. Bellen. 1998. Synaptic vesicle size and number are regulated by a clathrin adaptor protein required for endocytosis. *Neuron*. 21:1465–75.
- Zhang, J.Z., B. a Davletov, T.C. Südhof, and R.G. Anderson. 1994. Synaptotagmin I is a high affinity receptor for clathrin AP-2: implications for membrane recycling. *Cell*. 78:751–60.





# APPENDIX

---

## **MatLab routine for the generation of average mCLING intensity pictures from several ribbon-centered regions of interest (See Methods section 2.2.7.1, analysis type 4).**

The following MatLab package is based on 11 macros, presented here in the order they are required during the analysis. The start of every macro is marked with the symbols **%%** in bold.

### **%% Program Start**

```
function vesan

global movi rr xx yy filename chol b2 Movi3 pixel_size image_matrix
positioner pixel_size limits
global list mapname b rows cols A q s ijj jjj r1 firstred olds inner_radius
outer_radius matrix backmatrix old_movi
global alignsx alignsy rect fused not_fused sh hex hey rrl imagenr

% this set of macros allows the user to determine the positions of
% structures of interest such as synaptic ribbons, and then to average the
% areas of the cells that surround these structures.
% The image is shown in full color: blue for the ribbons (first frame
read), green
% for the second image read, red for the third image read. The user selects
a
% region of interest of any shape desired, around ONE ribbon,
% by using the left click (click and drag). The region of interest
% is drawn on the image in yellow.
% A new figure appears, showing:
% top left: the selected area in the ribbon channel
% top middle: the same area, in the green immunostaining channel
% top right: the same area, in the red immunostaining channel
% bottom left: the position of the ribbon selected
% The user can check and/or change the selection of the ribbon by using the
scroll bar at the bottom.
% Upon satisfactory selection, the user presses the "calculate" button.
% A square region, of 201 pixel width, is then selected for the region of
% interest, and its values in all three channels (ribbon, green
% immunostaining and red immunostaining) is saved in a .txt file
terminating
% with _spots
% One such file is saved for each ribbon analyzed.
% The next button moves the user to the next image, until all of the images
% are analyzed.
% The analysis is then repeated for all sub-folders containing such images.
% When the analysis is finished, the path to the folder containing all of
% the sub-folders that have been analyzed is written in the
```

## Appendix

---

```
% address_spots_1_by_both.m file
% This macro can be allowed to operate offline, overnight. It will produce
% averaged images for all channels: ribbon, green and red, and will save
% them in individual .txt and .tif files, in each sub-folder.
% The files contain the termination "_by_both", to indicate that both the
% information in the green and red channels has been taken into account.

cd 'C:\data_2012\data\New Folder';% the address of the folder to be worked
on

q=1; s=3;

limits=[8 3 5];

positioner=0;

imagenr=1;

[stat, mess]=fileattrib('*_ch00.tif');% looks for the files to be analyzed;
assumes that the ribbon images all end with a "_ch00.tif" termination
% The "green" immunostaining images all end with a "_ch00.tif" termination.
% The "red" immunostaining images (mCLING in our case) all end with a
"_ch01.tif" termination.
% Other terminations need to be chosen, according to the names of the files
that should be analyzed

dir *.tif;
pixel_size=20.20;

rr=mess(imagenr*2).Name
r4=mess(imagenr*2-1).Name

    r1=strcat(rr(1:numel(rr)-5), '0.tif');

    r2=strcat(rr(1:numel(rr)-5), '1.tif');

    filename=strcat(r4(1:numel(r4)-4));
    rr1=filename;
    filename=strcat(r4(1:numel(r4)-4), '.txt');

movi=[];

movi(:,:,1)=imread(r4);
movi(:,:,2)=imread(r2);
movi(:,:,3)=imread(r1);

old_movi=movi;

over=[];
over(:,:,2)=movi(:,:,2)*1/max(max(movi(:,:,2)));
over(:,:,1)=movi(:,:,3)*1/max(max(movi(:,:,3)));
over(:,:,3)=movi(:,:,1)*1/max(max(movi(:,:,1)));

sizz=size(movi);

STED=image(over, 'tag', 'him', 'cdatamapping', 'scaled');    colormap(summer);
```

```

axis square;

dd=icontrol('string','Step',...
    'style','pushbutton','callback','step',...
    'position',[100 0 50 30],'tooltipstring','one by one');
ee=icontrol('string','Stepback',...
    'style','pushbutton','callback','stepback',...
    'position',[150 0 50 30],'tooltipstring','one by one back');

m=icontrol('style','pushbutton','callback','sroi_next',...
    'position',[400 0 70 30],'string','Next');

chol=[];
inner_radius=10;
outer_radius=30;
image_matrix=[];
zz=[];
iii=0;jjj=1;
ijj=1;
backmatrix=[];
alignsx=[]; alignsy=[];
xx=[]; yy=[]; zz=[];
hex=[]; hey=[];

fused=[];
not_fused=[];

set(gcf,'windowbuttondownfcn','sroi_00y');
%sroi_align;

%% Manual selection
function sroi_00y;

global movi rr xx yy filename chol b2 Movi3 pixel_size image_matrix
global list mapname b rows cols A q s ijj jjj r1
global alignsx alignsy rect fused not_fused hey hex counter xses yyes

hfig=gcf;
button=get(hfig,'selectiontype');
if (strcmp(button,'extend'))

    l=get(gca,'currentpoint')

    hex(ijj)=round(l(1));
    hey(ijj)=round(l(3));

    xes=[hex(ijj)-50 hex(ijj)+50 hex(ijj)+50 hex(ijj)-50 hex(ijj)-50];
    yses=[hey(ijj)-50 hey(ijj)-50 hey(ijj)+50 hey(ijj)+50 hey(ijj)-50];

    line(xes,yses,'color','g');

    %figure;                imagesc(movi(hey(ijj)-50:hey(ijj)+50,hex(ijj)-
50:hex(ijj)+50,ijj));
    step;

```

```
elseif (strcmp(button, 'alt'))

l=get(gca, 'currentpoint')

alignsx(ijj)=round(l(1));
alignsy(ijj)=round(l(3));

line(alignsx, alignsy, 'linestyle', 'none', 'markeredgecolor', 'y', 'marker', 'o',
'markersize', 5, 'markerfacecolor', 'c');

elseif (strcmp(button, 'normal'))

counter=1;
xxes=[];
yyes=[];
set(gcf, 'windowbuttonmotionfcn', 'sroi_motion');
set(gcf, 'windowbuttonupfcn', 'sroi_2');

%
end;
%% Selection results (1)
function sroi_2

global counter xxes yyes ijv movi
global rr hex hey positioner alignsx alignsy pixel_size matrix filename
switcher pos1 small_movi

set(gcf, 'windowbuttonmotionfcn', 'sroi_3');
set(gcf, 'windowbuttonupfcn', 'sroi_3');

line(yyes, xxes, 'color', 'y');

pols=roipoly(movi(:, :, ijv), yyes, xxes);

ccc=find(pols==1);
[x y]=ind2sub(size(pols), ccc);

pos1(1)=min(x); pos1(2)=max(x); pos1(3)=min(y); pos1(4)=max(y);

small_movi=[];
siz=size(movi)
for i=1:siz(3)
i
movib=movi(:, :, i);
ccc=find(pols==0); movib(ccc)=0;
small_movi(:, :, i)=movib(pos1(1):pos1(2), pos1(3):pos1(4));
end;
```

```

    sroi_choose_region_autocorr_only;
%% Selection results (2): closing selection
function sroi_3

global movi rows cols A d c xx yy iii i bbb q s ijj

%%Moving selection
function sroi_motion

global counter xxes yyes switcher

l=get(gca, 'currentpoint');
    x=round(l(3));
    y=round(l(1));
    xxes(counter)=x; yyes(counter)=y;

if counter>1
    tx=[xxes(counter-1),xxes(counter)];
    ty=[yyes(counter-1),yyes(counter)];

    if switcher==1
        line('Xdata',ty, 'Ydata',tx, 'color', 'b');
    else

        line('Xdata',ty, 'Ydata',tx, 'color', 'r');
    end;

end;

    counter=counter+1;

%% Stepping through images
function step

global list mapname b movi rows cols A i xx yy zz iii bbb q s ijj jjj r
firstred olds inner_radius outer_radius matrix
global alignsx alignsy hex hey

% ijj is the frame number

ijj=ijj+1

if ijj<s+1
    if ijj==1
        colormap(summer(250));
    elseif ijj==2
        colormap(summer(250));
    elseif ijj==3
        colormap(hot(250));
    end;
    himg=image(movi(:, :, ijj)); axis square;

else ijj=q;

```

```

        if ijj==1
            colormap(summer(250));
        elseif ijj==2
            colormap(summer(250));
        elseif ijj==3
            colormap(hot(250));
        end;

    himg=image(movi(:,:,ijj)); axis square;

end;
%
% switch ijj;
%     case 1
%         textul=strcat('pHlourin');
%         text(15,35,textul,'FontSize',10,'color','g','BackgroundColor',[0.7
0.7 0.7]);
%     case 2
%         textul=strcat('Cy3');
%         text(10,35,textul,'FontSize',10,'color','r','BackgroundColor',[0.7
0.7 0.7]);
%     case 3
%         textul=strcat('647nC');
%         text(10,35,textul,'FontSize',10,'color','b','BackgroundColor',[0.7
0.7 0.7]);
%     case 4
%         textul=strcat('STED');
%         text(10,35,textul,'FontSize',10,'color','r','BackgroundColor',[0.7
0.7 0.7]);
%
% end
try
if numel(hex>1)

    xes=[hex(ijj)-50 hex(ijj)+50 hex(ijj)+50 hex(ijj)-50 hex(ijj)-50];
    yes=[hey(ijj)-50 hey(ijj)-50 hey(ijj)+50 hey(ijj)+50 hey(ijj)-50];

    line(xes,yes,'color','g');
end;
catch
end
%% Stepping back through images
function stepback

global list mapname b movi rows cols A i xx yy zz iii bbb q s ijj jjj r
firstred olds inner_radius outer_radius matrix
global alignsx alignsy hex hey
ijj=ijj-1
if ijj>q-1
    if ijj==1
        colormap(summer(250));
    elseif ijj==2
        colormap(summer(250));
    elseif ijj==3
        colormap(hot(250));
    end;
    himg=image(movi(:,:,ijj)); axis square;

    % set(himg,'cdata',movi(:,:,ijj));
else ijj=s;

```

```

        if ijj==1
            colormap(summer(250));
        elseif ijj==2
            colormap(summer(250));
        elseif ijj==3
            colormap(hot(250));
        end;
        himg=image(movi(:, :, ijj)); axis square;
    % set(himg, 'cdata', movi(:, :, ijj));
end;

%
%   switch ijj
%   case 1
%       textul=strcat('pHlourin');
%       text(10,35,textul,'FontSize',10,'color','g','BackgroundColor',[0.7
0.7 0.7]);
%   case 2
%       textul=strcat('Cy3');
%       text(10,35,textul,'FontSize',10,'color','r','BackgroundColor',[0.7
0.7 0.7]);
%   case 3
%       textul=strcat('647nC');
%       text(10,35,textul,'FontSize',10,'color','b','BackgroundColor',[0.7
0.7 0.7]);
%   case 4
%       textul=strcat('STED');
%       text(10,35,textul,'FontSize',10,'color','r','BackgroundColor',[0.7
0.7 0.7]);
%
%   end

    try
    if numel(hex>1)

        xes=[hex(ijj)-50 hex(ijj)+50 hex(ijj)+50 hex(ijj)-50 hex(ijj)-50];
        yes=[hey(ijj)-50 hey(ijj)-50 hey(ijj)+50 hey(ijj)+50 hey(ijj)-50];

        line(xes,yes,'color','g');
    end;
    catch
    end
%% Moving to the next image
function sroi_next;

global movi rr xx yy filename chol b2 Movi3 pixel_size image_matrix
positioner pixel_size limits
global list mapname b rows cols A q s ijj jjj r1 firstred olds inner_radius
outer_radius matrix backmatrix old_movi
global alignsx alignsy rect fused not_fused sh hex hey rrl imagenr

[stat, mess]=fileattrib('*_ch00.tif');

numel(mess)
imagenr=imagenr+1
positioner=0;
hex=[]; hey=[];
values_matrix=[];
movi=[];

```

## Appendix

---

```
if numel(mess)>2*imagenr | numel(mess)==2*imagenr

    imagenr
    2*imagenr*100/numel(mess)

[stat, mess]=fileattrib('*_ch00.tif');

dir *.tif;
%rr=input('The first confocal file      ','s');
%rr1= input('The STED file      ','s');
pixel_size=20.20; %input('What is the pixel size ?');

%if rr1=='1'
%   name=strcat(rr(1:numel(rr)-4),'.mat');
%   load(name);
%else
rr=mess(imagenr*2).Name
r4=mess(imagenr*2-1).Name

    r1=strcat(rr(1:numel(rr)-5),'0.tif');

    r2=strcat(rr(1:numel(rr)-5),'1.tif');

    filename=strcat(r4(1:numel(r4)-4));
    rr1=filename;
    filename=strcat(r4(1:numel(r4)-4),'.txt');

movi=[];

movi(:,:,1)=imread(r4);
movi(:,:,2)=imread(r2);
movi(:,:,3)=imread(r1);

old_movi=movi;

sizz=size(movi);

over=[];
over(:,:,2)=movi(:,:,2)*1/max(max(movi(:,:,2)));
over(:,:,1)=movi(:,:,3)*1/max(max(movi(:,:,3)));
over(:,:,3)=movi(:,:,1)*1/max(max(movi(:,:,1)));

STED=image(over,'tag','him','cdatamapping','scaled');    colormap(summer);
axis square;

dd=uicontrol('string','Step',...
    'style','pushbutton','callback','step',...
    'position',[100 0 50 30],'tooltipstring','one by one');
ee=uicontrol('string','Stepback',...
    'style','pushbutton','callback','stepback',...
    'position',[150 0 50 30],'tooltipstring','one by one back');

m=uicontrol('style','pushbutton', 'callback','sroi_next',...
```



```

        'position',[400 0 70 30],'string','Next');

%       sh=uicontrol('Style','slider','Callback',@lut,'Max',      255,
'Min',0,'Value',255,...
% 'SliderStep',[0.025 0.1], 'Position', [550 0 100 30]);

chol=[];
inner_radius=10;
outer_radius=30;
image_matrix=[];
zz=[];
iii=0;jjj=1;
ijj=1;
backmatrix=[];
alignsx=[]; alignsy=[];
xx=[]; yy=[]; zz=[];
hex=[]; hey=[];

fused=[];
not_fused=[];

set(gcf,'windowbuttondownfcn','sroi_00y');
%sroi_align;
else
    close all;

%       [stat, mess]=fileattrib('*_distances.txt');

end;
%% Processing the selected area
function automatic_sted_raj_cy3;

global positioner old_movi old_small_movi small_movi orange green sted
old_orange old_green pixel_size limits the_sizer pos1
global contrastor1 contrastor2 contrastor3 old_sted rr1 hex hey xxes yyes
background_orange background_green imagenr movi

limit_orange=limits(2);
limit_green=limits(1);
limit_sted=limits(3);

%limit_orange=3;
%limit_green=8;
%limit_sted=8;% 10 for normal old patches, 8 for new patches remaining, 6
for new patches
the_sizer=0;
figure;
% name the new area by increasing positioner
positioner=positioner+1;

% test whether the background is defined
% if numel(hex)<4
%     figure; text(0.3,0.5, 'Define background area');
%     pause(1);
%     close; close;
% end;

```

## Appendix

---

```
% name the new area by increasing positioner
positioner=positioner+1;

% % generate the background matrix
% sub_back=[];
% for i=1:4
%     sub_back(:,:,i)=old_movi(hey(i)-50:hey(i)+50,hex(i)-50:hex(i)+50,i);
% end;
%
% background_orange=mean2(sub_back(:,:,2));
% background_green=mean2(sub_back(:,:,1));

% generate the selected area matrix, and a second copy in "old_small_movi"
% with only the orange and STED images (atto confocal is by now irrelevant
old_small_movi=[];
old_small_movi(:,:,1)=small_movi(:,:,1);
old_small_movi(:,:,2)=small_movi(:,:,2);
old_small_movi(:,:,3)=small_movi(:,:,3);

%%%%%%%%
small_movi_filtered=[];
H=fspecial('average',3);
for i=1:3
    small_movi_filtered(:,:,i)=medfilt2(old_small_movi(:,:,i));
end;
small_movi_filtered(:,:,i)=imfilter(old_small_movi(:,:,i),H,'replicate');
end;

%%%%%%%%%%%% the actual images to work with, orange and sted
%
%     green=small_movi_filtered(:,:,1);
%     green=bpass(green,0,15);
%     orange=small_movi_filtered(:,:,2);
%     orange=bpass(orange,0,15);
%     sted=small_movi_filtered(:,:,3);
%
%     old_orange=orange;
%     old_sted=sted;
%     old_green=green;

%%%%%%%%%%%% getting a bw image of the area, saved as "pols"
pols=old_small_movi(:,:,1);
ccc=find(pols>0); pols(ccc)=1;

%%%%%%%%%%%%%%%%%%%%%%%%%%%%%%%%%%%%%%%%%%%%%%%%%%%%%%%%%%%%%%%%%%%%%%%%
%%%%%%%%%%%%%%%%%%%%%%%%%%%%%%%%%%%%%%%%%%%%%%%%%%%%%%%%%%%%%%%%%%%%%%%%
%
ccc_pols=find(pols==1);
%     contrastor1=icontrol('tag','fff',...
%         'style','slider','callback',{@sroi_levels1},...
%         'position',[200 0 100 30],'min',0,'max',(max(orange(ccc_pols))),...
%         'sliderstep',[0.0255 0.1]);
% set(contrastor1,'value',(mean(orange(ccc_pols)) + limit_orange));
% sroi_levels1;
%
%
%     contrastor2=icontrol('tag','fff',...
%         'style','slider','callback',{@sroi_levels2},...
%         'position',[300 0 100 30],'min',0,'max',(max(sted(ccc_pols))),...
%         'sliderstep',[0.0255 0.1]);
```

```

% set(contrastor2,'value',(mean(sted(ccc_pols)) + limit_sted));
% sroi_levels2;

    contrastor3=icontrol('tag','fff',...
        'style','slider','callback',{@sroi_levels3},...
        'position',[0 0 100 30],'min',0,'max',(max(green(ccc_pols))),...
        'sliderstep',[0.0255 0.1]);
set(contrastor3,'value',(mean(green(ccc_pols)) + limit_green));
sroi_levels3;

cleaning=icontrol('tag','clense','style','pushbutton',
'callback',{@make_do},...
    'position',[100 0 100 30],'string','Calculate');
%
%         cleaning2=icontrol('tag','clense','style','pushbutton',
'callback',{@make_do2},...
%         'position',[200 0 100 30],'string','Auto was
OK','tooltipstring','erase all drawings');
%
%         cleaning2=icontrol('tag','clense','style','pushbutton',
'callback',{@show_do},...
%         'position',[400 0 100 30],'string','Show
Auto','tooltipstring','erase all drawings');

subplot(2,3,1); imagesc(small_movi(:,:,1)); axis equal;
subplot(2,3,2); imagesc(small_movi(:,:,2)); axis equal;
subplot(2,3,3); imagesc(small_movi(:,:,3)); axis equal;

end
% function sroi_levels1(source,eventdata)
%
% global orange sted contrastor1 contrastor2 old_orange old_sted the_sizer
%
% orange=old_orange;
% hh=get(contrastor1,'value');
%
% ccc=find(orange<hh);orange(ccc)=0;
%
% %%%% orange
%
%
%
%         orange=imerode(orange,strel('disk',1));
%         orange=imdilate(orange,strel('disk',1));
%
% %         pk=pkfnd(orange,0,6);
% %         cnt=cntrd(orange,pk,6);
% %         pos=cnt(:,1:2);
% %         siz_pos=size(pos);
% %
% %         siz=size(pos)
%
%
%
%         bworange=im2bw(orange);
%         bwlorange=bwlabel(bworange);
%
%
%         for i=1:max(max(bwlorange))

```

## Appendix

---

```
% ccc=find(bwlorange==i);
%   if numel(ccc)<70
%       bwlorange(ccc)=0;
%   end;
% end;
%
% subplot(2,3,5);
% if the_sizer==1
%
%   imagesc(rot90(flipud(im2bw(bwlorange)),3));   axis equal;
%   else
%       imagesc(im2bw(bwlorange));   axis equal;
%   end;
%   hh
% end
% function sroi_levels2(source,eventdata)
%
% global orange sted contrastor1 contrastor2 old_orange old_sted the_sizer
%
% sted=old_sted;
% hh=get(contrastor2,'value');
%
% ccc=find(sted<hh);sted(ccc)=0;
%
% %%%% orange
%
%   sted=bpass(sted,0,30);
%
%   sted=imerode(sted,strel('disk',1));
%   sted=imdilate(sted,strel('disk',1));
%
%
%   pk=pkfnd(sted,0,6);
%   cnt=cntrd(sted,pk,6);
%   pos=cnt(:,1:2);
%
%
% sted2=rot90(flipud(sted),3);
% if the_sizer==1
%   subplot(2,3,6); imagesc(im2bw(sted2));   axis equal;
%
%   pk2=pkfnd(sted2,0,6);
%   cnt2=cntrd(sted2,pk2,6);
%   pos2=cnt2(:,1:2);
%   siz=size(pos2)
%
%   colors='rgbcmyk';
%
%   for k=1:siz(1)
%       p=randperm(numel(colors));
%
% line(pos2(k,1),pos2(k,2),'linestyle','none','marker','o','markeredgecolor',
% 'none','markerfacecolor',colors(p(1)));
%   end;
%
% else
%   subplot(2,3,6);
%   imagesc(im2bw(sted));   axis equal;
%
%   %   siz=size(pos)
% %
```

```

%         colors='rgbcmyk';
%         siz=size(pos);
%         for k=1:siz(1)
%             p=randperm(numel(colors));
%
line(pos(k,1),pos(k,2),'linestyle','none','marker','o','markeredgecolor','n
one','markerfacecolor',colors(p(1)));
%         end;
%
%
%
% end;
%
%
%
%
% hh
%
%
%
% end
function sroi_levels3(source,eventdata)

global orange green contrastor3 old_orange old_green old_small_movi greenx
greeny the_sizer

green=old_green;
hh=get(contrastor3,'value');

ccc=find(green<hh);green(ccc)=0;

%%%%%% orange

        green=imerode(green,strel('disk',1));
        green=imdilate(green,strel('disk',1));

%         pk=pkfnd(green,0,6);
%         cnt=cntrd(green,pk,6);
%         pos=cnt(:,1:2);
%         siz_pos=size(pos);
%
%         siz=size(pos)

        bwgreen=im2bw(green);
        bwlgreen=bwlabel(bwgreen);

        for i=1:max(max(bwlgreen))
ccc=find(bwlgreen==i);
            if numel(ccc)<10
                bwlgreen(ccc)=0;
            end;
        end;

bwlgreen=bwlabel(bwlgreen);

```

## Appendix

---

```
old_real_green=old_small_movi(:, :, 1);

greenx=[]; greeny=[];

    for i=1:max(max(bwlgreen))
ccc=find(bwlgreen==i);
    siz=size(bwlgreen);
    [xx yy]=ind2sub([siz(1) siz(2)],ccc);
    mm=old_real_green(ccc);
    greenx(numel(greenx)+1)=sum(xx.*mm)/sum(mm);
    greeny(numel(greeny)+1)=sum(yy.*mm)/sum(mm);
end;

        subplot(2,3,4); imagesc(im2bw(bwlgreen));        axis equal;

    hh

end
function make_do(source,eventdata)

global orange sted green rr1 positioner small_movi xxes yyes pixel_size
greenx greeny old_sted old_small_movi pos1 movi

siz=size(movi);    a=zeros(siz(1)+200,siz(2)+200);
for i=1:siz(3)
    a(101:100+siz(1),101:100+siz(2),i)=movi(1:siz(1),1:siz(2),i);
end;

green=a(:, :, 1);
red=a(:, :, 2);
sted=a(:, :, 3);

gmatrix=green(round(greenx(1))+pos1(1):round(greenx(1))+pos1(1)+200,round(greeny(1))+pos1(3):round(greeny(1))+pos1(3)+200);

redmatrix=red(round(greenx(1))+pos1(1):round(greenx(1))+pos1(1)+200,round(greeny(1))+pos1(3):round(greeny(1))+pos1(3)+200);

stedmatrix=sted(round(greenx(1))+pos1(1):round(greenx(1))+pos1(1)+200,round(greeny(1))+pos1(3):round(greeny(1))+pos1(3)+200);

rmmm=[];
rmmm(:, :, 1)=gmatrix;
rmmm(:, :, 2)=redmatrix;
rmmm(:, :, 3)=stedmatrix;

    dlmwrite(strcat(rr1, '_', num2str(positioner), '_spots.txt'), rmmm);
```

```
figure;
    subplot(1,3,1); imagesc(gmatrix); axis equal;
    subplot(1,3,2); imagesc(redmatrix); axis equal;
    subplot(1,3,3); imagesc(stedmatrix); axis equal;

    pause(1); close; close;
```

```
end
```

### %% Band pass filters

```
function res = bpass(image_array, lnoise, lobject, threshold)
%
% NAME:
%           bpass
% PURPOSE:
%           Implements a real-space bandpass filter that suppresses
%           pixel noise and long-wavelength image variations while
%           retaining information of a characteristic size.
%
% CATEGORY:
%           Image Processing
% CALLING SEQUENCE:
%           res = bpass( image_array, lnoise, lobject )
% INPUTS:
%           image: The two-dimensional array to be filtered.
%           lnoise: Characteristic lengthscale of noise in pixels.
%                   Additive noise averaged over this length should
%                   vanish. May assume any positive floating value.
%                   May be set to 0 or false, in which case only the
%                   highpass "background subtraction" operation is
%                   performed.
%           lobject: (optional) Integer length in pixels somewhat
%                   larger than a typical object. Can also be set to
%                   0 or false, in which case only the lowpass
%                   "blurring" operation defined by lnoise is done,
%                   without the background subtraction defined by
%                   lobject. Defaults to false.
%           threshold: (optional) By default, after the convolution,
%                   any negative pixels are reset to 0. Threshold
%                   changes the threshold for setting pixels to
%                   0. Positive values may be useful for removing
%                   stray noise or small particles. Alternatively, can
%                   be set to -Inf so that no thresholding is
%                   performed at all.
%
% OUTPUTS:
%           res:   filtered image.
% PROCEDURE:
%           simple convolution yields spatial bandpass filtering.
% NOTES:
% Performs a bandpass by convolving with an appropriate kernel. You can
% think of this as a two part process. First, a lowpassed image is
% produced by convolving the original with a gaussian. Next, a second
% lowpassed image is produced by convolving the original with a boxcar
% function. By subtracting the boxcar version from the gaussian version, we
% are using the boxcar version to perform a highpass.
%
% original - lowpassed version of original => highpassed version of the
% original
%
% Performing a lowpass and a highpass results in a bandpassed image.
```

## Appendix

---

```
%
% Converts input to double. Be advised that commands like 'image' display
% double precision arrays differently from UINT8 arrays.

% MODIFICATION HISTORY:
%     Written by David G. Grier, The University of Chicago, 2/93.
%
%     Greatly revised version DGG 5/95.
%
%     Added /field keyword JCC 12/95.
%
%     Memory optimizations and fixed normalization, DGG 8/99.
%     Converted to Matlab by D.Blair 4/2004-ish
%
%     Fixed some bugs with conv2 to make sure the edges are
%     removed D.B. 6/05
%
%     Removed inadvertent image shift ERD 6/05
%
%     Added threshold to output. Now sets all pixels with
%     negative values equal to zero. Gets rid of ringing which
%     was destroying sub-pixel accuracy, unless window size in
%     cntrd was picked perfectly. Now cntrd gets sub-pixel
%     accuracy much more robustly ERD 8/24/05
%
%     Refactored for clarity and converted all convolutions to
%     use column vector kernels for speed. Running on my
%     macbook, the old version took ~1.3 seconds to do
%     bpass(image_array,1,19) on a 1024 x 1024 image; this
%     version takes roughly half that. JWM 6/07
%
%     This code 'bpass.pro' is copyright 1997, John C. Crocker and
%     David G. Grier. It should be considered 'freeware'- and may be
%     distributed freely in its original form when properly attributed.

if nargin < 3, lobject = false; end
if nargin < 4, threshold = 0; end

normalize = @(x) x/sum(x);

image_array = double(image_array);

if lnoise == 0
    gaussian_kernel = 1;
else
    gaussian_kernel = normalize(...
        exp(-((-ceil(5*lnoise):ceil(5*lnoise))/(2*lnoise)).^2));
end

if lobject
    boxcar_kernel = normalize(...
        ones(1,length(-round(lobject):round(lobject))));
end

% JWM: Do a 2D convolution with the kernels in two steps each. It is
% possible to do the convolution in only one step per kernel with
%
% gconv = conv2(gaussian_kernel',gaussian_kernel,image_array,'same');
% bconv = conv2(boxcar_kernel', boxcar_kernel,image_array,'same');
%
```



```

% but for some reason, this is slow. The whole operation could be reduced
% to a single step using the associative and distributive properties of
% convolution:
%
% filtered = conv2(image_array,...
%   gaussian_kernel'*gaussian_kernel - boxcar_kernel'*boxcar_kernel,...
%   'same');
%
% But this is also comparatively slow (though inexplicably faster than the
% above). It turns out that convolving with a column vector is faster than
% convolving with a row vector, so instead of transposing the kernel, the
% image is transposed twice.

gconv = conv2(image_array',gaussian_kernel','same');
gconv = conv2(gconv',gaussian_kernel','same');

if lobject
    bconv = conv2(image_array',boxcar_kernel','same');
    bconv = conv2(bconv',boxcar_kernel','same');

    filtered = gconv - bconv;
else
    filtered = gconv;
end

% Zero out the values on the edges to signal that they're not useful.
lzero = max(lobject,ceil(5*lnoise));

filtered(1:(round(lzero)),:) = 0;
filtered((end - lzero + 1):end,:) = 0;
filtered(:,1:(round(lzero))) = 0;
filtered(:,(end - lzero + 1):end) = 0;

% JWM: I question the value of zeroing out negative pixels. It's a
% nonlinear operation which could potentially mess up our expectations
% about statistics. Is there data on 'Now centroid gets subpixel accuracy
% much more robustly'? To choose which approach to take, uncomment one of
% the following two lines.
% ERD: The negative values shift the peak if the center of the cntrd mask
% is not centered on the particle.

% res = filtered;
filtered(filtered < threshold) = 0;
res = filtered;

%% Post-processing of selection, to obtain average images
function address_spots;

cd 'C:\data_2012\sinem';% Folder containing sub-folders that have just been
analyzed

cellb={};

[dsstat, dmmess]=fileattrib('*');
for i=1:numel(dmmess)
    if dmmess(i).directory
        cellb{numel(cellb)+1}=dmmess(i).Name;
    end;
end;
end;

```

## Appendix

---

```
for abcdef=1:numel(cellb);

    abcdef
    name=cellb{abcdef};
    cd(name);

% global pixel_size;
close all;
pixel_size=20.2;

[stat, mess]=fileattrib('*_spots.txt');
if stat==1
    redm=[];
    greenm=[];
    redm=zeros(201,201);
    greenm=zeros(201,201);
    matcounter=0;

    matrix=dlmread(mess(1).Name);
    az=matrix(1:201,1:201);
    red=matrix(1:201,403:603);
    counter=1;
    for klm=2:numel(mess)
        klm*100/numel(mess)

        matrix=dlmread(mess(klm).Name);
        az2=matrix(1:201,1:201);
        red2=matrix(1:201,403:603);
        %%%%%%%%%%%%%%%turn around

    for klmmm=1:72

        aa=imrotate(red2,klmmm*5);
        siz=size(aa);half=round(siz(1)/2);
        aa=aa(half-100:half+100,half-100:half+100);
        bb=imrotate(green2,klmmm*5);
        siz=size(bb);half=round(siz(1)/2);
        bb=bb(half-100:half+100,half-100:half+100);

        minima(klmmm)=corr2(aa(50:150,50:150),red(50:150,50:150))*corr2(bb(50:150,50:150),green(50:150,50:150));
    end;
    %%%%%%%%%%%%%%%flip
    for klmmm=1:72

        aa=imrotate(flipud(red2),klmmm*5);
        siz=size(aa);half=round(siz(1)/2);
        aa=aa(half-100:half+100,half-100:half+100);
        bb=imrotate(flipud(green2),klmmm*5);
        siz=size(bb);half=round(siz(1)/2);
        bb=bb(half-100:half+100,half-100:half+100);

        minima(klmmm+72)=corr2(aa(50:150,50:150),red(50:150,50:150))*corr2(bb(50:150,50:150),green(50:150,50:150));
    end;
end;
```

```

end;

ccc=find(minima==max(max(minima)));
try
pos=ccc(1);
catch
end;

if pos<72
    aa=imrotate(green2,pos*5);          siz=size(aa);half=round(siz(1)/2);
aa=aa(half-100:half+100,half-100:half+100); green2=aa;
    aa=imrotate(red2,pos*5);  siz=size(aa);half=round(siz(1)/2); aa=aa(half-
100:half+100,half-100:half+100); red2=aa;
    aa=imrotate(az2,pos*5);  siz=size(aa);half=round(siz(1)/2); aa=aa(half-
100:half+100,half-100:half+100); az2=aa;

else
    aa=imrotate(flipud(green2),pos*5);  siz=size(aa);half=round(siz(1)/2);
aa=aa(half-100:half+100,half-100:half+100); green2=aa;
    aa=imrotate(flipud(red2),pos*5);    siz=size(aa);half=round(siz(1)/2);
aa=aa(half-100:half+100,half-100:half+100); red2=aa;
    aa=imrotate(flipud(az2),pos*5);    siz=size(aa);half=round(siz(1)/2);
aa=aa(half-100:half+100,half-100:half+100); az2=aa;
end;

%turn_matrix=turn_matrix/2;
counter=counter+1;
green=(green+green2);
red=(red+red2);
az=(az+az2);

end;
% imagesc(turn_matrix); axis equal; drawnow;

dlmwrite('ribbon_matrix_by_both.txt',az/counter);
dlmwrite('green_matrix_by_both.txt',green/counter);
dlmwrite('red_matrix_by_both.txt',red/counter);

a=dlmread('ribbon_matrix_by_both.txt');
b=dlmread('green_matrix_by_both.txt'); c=dlmread('red_matrix_by_both.txt');
figure;

imwrite(uint8(a),'ribbon_matrix_by_both.tif','tiff');
imwrite(uint8(b),'green_matrix_by_both.tif','tiff');
imwrite(uint8(c),'red_matrix_by_both.tif','tiff');

subplot(2,2,1); imagesc(a); axis equal; colormap(jet);
subplot(2,2,2); imagesc(medfilt2(b)); axis equal; colormap(jet);
subplot(2,2,3); imagesc(medfilt2(c)); axis equal; colormap(jet);

end;

```

end;

# CURRICULUM VITAE

---

## Natalia Hasel Revelo Nuncira

Humboldtalle 23  
37073  
Goettingen, Germany  
nrevelo@gwdg.de

### EDUCATION

- 2009 - 2014** Enrolled as PhD student in the MSc/PhD International Max Planck Research School in Neuroscience and the Göttingen Graduate School of Neurosciences and Molecular Biosciences (GGNB) from the Georg-August-Universität, Göttingen.
- 2008 - 2009** Master year at the MSc/PhD International Max Planck Research School, Neuroscience Program. Göttingen, Germany.  
Total grade of the Master's examinations: 1.33 = A (excellent)
- 2003 - 2008** B.Sc. in Biology (with Honours). Universidad Nacional de Colombia  
**Academic Awards:** Honor matriculation and tuition fee exemption for the best Grade Point Average, Universidad Nacional de Colombia: I-2003, I-2004, II-2004, I-2005, II-2005, I-2007, II-2007.  
**Cumulative Grade point average (Max. 5):** 4.4  
Top ranked student in both the Biology department and the Natural Sciences Faculty

### PUBLICATIONS

- Revelo N.H.\***, Kamin D.\*, Truckenbrodt S., Wong A.B., Reuter K., Reisinger E., Moser T., Rizzoli S.O.° (2014) A new probe for super-resolution imaging of membranes elucidates trafficking pathways. *J Cell Biol.* 205(4), 591–606.
- Kamin, D.\*, **Revelo N.H.\***, Rizzoli S.O.° (2014) FM Dye Photo-oxidation as a Tool for Monitoring Membrane Recycling in Inner Hair Cells. *PLoS One.* 9:e88353. doi:10.1371/journal.pone.0088353.
- Revelo N.H.°**, Rizzoli S.O. (2015) Application of STED microscopy to cell biology questions. In: Verveer P. Advanced Fluorescence Microscopy: Methods and Protocols. *Methods Mol Biol.* 1251, 213–30. doi:10.1007/978-1-4939-2080-8\_12
- Regen, T., van Rossum, D., Scheffel, J., Kastriti, M.E., **Revelo, N.H.**, Prinz, M., Brück, W., Hanisch, U.K. (2011) CD14 and TRIF govern distinct responsiveness and responses in mouse microglial TLR4 challenges by structural variants of LPS. *Brain Behav. Immun.* 25:957-970.

\* Equal contribution

° Corresponding Author

## RESEARCH EXPERIENCE

- 05.2011 – present**    **PhD project.** Synaptic vesicle recycling in the inner hair cell.  
Dr. Silvio Rizzoli. Laboratory for STED microscopy of synaptic function. European Neuroscience Institute Göttingen.  
Experience: STED microscopy of synaptic vesicle recycling in inner hair cells from mice.
- 10. 2009 – 04.2011**    **PhD project.** Localized signaling reactions in the developing growth cone during navigation  
Prof. Dr. Fred S. Wouters. Laboratory for Molecular and Cellular Systems. Department of Neuro- and Sensory Physiology. University Medicine, Göttingen.  
Experience: Epifluorescent and confocal imaging of FRET based molecular probes. Design and cloning of FRET based biosensors for intracellular cyclic nucleotides levels.
- 05.2009 – 06.2009**    **Lab rotation.** Design and evaluation of molecular replacement vectors for the analysis of signaling mechanisms in long term synaptic plasticity.  
Dr. Oliver Schlüter, European Neuroscience Institute Göttingen (ENI-G)  
Experience: Western Blot, cloning, electrophysiology, coexpression of vectors in HEK293 cell cultures.
- 03.2009 – 04. 2009**    **Lab rotation.** Effect of different LPS chemotypes on microglial TLR4 pathways  
Prof. Dr. Uwe-Karsten Hanisch. Neuropathology Department. Klinikum der Georg-August-Universität Göttingen.  
Experience: primary microglia cell culture, microglia stimulation, ELISA
- 01.2009 – 02.2009**    **Lab rotation.** Imaging of conformational changes in the FAT and FERM domains of the Focal Adhesion Kinase (FAK) using FRET based biosensors.  
Prof. Dr. Fred S. Wouters – Dr. Gertrude Bunt. Laboratory for Molecular and Cellular Systems. Dept. of Neuro- and Sensory Physiology. Center II, Physiology and Pathophysiology. University of Göttingen.  
Experience: REF52 cell culture and transfection, cloning, confocal microscopy, acceptor photobleaching FRET analysis.
- 03.2008 – 08.2008**    **Research project.** Content-Based Retrieval System for Histological Images  
Dr. Fabio González, Dr. Clara Spinel Gómez. Universidad Nacional de Colombia  
Experience: Histological images acquisition from cat and mouse tissues.
- 02.2007 – 12.2007**    **Bachelor thesis.** Schwann cells and endoneural fibroblasts tridimensional culture in collagen matrix.

Dr. Clara Spinel Gomez. Universidad Nacional de Colombia

Experience: Primary and collagen tridimensional cultures from sciatic nerve cells.

**08.2006 - 11.2006** **Practical training.** Dynamics of the functional changes in the facial primary motor cortex induced by the peripheral injury of the contralateral facial nerve.

Dr. Julieta Troncoso. Universidad Nacional de Colombia

Experience: electrophysiological recordings from primary motor cortex after contralateral facial nerve lesion.

### SCHOLARSHIPS AND AWARDS

**07.2014** Selected as participant for the Lindau Nobel Laureate Meeting for Medicine and Physiology

**09.2012** Poster Presentation Prize at the Horizons in Molecular Biology Symposium.

**04.2012 - 10.2013** Mentee of the Dorothea Schlözer Mentoring Programme of the Georg-August-Universität Göttingen.

**09.2008 - 09.2009** Stipend of the Excellence Foundation for the Promotion of the Max Planck Society

**10.2007** Academic Visit to the Federal Republic of Germany.  
DAAD Scholarship (Deutscher Akademischer Austausch Dienst).  
October 14 - 25, 2007.

### ORGANIZATION OF ACADEMIC EVENTS

**2012 - 2013** Organizer of the 2<sup>nd</sup> Women's Careers and Networks Symposium from the Göttingen Graduate School of Neurosciences and Molecular Biosciences (GGNB). March 6, 2013. Göttingen.

**2010 - 2011** Organizer of the 1<sup>st</sup> Women's Careers and Networks Symposium from the Göttingen Graduate School of Neurosciences and Molecular Biosciences (GGNB). November 3, 2011. Göttingen.

**2010 - 2011** Organizer of the Neurizons Meeting from the International Max Planck Research School of Neuroscience in Göttingen. May 25 - 28, 2011. Göttingen.

**01.2006 - 10.2007** Organizer and General Secretary of the 1<sup>st</sup> National Congress of Biology Students. Biology Department, Natural Sciences Faculty, Universidad Nacional de Colombia

### WORK AND TEACHING EXPERIENCE

**05.2011 - Present** Position: Researcher  
Employer: European Neuroscience Institute, University Medicine, Göttingen.

- 10.2009 – 05.2011** Position: Researcher  
Employer: Department of Neuro- and Sensory Physiology, University Medicine, Göttingen.
- 12. 2010** Preparation of the Light Microscopy and FLIM demo for the Göttingen Neuroscience Program first year students.
- 03.2010** GGNB extended methods course in advanced light microscopy. Tutor during the hands-on course on FRET imaging.
- 03.2007 – 08.2008** Position: Researcher  
Employer: International Physics Center, Biophysics Research Group. Colombia
- 01.2007 – 08.2008** International Physics Center, Bogota, Colombia. Biophysics Research Group.
- 02.2007 – 07.2007** Position: Tutor  
Subject: Plant Physiology  
Employer: Natural Sciences Faculty, Universidad Nacional de Colombia
- 02.2006 – 08.2008** Animal physiology Research Group  
Directed by Dr. Edgar Cristancho, assistant professor  
Biology department, Universidad Nacional de Colombia



“La vida no es la que uno vivió, sino la que uno recuerda y cómo la recuerda para contarla”.

“Life is not what one lived, but what one remembers and how one remembers it in order to  
recount it”.

**Gabriel García Márquez**

Colombian Nobel Laureate for Literature

1927-2014